DEEP CONVECTION OCCURRING ABOVE A STABLE PLANETARY BOUNDARY LAYER

by

Bradley Roy Colman

B.S., Montana State University
(1977)

Submitted to the Department of
Earth, Atmospheric and Planetary Sciences
in Partial Fulfillment of the Requirements for the

Degree of

DOCTOR OF SCIENCE

at the

MASSACHUSETTS INSTITUTE OF TECHNOLOGY

© 1984, Massachusetts Institute of Technology

Signature of Author _____
Department of Earth, Atmospheric and
Planetary Sciences, February, 1984

Certified by: _____
Professor Frederick Sanders
Thesis Supervisor

Accepted by: _____
Professor Theodore R. Madden
Chairman, Departmental Committee
on Graduate Students

WITHDRAWN
MASSACHUSETTS INSTITUTE OF TECHNOLOGY
AUG 31 1984
LIBRARIES

DEEP CONVECTION OCCURRING ABOVE A STABLE PLANETARY BOUNDARY LAYER

by

Bradley Roy Colman

Submitted to the Department of Earth, Atmospheric, and Planetary Sciences in February, 1984 in partial fulfillment of the requirements for the Degree of Doctor of Science in Atmospheric Sciences

ABSTRACT

We have studied the observed characteristics of "elevated convection", defined as thunderstorm activity that occurs in an environment having a gravitationally stable planetary boundary layer overlain by a less stable layer. We have focused specifically on elevated convection occurring above a frontal inversion, but have made no *a priori* assumption about the generating mechanism.

First, a climatology of elevated convection for the United States was completed. The data set used in the study contains 1093 observations over a four-year period, which were collected from the 00 GMT and 12 GMT NMC surface analyses. Second, an investigation into the elevated convection that occurred during the AVE-SESAME I experiment of 10, 11 April 1979 was conducted. The study was built upon a very detailed radar analysis that was the result of compositing hourly photographs of the PPI scopes from seven different radar sites. The elevated convection was found to dominate the storm total precipitation amounts, helping to substantiate the importance of understanding these storms.

A composite of the data set showed that the typical elevated thunderstorm is found to the northeast of an associated surface low pressure center, and north of a warm front in a region with northeasterly surface winds. The planetary boundary layer is generally very stable with respect to both the 500-mb and 850-mb air. The convection is usually found in the left exit region of a low-level wind maxima and in strong warm advection flanked by an area of strong deformation. There is generally very little latent instability anywhere in the sounding, with the atmosphere nearly moist adiabatic.

The annual frequency distribution of elevated convection was found to be bimodal, with the primary peak in April and the secondary peak in September. The geographical distribution has the major concentration of events occurring in the area from the central Gulf Coast northward into the Mississippi and Ohio River drainages. It was shown that nearly all winter season (December through February) thunderstorms east of the Rocky Mountains are of the elevated type with the exception of

those over the Florida Peninsula, where ground-based convection persists throughout the year. Most of this winter season elevated convection was found to occur very near the Gulf Coast during periods of extensive overrunning ahead of migrating cyclones across the southern tier of states.

In the case study, the convection was observed to occur in three convective impulses. The initial development of each one took place in the warm sector, and subsequently propagated onto the frontal surface. Numerous pressure waves were observed in association with the elevated convection, yet, were not found to be important in the triggering of the elevated thunderstorms. During the lifetime of these impulses, mesoscale updrafts developed and moved with the convective area, maintaining a nearly steady-state system with strong low-level inflow.

An investigation of a convective band that formed above the frontal surface revealed that the development likely took place in two steps. Initially, high θ_e air overlying the frontal inversion was stable to vertical displacements, but inertially unstable. Then, along the path of the unstable parcel, the thermodynamic structure changed, and the parcel apparently became grativationally unstable, resulting in upright convection.

Thesis Supervisor: Dr. Frederick Sanders

Title: Professor of Meteorology

To all of my family

and

In loving memory of my grandfather

TABLE OF CONTENTS

ABSTRACT 2

DEDICATION 4

TABLE OF CONTENTS. 5

CHAPTER 1: INTRODUCTION. 6

CHAPTER 2: BACKGROUND. 11

CHAPTER 3: CLIMATOLOGICAL SURVEY 22

3.1 Introduction 22
3.2 Data Source and Selection Process. 24
3.3 Geographical, Seasonal, and Diurnal Variations 29
3.4 Dynamic and Thermodynamic Environment. 56
3.5 Synoptic Types 80
3.6 Discussion 92

CHAPTER 4: AN INVESTIGATION OF ELEVATED CONVECTION DURING AVE-SESAME I 95

4.1 Introduction 95
4.2 Data Sources 99
4.3 Synoptic Overview. 103
4.4 Stability Analysis 125
4.5 Radar Analysis 132
4.6 Mesoscale Analysis of Convective Impulses. 160
4.7 Gravity Wave Analysis. 189
4.8 Discussion 195

CHAPTER 5: CONCLUSIONS. 200

REFERENCES 211

APPENDICES

I Upper-Air Soundings from AVE-SESAME I. 216
II AVE-SESAME I Grid Point Data Set 218
III Complete Set of Mesoscale Surface Analyses 220
IV Complete Set of 850-mb and 500-mb Analyses 232

ACKNOWLEDGEMENTS 241

BIOGRAPHICAL NOTE. 243

CHAPTER 1: INTRODUCTION

Deep convection, as evidenced by the occurrence of thunderstorms, is frequent and widespread. Conceptually, the air-mass thunderstorm is the simplest and most easily understood. Surface diabatic effects, both heating and moistening, act to create a boundary layer that is gravitationally unstable to vertical displacements. This surface heating is immediately realized as an increase in the ambient temperature, and when the vertical lapse rate of temperature in the environment exceeds the dry-adiabatic lapse rate, the sensible and latent heat are transported and mixed upward by turbulence and small-scale convective overturning. Through a continuation of this process, or perhaps by forced lifting, the rising surface air cools sufficiently to produce condensation, which provides an additional source of heating from the phase change of vapor to liquid. This latent heating acts to balance part of the cooling from the adiabatic expansion of the rising air. In an environment where the temperature lapse rate exceeds that of the rising moist air, the rising air will become positively buoyant, its internal energy being converted to kinetic and potential energy. The air then continues to rise until it becomes negatively buoyant, generally near the tropopause. This type of thunderstorm, generally consisting of a single cell in a non-sheared environment, has a lifetime of an hour or two, and occurs over many regions of the globe.

In the mid-latitudes, migratory cyclones and anticyclones are important in creating an environment that is conducive to this and

other types of convection. The circulations of these systems are capable of transporting heat and moisture over large distances. For example, they can transport the moist maritime boundary layer over strongly heated land to create strong convective instability. In addition, the cyclones have associated fields of divergence and vertical velocities that can act to produce favored regions of thunderstorm development. The cold-frontal rainband is an example of the cyclone determining the position of the convection.

Furthermore, these cyclones typically develop in regions of strong baroclinity and are thus characterized by vertical wind shears. These vertical shears can influence the characteristics and lifetimes of the associated convection; warm-sector squall lines and super-cell thunderstorms are examples of deep convection where shear is an important factor. The lifetimes of these systems are generally much longer than those of air-mass thunderstorms.

In addition to these basic types of deep convection, observations have shown the existence of thunderstorms that occur above a low-level inversion (Fujita, 1963; Ferguson, 1967). The purpose of this thesis is to investigate this "elevated convection" as it occurs in association with extratropical cyclones. Initially, let this be defined as thunderstorm activity that occurs in an environment that is characterized by a gravitationally stable planetary boundary layer stable planetary boundary layer overlain by a layer that is less stable. There is not an <u>a priori</u> assumption that the generating instability is gravitational or even that any hydrostatic instability is present. Here and in the remainder of this dissertation,

hydrostatic instability will be used to describe the existence of a layer in the atmosphere where positive buoyancy is felt by a given parcel of air moving through the static environment. If the total integrated buoyancy for a parcel from its original position to its cloud top position is positive, the sounding is said to have latent instability (Darkow, 1982). Potential instability refers to the possible development of an hydrostatically unstable lapse rate as an entire layer is lifted and becomes saturated ($\partial\theta_e \partial z<0$). It is reasonable to assume that lightning, the identifying characteristic of elevated convection, requires vertical velocities on the order of one meter per second or more (personal communication, R. E. Orville, 1982). With the vertical velocities generally associated with synoptic-scale cyclones an order of magnitude less, it is postulated that a smaller scale instability is present. It is this instability that we will investigate.

The required stratification for elevated convection is typically found in the overrunning region extending away from the surface warm and cold fronts associated with extratropical cyclones (i.e., those regions other than the classical warm sector). The importance of overrunning precipitation for the south-central United States was discussed by Muller (1977). Although not differentiating the type of precipitation as convective or stratiform, he found that for New Orleans, from 1971-1974, 17% of the total precipitation was a result of frontal overrunning, most of which fell from winter to mid-spring. The frequency and extent of thunderstorms occurring in an overrunning

situation is not known. Furthermore, with the possibility that such storms play a role in heavy precipitation, synoptic development, and severe events, it is an important topic of research.

Also, the similarities and differences between thunderstorms rooted in the boundary layer and those that occur above a frontal surface are not known. It is not understood whether the mechanisms that initiate boundary layer thunderstorms are responsible for elevated thunderstorms or if other mechanisms exist. The structure of elevated thunderstorms has only been touched on previously. If elevated convection has mesoscale structure, an interesting question is whether any of the proposed mechanisms for classical convection are responsible for that structure. These mechanisms, as well as the background of our present understanding of small-scale structure above frontal surfaces, will be discussed in the next chapter.

The approach of this thesis will be to present first a comprehensive climatology of elevated convection for the United States. The spatial and temporal variations of elevated thunderstorms will be included as well as the mean thermodynamic and dynamic structure of the large-scale environment. This part of the thesis is presented in chapter 3.

Then, to ascertain the detailed structure of elevated convection, a mesoscale analysis of the AVE-SESAME I experiment is presented in chapter 4. This well-observed storm was associated with extensive elevated convection and serves as an excellent example of the great

complexity of structure of elevated convection.

Finally, chapter 5 will summarize the findings, state the conslusions of this study, and suggest problems for future research.

CHAPTER 2: BACKGROUND

The descriptive models of the extratropical cyclone, put forth by the Norwegians (Bjerknes, 1919), have stood up reasonably well against the test of time. This apparent success may have contributed to a division in research between the large scale (>1000 km in horizontal extent) and the convective scale (≈10 km in horizontal extent). Without considering the smaller scale processes great advances were made in understanding the physics of extratropical cyclones through baroclinic instability theory (Charney, 1947; Eady, 1949). On the other hand, early work on thunderstorms focused on the forecasting of the associated severe events. In so doing, the investigators looked at the characteristics of the larger-scale environment of the convection and found that features typifying extratropical cyclones were apparently important in the development of severe convection. Fawbush *et al.* (1951) looked at tornadic storms and found that vertical wind shear, temperature advection and vorticity patterns, all characteristic of a baroclinic environment, were important indicators of convection. Another frequently observed relationship is the occurrence of thunderstorms with the passage of a cold front. The large majority of severe convective events occur in the warm sector associated with supercells, pre-frontal squall lines or cold frontal rainbands and the main emphasis of research on thunderstorms is now focused in that direction. Warm sector events and thunderstorms that occur simultaneously with the passage of a surface cold front will not

be addressed in this dissertation.

Perhaps equally familiar, but receiving far less attention, are thunderstorms that occur above a frontal surface in an overrunning situation. The classic description of the warm front is of warm air that gradually ascends over a wedge of cold air, accompanied by widespread stratiform clouds and precipitation. Since the occurrence of thunderstorms near the warm front is not an element of this basic model, they have often been overlooked. Frequently, this convection is described as "a few embedded thunderstorms" (Weber and Wilderotter, 1981) without knowledge of anything about the source or structure of these storms.

The identification of smaller scale structures became possible as observation techniques improved. Identifying small scale structure in warm-frontal bands was aided by the use of autographic rainguage networks (e.g., Harrold, 1973) and the development of radar. Mesoscale features associated with extratropical cyclones were first observed using radar in the early 1950's. Marshall (1953) identified 'generating elements' in the mid-troposphere (≈15,000 ft), spaced aboud 30 km apart, and associated with the observed streaking of snow as it fell through a sheared environment. Marshall suggested that the 'generating elements' were advected by the upper level winds and regulated the observed snowfall.

Gunn et al. (1954) extended the work of Marshall by looking at winter precipitation events at Montreal, Canada. Of the 22 cases investigated, all of which had frontal inversions, 19 of them

exhibited small-scale structure. Of these cases, those that had instability above the frontal surface sufficient to support convective activity (7 of the 22) showed the least amount of mesoscale organization. On the days with instability, the echoes were usually in the vicinity of the frontal surface and extended upward an average of 4,500 ft.

Austin and Houze (1970) were the first to classify a nesting of the various sizes of precipitation areas associated with cyclones. They felt that two distinct mesoscale sizes (in areal extent) existed between the convective scale and the synoptic scale. They identified these sizes as the large mesoscale area (LMSA) covering 10^3 to 10^4 km^2, and the small mesoscale area (SMSA) covering 50 to 10^3 km^2. The nesting was such that the LMSA consisted of several distinct SMSA's which in turn contained the individual convective elements. In studying a variety of storms in New England with both radar and precipitation gauges, they found that LMSA's lasted from 2-5 hours and SMSA's on the order of 1 hour. The identification of these intermediate scales was important in directing future research in that no previously known lifting mechanism was of that scale. This was particularly true since observational studies showed that mesoscale structure associated with extratropical cyclones was nearly ubiquitous. As it became clear that a large fraction of the precipitation that occurs in conjunction with cyclonic-scale vertical motions in frontal zones is in the form of bands and showers, researchers (e.g. Elliot and Hovind, 1965; Kreitzberg and Brown, 1970)

concentrated on the associated dynamics and thermodynamics.

Early on, Hewson (1937) demonstrated a relationship between potential instability in the warm sector and the subsequent rainfall associated with the warm front. As the potential instability for any layer in the troposphere of the warm sector increased, he observed a corresponding increase in the precipitation amount north of the front. Normand (1938) discussed the release of latent instability through the lifting of a potentially unstable layer and Dexter (1944) suggested this as the acting mechanism for warm frontal thunderstorms.

Kreitzberg and Brown (1970) found that convection observed above a frontal surface was frequently aligned parallel to the wind shear in the convective layer and advanced eastward more rapidly than the surface front. They associated the generation of potential instability with the rapid advance of a 'pre-frontal cold surge' in the mid-troposphere. Their proposed scenario incorporated the release of that potential instability by the synoptic-scale ascent. The convective mixing was apparently so efficient that the atmosphere became barotropic, reestablishing a baroclinic zone farther west. This rather discontinuous process of overrunning is in sharp contrast to the previously proposed slow stable ascent associated with the warm frontal process. They identified distinct warm tongues that had apparently been transported over the frontal surface to establish regions of strong potential instability. They reported a strong correlation between the convection and these 'baroclinic leaves' and thus concluded that it was the thermodynamics that governed the

mesoscale patterns.

The University of Washington's CYCLonic Extratropical Storms (CYCLES) Project (see for example, Hobbs et al. 1980) has contributed a great deal of information about the microphysical and mesoscale structure of several types of bands associated with synoptic-scale cyclones. Herzegh and Hobbs (1980) discussed several rainbands positioned perpendicular to a warm front that they felt were associated with generating cells aloft.

A CYCLES case study presented by Matejka et al. (1980) showed results similar to those of Kreitzberg and Brown (1970) with rainbands in potentially unstable air behind a pre-frontal cold surge above the warm front. They felt these bands, aligned perpendicular to the background wind, were the result of the release of potential instability generated by the overrunning of the warm front by the cold air.

The release of potential instability by synoptic-scale motions was investigated numerically by Kreitzberg and Perkey (1976 and 1977). They proposed that large-scale convergence provided sufficient lift to release the instability. In their numerical simulation they used a sounding that showed potential instability above a warm-frontal zone. A cumulus cloud parameterization model was used that allowed for instability in more than one layer. The layer with the largest integrated buoyancy (which they called the level of maximum releasable instability) was selected as the initial cloud base. The initial moisture field showed a peak above the frontal surface with a

sinusoidal decrease on both sides with a wavelength of 720 km. The initial widespread cyclonic-scale ascent had a peak value of 7.5 cm/s at mid-levels. Early in the run 'convection' was very active above the frontal surface with the convective plume showing a peak in the vertical velocity of 8 m/s, clearly strong enough to generate lightning.

The convective heating, in turn, forced low-level convergence and increased the vertical motion on the mesoscale from 7.5 cm/s to 14.4 cm/s at 6 km. The mean subsidence from the parameterized convection was more than offset by the corresponding mesoscale ascent keeping the environment saturated. Most of the potential instability was effectively removed by the convection at 460 minutes into the integration with the wavelength of the area affected by convection limited to about 1/3 that of the moisture wavelength.

An interesting result of their experiment is that after the convection neutralized the environment, the existing mesoscale circulation, originally established by the convective heating, did not decay but actually narrowed and intensified. The resurgence of the circulation peaked at about 10 hours into the run with a maximum vertical velocity of over 21 cm/s. This mesoscale circulation was apparently driven by the diabatic heating of the stable condensation. Interestingly, most of the precipitation from the run fell after the stable mesoscale circulation became dominant. This suggests that mesoscale circulations can be initiated by convection and can actually persist and strengthen after all latent instability

has been released. The remaining updrafts in the hydrostatically neutral atmosphere can produce substantial amounts of precipitation.

Brown (1979) showed the development of a similar circulation system in his numerical simulation of saturated mesoscale anvils. He found that the positive feedback between the mid-tropospheric heating and convection was possible as long as there was subsidence in the cloud base environment. The subsidence acted to maintain a warm trough and an inwardly directed pressure gradient that forced the low-level convergence.

Further advances in the understanding of mesoscale circulations came with the application of symmetric instability. Emanuel (1979) and Bennetts and Hoskins (1979) developed the theoretical models that define the circulation that develops in the presence of strong vertical shear for both dry and moist atmospheres, respectively. The instability is manifested as slanted two-dimensional rolls aligned along the mean baroclinic shear. This dynamic instability is appealing in that it provides a lifting mechanism that acts on the mesoscale.

Bennetts and Sharp (1982) investigated the growth rate of conditional symmetric instability and tested their results with observations. Rainbands were observed in 80% of the cases where there was predicted growth. However, the growth rate of conditional symmetric instability is much slower than that for cumulus convection and would therefore be dominated by convection if both instabilities were present.

An interesting question is what determines when and where the convection breaks out after the thermodynamical environment conducive to convection has been established. Many recent studies of deep cumulus convection have investigated the various mechanisms to which the actual initialization of the storms can be attributed. Circulations associated with cold fronts (Koch and McCarthy, 1982), low-level jets (Means, 1944; Pitchford and London, 1962), drylines (Schaefer, 1973), and thunderstorm outflow boundaries (Fujita, 1963) have all been shown to trigger convection in some situations. Boundary-layer processes such as surface heating and moistening to remove a stable cap (Colby, 1983), or circulations driven by irregularities in surface heating forcing convergence (e.g., the 'inland sea-breeze', Sun and Ogura, 1979), shown to be important for some convection, are not possible triggering mechanisms for elevated convection if the convection originates above the frontal inversion.

Gravity waves have also been proposed as a possible triggering mechanism for thunderstorms. Observations have shown that in some cases gravity waves can be ducted and propagate great distances without dissipating (e.g., Bosart and Cussen, 1973). Lindzen and Tung (1976) showed that the stratification required to trap a gravity wave is a stable layer adjacent to the surface overlain by an unstable layer which contains a critical level for the propagating wave. Qualitatively this is the same environment as that required for elevated convection. The coexistence of elevated convection and ducted gravity waves in the same environment was clearly shown by

Ferguson (1967). Lindzen (1974) discussed wave-CISK (conditional instability of the second kind) in which latent heat released in convection appears capable of efficiently forcing the gravity waves, which in turn act to organize the convection. This process requires a vertically propagating wave so that there is a phase shift with height. However, since the waves associated with elevated convection are most likely trapped, there is not a phase shift with height and the wave-CISK argument does not work. This leaves the possibility that the vertical displacement associated with the wave can lift the environment to the point that it becomes hydrostatically unstable and thus trigger convection. Several case studies have shown a strong modulation of convection by ducted gravity waves (e.g., Miller and Sanders, 1980). However, the actual initialization of convection by this process has not been clearly demonstrated. Uccellini (1975) felt he was able to show this, yet, as will be discussed in chapter 4, his model appears incompatible with his data.

The actual number of case studies involving elevated convection is very small. Ferguson (1967) examined a squall line, accompanied by snow, small hail and gusty surface winds, that travelled over a low-level arctic-frontal zone for nearly 1000 km at a speed of approximately 20 m/s. The squall line appeared to form ahead of and parallel to a diffuse arctic cold front and at right angles to an east-west oriented stationary front. The southern end of the line extended well south of the surface front. There was a low-level west-southwesterly jet in the warm sector, however Ferguson did not

investigate any possible relationship between it and the line. He did feel the line was significant enough to affect short-range forecasting and even speculated that such waves could influence the subsequent formation of synoptic-scale short-wave troughs.

A case study of a long-lived mesoscale circulation system was presented by Sanders and Paine (1975). In their case, an advancing cold front was able to trigger deep cumulus convection above the frontal surface as a moist potentially unstable boundary layer was displaced upward. Once the convection was initiated, an intense mesoscale downdraft-updraft couplet developed. This circulation developed into a nearly steady-state situation producing large amounts of rainfall. Thunder was heard up to five hours after the frontal wind shift, yet the atmosphere was essentially neutrally stratified two hours after the front had passed. The remaining circulation was apparently maintained by a cooling and heating couplet, the cooling from the evaporation of cloud tops into the drier air aloft and the heating being the result of the adiabatic ascent of moist air. In many ways this system resembled the one modelled by Brown (1979).

The above discussion has outlined the highlights of the development of our present understanding of sub-synoptic scale structure associated with extratropical cyclones. It seems reasonable to assume that elevated convection (as previously defined) is an element of this structure and with that in mind we can make several points about the reason for doing this work. To date, climatologies of sub-synoptic scale structure specifically associated

with extratropical cyclones have been limited in regional extent due to the use of radar and small-scale raingauge networks. The studies have generally dealt with precipitation and precipitation intensity without specifically identifying precipitation that is accompanied by lightning. The choice of lightning, a routinely reported phenomenon, as an identifier makes possible a comprehensive study without requiring a special project.

CHAPTER 3: CLIMATOLOGICAL SURVEY

3.1 INTRODUCTION

Studies of the spatial and temporal variation of atmospheric phenomena, as well as their specific characteristics, have served as the cornerstone of synoptic meteorology since its infancy. The knowledge of these various features has often led to the development of hypotheses on the structure and physical processes associated with such phenomena. These original ideas have then served to motivate the development and testing of subsequent theories. The bulk of such descriptive meteorology was done during the early part of this century with a gradual shift in recent years towards more theoretical approaches. This shift has not precluded the writing of important fundamental observational papers, such as Sanders and Gyakum (1980) on the 'bomb' or Bonner (1968) on the low-level jet. It is important to continue the use of descriptive meteorology and climatology in motivating theory and not to limit the use of observations to serving merely as examples of an independently derived theory. It is in this light that we have established the seasonal, diurnal, and geographical variation of elevated convection in the United States.

This chapter will be devoted to the presentation of a descriptive climatology of elevated convection associated with extratropical baroclinic systems. There have been many previous climatological studies done on thunderstorms (e.g., Alexander, 1935; Shands, 1948;

Court and Griffiths, 1982) which have undoubtedly included elevated convection in their data sets. To date, no study has distinguished this type of convection as a separate entity, let alone determined a specific climatology. Instead of devoting an entire section to reviewing these general studies, an attempt will be made to incorporate specific parts to support or contrast various conclusions that are being drawn in this chapter.

In this part of the study we will define an elevated thunderstorm as a thunderstorm that occurs on the 'cold' side of an analyzed synoptic-scale surface front, the thunderstorm itself being identified by an inspection of plotted surface hourlies on NMC surface maps. The thunderstorm should have an identifiable 'elevated source' of air above the boundary layer that has more latent instability than the air at the surface. The frontal inversion is then acting as a lower boundary for the convective storm.

This particular study utilized the standard National Weather Service upper-air and surface analyses over a four year period as a data source to collect a large number of individual cases. All surface fronts were accepted without further investigation as being that type analyzed by the National Meteorological Center (NMC).

Section 3.2 describes the details of the data source and the individual selection process. Section 3.3 deals with the geographical, seasonal, and diurnal variations of elevated convection, while section 3.4 presents a summary of the environment with which this type of convection is associated. Section 3.5 illustrates the

associated synoptic types and, finally, a summary of the chapter is presented in section 3.6.

3.2 DATA SOURCE AND SELECTION PROCESS

To collect a large sample of observations of elevated thunderstorms, it was first necessary to design a procedure that was not only successful at selecting the correct observations, but was also feasible to do in a reasonable amount of time. For this purpose, the National Weather Service analyses that are routinely archived at the Massachusetts Institute of Technology were utilized since they were both immediately available and a four-year archive is continually maintained. The maps used were the standard surface analysis, 850-mb constant-pressure analysis and 500-mb constant-pressure analysis for North America. It was necessary to limit the study to 00 GMT and 12 GMT, which correspond to the twice-daily upper-air observations, to avoid interpolation in both space and time in determining the upper-level characteristics. The four-year period that was used in the study ran from September 1978 to August 1982. Table 3.1 summarizes this period and the number of surface maps that were available. The number of maps utilized for each month was approximately the same, with slightly more in March and November and slightly fewer in February and December.

A specific set of criteria was used in the selection of events. These criteria were applied to an observation plotted on a surface

Table 3.1

Year	Jan	Feb	Mar	Apr	May	June	July	Aug	Sep	Oct	Nov	Dec	Total
1978	-	-	-	-	-	-	-	-	46	51	59	44	200
1979	54	47	58	49	59	57	60	56	52	47	55	46	640
1980	54	50	60	44	50	50	46	54	49	55	56	52	620
1981	60	45	57	60	53	51	54	46	53	54	55	51	639
1982	48	54	60	54	56	56	58	58	-	-	-	-	444
Total	216	196	235	207	218	214	218	214	200	207	225	193	2543
% of possible available	87%	87%	95%	86%	88%	89%	88%	86%	83%	83%	94%	78%	87%

Table 3.1. Summary of the available surface maps for the four year period of study. 00 GMT and 12 GMT were used, giving a possible two maps for each day. Monthly and yearly sums are shown as well as the percentage of the total possible.

map, which was reporting a thunderstorm, to determine if the thunderstorm was likely to have originated from an elevated source. These criteria are listed below.

1. The observation had to lie on the cold side of an analyzed front which showed a clear contrast in temperature, dew-point temperature, and wind.

2. The station's wind, temperature, and dew-point temperature had to be similar to the immediately surrounding values.

3. An apparent source of air with higher equivalent potential temperature had to lie on the warm side of the analyzed front.

When interpreting the collected data, we will assume that the air above the frontal surface had previously existed as a surface boundary layer. With this in mind, the third criteria was necessary to ensure that the overriding air had more convective potential than the underlying boundary layer. Some frontal boundaries separating warm, moist air and hot, dry air were found to either have no gradient in θ_e or higher θ_e's on the cooler side.

When an observation was found that met these three criteria the event was recorded and the station's temperature, dew-point temperature, wind direction, and altimeter setting were recorded. A log was kept of the orientation with respect to the associated low center (if one existed) and analyzed front, as well as a simple sketch of the synoptic configuration. The distance, normal to the front, that the thunderstorm was displaced into the cold air was also recorded. If more than one station was reporting a thunderstorm each one was recorded as an individual event. Over the 48 months studied, a total of 1378 events were selected using these criteria.

The next step in the survey was the collection of the corresponding upper-air data for each event. The parameters used were the 850-mb temperature, dew-point temperature, wind speed, and wind direction as well as the 500-mb temperature, wind speed, and wind direction. The 850-mb geopotential height was recorded to allow the calculation of the station pressure. It was necessary to interpolate between soundings to estimate these values for those stations that were not radiosonde stations. An inspection of the wind field gave the qualitative relationship between an event and both the exit/entrance region and cyclonic/anticyclonic shear region of a wind maximum (if one existed). In this chapter a wind maximum will be defined as an identifiably stronger wind ($\geq$ 5 knots on the plotted charts) at one or more stations when compared with the immediately surrounding stations. If the estimated horizontal wind shear was cyclonic (anticyclonic) the event was recorded as being on the cyclonic (anticyclonic) side of the wind maximum. If the flow was estimated to be difluent (confluent) the event was recorded as being in the exit (entrance) region. If the winds over several of the surrounding stations were uniform, no wind maximum was identified and a null case was recorded.

The compiled data were then put into a data file on a PDP-11/44. After the data were entered, further requirements were placed on the collected events. A filtering program was run that eliminated all events where 1) the calculated surface pressure was less than 860 mb so that the 850-mb air was the surface air or 2) the surface air, when

lifted pseudo-adiabatically to 500 mb, was the same temperature or warmer than the 850-mb air lifted to 500 mb. A total of 285 cases were eliminated. Most of those eliminated were from June, July, and August (164); most likely the result of poorly defined and/or analyzed fronts. In the remaining nine months, 18 cases were thrown out because the surface pressure was too low and 103 cases were eliminated due to no change or a decrease in the potential temperature from the surface to 850 mb.

It is possible that cases of elevated convection that occurred in mountainous regions may have been wrongly removed by the criteria requiring horizontal homogeneity in temperature and wind with surrounding stations. Also, those cases where the surface elevation was near or above the 850-mb level would have been eliminated. The effect of these biases will be discussed in the next section.

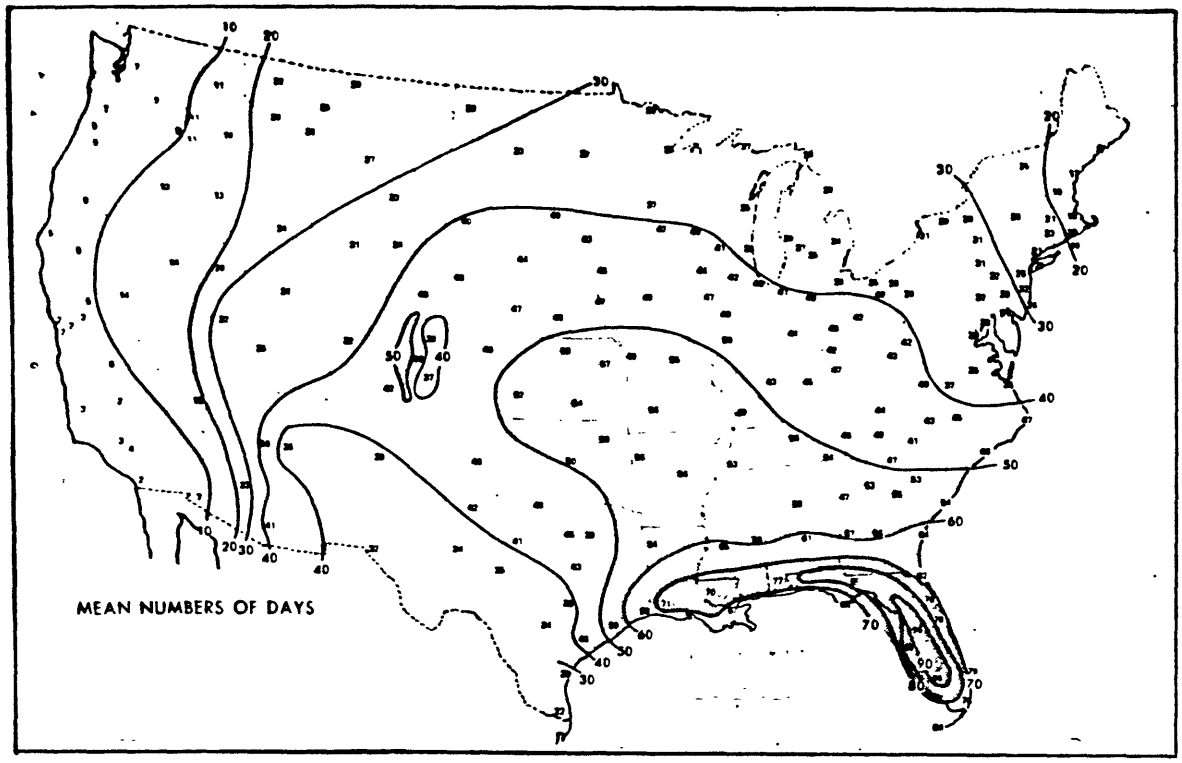
The final data set contains 1093 cases recorded over the four year period. It is felt that this set of observations consists only of cases where the 'classical' concept of cumulus convection was not occurring. The instability was evidently taking place above the frontal inversion, with vertical velocities that were strong enough to generate the observed lightning and precipitation. This filtered data set was then used to construct the climatology of elevated convection presented here. It was possible to look not only at the geographical and seasonal variations but also at some of the thermodynamic and dynamic characteristics of the observed environment. The following sections will summarize these results.

3.3 GEOGRAPHICAL, SEASONAL, AND DIURNAL VARIATIONS

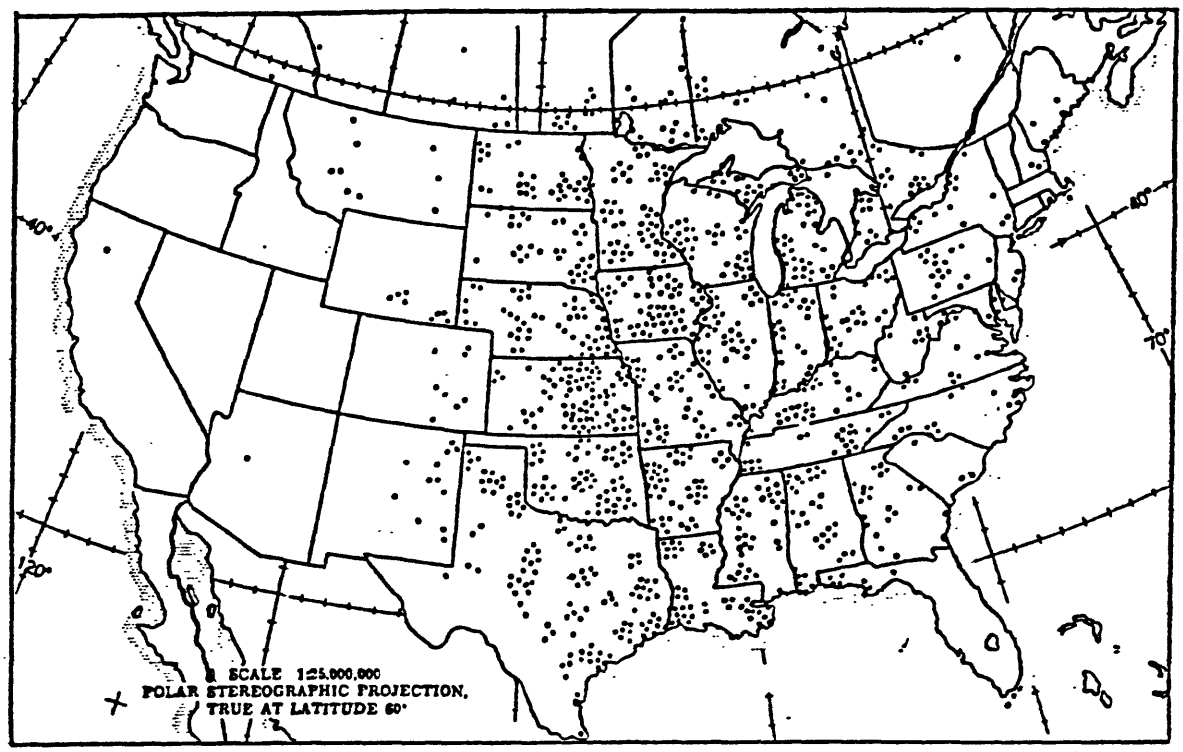
GEOGRAPHICAL AND SEASONAL

Figure 3.1(a) shows the mean annual number of days with thunderstorms of any type and Figure 3.1(b) shows the geographical distribution of the total sample of 1093 cases in this study. The apparent localized clustering of points is a result of multiple observations for a single station. The greatest concentration of events extends from the central Gulf Coast northward to the upper Mississippi and Ohio River Valleys, with the western edge running north-south along the eastern slope of the Rockies. The maximum in the distribution for elevated thunderstorms extends much farther north than that for all thunderstorms. The sharp cutoff in the frequency distribution over south-western Texas is positioned along the southward extending axis of the climatologically preferred region of cyclogenesis in eastern Colorado. This is apparently the western limit of low-level moisture penetration from the Gulf of Mexico. West of this axis the low-level circulation associated with developing cyclones would be unfavorable for transporting moisture from the Gulf of Mexico into the synoptic system. A similar cutoff is observed in the total distribution of thunderstorms.

The region of high concentration shows a gradual decrease in events towards the East Coast. This gradient is only evident over the



(a)



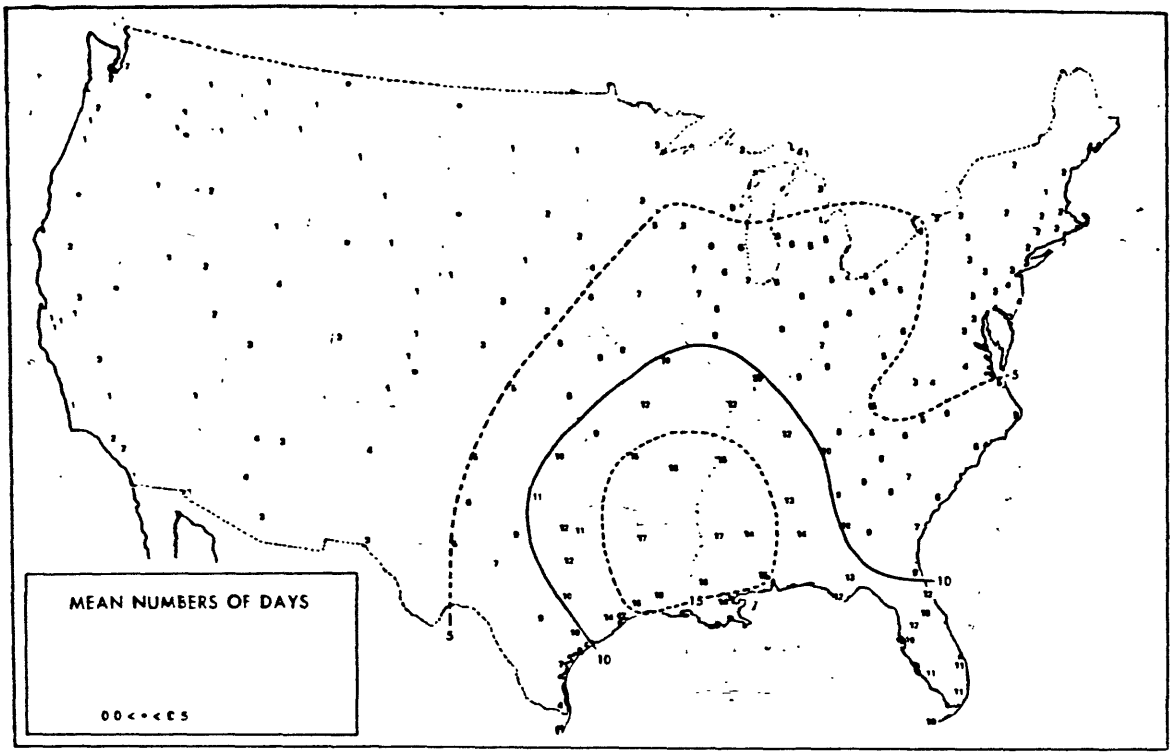
(b)

Figure 3.1(a). The mean annual number of days with thunderstorms, by station, 1951-1975 (Court and Griffiths, 1982). (b). The distribution of the 1093 cases of elevated convection identified over the four year period from September, 1978 to August, 1982.

Northeast in the distribution for all thunderstorms, which shows a north to south gradient from Virginia to a maximum in Florida. The most striking contrast between the two distributions is over the Florida Peninsula where no elevated thunderstorms were observed.

Figure 3.2(a) shows the observed distribution of the mean number of thunderstorm days for the months October through March compiled by Court and Griffiths (1982) for the period 1951-1975, and Figure 3.2(b) shows the corresponding distribution of the events observed in this study. The distribution of elevated thunderstorms compares favorably with the distribution of thunderstorm days. Such characteristics as the strong gradient of events across Texas and the central Gulf coast maximum are clearly present in both distributions. The near absence of observed elevated thunderstorms over the western United States in the present study, although possibly an artifact of the effect of irregular and mountainous terrain on the selection process, seems to be well supported by the low number of mean thunderstorm days. Once again the largest contrast between the distributions is over the Florida Peninsula where the absence of elevated thunderstorms suggests the persistence of convection rooted in the boundary layer throughout the year.

To get a better indication of what fraction of observed winter-season thunderstorms are of the elevated type, a projection can be made of the number of events expected from a given sample of observations using the frequency percentage of occurrence of thunder. Values of the observed frequency of thunder for the winter-season



(a)

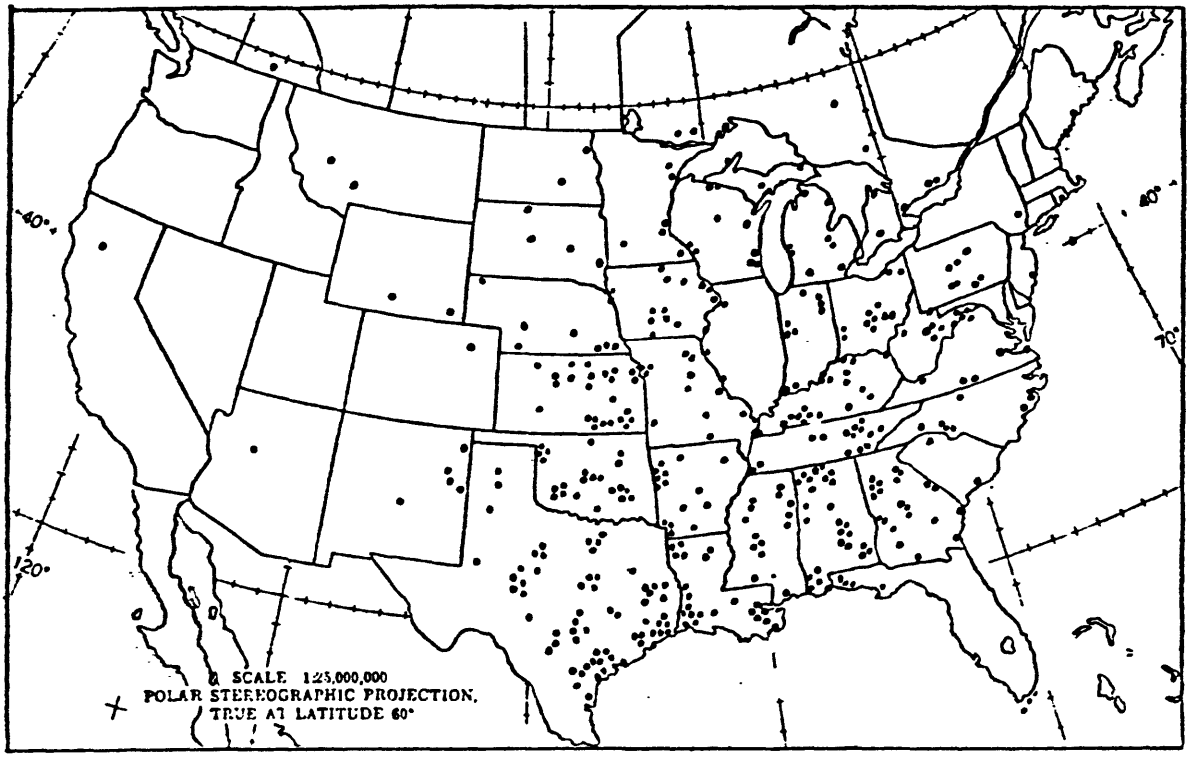
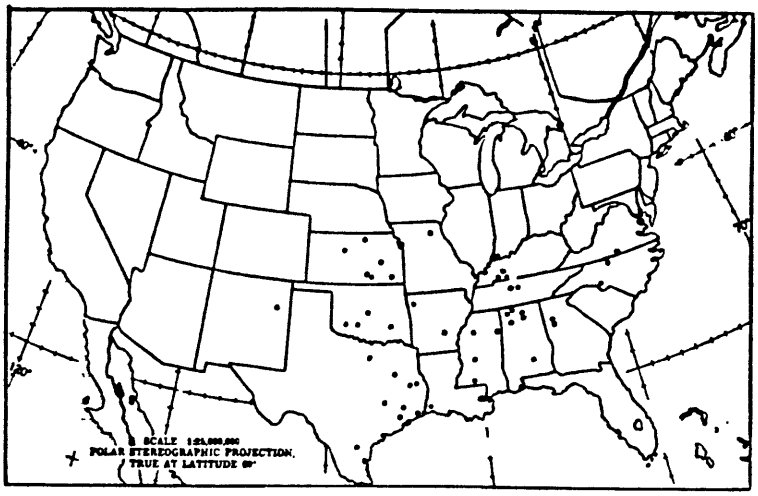


Figure 3.2. (a) The mean number of days with thunderstorms during winter, by station, for the period October through March, 1951-1975. (after Court and Griffiths, 1982). (b) The location of elevated thunderstorm cases in this study for the period October through March, 1978-1982.

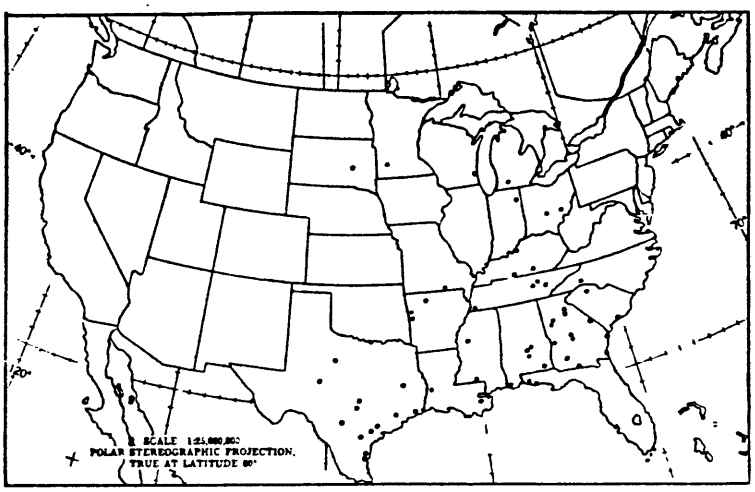
(defined as the months December through February) were obtained from the Airway Meteorological Atlas of the United States (United States Weather Bureau, 1946) and represented the percent fraction of all hourlies for that individual station that included a report of thunder. The maximum value was 0.5% for Houston, Texas. The average number of observations used for each station was 59,355 with a range in sample size of from 17,544 for Danville, Virginia to 85,133 for Chicago, Illinois. A group of 35 stations was selected which contained all those stations east of the Rockies that had a frequency percentage greater than or equal to 0.1%. The group did not include stations in Florida. Adjusting the present study for missing maps, a total of 605 maps over the four winter seasons were used giving a total of 21,175 observations from the 35 stations. Utilizing the sum of the individual percentages the projected total number of observations reporting thunder for the 35 stations was 40 while the observed total was 33 (82.5% of the projected total). The observed value is most likely low since it has been assumed that all 35 stations were plotted on each of the maps inspected, not allowing for station reports that were missing. This result is strongly suggestive that nearly all winter-season thunderstorms over the United States east of the Rockies, with the exception of the Florida Peninsula, are of the elevated type.

Figure 3.3(a-l) shows the four-year monthly spatial distributions for the study period. The frequency distributions will be presented in the next part, however, some understanding of them may be obtained

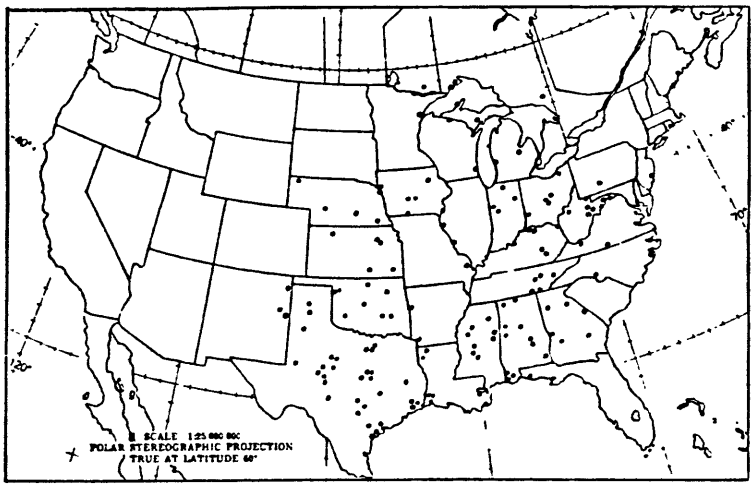
Figure 3.3(a-l). Monthly composites of the distribution of elevated thunderstorm events for the four year period from September, 1978 to August, 1982.



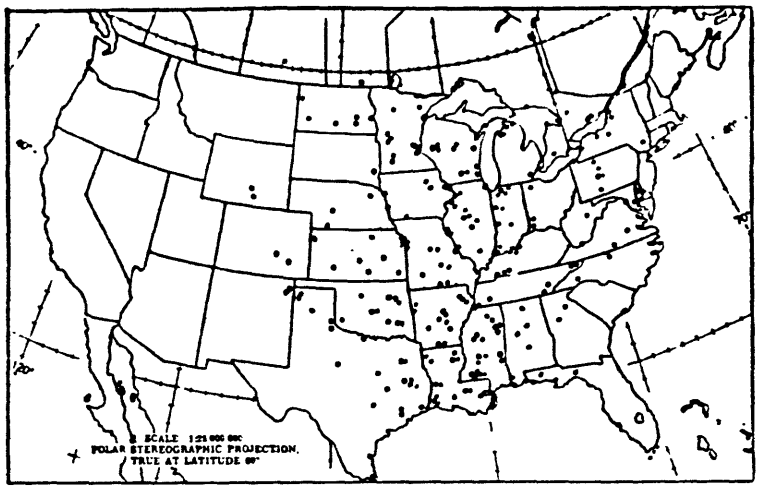
(a) January



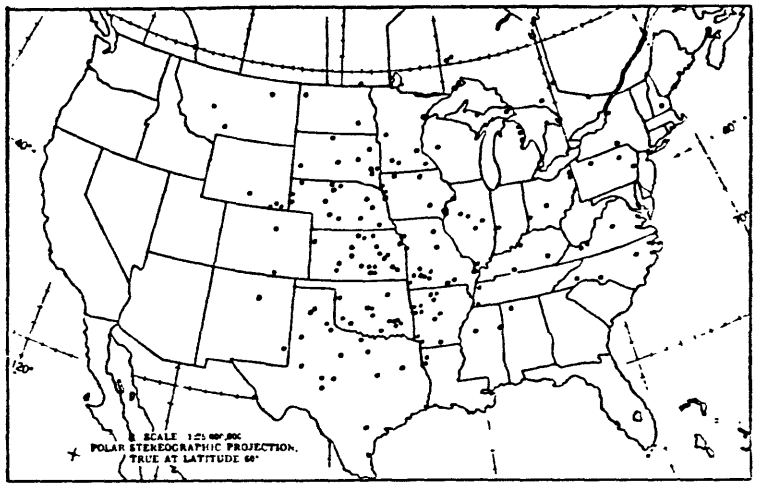
(b) February



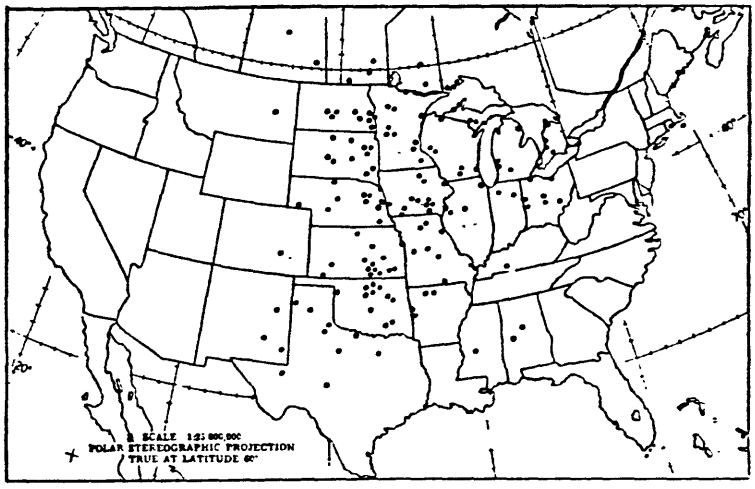
(c) March



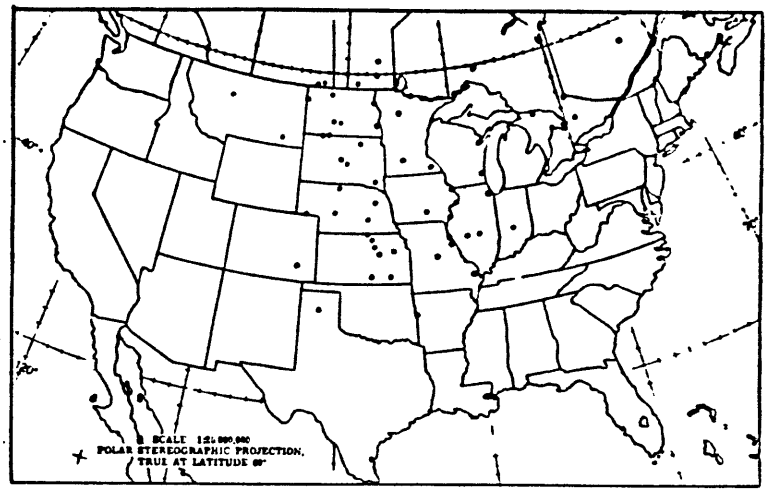
(d) April



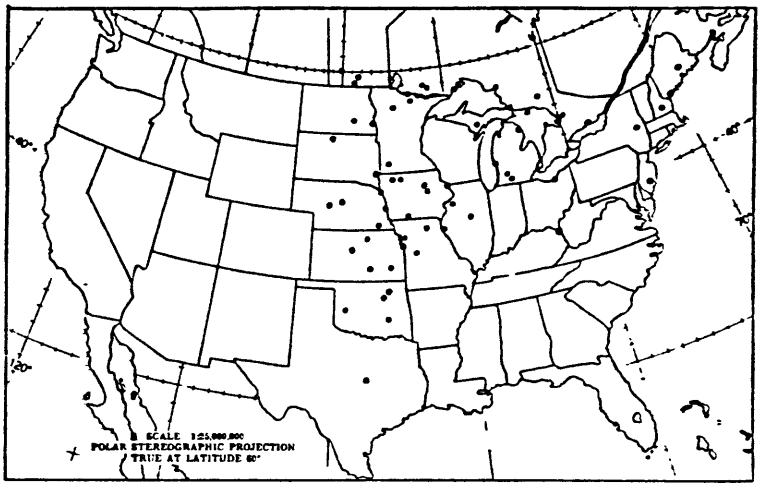
(e) May



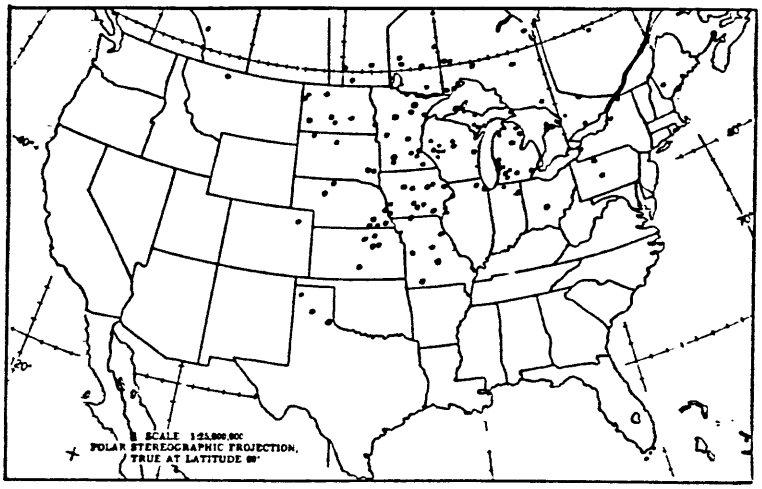
(f) June



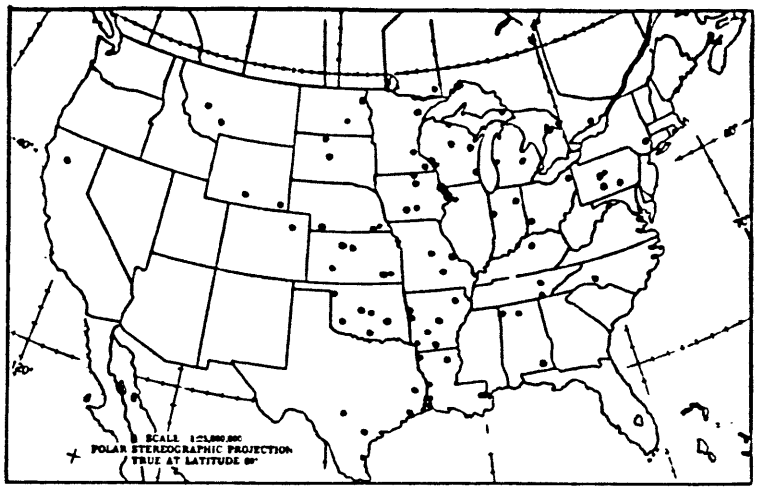
(g) July



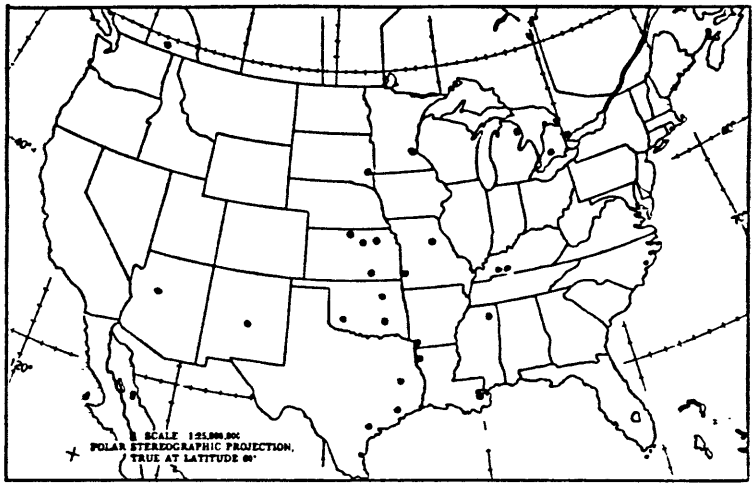
(h) August



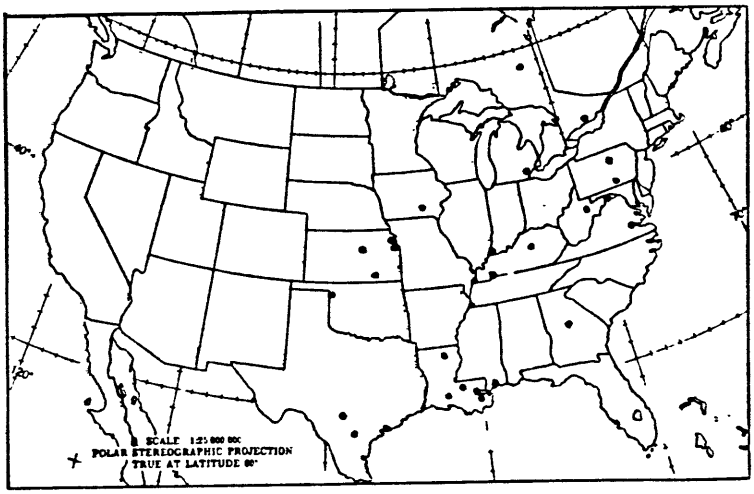
(i) September



(j) October



(k) November



(l) December

from figure 3.3 as all events are plotted. January and February show a maximum of occurrences over the south central United States. The January events were limited to the Gulf Coast with the exception of one year (1982) that accounted for all of the northern events for that month. This concentration of events along the Gulf Coast would appear to be tied to the development of the southern storm track (see Figure 3.4) that is able to tap the maritime air from over the warm Gulf of Mexico. March shows a continuation of events along the Gulf Coast with additional occurrences well to the north. As with January, part of the northwest expansion is explained by a rather anomalous year (1979).

April shows a large northward expansion of the maximum concentration while retaining the high frequency along the Gulf Coast. This is correlated with the increase in solar heating of the surface layer at a time when extratropical cyclones are still frequent and widespread over the United States. The month of May shows a shrinkage and a northwestward shift of the center to the central Great Plains. A very striking change from April to May is the rapid decline of events on the Gulf Coast. This is probably the result of two changes taking place; first, fewer synoptic systems travel across the Gulf Coast in May than in April. Second, and perhaps more important, is the relaxation of the temperature contrast between the land and the water. A sharp land to sea temperature contrast frequently contributes, through diabatic effects, to the in situ development of a front along the coast. In the absence of this local effect, the

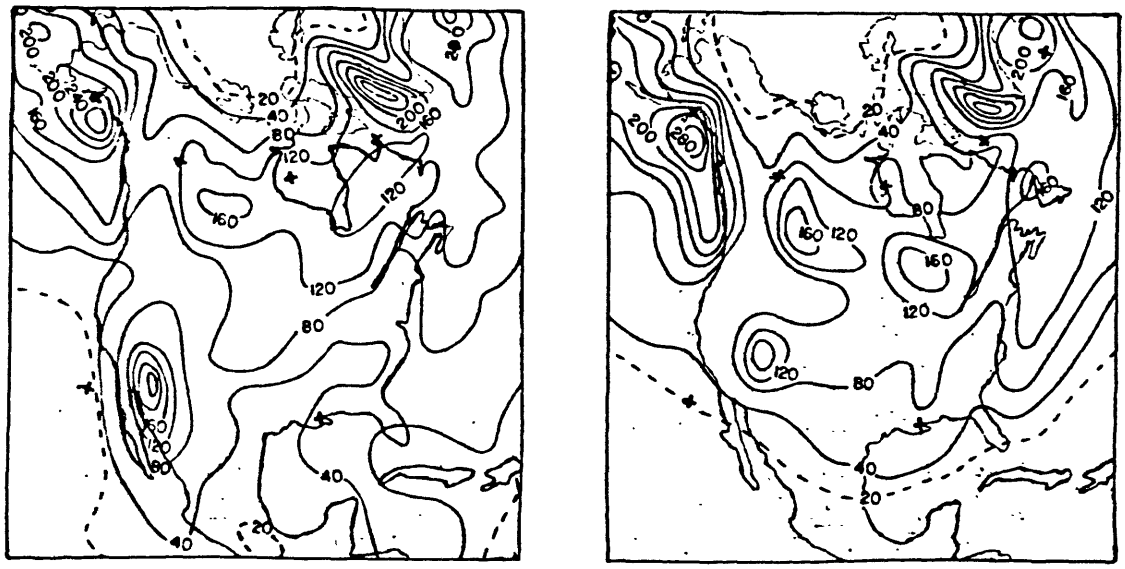


Figure 3.4. The number of lows per normalized 5° X 5° tessera on 1230 GMT sea-level pressure maps. (a) September through November, 1899-1939 (b) December through February, 1899-1939. (U.S.W.B., 1957)

occurrence of overrunning along the coast decreases dramatically (Hsu, 1981) resulting in the decrease of elevated convection.

The northwestward shift continues with the month of June. In July and August the distributions become more scattered with a decrease in events over Texas and Oklahoma from those observed in June.

In September the maximum concentration is over the northern Great Plains with very little southern extent. This northern maximum is tied to the early season storm track across southern Canada which limits the southern advance of cold air to the northern tier of states. The absence of cold air would appear to be the limiting factor since there is not a lack of latent instability over much of the United States as is evidenced by the presence of ground-based convection throughout the summer.

The September maximum concentration is what should be expected if compared with the cyclone frequency distribution for the fall (Figure 3.4(a)) which shows a minimum in the number of lows extending from the western Gulf Coast east-northeastward across the United States, explaining the limited southern extent.

October shows a dispersion in the distribution to cover the full north to south extent of the Mississippi basin. This dispersion continues, and in November and December the events become widely scattered showing no preferred region. Unfortunately, with so few cases it is not possible to determine which are anomalous events and which represent consistent changes in the annual distribution. Figure

3.4 shows more than a doubling of the number of lows over the lower Mississippi River from fall to winter and it is this increase that accounts for the development of the concentration already discussed for January.

Figure 3.5(a) shows the frequency distribution of all events by month. From a minimum in November there is a gradual recovery through the month of February associated with the increased frequency of lows along the Gulf Coast. There is then a rapid increase to the primary peak in the distribution in April. This April peak is associated with strong instability (the result of the upper atmosphere being cold and the surface boundary layer being rapidly heated prior to being lifted over the frontal surface), and the frequent advances of cold Canadian air southward. These conditions combine to create an optimum situation for elevated convection. In May the frequency drops to slightly higher than that for March most likely due to a decline in synoptic systems and frontal strength. The high frequency of events continues into June before a rapid decrease to a relative minimum in July. This minimum is the result of a decrease in the number of extratropical cyclones over the United States as well as a general decrease in the thermodynamic instability (Johns, 1982). The frequency then increases to a secondary maximum in September, as the number of lows increases, before rapidly dropping to the minimum in November. This minimum is most likely the result of a combination of the low sun angle (i.e., a minimum in surface heating) and the absence of cold surface air early in the winter season.

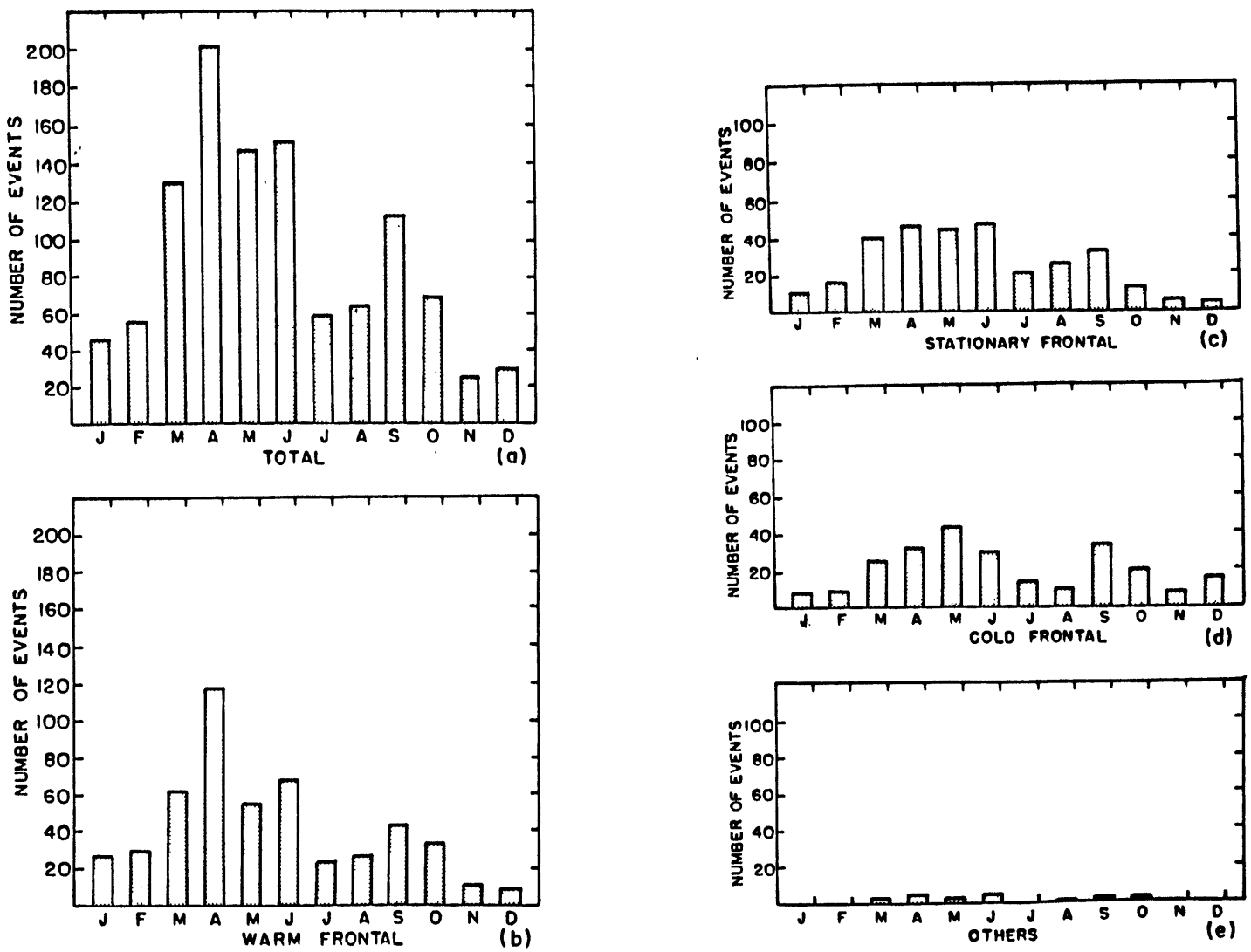


Figure 3.5. The frequency distributions, by month, of the elevated thunderstorm events for a) the total sample, b) the warm frontal cases, c) the stationary frontal cases, d) the cold frontal cases and e) others (see text for explanation).

Thus, the annual variation of elevated convection is bimodal with a primary maximum in April and a secondary maximum in September. The distribution is a result of the combination of a winter maximum in extratropical cyclones and a late spring maximum in thermodynamic instability.

Further insights are possible if the population of events is divided according to the particular type of front with which they are associated. Figures 3.5(b-d) show the monthly distributions for warm, stationary, and cold fronts, respectively. Figure 3.5(e) shows the distribution for those events where the report is positioned in the occluded part of the storm with no clear relationship with either the warm or cold front ('others').

During the fall, September through November, the distributions for the three frontal types show a similar decrease. The warm-frontal storms show a sharp increase in January, from the minimum in December, which is reflected in the concentration of events along the Gulf Coast (see Figure 3.3(a)). The rest of the warm-frontal distribution is very similar to the distribution for the entire sample.

The stationary-frontal distribution shows an interesting flattening from the spring through June. This is likely the result of an increase in analyzed stationary fronts as the storm track migrates northward, increasing the number of trailing fronts over the United States.

The distribution for cold-frontal elevated convection shows a slightly different characteristic. There is a slight peak in December

which is not easily explained on physical grounds but is possibly the result of a few anomalous events that have combined to show a detectable peak in a rather small sample size. The cold-frontal type does show a consistent increase from January through the month of May. This type does not show the same decrease in events from April to May as with the other two frontal types. The summer minimum is also shifted by one month to August.

Figures 3.6(a-c) show the percent occurrence of each frontal type by month. Warm-frontal cases make up nearly half of the total sample, with stationary-frontal and cold-frontal cases each accounting for one quarter of the events. The observed monthly variations show an increased percentage of warm-frontal cases from January through April. This is also the period with a rapid increase in the number of events and is presumably associated with the increased insolation and continued strong frontal contrasts. The fraction of cold-frontal cases is larger during the fall months and then again in May. During the summer months, when the westerlies are generally weaker and displaced farther north, a higher percentage of cases occur with stationary fronts.

INTERANNUAL VARIATION

Owing to the dependence of the investigated elevated convection on the existence of a synoptic-scale front, a correlation would be expected between the region of convection and the large-scale circulation pattern if the fronts are typically associated with

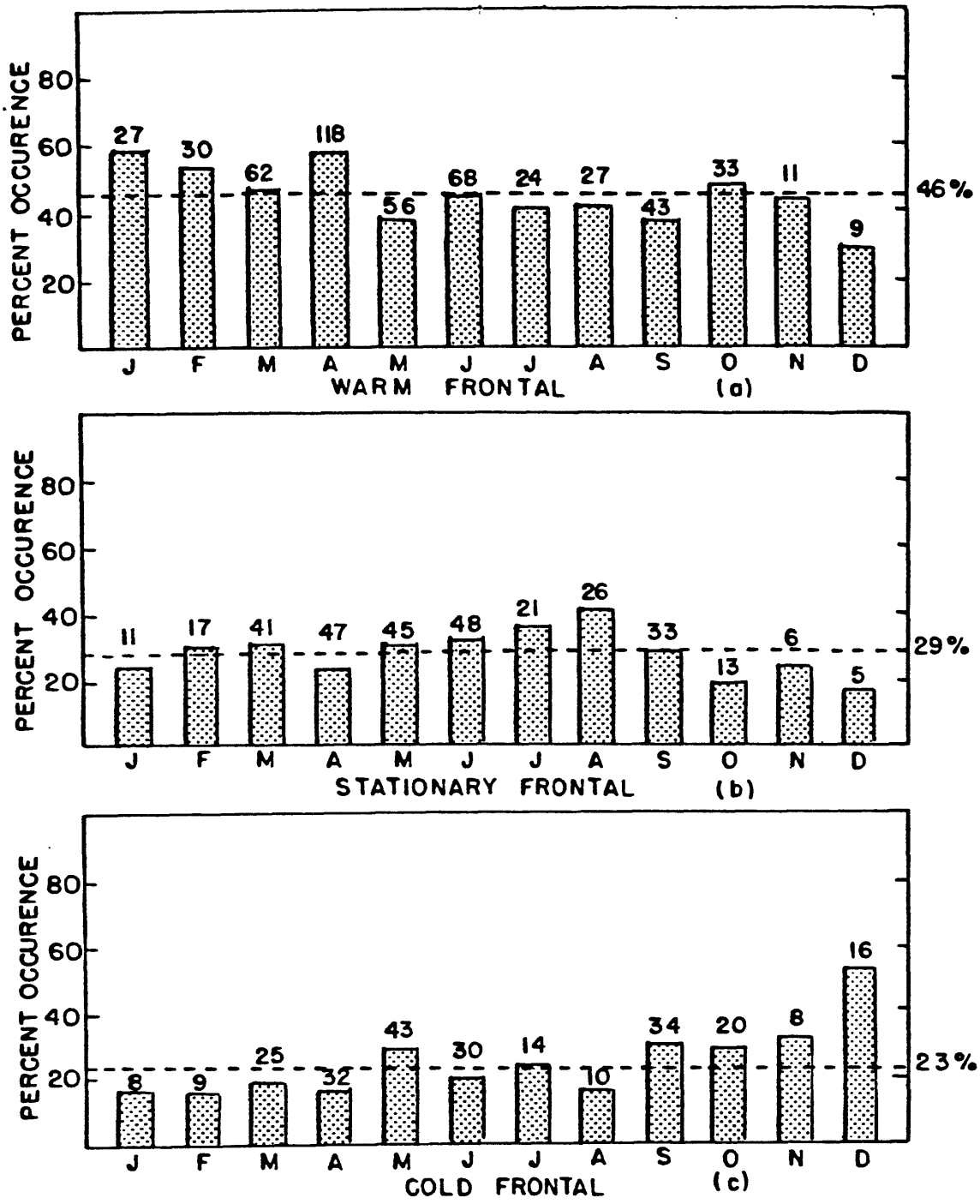
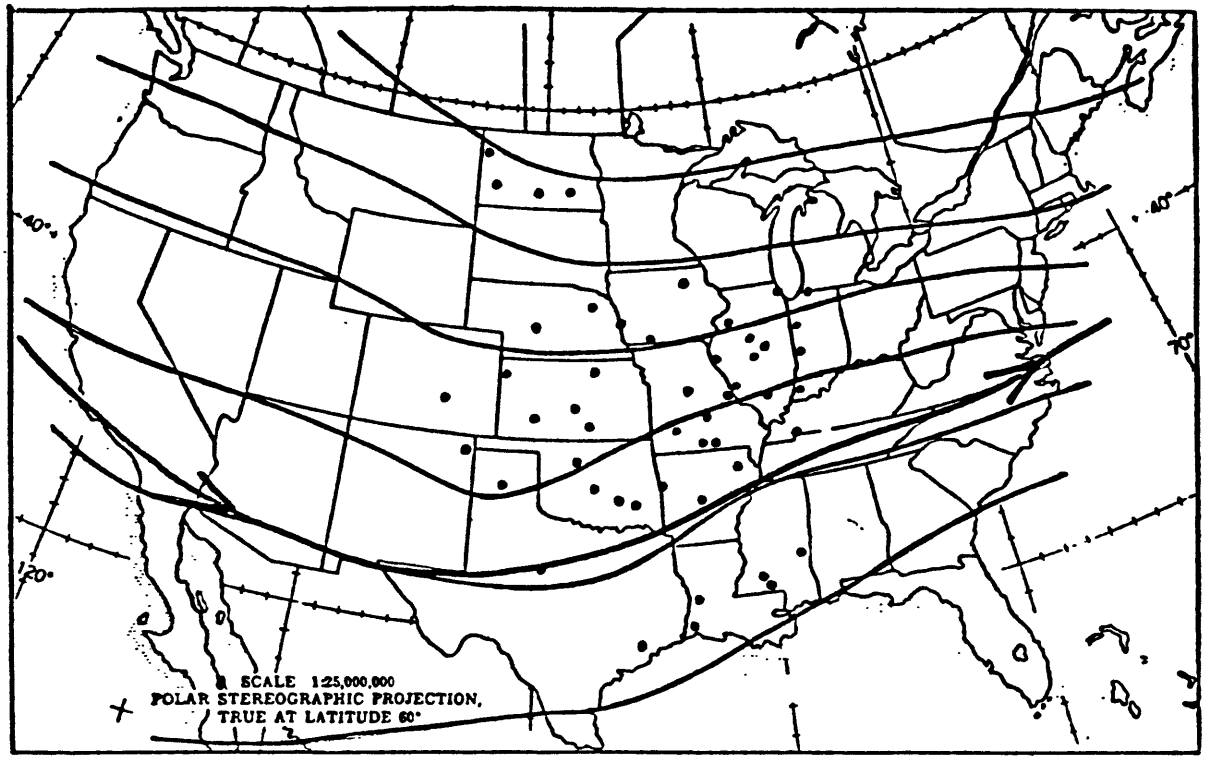


Figure 3.6. The monthly fractional percentage of the total sample for a) warm fronts, b) stationary fronts, and c) cold fronts. The annual percentage is shown by the dotted horizontal line with the sample size above each bar.

mid-latitude baroclinic systems. It has already been pointed out in the last section how some of the distributions were affected by a large year-to-year variation. This interannual variation is easily seen in Figures 3.7 (a & b) which contrast April, 1979 with April, 1980. The elevated convection occurs downstream from the mean trough position and generally on the cyclonic side of the mean 700-mb jet position. This clear dependence is suggestive that elevated convective regimes occur and are determined by fluctuations in the large-scale circulation.

DIURNAL VARIATION

The diurnal variation of convection has been frequently discussed. Unfortunately, most of the previous work has been focused on identifying the diurnal pattern of convection over the summer, the period of greatest activity. With the relatively small sample sizes for winter-season convection the various attempts at identifying a diurnal oscillation have not been conclusive. Shands (1948), in discussing the probability of thunderstorms beginning during each quarter day (6 hour groupings) during the winter season (Dec.-Feb.), remarked that "there is a tendency toward the equalization of probabilities in all four periods of the day". His data suggested an early morning (06-12 LST) minimum in thunderstorm occurrence, particularly along the central Gulf Coast. He attributed this to the increased stability of the boundary layer in the morning. Although he



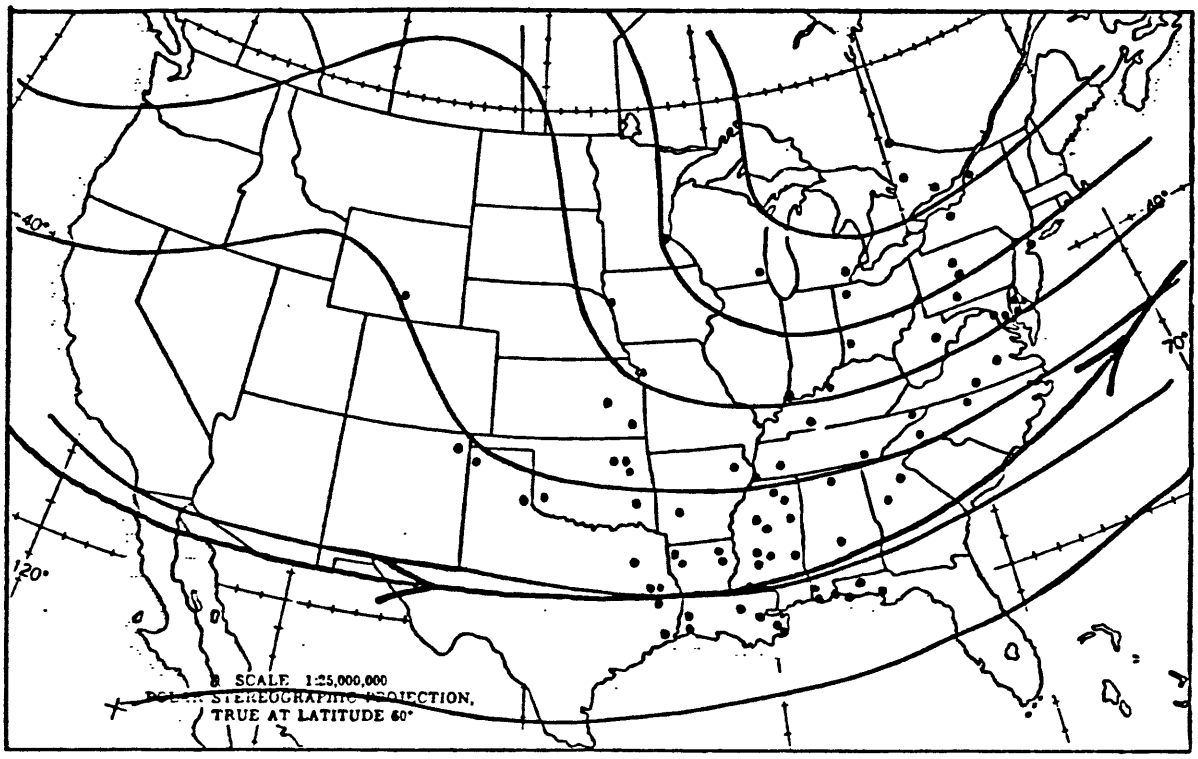


Figure 3.7. The distribution of events for a) April, 1979 and b) April, 1980. Solid lines represent the 700-mb mean height field, with the mean jet position marked by a heavy arrowed line.

suggested a corresponding afternoon maximum, it was not evident in his data. The highest probability at a single station (Vicksburg, 3.3%) did occur between 12-18 LST, but the pattern was not consistent for all stations.

The Airway Meteorological Atlas of the United States (United States Weather Bureau, 1946) shows an evening maximum and a mid-day minimum for Little Rock, Arkansas, Shreveport, and New Orleans, Louisiana for the month of January (See Figure 3.8). Contrarily, the pattern for Houston, also shown in Figure 3.8, is opposite in phase.

Wallace (1975), grouping neighboring stations to get larger sample sizes, concluded that a "substantial" diurnal cycle in winter-season convective activity (Dec.-Feb.) exists and has a nocturnal maximum. He notes that Florida and southern Georgia, displaying a late afternoon (≈18 LST) maximum, are exceptions. This is in agreement with the previously suggested persistence of insolational thunderstorms in this region throughout the winter. Figure 3.9(a) (Wallace, 1975) shows a vectorial display of the diurnal cycle in thunderstorm frequency during the winter season. The region corresponding to the maximum frequency of elevated convection for the winter season (see Figure 3.2(b)) shows a consistent midnight maximum. Figure 3.9(b) shows Wallace's diurnal cycle for summer season thunderstorms. The contrast between the two seasons is striking. A strong, late afternoon maximum prevails over most of the country in the summer, intimately associated with the maximum in insolational heating. The one exception is the area with a nocturnal

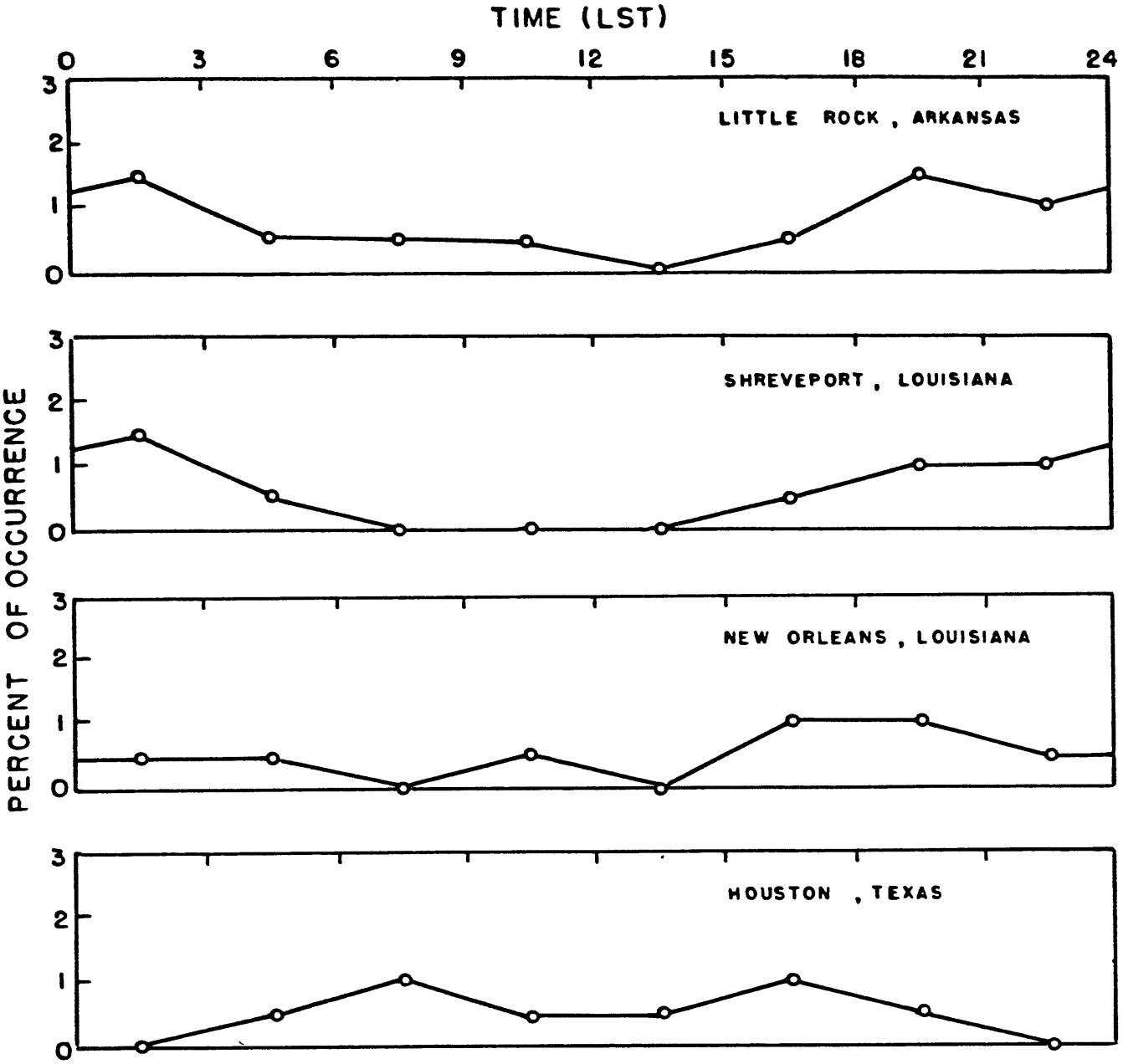


Figure 3.8. The percent occurrence of thunder in hourly airway surface observations for the month of January, for three hour periods (the station names are shown on each plot). (U.S.W.B., 1946)

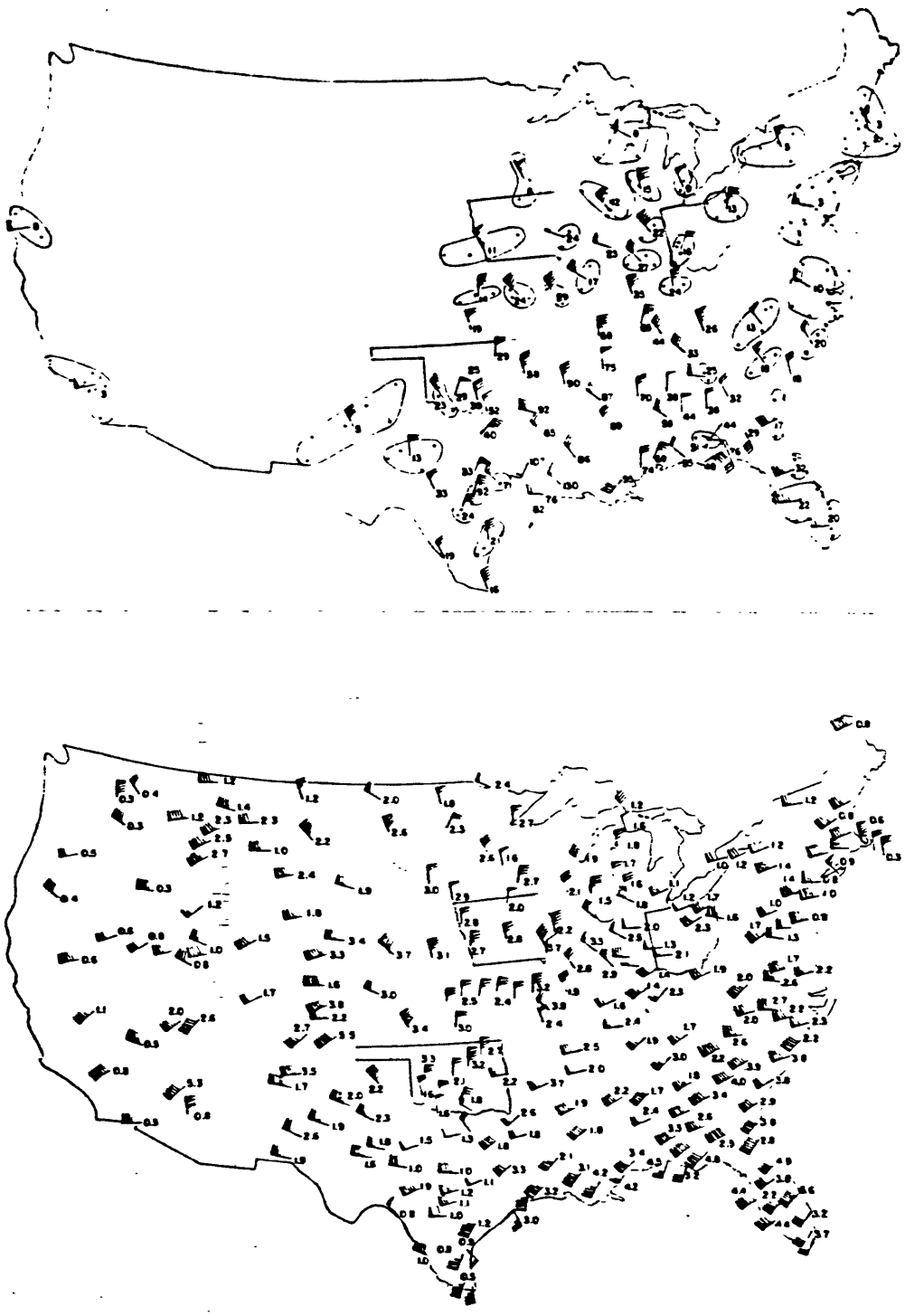


Figure 3.9. (a) The diurnal cycle in thunderstorm frequency during the winter season (December-February). The phase is indicated by the orientation of the vector. A vector pointing from the north indicates a midnight maximum (LT), one pointing from the east is a 0600 LT maximum, and so on. Barbs indicate 'normalized amplitude' of the diurnal cycle, defined as the amplitude of the first harmonic divided by the 24-h mean. Each half barb represents 5%, each full barb 10%, and each flag 50%. The plotted numbers are the 24-h mean frequencies expressed in hundredths of percent of hours with thunderstorms. Dots represent stations that were grouped together. (b) The diurnal cycle in thunderstorm frequency during the summer season (June-August). Plotting convention the same as for (a) except that mean frequencies are expressed in percents. (Wallace, 1975)

maximum over the central plains states typically associated with a maximum in low level jet occurrences. Clearly, winter-season thunderstorms display characteristics that suggest they are separate phenomena and not merely the minimum in an annual cycle of convection characterized by summer-season convection.

With only twice-daily observations being used in this study, it is not possible to independently examine the diurnal cycle. The total sample of 1093 cases consists of 458 events at 00 GMT and 635 events at 12 GMT. With 00 GMT, the center of Shand's suggested maximum, corresponding to 18 LST in the region of maximum occurrence, it is surprising to see that it contains the smallest sample. The 12 GMT maximum is in better agreement with Wallace's result suggesting a late night or early morning maximum.

Dexter (1944), in discussing warm-frontal precipitation and thunderstorms, differentiated between the development of potential instability and the realization of latent instability. He felt that a late evening and early morning maximum could be explained by the time lag between the time the surface boundary layer in the warm sector is heated and moistened, and the time when the instability is actually released over the warm-frontal surface. Dexter's impression was that this delay between development and realization would be between six and ten hours. He also felt that when the boundary-layer air starts to cool in the evening, resulting in a lowering of the lifted condensation level (LCL), the thunderstorms would occur closer to the frontal boundary. It would not seem that this argument is valid,

since, although the LCL is lowered as the boundary layer cools, the level of free convection (LFC) increases and would require more lift before the instability is realized. Further cooling of the air during the night would eventually destroy the instability and result in a late morning and early afternoon minimum.

In the present study there does not appear to be any support for Dexter's suggested fluctuation in the positioning of the convection with respect to the front. Out of a total sample size of 1025 complete observations, 703 events had an 850-mb wind with a cross-frontal component towards the cold air. Using the cross-frontal component of the 850-mb wind and the measured distance of the thunderstorm from the frontal boundary it is possible to estimate a travel time for the air above the frontal surface. The median travel time for the 703 events was 7.7 hours. The medians for the individual groups for 00 GMT and 12 GMT were different by only 0.4 hours with the 00 GMT median the shortest. The median is used here to eliminate the effect of unrealistically large values of travel time for very small cross-frontal angles. The average distances were 2.2 and 2.3 degrees of latitude for 00 GMT and 12 GMT, respectively. The cross-frontal angles were also essentially the same with 51 degrees for 00 GMT and 53 degrees for 12 GMT. (Dexter (1944) had suggested that the cross-frontal angle would be greater at night.) The median travel time does, however, fall within Dexter's suggested range of 6-10 hours.

Wallace (1975) felt that a nighttime increase in the static

stability of the boundary layer would create a decrease in the frictional drag and allow for higher wind speeds and thus more frontal lifting. In this study, neither the total wind speed nor the cross-frontal component show this diurnal fluctuation. The average 850-mb wind speed for the 703 events was 25 kts. and 23 kts. for 00 GMT and 12 GMT, respectively. The cross-frontal components averaged 18 kts. at 00 GMT and 17 kts. at 12 GMT. Contrary to Wallace's suggestion, the difference is towards slightly faster wind speeds in the evening, although the contrast is so small that it is most likely insignificant.

Figure 3.10 breaks the sample down into histograms for the total group and individual groups according to observation time (00 GMT or 12 GMT). For eight out of the twelve months (Figure 3.10(a)) there were more events recorded at 12 GMT than at 00 GMT. The months for which this was not true were January, March, September, and December. An inspection of Figure 3.10(d) shows that for seven of the months there were more events associated with cold fronts at 00 GMT than at 12 GMT. Recall that, for September through December and in March, the percent frequency of events associated with cold fronts was higher than for the total sample. Also, for each of these months more than twice as many events associated with cold fronts occurred at 00 GMT than 12 GMT. For the twelve month sample of those cases occurring with cold fronts, 140 events were at 00 GMT while only 109 events were at 12 GMT. It is easy to see from Figure 3.9(b) that far more events were associated with warm fronts at 12 GMT (308) than at 00 GMT

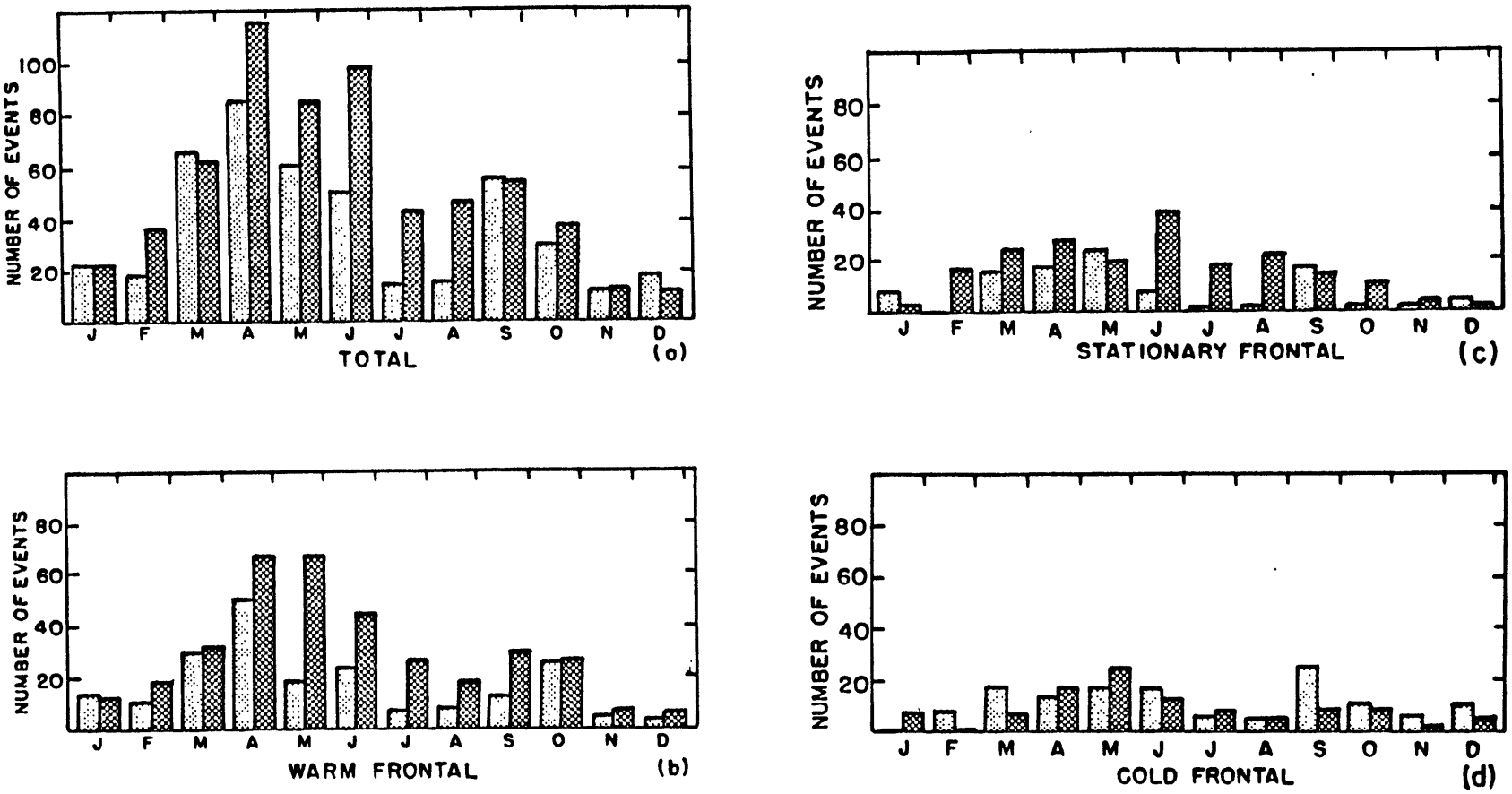


Figure 3.10. Histogram of the number of events observed at 00 GMT (light shading) and 12 GMT (dark shading) for a) total sample, b) warm fronts, c) stationary fronts, and d) cold fronts.

(200). Similarly, for those associated with stationary fronts 207 were at 12 GMT and 106 at 00 GMT.

It seems that the most significant conclusion to be drawn is that the diurnal cycle of winter-season convection, and thus elevated convection, has a clear dependence on frontal type. The convection associated with warm and stationary fronts is more frequent at 12 GMT while that associated with cold fronts is more common at 00 GMT. A clear insolational dependence may be obscured by a range in travel times, of the type suggested by Dexter, affecting the delay in the release of the instability. The scenario is then that the surface boundary layer air reaches a maximum in internal energy during the afternoon prior to being transported over the front. This energy is subsequently released over the frontal surface as elevated convection delayed by the travel time of the source air.

3.4 DYNAMIC AND THERMODYNAMIC ENVIRONMENT

DYNAMIC ENVIRONMENT

Figure 3.11 shows the relative position of the 845 cases with identifiable low centers. The greatest frequency of elevated convection occurs in a sector that runs from just north of the low center to the east-northeast. The region extends to more than five degrees of latitude from the low center before a sharp cutoff occurs farther to the east at what is likely a reflection of the surface

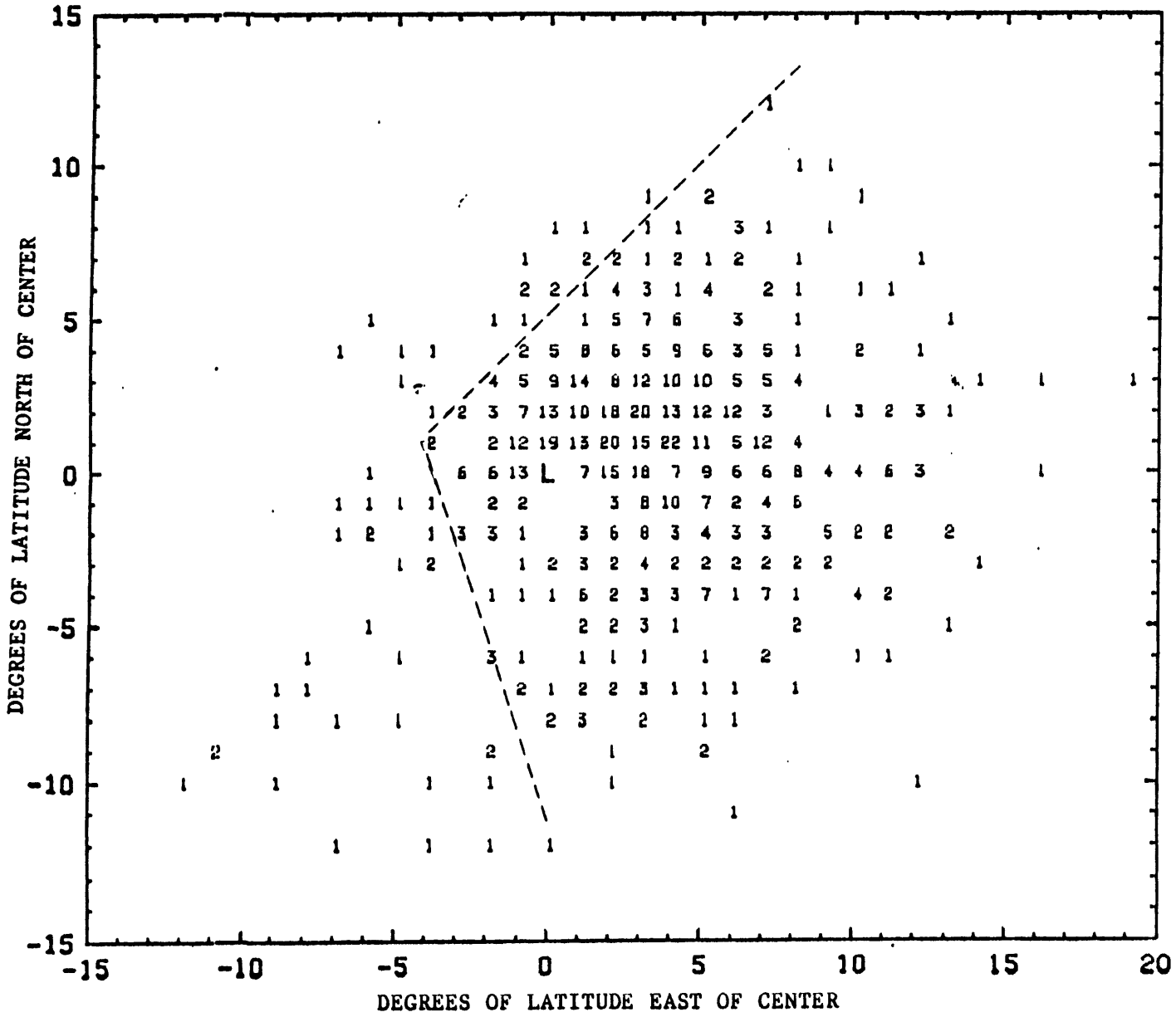


Figure 3.11. A composite of the number of events that were recorded at a given position with respect to the associated surface low-pressure center. The dashed lines delineate the region of maximum occurrence. The degree of latitude (60 nm, 110.8 km) is used as the unit of distance.

ridge line. There is an extension of this area of maximum frequency by several degrees to the south at about 4 or 5 degrees east of the low center. Sanders (1971), using a diagnostic quasi-geostrophic model, showed that the maximum destabilization associated with a developing cyclone occurred to the east-northeast of the surface low-pressure center (≈1/4 L) and was the result of warming by low-level temperature advection and cooling in the mid-troposphere through adiabatic cooling. In this study the observed maximum in events agrees very well with this region of large-scale destabilization.

A sharp decrease in occurrences is evident along a northeast to southwest line to the north of the surface center, which then turns south-southeasterly northwest of the low. This line forms the western edge of the area of frequent occurrence of elevated convection. These cutoffs in the frequency are strongly related to features of the upper-level flow.

A composite of the mean wind direction at each location (Figure 3.12) shows the flow pattern for the surface, 850 mb, and 500 mb. From the surface composite (Figure 3.12(c)) it can be seen that the greatest frequency of events occurs with an east or northeast surface wind. The dashed lines from Figure 3.11, which outline the area of greatest activity, have been added to Figure 3.12.

The 850-mb composite shows an uninterrupted southerly flow from the region south of the surface center to the area of maximum frequency of thunderstorms. This flow illustrates the position of a

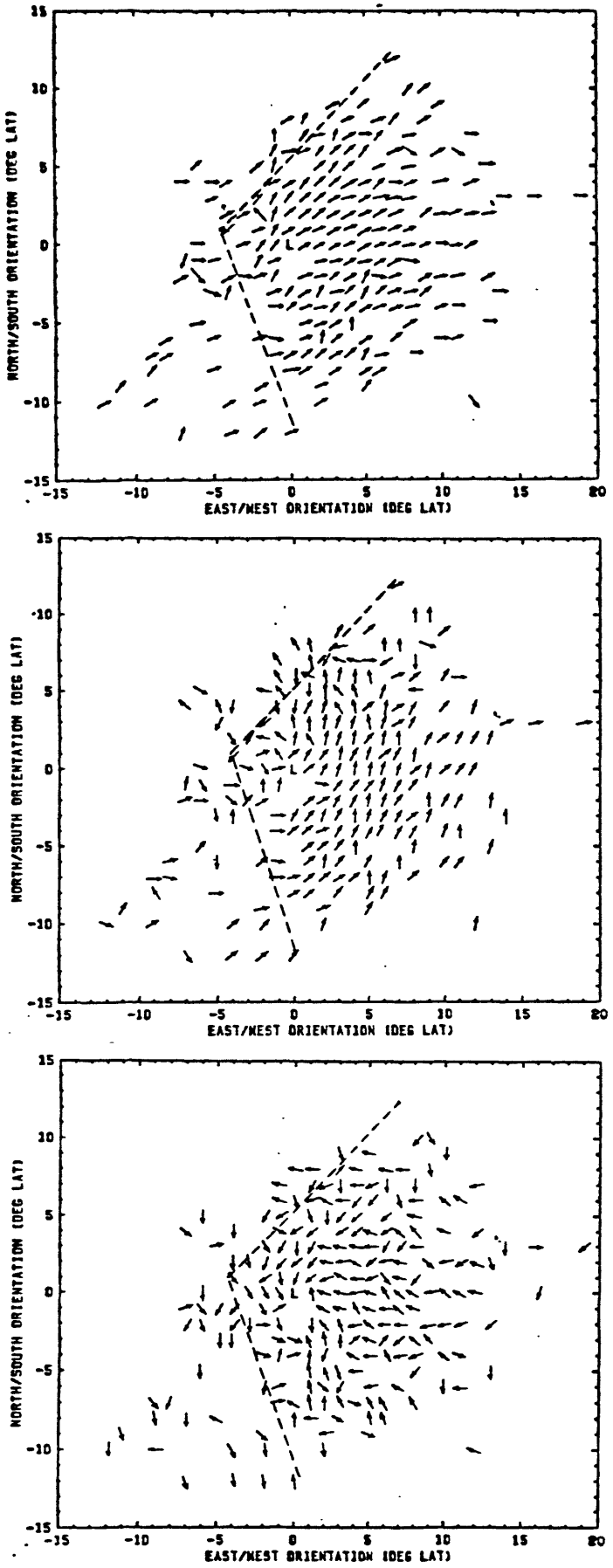


Figure 3.12. A composite of the mean wind direction at a) 500 mb, b) 850 mb and c) the surface for all the cases observed at a given position with respect to the associated surface low-pressure center. Dashed lines are as defined in Figure 3.11.

low-level wind maximum (not shown), that is recurrently observed at 850 mb in these cases. Frequently, as will be shown later, an area of deformation is positioned southwest to northeast at the exit region and/or along the cyclonic shear side of this wind maximum. A sharp cutoff in active elevated convection is observed along the associated axis of dilatation which is reflected by the limit in events north of the low.

The southern part of the western limit appears to be closely associated with the 850-mb trough axis. Ahead of the trough, in the region of active elevated convection, strong warm advection is almost always observed. The few events that occurred with a northerly component to the 850-mb wind can be explained in one of several ways. First, in those regions where such events were recorded, the surface layer is characterized by winds with a northerly component (see Figure 3.12). In this situation, it is possible that the 850-mb wind is representative of the flow in the boundary layer. Second, the errors associated with the linear interpolation used to obtain intermediate conditions from conventional rawinsondes are such that it would be difficult to avoid including incorrect values, particularly in regions of strong shear and small-scale variations. A third possibility is that the flow is completely cut off through the depth of the troposphere and the convection is taking place in the return flow northwest of the center. Although not common, this does occur and a case will be shown later in this chapter. Finally, the observation could be dominated by a mesoscale circulation and not be

representative of the large-scale flow.

The preferred region of convective activity extends well into the 500-mb anticyclonic flow ahead of the trough. The maximum frequency is positioned very near the inflection point in the composite 500-mb flow field. 40% of the cases occurred in the region downstream from the inflection point in the 500-mb flow. In contrast, 77% of the events were in the cyclonically curved region of the flow at 850 mb.

There is a very strong relationship between the location of the elevated convection and an associated local wind maximum. Figure 3.13 shows a simple composite of the number of events positioned with respect to a wind maximum at the 850-mb and 500-mb levels. 44% of the cases were downwind from the maximum wind region and on the cyclonic shear side of the maximum at the 850-mb level. At 500 mb the pattern differs in that the convection is positioned downwind and on the anticyclonic shear side of the jet. This quadrant of the 500-mb jet encompasses 38% of the events.

Figures 3.14 (a & b) show the scatter diagrams for the wind direction and speed between 850 mb and 500 mb. The direction veers slightly with height from about 210 degrees at 850 mb to 240 degrees at 500 mb. The speed generally increases with height between the two levels with an average increase of 32 knots. The increases tend to be larger for the lighter 850-mb winds and smaller for the stronger 850-mb winds. In contrast, the directional shear between the surface and 850 mb is extreme (see Figure 3.15). The surface wind direction is generally northeasterly, with the 850-mb direction almost 180 degrees

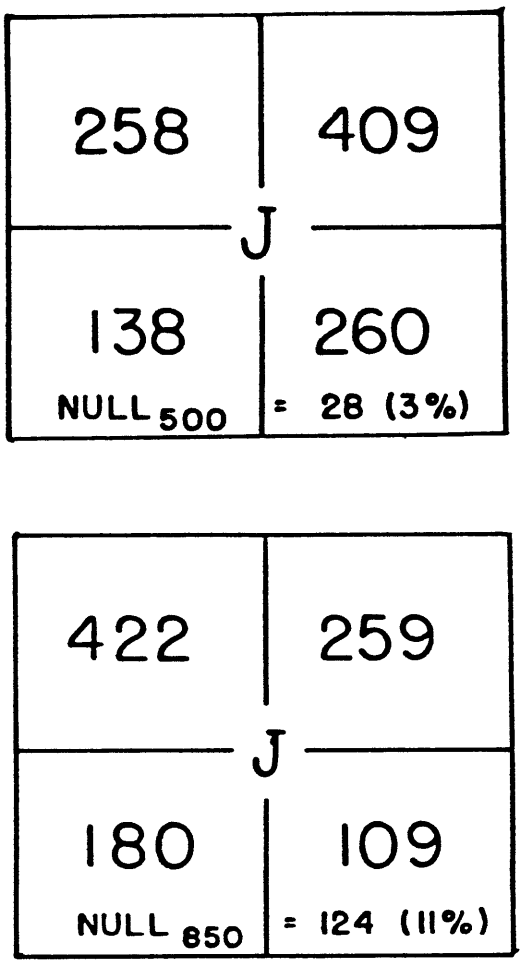


Figure 3.13. The number of events that were observed in each sector of a relative wind maxima (see section 3.2 for definition). The wind maxima position is indicated by the large J. Null cases are those where no wind maximum was observed.

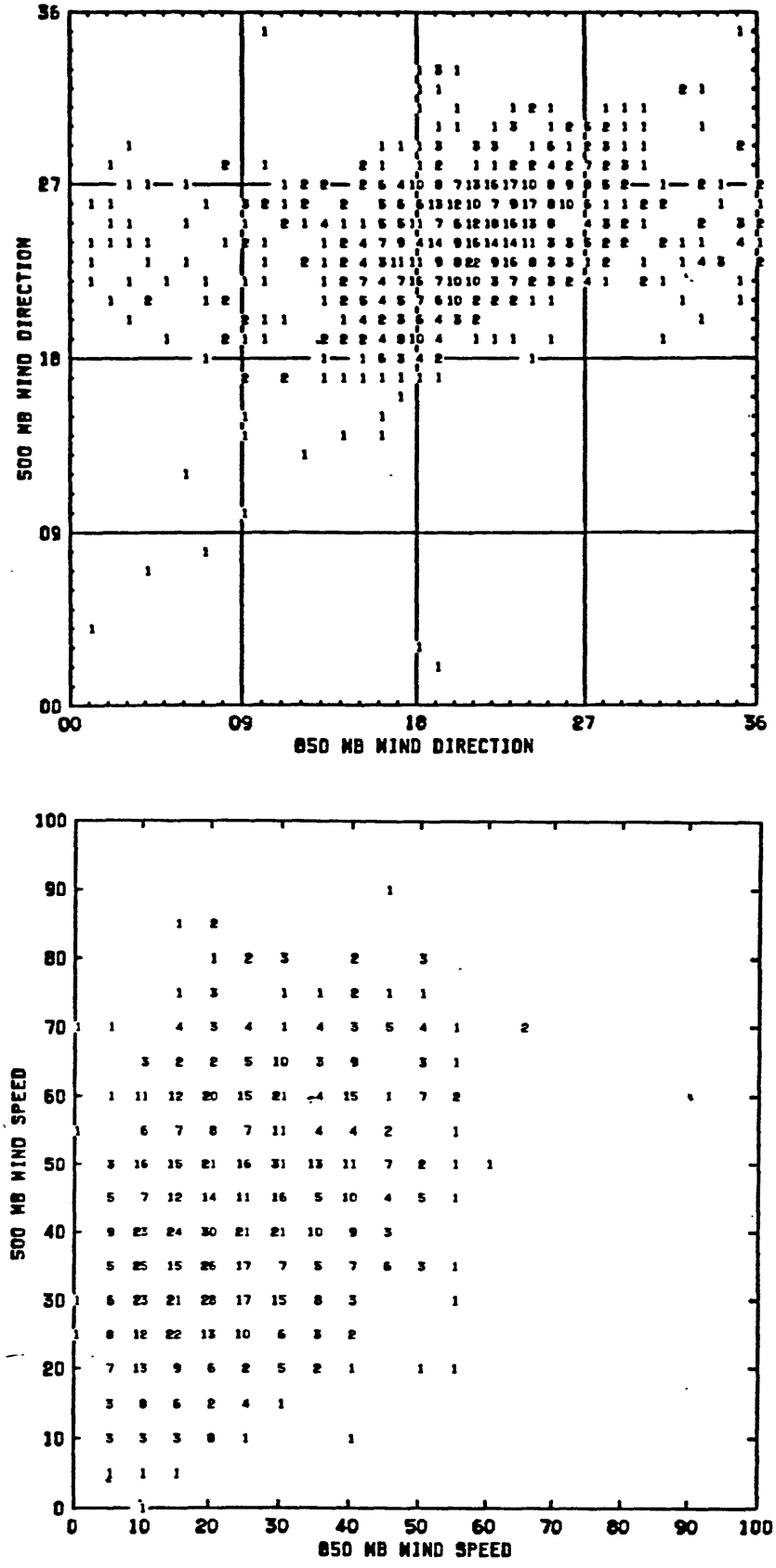


Figure 3.14. A composite of the number of events positioned according to a) the 850-mb and 500-mb wind direction (degrees) and b) the 850-mb and 500-mb wind speed (knots).

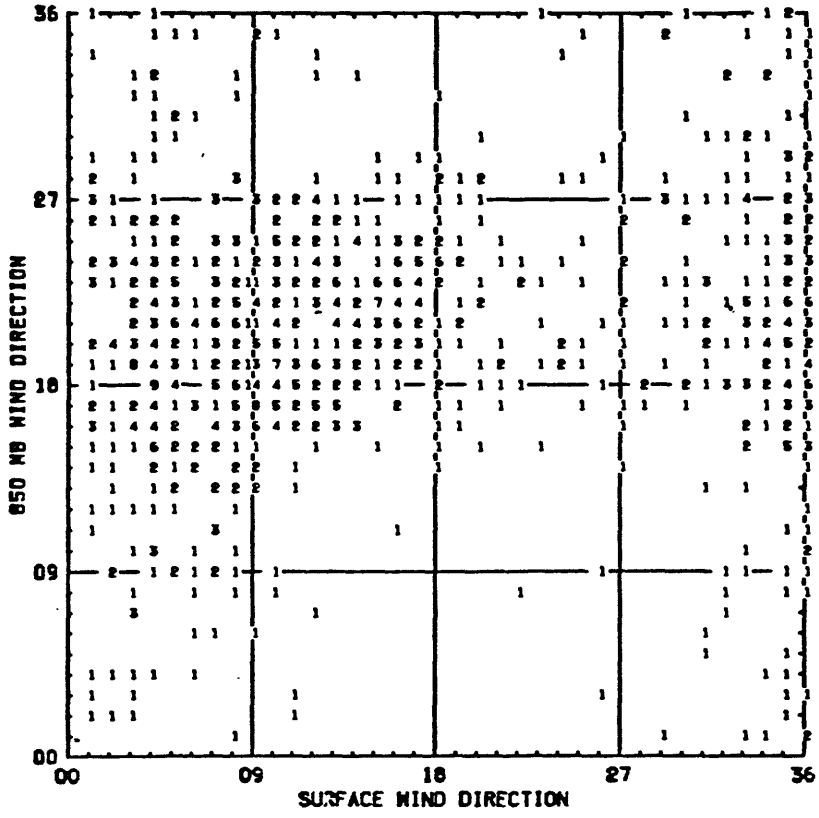


Figure 3.15. A composite of the number of events positioned according to the surface and 850-mb wind direction.

out of phase.

As a control, a random sampling of 594 soundings was selected from a six month period (February through July, 1983) from the standard radiosonde network for the 48 contiguous United States. Figure 3.16 shows the comparable scatter diagram to Figure 3.14 but for the control sample. The diagram has been normalized by the number of elevated thunderstorm events to allow direct comparison between the two figures. The wind directions are similar between the two sets, though, not surprisingly, the scatter for the control set is greater. The tendency for the wind to veer is still present although not quite as strong. One obvious difference between the two sets is the absence of elevated convection when there is an easterly component or a large northerly component to the 500-mb wind.

The most striking contrast between the climatology sample and the control sample is in the wind speed. Elevated convection occurs in situations with stronger winds at both levels and a stronger shear between them than the control soundings.

It has already been mentioned that elevated convection was observed to be associated with all three types of fronts analyzed by NMC on the surface analyses. Recall that 46% of the events were associated with warm fronts, 29% with stationary fronts, and 23% with cold fronts. Figure 3.17 shows the histograms, for each type of front, of the distance normal to the front, that the event was recorded. The histograms have been normalized by the total number of events associated with warm fronts. The mean distances for warm

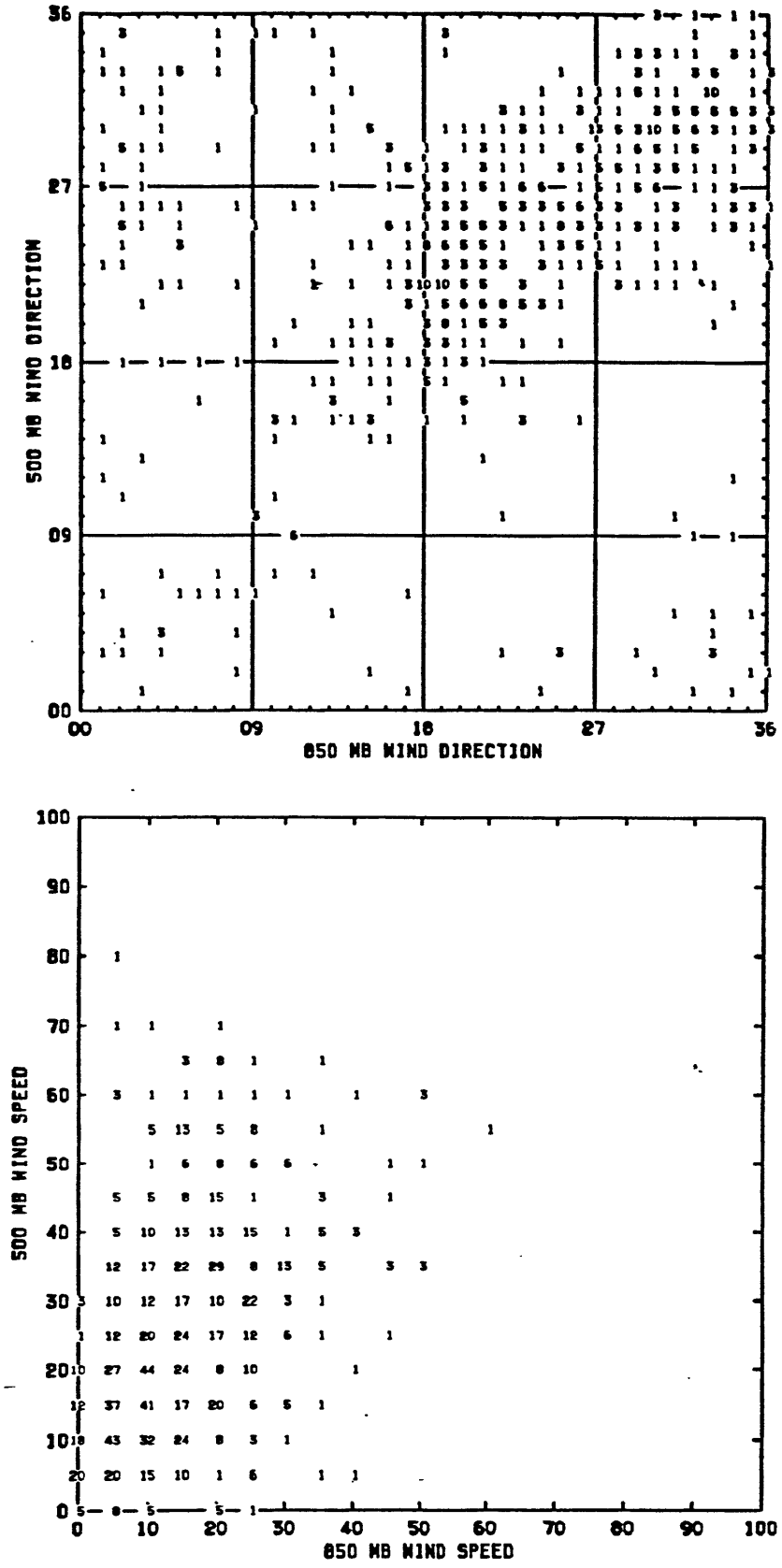
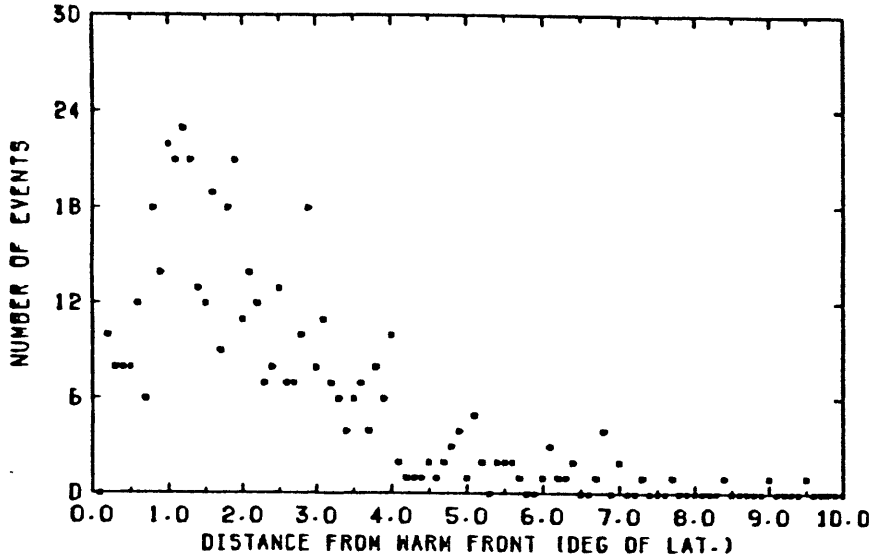
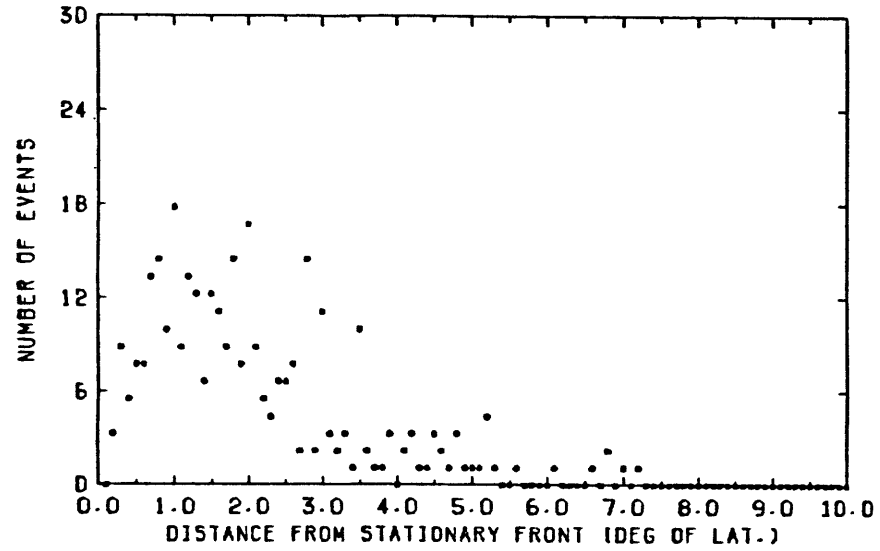


Figure 3.16. Same as Figure 3.14 except it is for the control sample of upper air soundings (6-month sample).





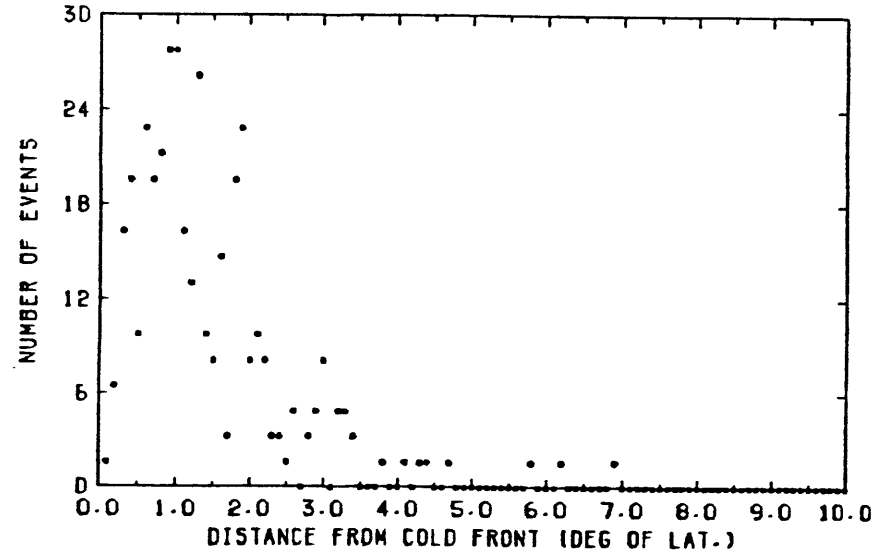


Figure 3.17. Histogram of events with respect to the distance from a) warm fronts, b) stationary fronts, and c) cold fronts.

fronts and stationary fronts were 2.3 and 2.0 degrees of latitude, respectively. The appearance of the histograms for the warm and stationary fronts is very similar, with only a slight suggestion that the elevated convection occurring with warm fronts had a tendency to be displaced slightly farther into the cold air. The mean distance for those associated with cold fronts was 1.4 degrees of latitude. This disparity between frontal types would even be greater had frontal motion been included. This difference would give a much shorter travel time for cold fronts and, as discussed previously, would explain the differences observed in the diurnal oscillation.

One of the criteria used in filtering the original data set to eliminate wrongly collected cases was that the surface air had less latent instability than the 850-mb air. This essentially required the frontal inversion to be located below the 850-mb level at the position of the storm. It might be expected that a large number of those cases eliminated would have been those that occurred at large distances from the surface front, however, very few were. This suggests that a shallow frontal slope is generally present when elevated convection occurs.

THERMODYNAMIC ENVIRONMENT

The separation of charge necessary to generate a lightning bolt is commonly attributed to the turbulence associated with strong vertical velocities. Observations suggest that these velocities should be on the order of a meter per second or more. It has been

known since the late 1940's (based upon observations from the Thunderstorm Project) that very strong updrafts and downdrafts (>25 m/s) are present in large cumuliform clouds. The instability active in creating such clouds is gravitational, resulting from the release of latent heat in the rising air column creating thermal buoyancy for the cloud.

This association between cumulus convection and lightning is well indoctrinated in the teachings of meteorology. In the last few years another instability has been shown to play a role in mesoscale convection. Emanuel (1979) discussed the role of inertial instability in convective systems and was able to show that the instability is mesoscale in extent. In later work (Emanuel, 1983) he suggested that in a strongly baroclinic atmosphere the centrifugal imbalances may not be negligible and could actually account for vertical velocities of a few meters per second. Also, strong vertical shear would likely be present and could possibly play a role in atmospheric electrification. This section will discuss the possible instabilities present in elevated convection.

Using the altimeter setting and the known station elevation it is possible to calculate the station pressure. Then, from the temperature and dew-point temperature, conservative thermodynamic quantities can be determined. These are used to calculate 'parcel' characteristics at different pressures which are compared with the observed environment to estimate the latent instability of the atmosphere.

Figure 3.18 shows the lifted indices for the surface air (SLI) and the 850-mb air (LI-850), respectively. The lifted index is defined as the ambient 500-mb temperature minus the temperature of a parcel of air lifted pseudo-adiabatically to 500 mb. The mean SLI was 7.4°C with only a few cases showing positive buoyancy. The extreme stability of the surface air is characteristic of elevated convection. The LI-850 shows a much narrower distribution than the SLI, with a mean of 0.6°C and a standard deviation of 3.5°C. The normal curve, drawn on the figure, shows good symmetry and fit.

In the selection of cases, surface air was required to be colder, when lifted to 500 mb, than the 850-mb air was when lifted to 500 mb. This did not require that the surface air be colder than the 850-mb air when lifted to 850 mb. Figure 3.19 shows the 'cap' for the surface air at 850 mb (i.e., the temperature deficit of the surface air passing through 850 mb). The surface air was colder in essentially all cases. The strong peak in this distribution away from neutrality (≈5°C) is suggestive that strong surface stability is required for elevated convection and is not merely a consequence of definition. The sharper the thermodynamic contrast is between the boundary layer and the free atmosphere, the more complete the decoupling between the two layers would be. The decoupling would act to decrease the drag on the free atmosphere, approximating a free-slip boundary at the interface, and possibly allow for a more efficient convective overturning. Hsu (1981) investigated the relationship between frontal overrunning and the temperature difference across the central Gulf

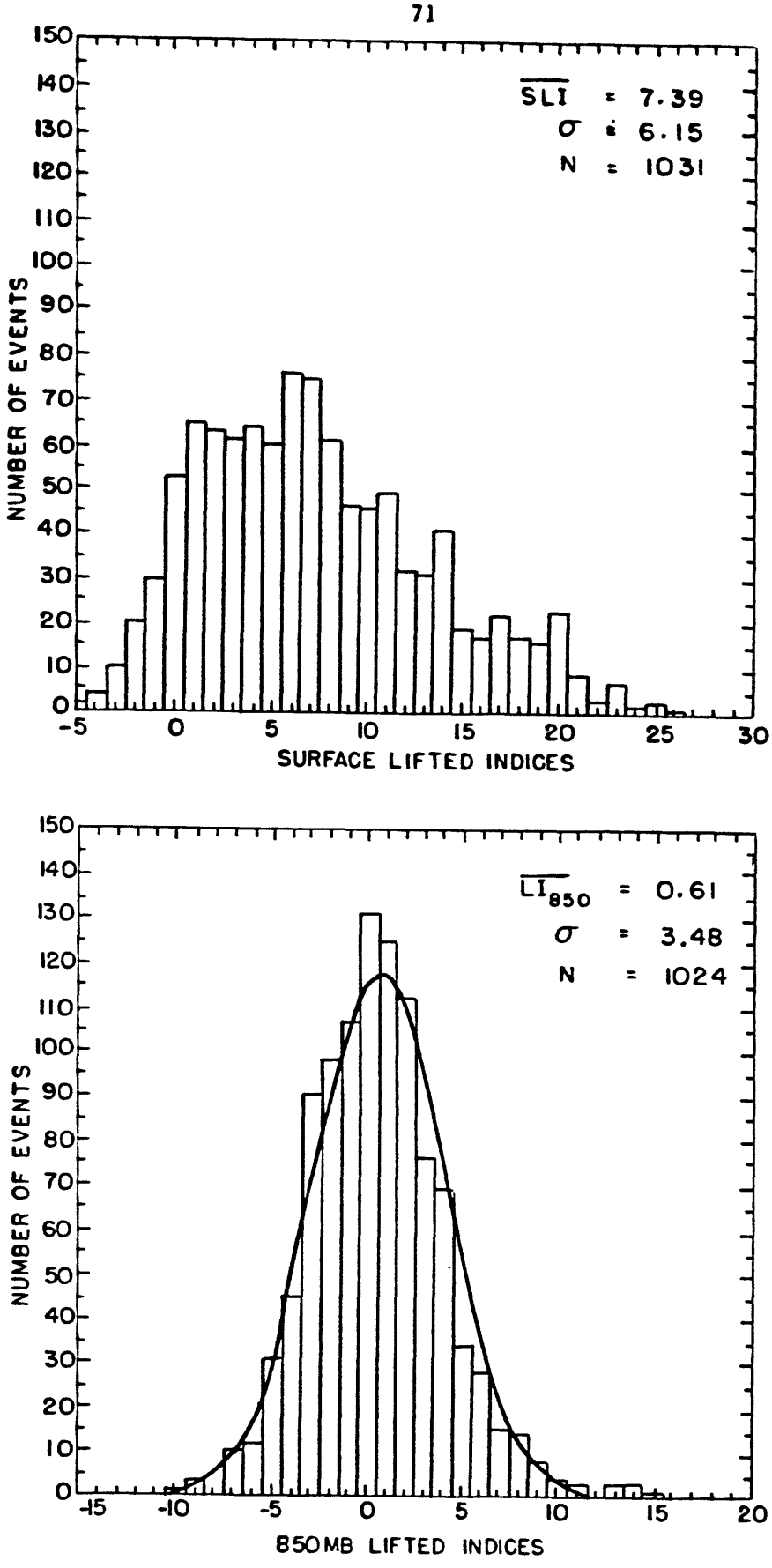


Figure 3.18. Histogram of the a) surface lifted indices (°C) and b) 850 mb lifted indices (°C). See text for definition of indices. The normal curve plotted on (b) was fitted using the mean and standard deviation of the data set.

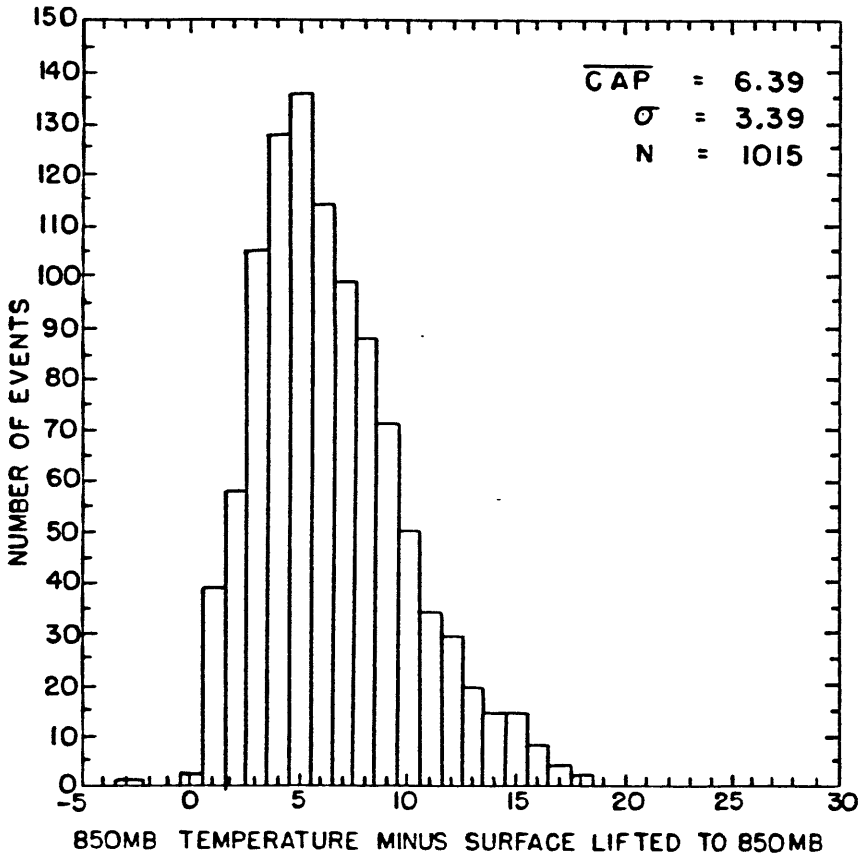


Figure 3.19. Histogram of the 'cap' of the surface air at 850 mb. (°C). See text for definition.

Coast. He found a dramatic increase in frontal overrunning as the air over the land became increasingly colder than the air over the water. Figure 3.20 shows the relationship he found between the monthly percentage of frontal overrunning and the monthly mean offshore to onshore temperature differences.

The equivalent histogram for LI-850 was calculated using the 6-month control data set (Figure 3.21). The distribution is considerably flatter than the one for the thunderstorm data set. There is still a sharp decrease to the left of the neutral point, reflecting the control that convection has on the stability of the atmosphere. There is a similar peak at neutral or moist adiabatic. If individual months are investigated (see Figure 3.22) it is clear that this moist adiabatic peak is from the summer months and represents the convectively processed environment that is characteristic of that season. On the other hand, very few of the cases in March were moist adiabatic. Therefore, the strong peak that we have observed for elevated thunderstorms suggests that they occur in an atmosphere thermodynamically similar to the typical summer atmosphere.

The fact that the mean LI-850 is stable raises the question about the role of latent instability in elevated convection. It should first be pointed out that there is no <u>a priori</u> reason to believe that the most unstable air will always be found at 850 mb. However, qualitative inspection of many cases has shown that, in most situations, as long as the inversion is below 850 mb, the air at

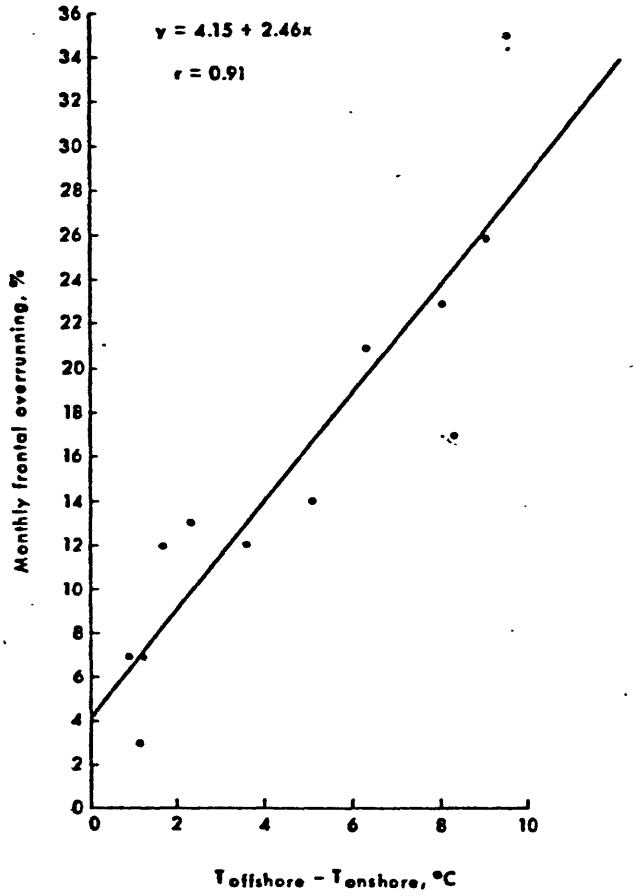


Figure 3.20. The relationship between monthly frontal overrunning, expressed in percent of hours observed per month, and the mean offshore-onshore temperature difference. (Hsu, 1981).

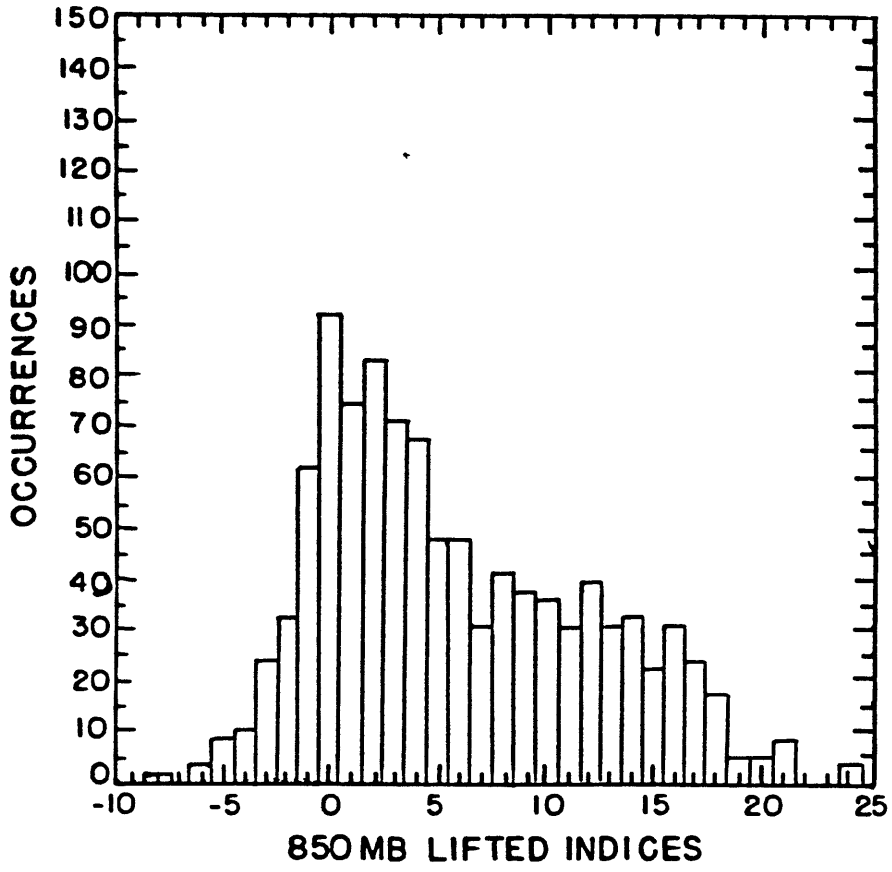


Figure 3.21. Convention same as Figure 3.18(b) except for control sample of upper air soundings (6-month sample).

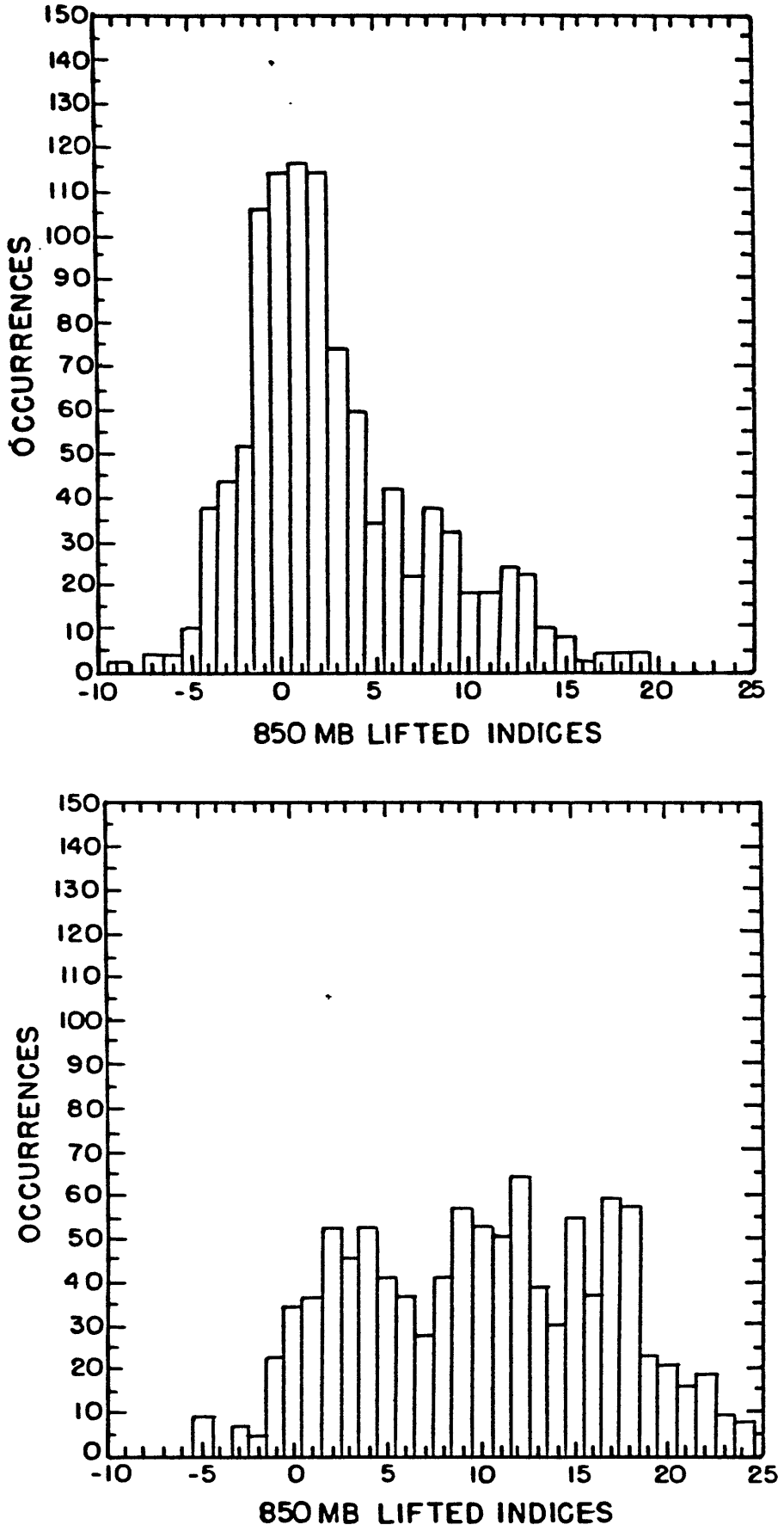


Figure 3.22. (a) Convention same as Figure 3.18(b) except it is for the control sample of upper air soundings for July. (b) Convention same as (a) except it is for March.

850 mb is representative of the air with the highest equivalent potential temperature. Thus, the error would be to underestimate the latent instability, but by presumably only a small amount.

If local conditional symmetric instability is a contributing factor in elevated convection, it could aid in overcoming slight parcel stability. Figure 3.23 shows a scatter diagram of wind shear vs. the LI-850. Although the correlation is very low, the linear regression shows stronger gravitational stability balanced by stronger shear and thus a larger centrifugal contribution. The zero intercept of -0.83°C, although admittedly small, shows hydrostatic instability when the inertial contribution drops to zero.

An estimate of the correction that should be applied to the parcel temperature to allow for the centrifugal contribution is given by Emanuel (1983) as

$$\Delta T_{AKE} = \frac{1}{2} \frac{T_{v0}}{g} \frac{f}{\eta(z)} \frac{d}{dz} \left(V_E - V_0\right)^2$$

where T_{v0} is the parcel temperature, $\eta(z)$ the vertical component of absolute vorticity, V_E the environmental V and V_0 the parcel's V. By taking $\eta(z)$ constant and equal to f, and the 500-mb and 850-mb winds

for V_E and V_0, respectively, it is possible to calculate ΔT_{AKE} for the individual events in this study. Figure 3.24 shows the histogram for the LI-850 with the centrifugal contribution included

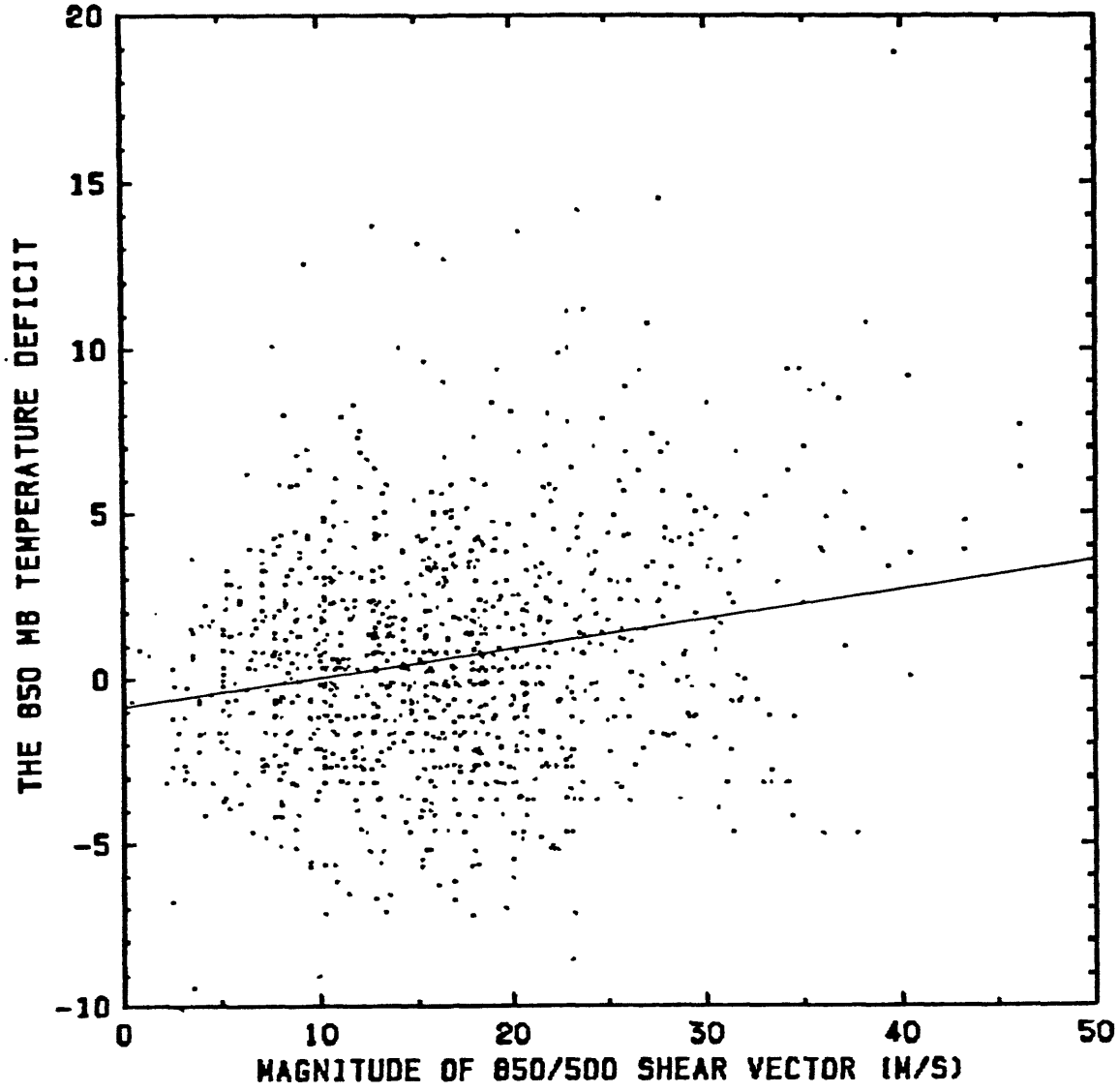


Figure 3.23. Scatter diagram correlating the layer shear from 850 mb to 500 mb to the 850-LI for the thunderstorm data set.

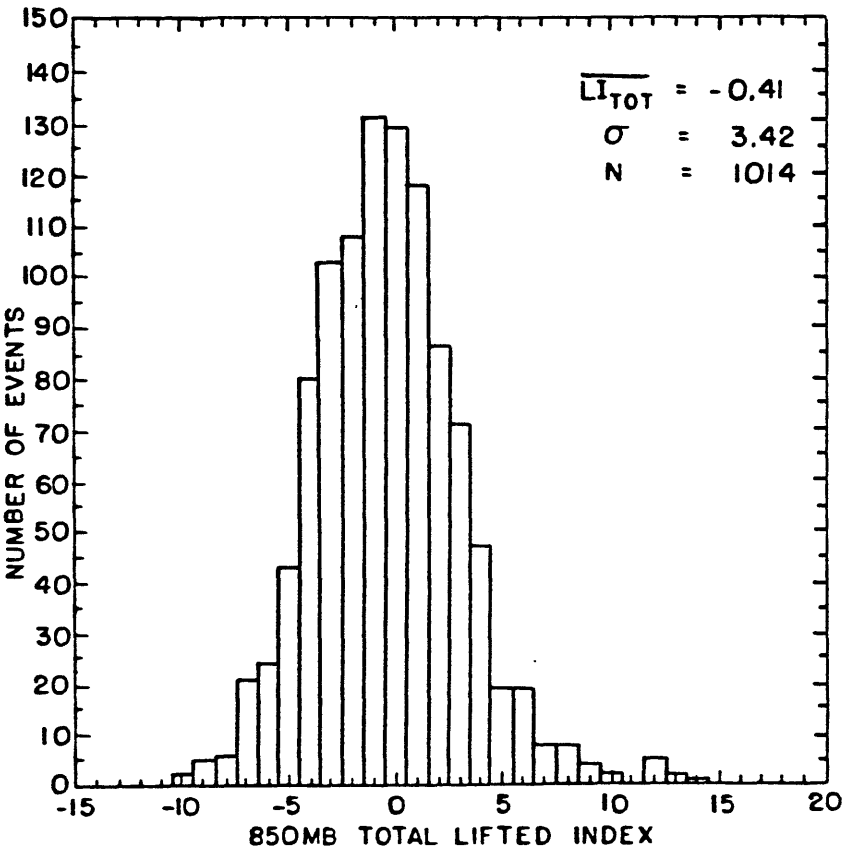


Figure 3.24. Convention same as Figure 3.18(b) except that the inertial contribution, ΔT_{AKE}, has been included (see text for explanation).

(LIT-850). The correction was able to balance the slight hydrostatic stability present and put the mean at -0.41°C, which is essentially neutral. There was also a slight reduction in the variance of the distribution which indicates a tendency for larger centrifugal contributions in those cases with less latent instability.

Figure 3.25 shows the gravitational and centrifugal contributions to the LIT-850 by month. A positive value implies stability. The monthly mean event is gravitationally unstable for the period April through September. There are two apparent peaks in the gravitational stability, one in November and the other in February. For the period from February through April both contributions are increasingly more unstable which correlates well with the peak frequency of occurrence in April. The centrifugal contribution is surprisingly constant over the twelve months with a difference of 0.73°C between the minimum in August and the peak in April. This annual variation in the amount and type of instability present suggests that the active mechanism may not always be the same, unfortunately, it is not possible to draw further conclusions from the composite data.

3.5 SYNOPTIC TYPES

As is usually the case with mesoscale events, elevated convection tends to occur most frequently in certain, very similar, synoptic situations. This section will present six different episodes of elevated convection that will serve to exemplify which synoptic types are most common. A 'snapshot' of each case will be shown with

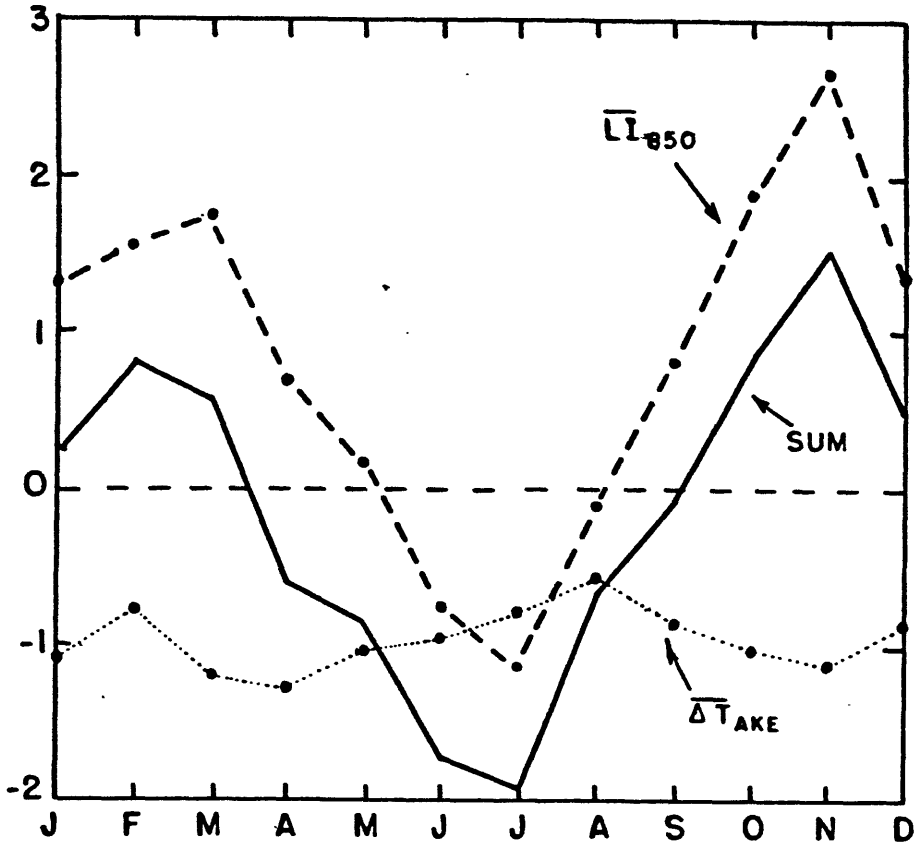


Figure 3.25. The monthly mean contribution to the total lifted index at 850 mb (°C). The inertial contribution is light dotted, the hydrostatic contribution is dashed and the total lifted index is solid.

analyses for the surface, 850 mb, and 500 mb. To keep the discussion qualitative, the figures show only the contoured fields of height and temperature for the upper-air, and isobars for the surface maps. To identify the thermal contrast across the front, the surface maps have at least one complete station plot on each side of the front. In addition, the weather is plotted for each station reporting an elevated thunderstorm.

Figure 3.26(a). This is a very common synoptic situation for elevated convection, particularly along the Gulf Coast. The trailing cold front from an initial baroclinic system drops southward and, in this case, is positioned over the western Gulf of Mexico. Then, a subsequent short-wave moving out of the long-wave trough position forces a secondary circulation to develop along the front with intense warm advection downstream from the 850-mb center. Strong deformation is usually found on an axis that extends along the boundary between this warm advection and the cold advection, associated with the previous system, ahead and to the north of the secondary circulation. This axis marks the northern extent of the elevated convection. The strong ridging and northerly flow north of the system is crucial in maintaining the cold, low-level, north-northeasterly flow. In the example shown, the elevated thunderstorms extend well to the west of the surface center over strong cold advection in the boundary layer.

Figure 3.26(b). In this case, a large, cold anticyclone is

established over the United States, with the surface thermal gradient south of the upper-level jet stream. In response to an upper-level short wave moving out of the Rockies there are surface-pressure falls in the lee of the Rockies and an accompanied Gulf return flow that enhances the thermal gradient. The mid-level circulation, already in existence over the West, seems to advance over the cold air, establishing strong warm advection above the boundary layer. In fact, depending upon the strength of the anticyclone, the cold air may continue to advance southward delaying the development of a surface cyclone. The convection can extend well to the north of the surface front and is frequently accompanied by snow over the western Great Plains during mid-winter.

Figure 3.26(c). Another very common synoptic situation, particularly in the spring, is associated with a split flow around a sagging upper level short-wave. The short-wave is progressive and appears to move in tandem with another wave, positioned downstream and embedded in the northern branch of the flow. A strongly frontogenetical deformation zone develops between the two surface cyclones, with the axis of deformation defining the northern extent of elevated convection. The cold air is maintained by ridging behind the northern system, allowing an area of prolonged elevated convection to follow the track of the storms.

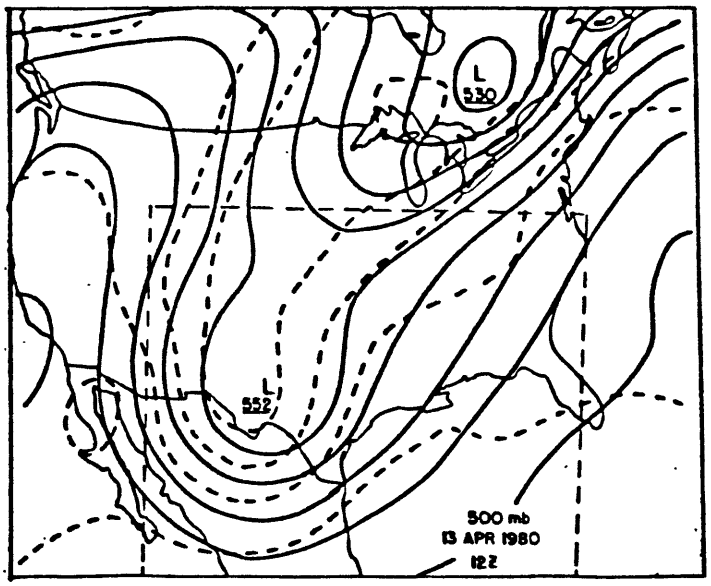
Figure 3.26(d). The most prolonged outbreaks of elevated

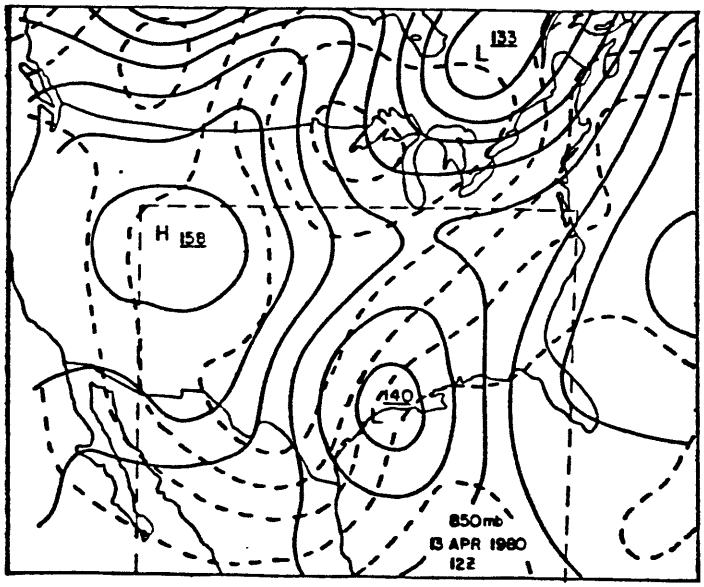
convection occur when a strong system undercuts an established large-scale ridge. The 500-mb height analysis displays a typical Rex flow pattern (Rex, 1950) during the most convectively active period. The southerly winds to the south of the front are the result of a surface cyclone that develops in response to the upper-level forcing. The 500-mb ridge to the north maintains the strength of the surface anticyclone and thus the east to northeast surface winds on the north side of the front. An area of deformation northeast of the surface center, frequently identifiable at 850 mb, is clearly visible in this case. The system moves slowly toward the east with the convectively active region, limited in northward extent by the deformation at 850 mb, but stretching many degrees of latitude toward the east.

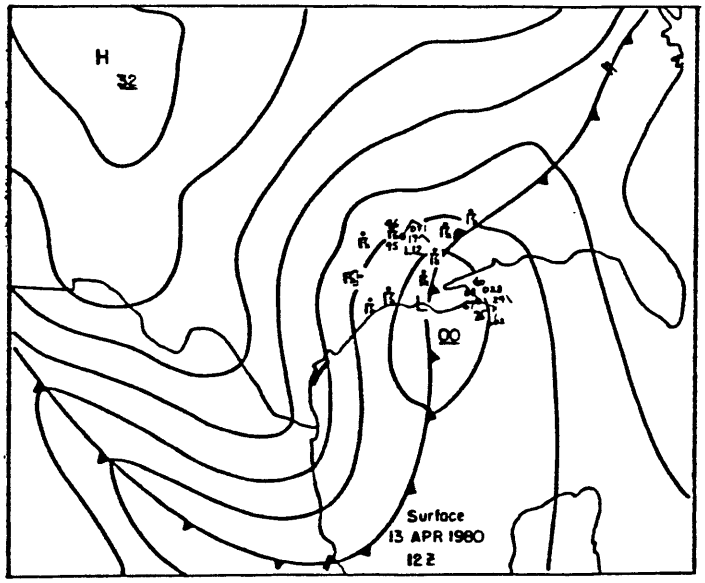
Figure 3.26(e). If a baroclinic system cuts off when there is still active warm advection present, it is possible for elevated convection to occur to the west of the surface center with northerly flow at all levels. In this case there is a strong inversion separating the cold advection in the boundary layer from the warm advection at 850 mb. This type should not be confused with the cold air thunderstorm which is found in the same sector of the storm but occurs with cold advection at all levels and strong surface heating.

Figure 3.26(f). If cold air exists at the surface, to the east of a rapidly deepening cyclone, the intense warm advection in the low levels will override the cold boundary layer. In this situation there

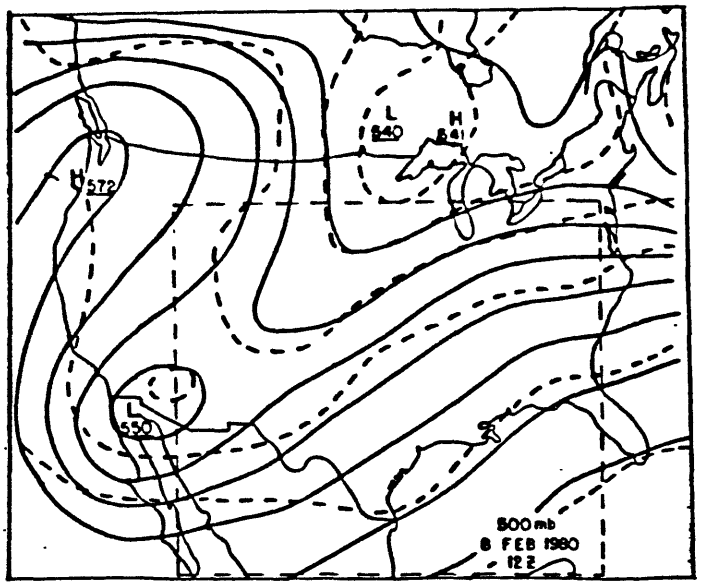
Figure 3.26(a-f). Synoptic snapshots of large-scale patterns that frequently have associated elevated thunderstorms. The top and middle panels show isohypses and isotherms for 500 mb and 850 mb, respectively. The bottom panel shows the sea-level isobars and surface frontal positions. Plotted stations follow conventional model. The area covered by the surface map has been lightly dashed on the upper two panels.

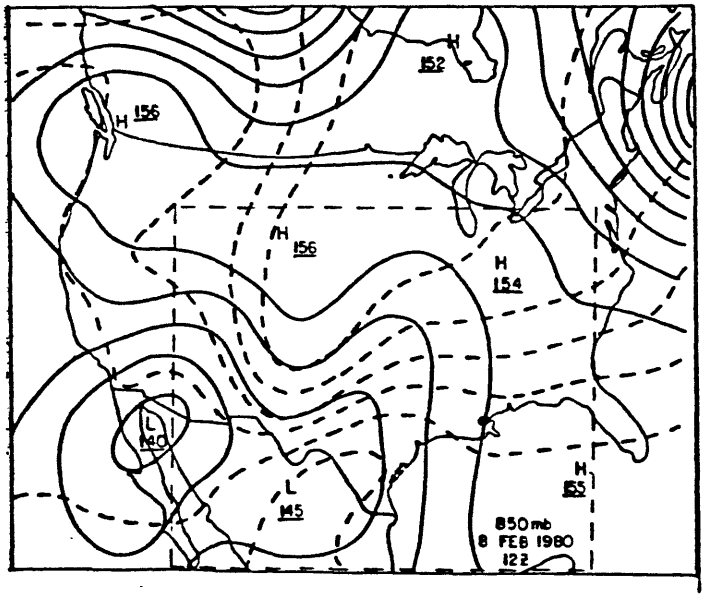

L
530
552
500 mb
13 APR 1980
12Z

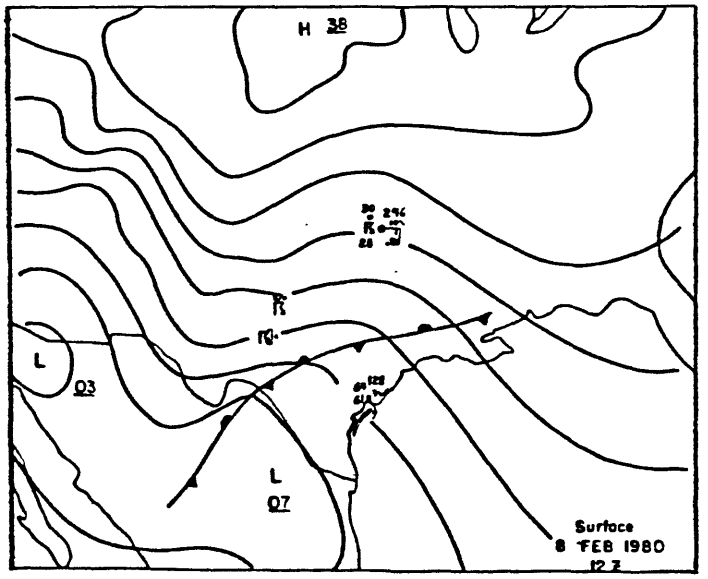

133
L
H 158
140
850mb
13 APR 1980
12Z


H
32
00
Surface
13 APR 1980
12Z

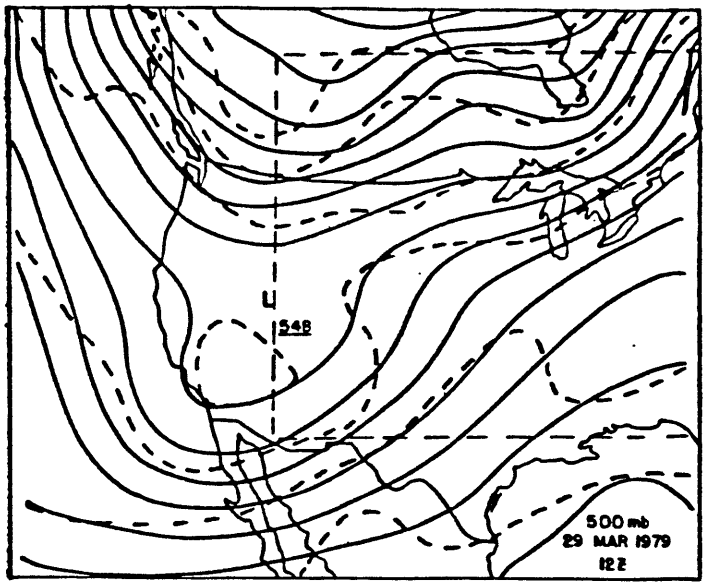
(a)

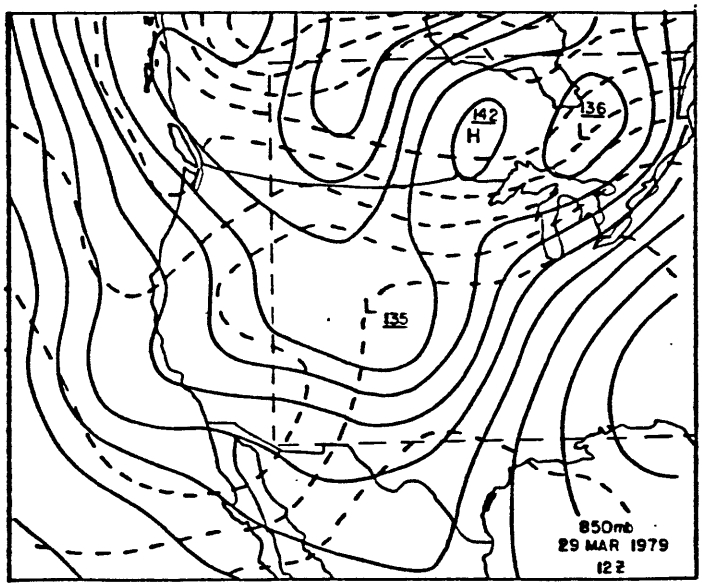

L
840
H
841
H
572
L
550
500 mb
8 FEB 1980
12 Z

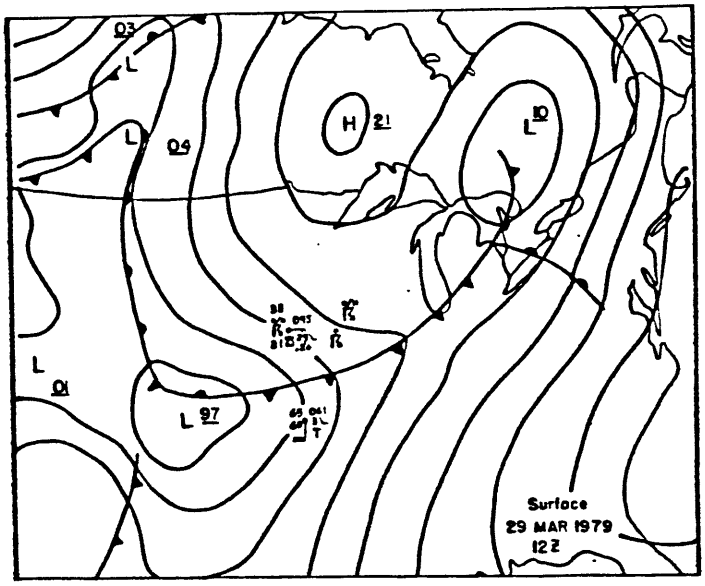

H
152
H
156
H
156
H
154
L
140
L
145
H
155
850 mb
8 FEB 1980
12 Z


H
38
L
03
L
07
Surface
8 FEB 1980
12 Z

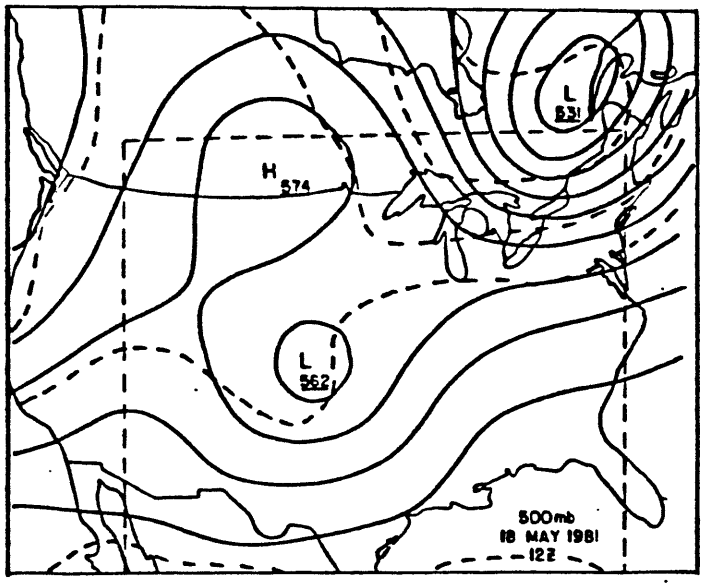
(b)

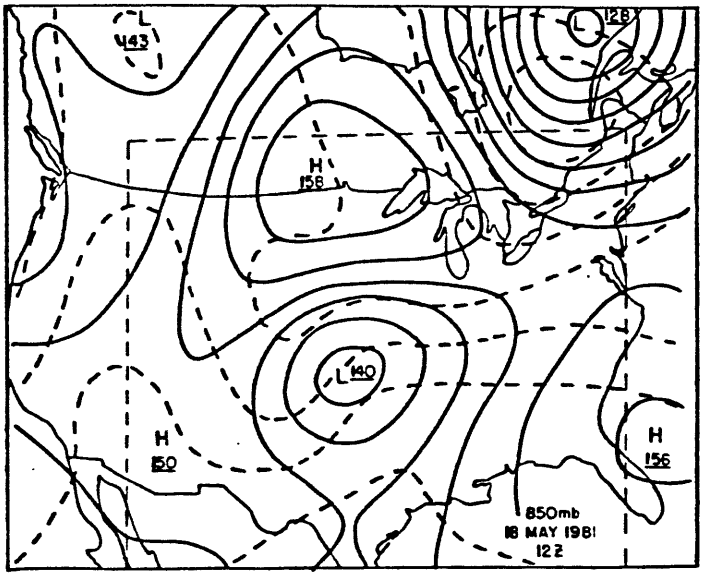

L
548
500 mb
29 MAR 1979
12Z

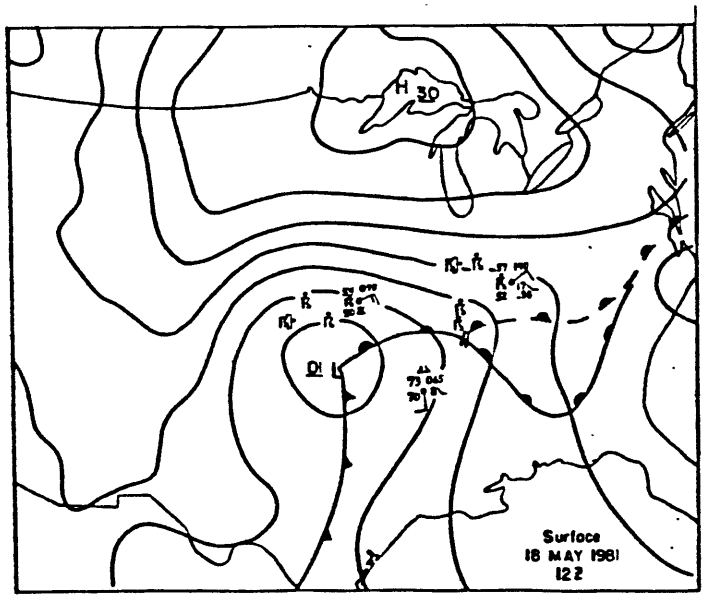

142
H
136
L
L
135
850mb
29 MAR 1979
12Z


03
L
L
04
H
21
L
10
L
01
L
97
Surface
29 MAR 1979
12Z

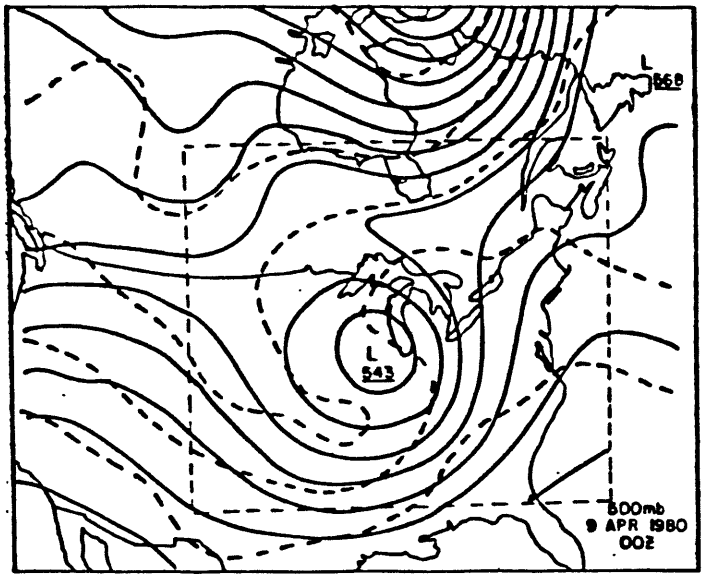
(c)

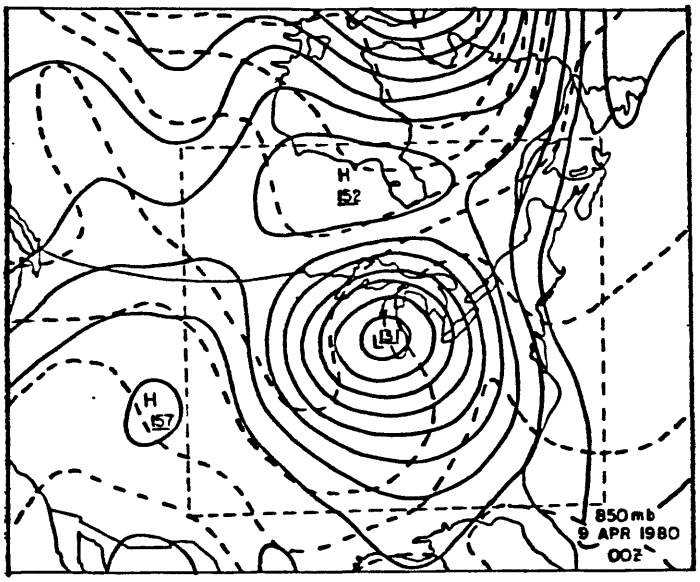

L
531
H
574
L
562
500mb
18 MAY 1981
12Z

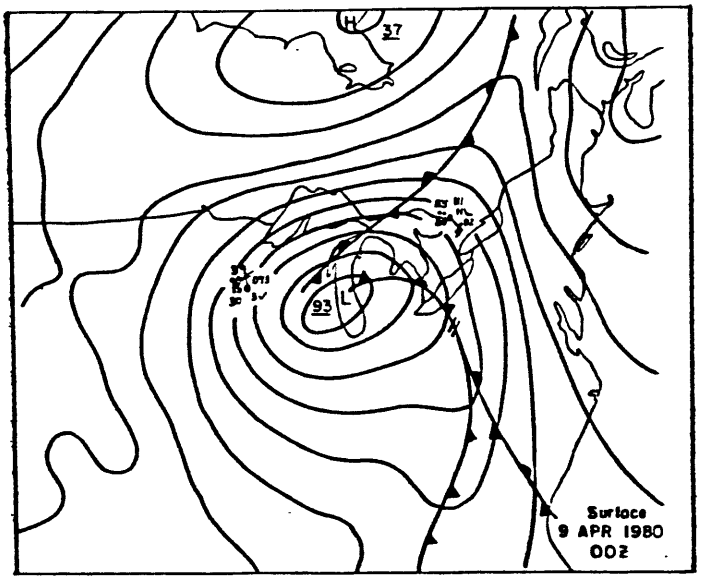

L
143
L
128
H
156
L
140
H
150
H
156
850mb
18 MAY 1981
12Z


H
30
L
Surface
18 MAY 1981
12Z

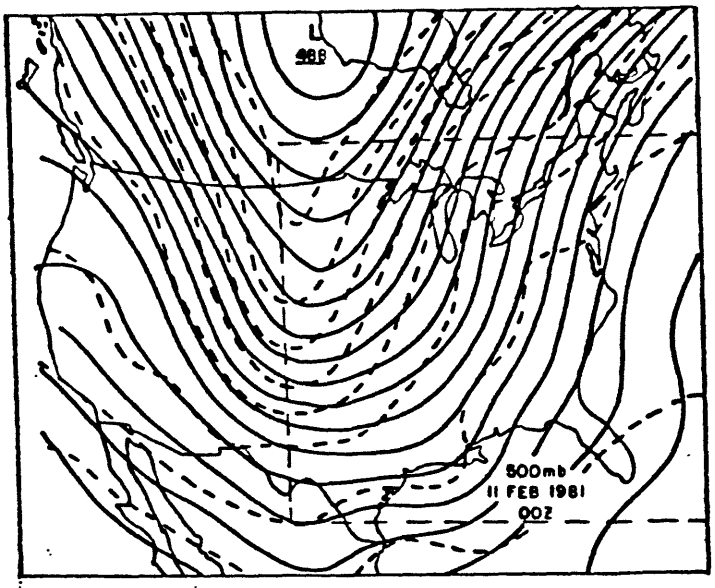
(d)

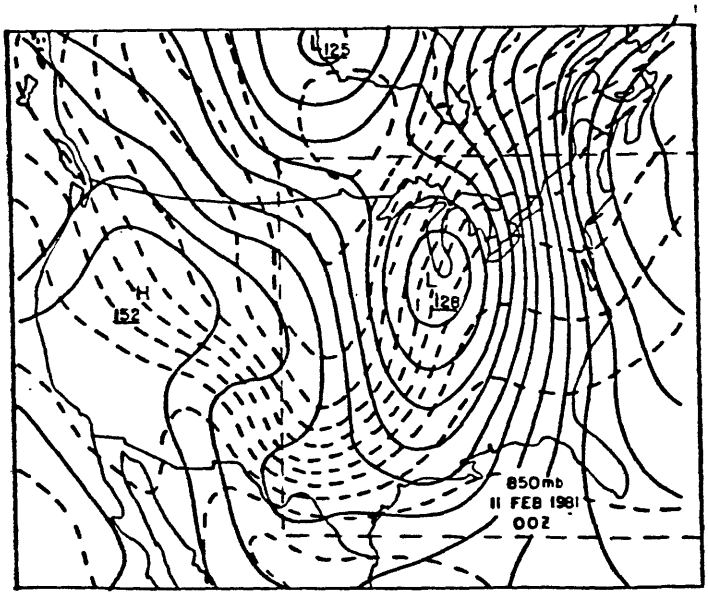

L
869
L
543
500mb
9 APR 1980
00Z

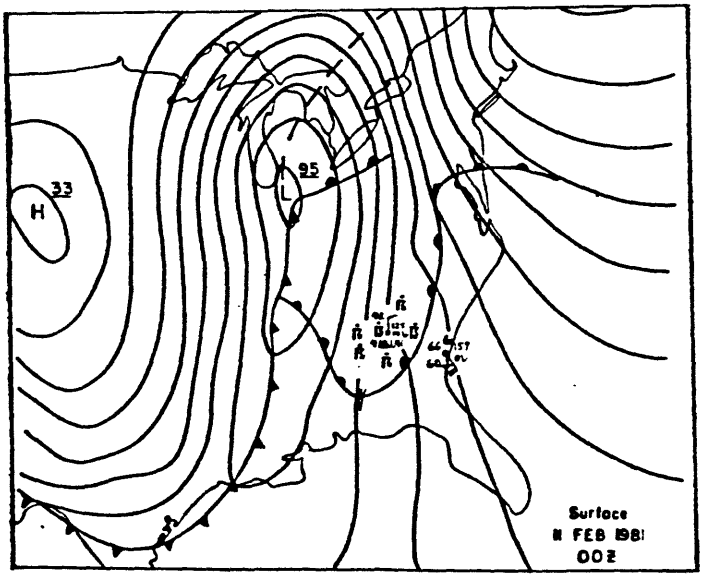

H
152
L
131
H
157
850mb
9 APR 1980
00Z


H
37
93
L
Surface
9 APR 1980
00Z

(e)


L
988
500mb
11 FEB 1981
00Z


L
125
H
152
L
128
850mb
11 FEB 1981
00Z


95
L
33
H
Surface
11 FEB 1981
00Z

(f)

is not a synoptic-scale dynamic maintenance of the cold surface layer, but rather, the advance of the warm air is retarded by surface or mesoscale effects. Small mountain barriers (e.g., the Ozark or Appalachian Mountains) can act to protect a cold surface layer from the advance of the warm air. Coastal fronts found along the Atlantic Coast and western Gulf Coast (Bosart et al., 1972) can also act as efficient barriers. The elevated convection can be intense but is usually short lived in the absence of forcing to maintain the cold air, and ends when the cold air is dislodged. The rapid decrease in reported thunderstorms, upon the dissolution of the warm front, suggests that an active role is being played by the cold boundary layer. The advance of the warm front is erratic and often discontinuous, suggesting downward mixing of warm air to the ground.

3.6 DISCUSSION

In this chapter, elevated convection has been characterized as deep convection that is isolated from surface diabatic effects by a relatively more stable planetary boundary layer than the lower layer of the overriding free atmosphere. This structure is contrary to the 'classical' concept of cumulus convection in which surface sensible and latent heat fluxes in the planetary boundary layer contribute to the destabilization of the atmospheric column. It has been shown in this chapter that, in the absence of these surface effects, convection at least strong enough to generate lightning can occur

above a frontal surface. Indeed, nearly all winter season (December though February) thunderstorms have been shown to be of this type.

An investigation into the distribution and frequency of elevated convection over four years has been discussed. The results show a bimodal frequency distribution with a primary maximum in April and a secondary maximum in September. It has been proposed that this is determined by the intersection of the annual distributions for convective instability and mid-latitude cyclones over the United States.

The diurnal variation, which does exist, seems to be influenced by a delay in the release of the instability as the air travels over the frontal surface. As a result, elevated convection associated with warm and stationary fronts occurs more frequently at 12 GMT than 00 GMT while the opposite is true for cold fronts where the convection is not displaced as far over the cold air. Recall that we initially made the assumption that the source air existed as a surface boundary layer prior to being transported over the frontal surface. This assumption is consistent with the data and the observed dependence on frontal type.

The thermodynamic stability of the overriding atmosphere has been found to be slightly positive in the mean. However, for individual cases, the stability varied fron moderately unstable to moderately stable. When the centrifugal contribution was included the mean was shifted by about 1°C, to slightly unstable. What instability is present seems to be highly case dependent. Clearly for those cases

where the LI-850 approached -10°C the active instability was gravitational and the convection upright. On the other hand, for those cases where the LI-850 is 0°C or positive, the characteristic of the mechanism is not clear from these data. The case study presented in the next chapter offers insight into this structure, and we will thus wait until then for further discussion. The fluctuation in the mean monthly LI-850 is also suggestive that more than one mechanism can generate an elevated thunderstorm.

The results have suggested that a shallower, more sharply defined front is more favorable for elevated convection. The preference for a shallow slope is contrary to the notion that the front provides the necessary lift to release latent instability from a potentially unstable layer as Dexter (1944) suggested. He felt that the actual thunderstorms were triggered by shear generated turbulence at the frontal surface. In the case study done by Ferguson (1967) the convection appeared to propagate onto the frontal surface from the warm sector and was thus triggered in a classical fashion from the boundary layer.

In order to gain a better understanding of the processes involved in elevated convection and the associated triggering mechanisms, the next chapter will discuss a detailed case study of elevated convection.

CHAPTER 4: AN INVESTIGATION OF ELEVATED CONVECTION DURING AVE-SESAME I.

4.1 INTRODUCTION

The first AVE-SESAME experiment (see next section) had the paradoxical fortune of being run on the 10th and 11th of April 1979, the day of the Red River Valley tornado outbreak. This noteworthy storm contained most of the phenomena commonly associated with severe weather outbreaks (e.g., dryline, strong overlying inversion, jet streak, etc.). The storm left 56 people dead, 1916 injured and damage estimates that totaled several hundred million dollars.

The wealth of observations collected by project SESAME has proven to be a mecca for the observational meteorologist. Studies already completed by Carlson et al. (1980), Fuelberg and Jedlovec (1982), and Negri (1982) have investigated the small-scale aspects of the tornadic storms, with a special emphasis placed on the severe storm that spawned the devastating Wichita Falls tornado. Figure 4.1.1 shows a composite of the severe weather events observed during AVE-SESAME I. It can be seen that there were two major areas of severe weather that consisted of tornadoes, strong winds, heavy rain, hail, flooding and duststorms. These two areas of severe weather attract attention to north central Texas and central Oklahoma. On the other hand, an

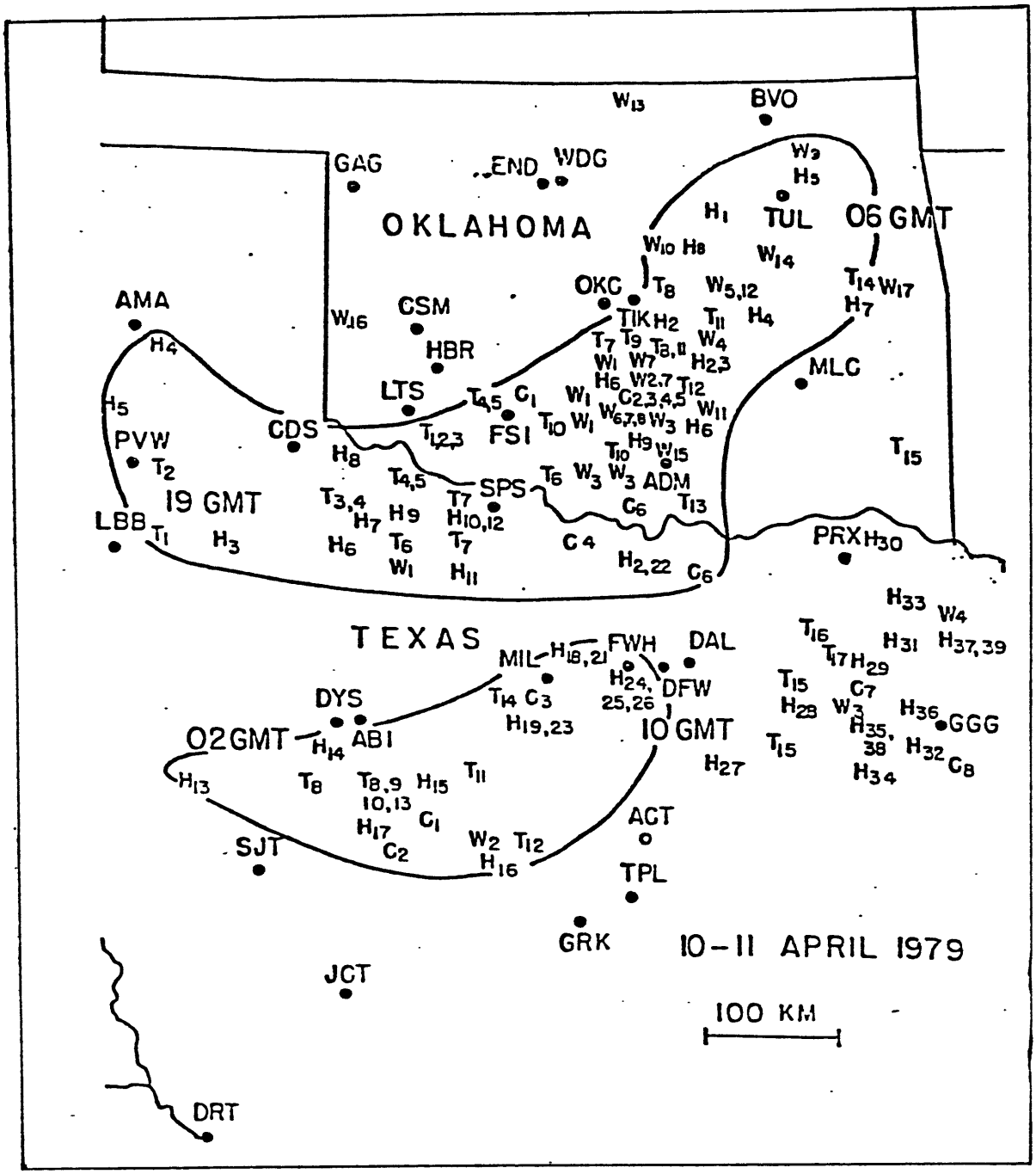


Figure 4.1.1. Map of severe weather events for 10-11 April 1979. T, W, H, and C denote tornado, damaging wind, large hail, and funnel cloud, respectively (Sanders, 1983).

inspection of the precipitation amounts from the storm shifts attention to a region northeast of the areas of severe weather where heavier and more widespread precipitation occurred. A composite of the storm total precipitation prepared from the climatological station network is shown in Figure 4.1.2. This heavier precipitation was almost exclusively the result of an extensive outbreak of elevated convection.

The purpose of this chapter is to examine in detail the synoptic-scale and mesoscale aspects that led to the development of this elevated convection. Section 4.2 will describe the data sources used for the study. Section 4.3 will present a synoptic overview of the case, with section 4.4 discussing the gravitational stability. A radar analysis of the mesoscale structure of the elevated storms is presented in section 4.5. The purpose of these first few sections is to establish the characteristics of the convection and to verify that the convection was not rooted in the boundary layer.

With the laying of groundwork completed, a more detailed presentation of several of the convective elements is discussed in section 4.6. Utilizing these detailed analyses we are then able to discuss the physical processes that account for the elevated convection observed in this case study. The association with gravity waves and their possible role in triggering the convection is presented in section 4.7. Finally, a summary of the case is given in section 4.8.

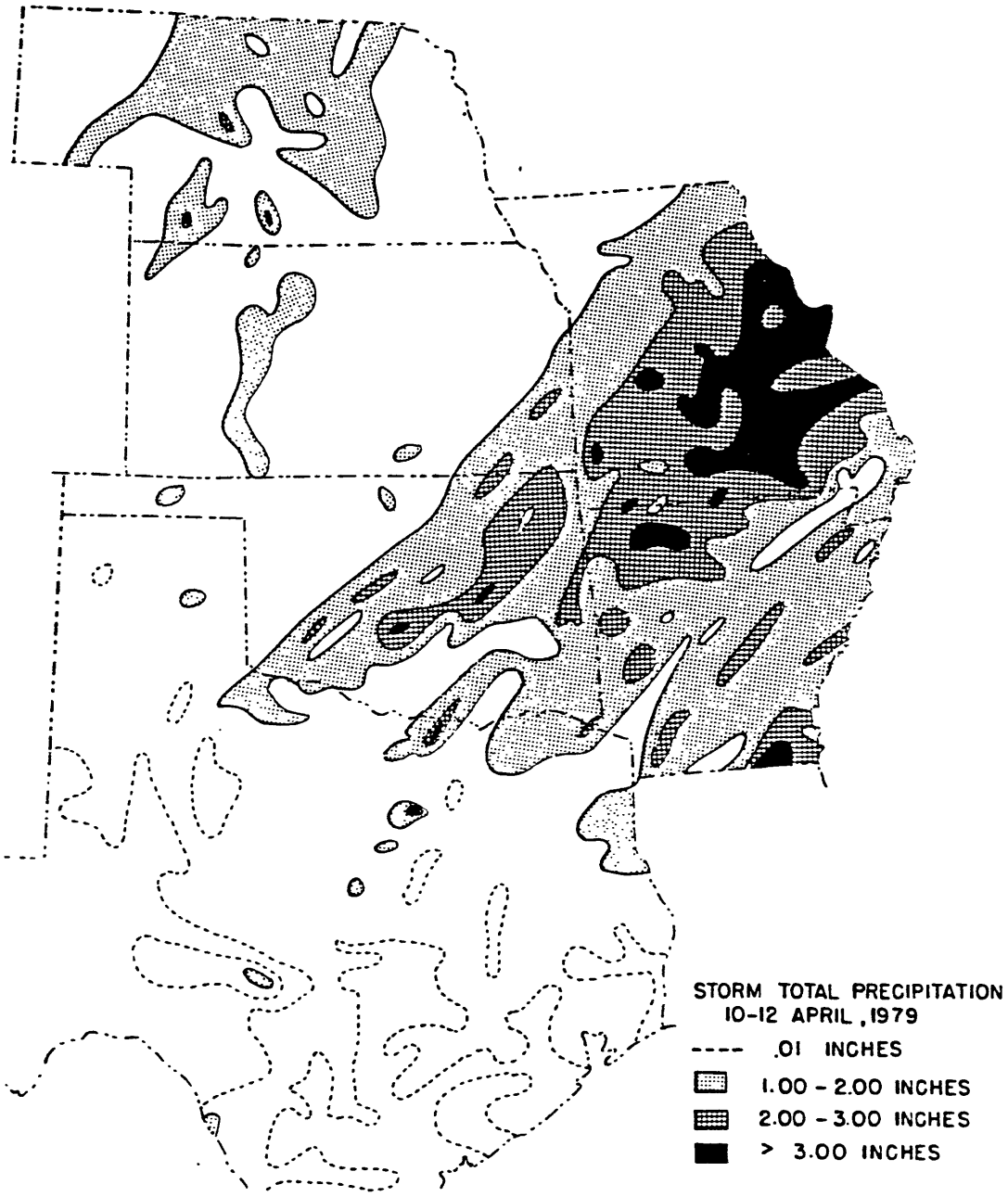


Figure 4.1.2. The storm total precipitation compiled from the U.S. Climatological daily precipitation records.

4.2 DATA SOURCES

The number of observational studies that have been able to investigate the interaction between the larger scale and the mesoscale has been limited by the resolution of the conventional network of upper-air data collection. This network is not able to resolve sub-synoptic and mesoscale systems adequately, making it necessary to execute specific experiments, with a higher density data collection, in order to obtain this information for research purposes.

In 1964 NASA initiated the Atmospheric Variability Experiment (AVE). Their goal was to obtain high resolution data sets during meteorological conditions that contained different types of mesoscale systems. Nine separate experiments were conducted. These data sets have aided in the development of a better understanding concerning the formation, maintenance and decay of mesoscale systems. As a continuation of this approach another field program was conducted in the spring of 1979. Project Severe Environmental Storms and Mesoscale Experiment (SESAME) collected data sets that utilized all of the existing observational abilities. SESAME further extended the time and space resolution of AVE, resolving meso-meteorological systems whose wavelengths range from < 100 km to 1000 km and whose time-scales vary between 1.5 hours and 24 hours. One basic hypothesis of SESAME was that severe storm systems are phenomena of the meso-β scale (25 km to 250 km), comprised of individual elements of the meso-γ scale (2.5 to 25 km), and are organized or initiated by processes on the meso-α scale (250 to 2,500 km). This strong dependence between scales has

already been demonstrated in the previous chapter where it was found that the preferred area for the occurrence of elevated convection was determined by the large-scale circulation.

A knowledge of the specific meteorological situation with respect to these different scales is therefore a requirement of any data set that is to be used for a detailed case study of elevated thunderstorms. SESAME data sets are unprecedented in this respect and, for that reason, this case (AVE-SESAME I; 10 and 11 April 1979), was chosen. Following is a summary of SESAME and the different observations available.

SESAME was carried out in two phases, each related to a domain size: first, a regional domain covering a 1500 km square region in the central United States; second, a storm-scale domain covering a 400 km square area. This nesting of domains is shown in figure 4.2.1. There were six individual 24-hour experiments, three for each phase. The specific operating dates were selected on the likelihood of the development of severe weather.

AVE-SESAME I was a regional domain experiment. 23 of the existing National Weather Service sites in the 1500 km square region released soundings at 3-hourly intervals. There were an additional 18 supplemental sites for a total of 41 rawinsonde sites for the experiment. The supplemental sites provided enhancement over the whole region. The processed data set used in this study consists of data at 25-mb intervals and was obtained on both magnetic tape and hard copy. For a detailed discussion of the data set refer to Appendix I.

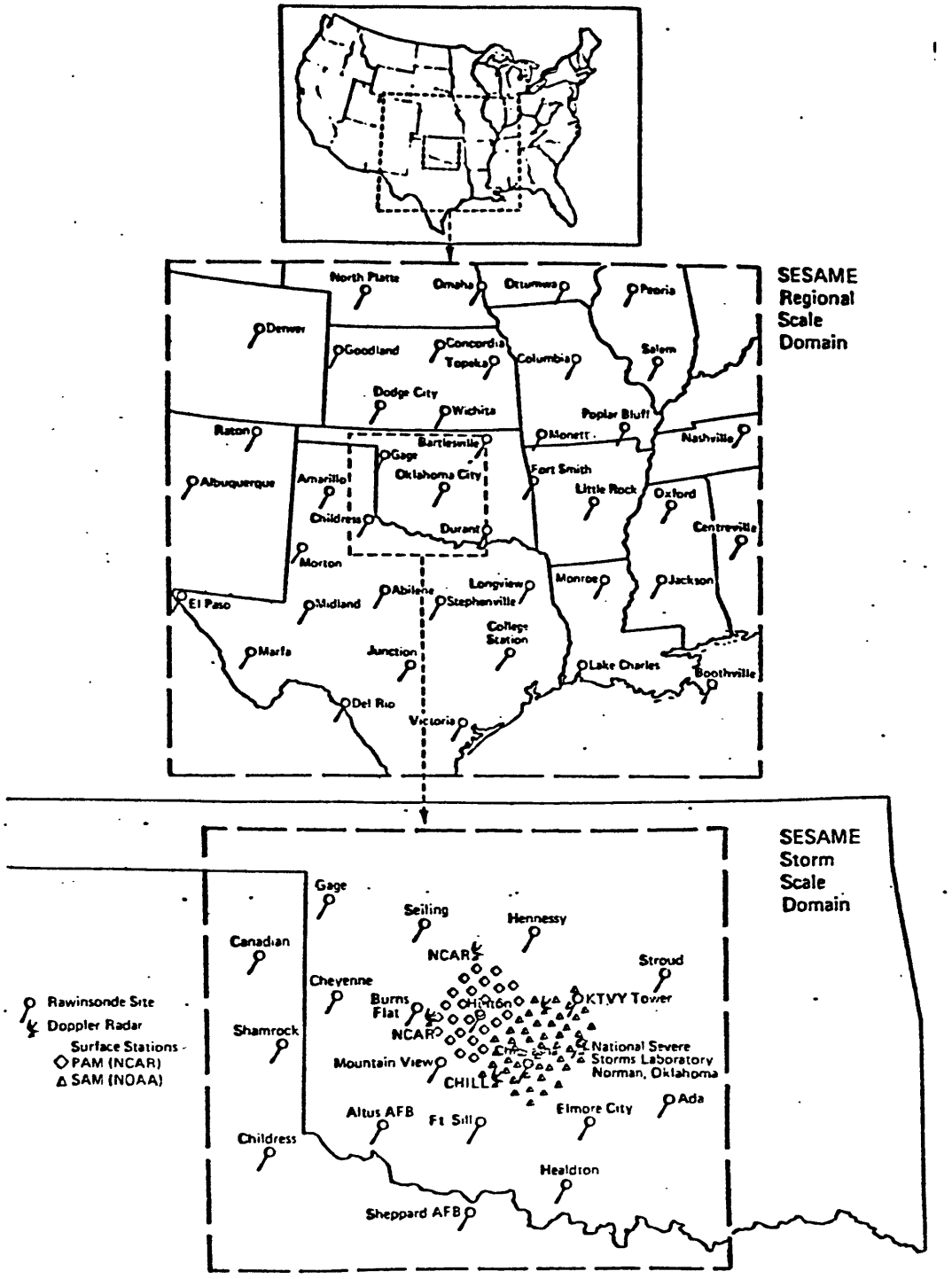


Figure 4.2.1. The observing networks for AVE-SESAME 1979 (Alberty and Barnes, 1979).

In addition to the processed rawinsonde soundings, a grid point data set was obtained from Purdue University, which had values every 50 mb from 950 mb to 100 mb, as well as surface data. The grid spacing was one degree of latitude by one degree of longitude with a domain bounded by 42°N, 85°W, 28°N and 107°W. This data set contained geopotential, u-velocity, v-velocity, temperature, relative humidity and p-velocity (ω). Refer to Appendix II for a more detailed discussion of this data set and a map showing the grid domain. In this study the vertical p-velocities from the data set were used directly. The data set was also used to derive the geostrophic wind, SLI's, LI-850's and divergence.

A large set of hourly surface observations was collected using two sources. A magnetic tape obtained from the Florida State University Archive contained all the synoptic and airway observations that were obtained via the AWN (air weather net) for the period 00 GMT 10 April to 23 GMT 11 April, 1979. In addition, this set was supplemented using Service A observations available on hard copy from 14 GMT 10 April to 05 GMT 11 April. An incomplete set of microbarograph traces was also obtained.

Daily precipitation records for Nebraska, Kansas, Missouri, Oklahoma, Arkansas and Texas were ordered from the National Climatic Center (NCC). Radar films were also purchased from the NCC to complete a detailed analysis of the individual convective elements. These films consisted of photographs of the plan position indicator

(PPI) scope at intervals ranging from as often as every 40 seconds to at least every 5 minutes. Satellite pictures were also used to locate some of the early areas of cloud development.

4.3 SYNOPTIC OVERVIEW

The surface analysis for 12 GMT 10 April, 1979 is shown in Figure 4.3.1. A large surface ridge was established over the eastern United States with a developing southerly flow over the western Great Plains. Farther west, a large cyclonic circulation was centered over southeast Wyoming. Light precipitation was being reported at several locations in a band extending from Montana southeastward toward Missouri. The 1435 GMT 10 April radar summary (Figure 4.3.2) shows that the precipitation was generally showery with the maximum cell tops being reported to be 24,000 ft over northwest Arkansas. The cells and echo areas were moving off toward the northeast, associated with a clearly defined short wave at 500 mb over Kansas. See figure 4.3.3 which shows the upper-air analyses for 12 GMT 10 April.

Another feature at 500 mb was a strong difluent short-wave trough digging southeastward from the Northwest. The surface cyclone over southeast Wyoming was redeveloping in response to this advancing wave. The isotach analysis for 850 mb shows a broad region of southerly winds greater than 20 kts. extending from the Gulf Coast to the Canadian border with a wind speed maximum over the eastern Panhandle of Oklahoma exceeding 40 kts.

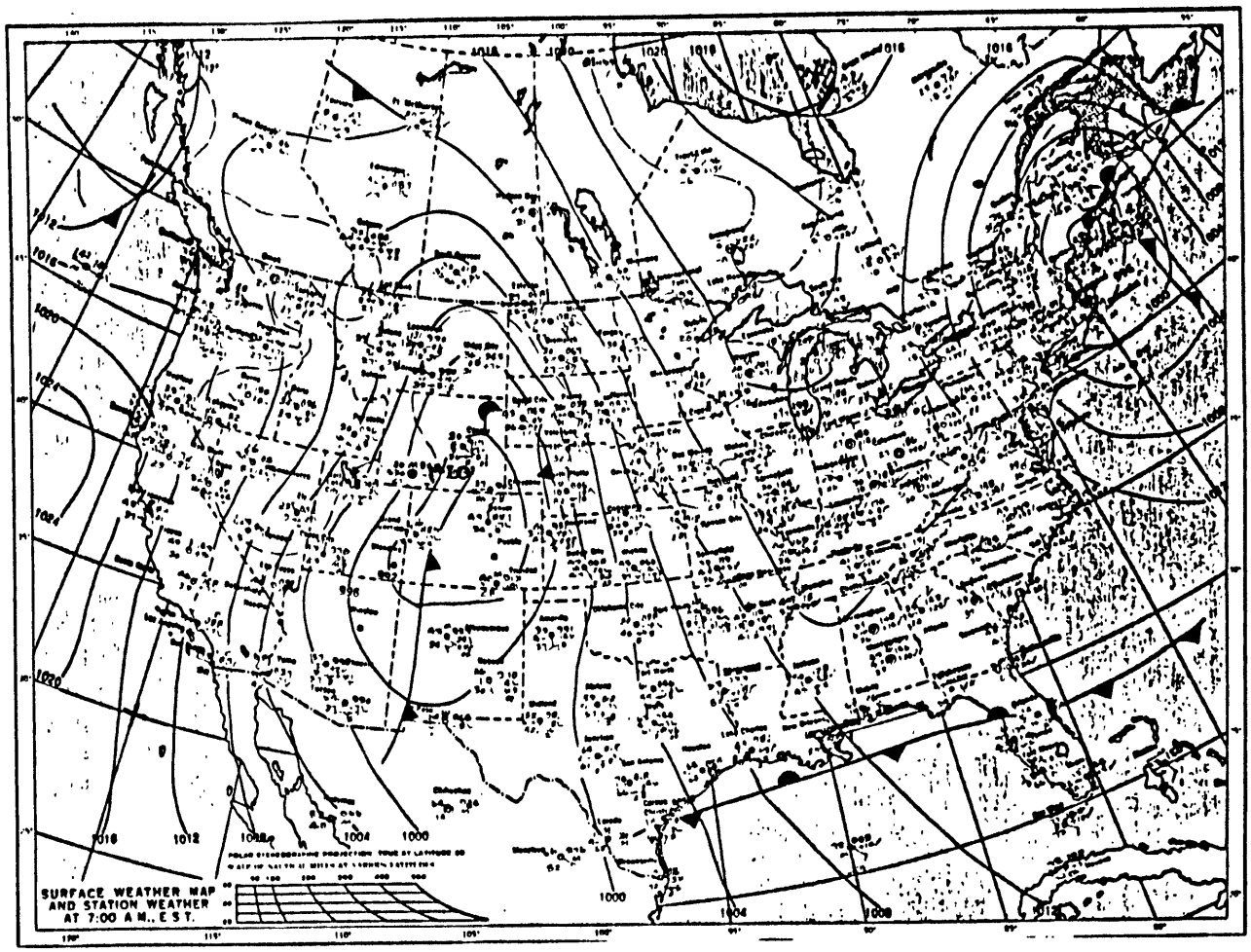


Figure 4.3.1. The surface analysis for 1200 GMT 10 April 1979 (U.S. Dept. of Commerce, 1979).

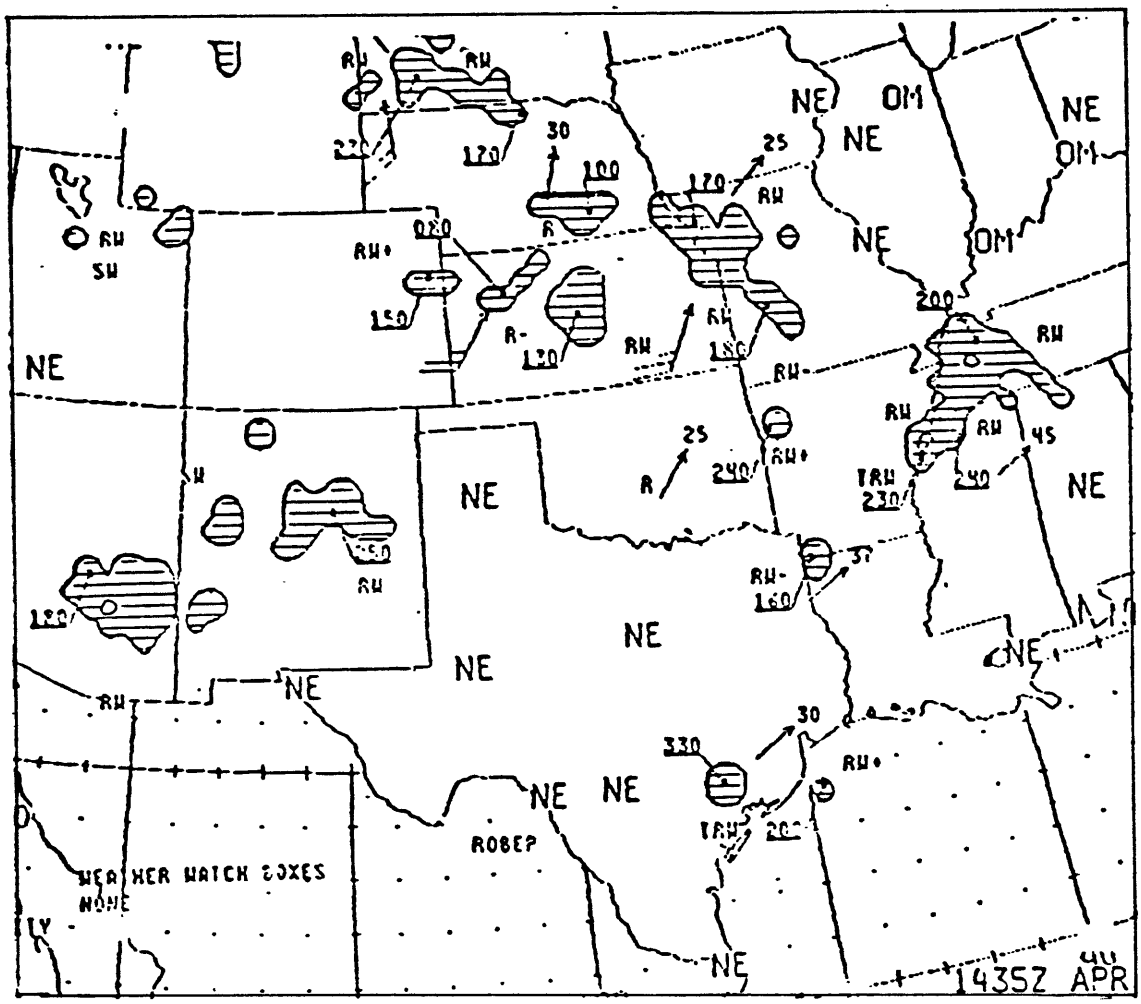
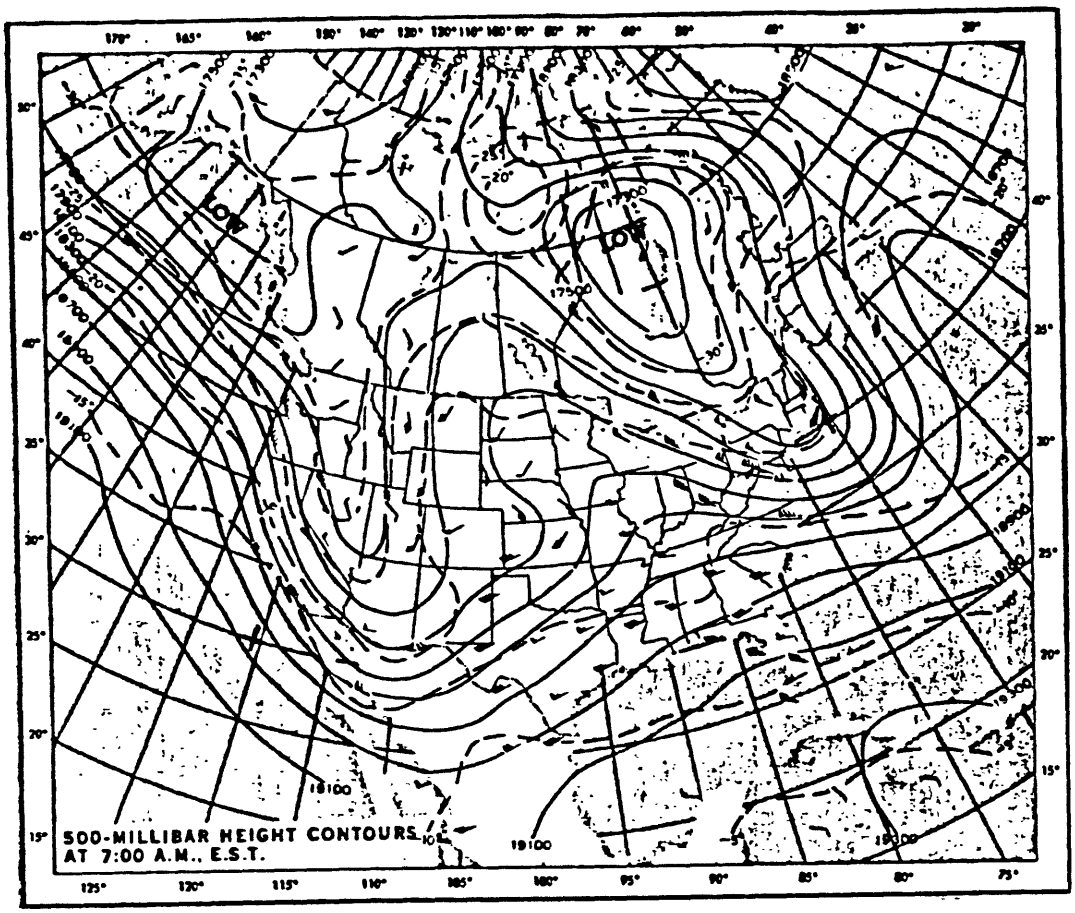


Figure 4.3.2. The 1435 GMT 10 April 1979 radar summary showing the areas of precipitation (shaded), cell tops in hundreds of feet, directional barbs (group motion) and directional vectors (individual cell motion).



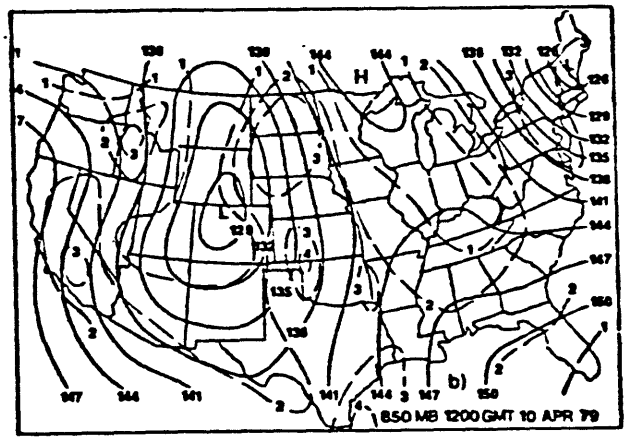


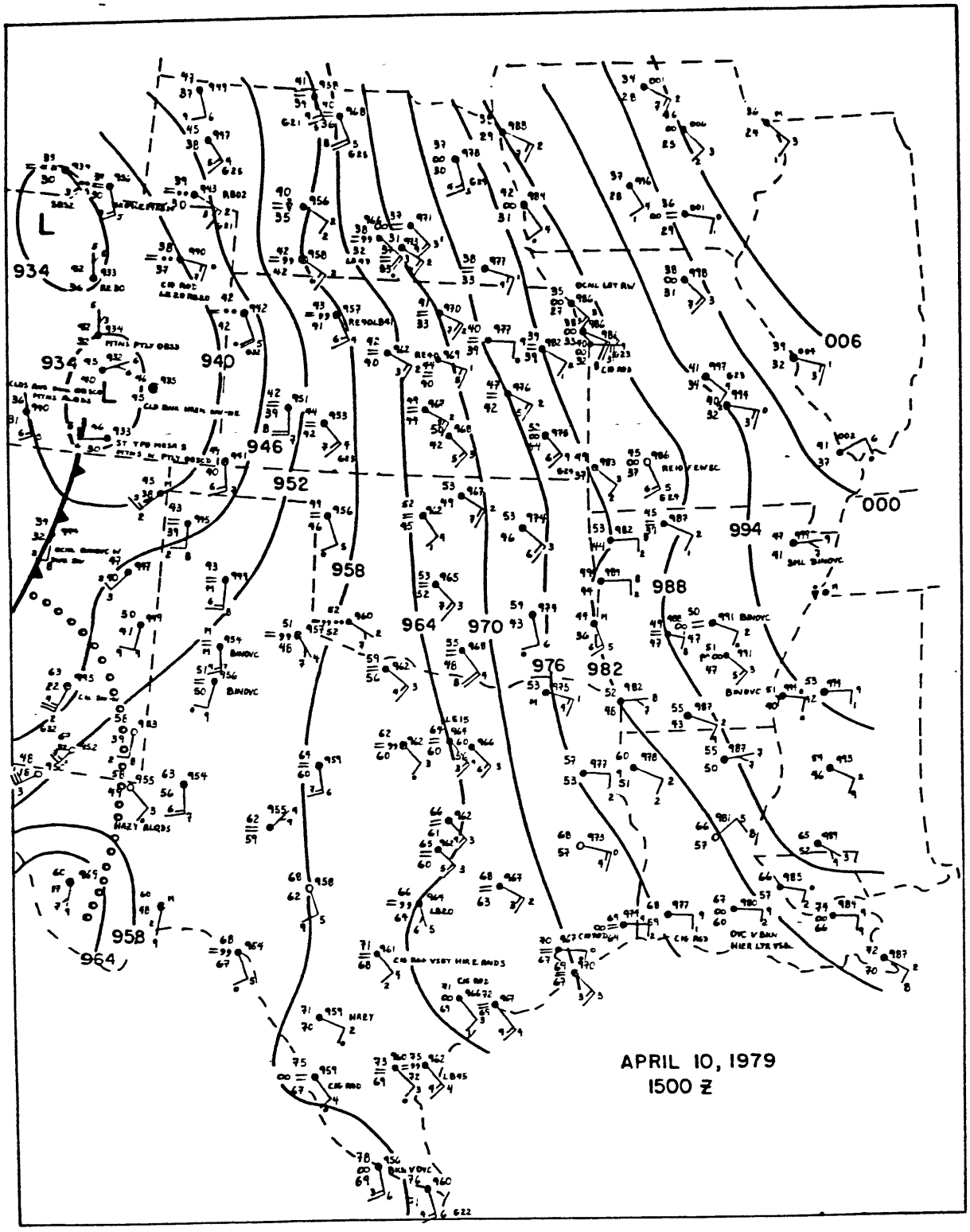
Figure 4.3.3. (a) The 500-mb analysis for 1200 GMT 10 April 1979. The solid lines are height contours (ft). The dashed lines are isotherms (°C). The wind barbs are in knots (U.S. Dept. of Commerce, 1979). (b) The 850-mb analysis for 1200 GMT 10 April 1979. The solid lines are height contours (dm). The dashed lines are isotachs, labeled in tens of knots (Moore and Fuelberg, 1981).

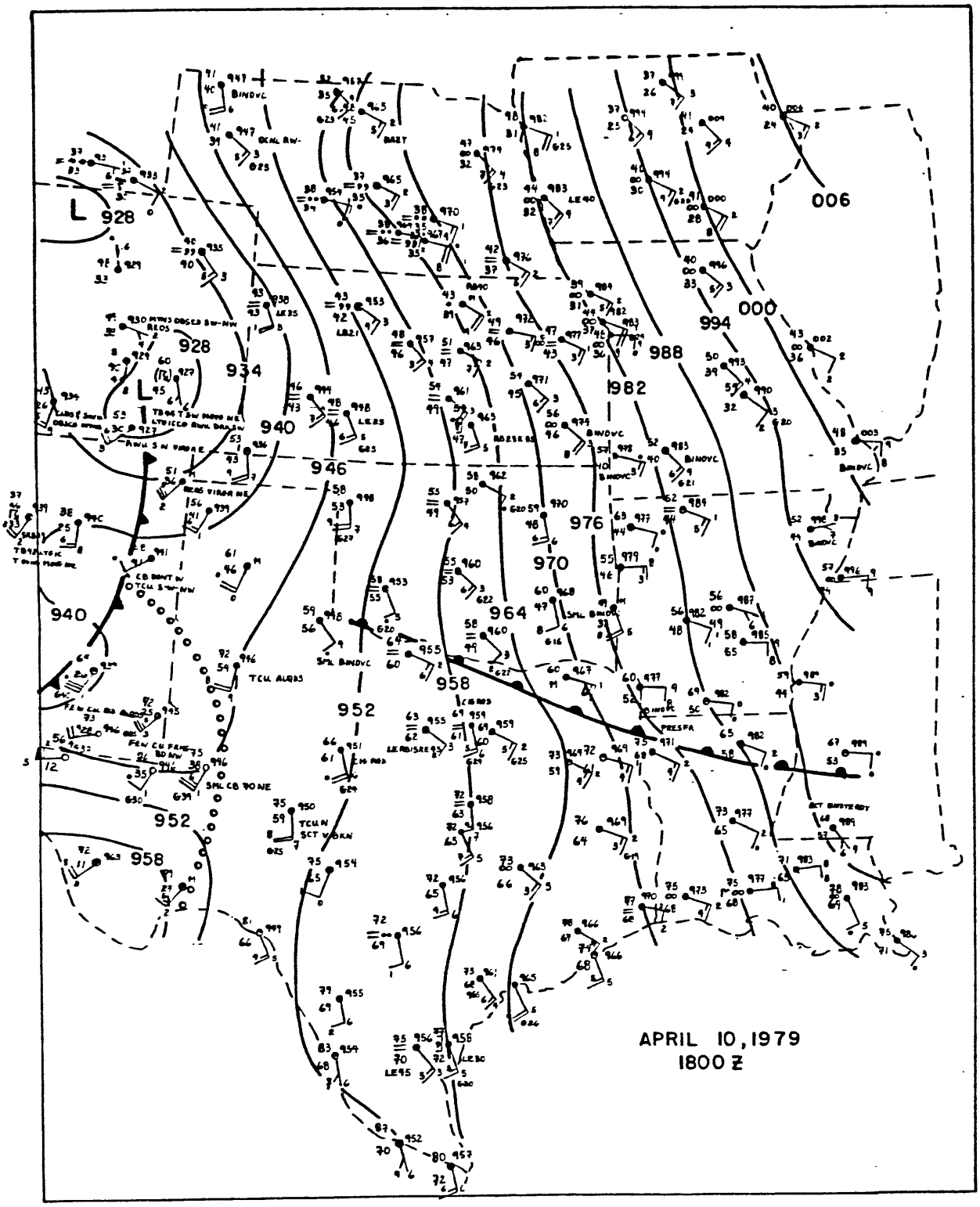
This synoptic situation is similar to type (b) discussed in the previous chapter where the surface front from a preceding system has pushed well south of the new upper-level forcing. The Gulf return flow established by the new system is illustrated in this case by the strong southerly winds at 850 mb.

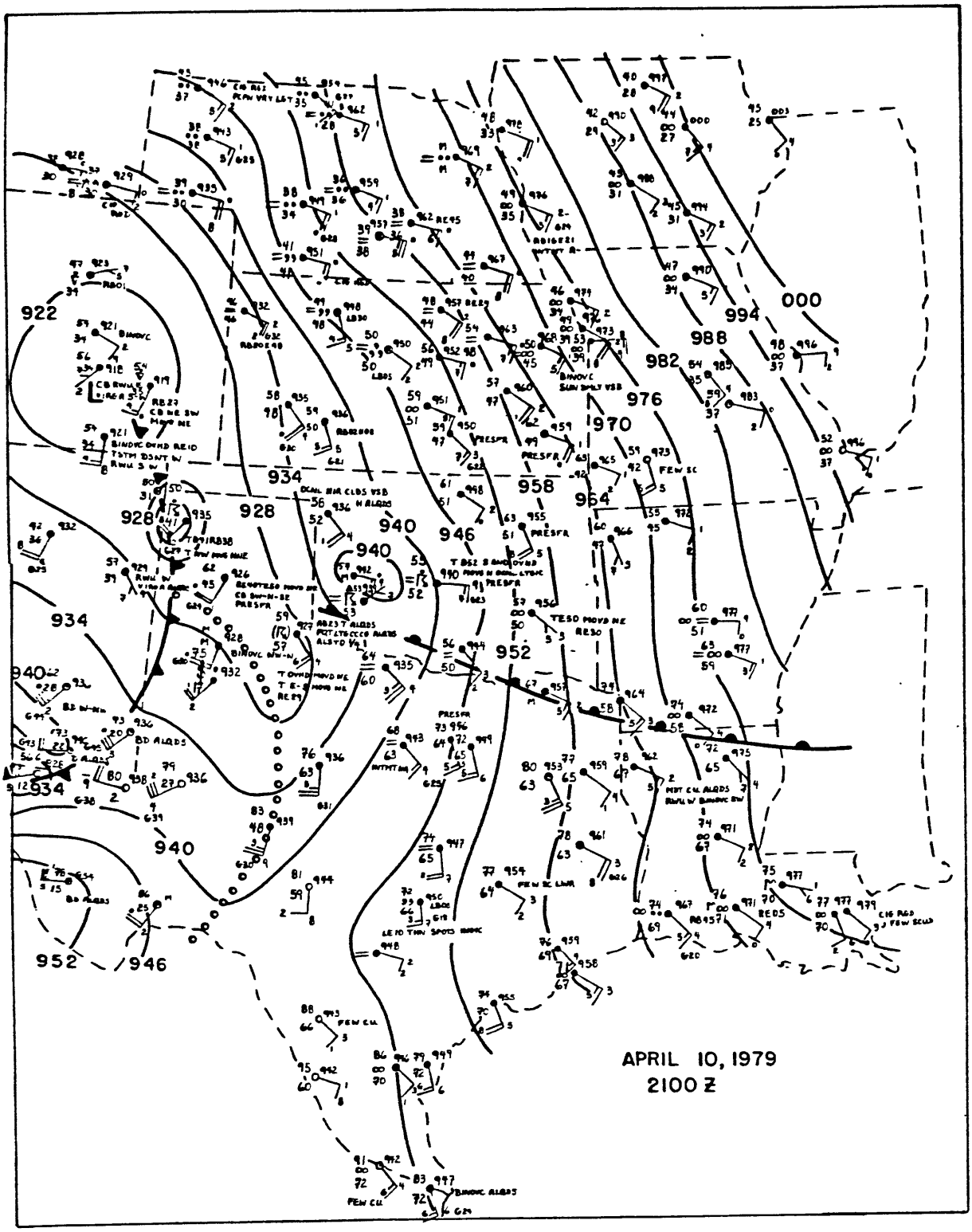
Figure 4.3.4 is a series of 3-hourly mesoscale surface analyses for the period from 15 GMT 10 April to 03 GMT 11 April, and 21 GMT 11 April. The entire series of surface maps from 15 GMT 10 April to 21 GMT 11 April every three hours, plus the upper-air analyses for 850 mb and 500 mb from 15 GMT 10 April to 12 GMT 11 April every three hours, are available in Appendix III for reference. At 15 GMT the surface temperatures ranged from the mid-thirties over Iowa to the upper seventies near Brownsville, Texas. Although this is a very large temperature range there was not a clearly defined warm front. A dryline was positioned over eastern New Mexico and western Texas. At 18 GMT the dryline had advanced farther into Texas and a developing surface warm front was defined by a weak pressure trough and a temperature/moisture contrast. A strong jet streak which was moving into the region is evident at 500 mb over southwest Texas on the 500-mb analysis for 18 GMT 10 April (figure 4.3.5).

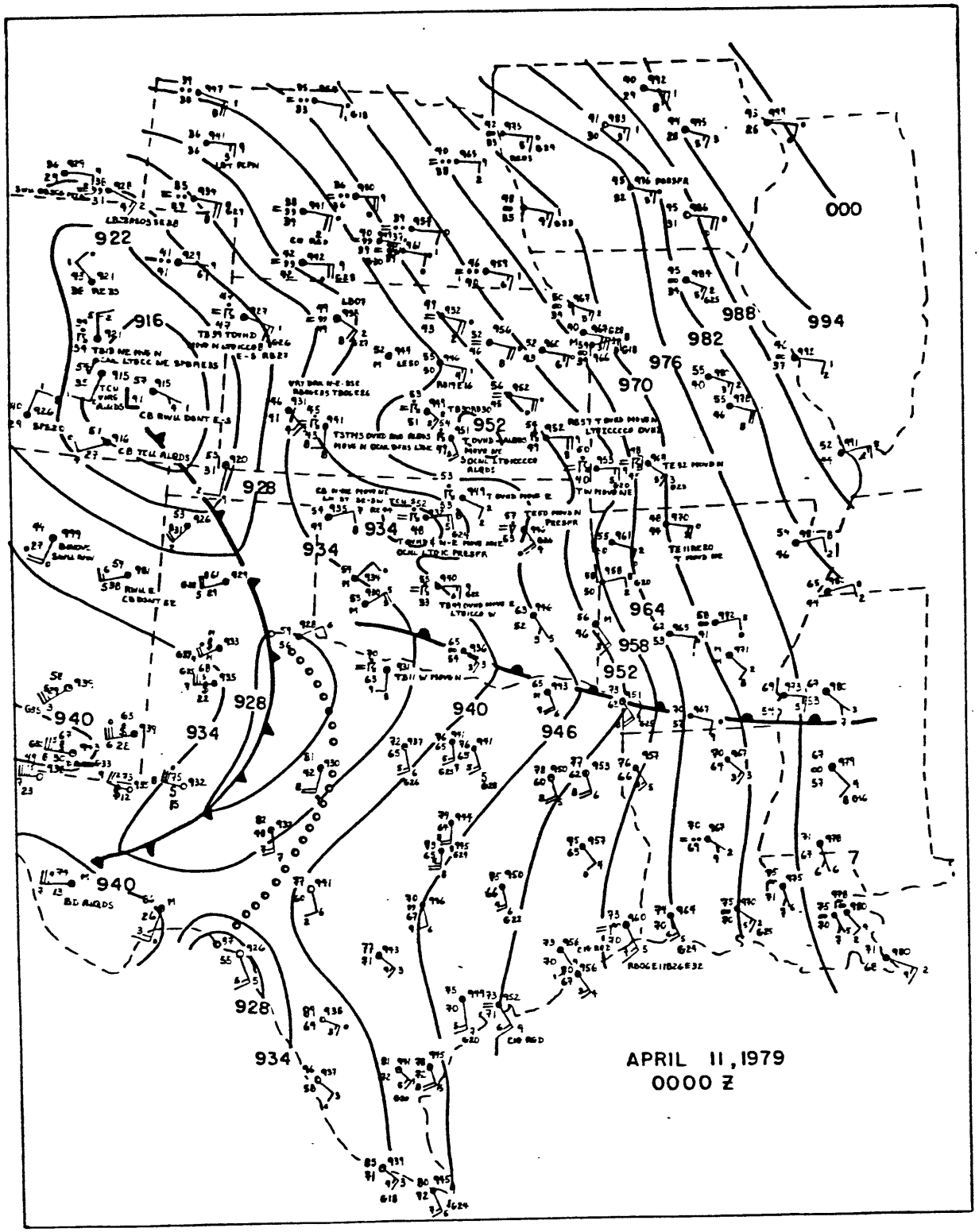
The first convection broke out in two regions just before 18 GMT. Several parallel convective lines formed just north of the dryline over the Texas Panhandle while another convective line developed in an east to west orientation across northern Texas. These two regions are evident in the satellite picture from 18 GMT (see

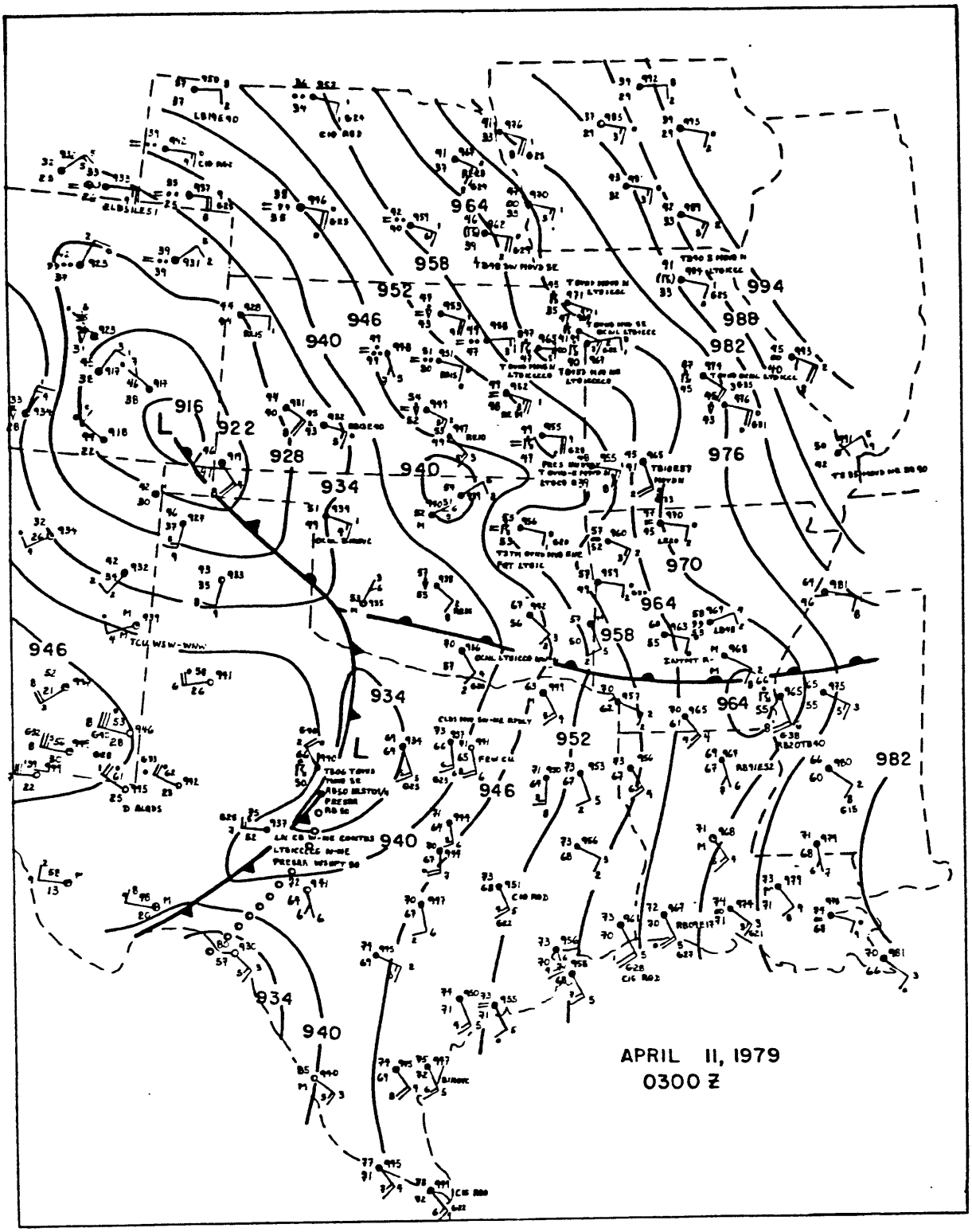
Figure 4.3.4. Mesoscale Surface Analyses for the period from 1500 GMT 10 April 1979 to 0300 GMT 11 April 1979 (every 3 hours) and 2100 GMT 11 April 1979. The solid lines are isopleths of altimeter setting (970 = 29.70" of Hg). The station model is conventional, with temperatures in °F and wind in kts. The position of the dry line is marked with a line of circles.

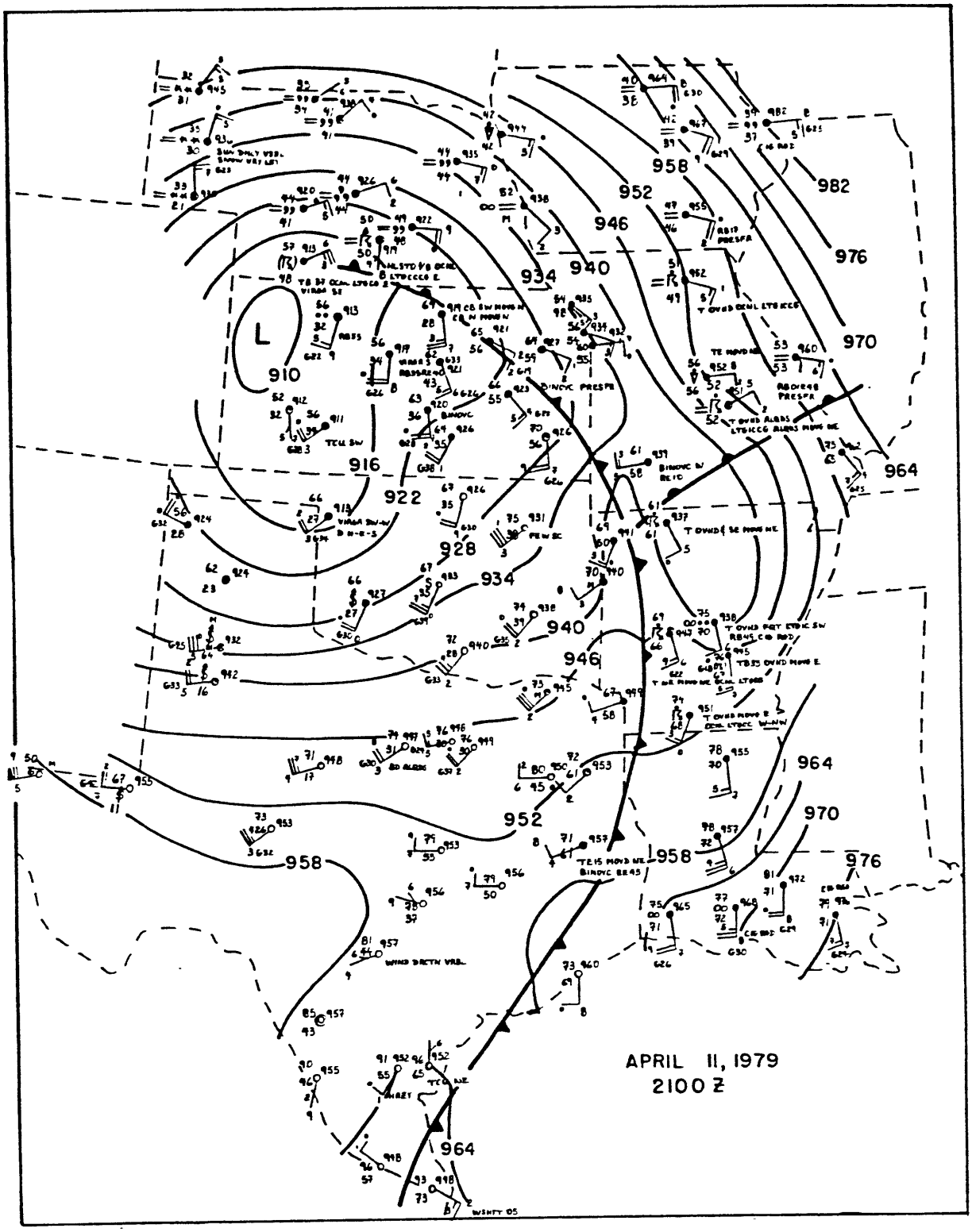

APRIL 10, 1979
1500 Z


APRIL 10, 1979
1800 Z


APRIL 10, 1979
2100 Z


APRIL 11, 1979
0000 Z


APRIL 11, 1979
0300 Z


L
910
916
922
928
934
940
946
952
958
964
970
976
982
APRIL 11, 1979
2100 Z

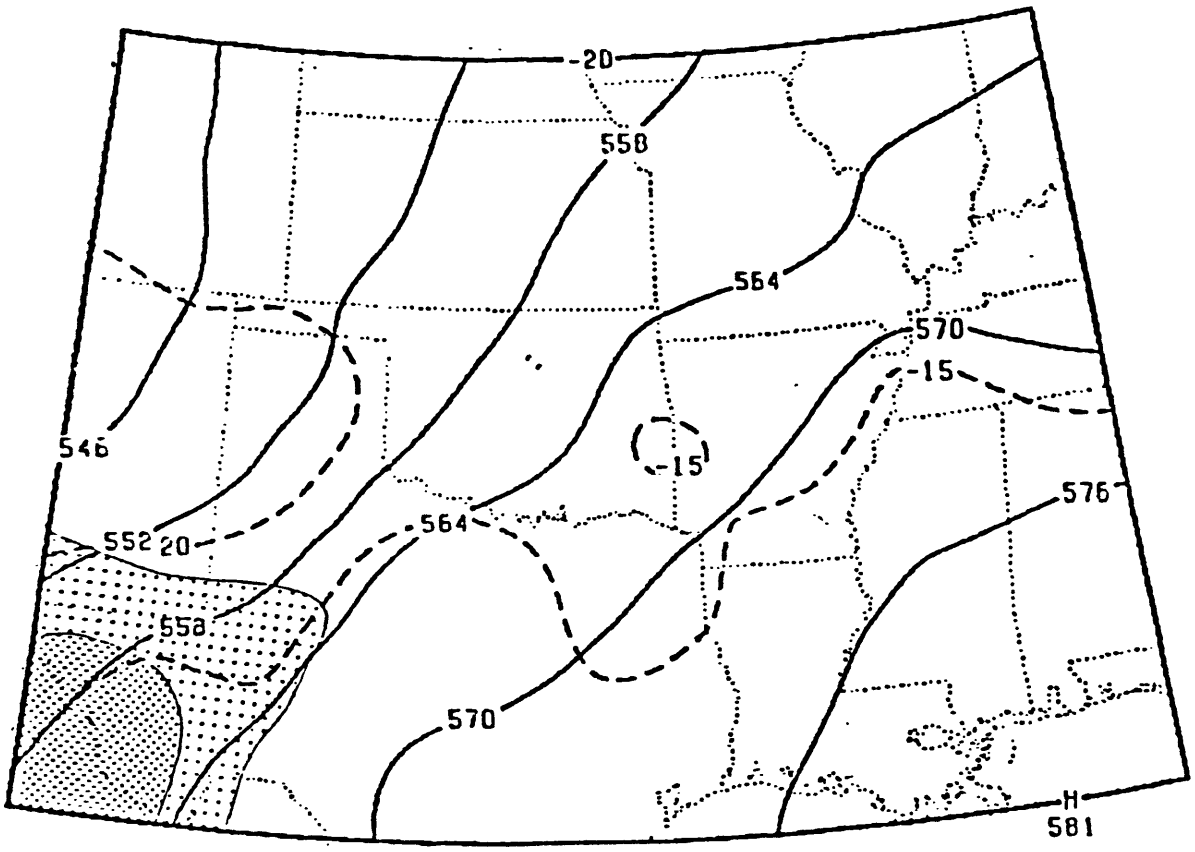


Figure 4.3.5. The 500-mb analysis for 1800 GMT 10 April 1979. The solid lines are height contours (dm). The light shading is for wind speeds 30-39 m/s and dark shading for wind speeds 40-49 m/s. The dashed lines are isotherms (°C).

Figure 4.3.6). General cloud cover is seen extending from the Texas Gulf Coast northward into Nebraska. The cloud deck was generally shallow with the convection protruding above.

At 21 GMT the first plotted elevated thunderstorms are found over Oklahoma. Oklahoma City (OKC) is reporting a thundershower with a temperature of 55°F and a 52°F dew-point, representative for the area north of the warm front. The geographical locations of the stations referenced in this chapter are all shown in Figure 4.8.1 at the end of this chapter. These temperatures give a lifted temperature of -19°C at 500 mb. The OKC sounding at 2005 GMT showed an ambient 500-mb temperature of -15.5°C. Figure 4.3.7 shows the plotted sounding. The frontal inversion is clearly defined in both the reported winds and temperature. The 850-mb air shows a 0.1°C depression and essentially no negative area (the moist pseudo-adiabat for the air at 850 mb has been plotted). The 850-mb air is 3.3°C positively buoyant at 500 mb and remains positively buoyant until 300 mb. This convection is clearly not rooted in the boundary layer.

AT 00 GMT 11 April numerous stations in Kansas, Missouri and Oklahoma are reporting thunderstorms. These are all occurring where the planetary boundary layer is stable and are of the elevated type. This will be discussed in more detail in section 4.4. The pressure field shows a lot of small-scale structure in the region of the convection. This is very characteristic of elevated convection and is apparently the manifestation of ducted gravity waves as will be discussed in section 4.7. During this same period the upper level jet

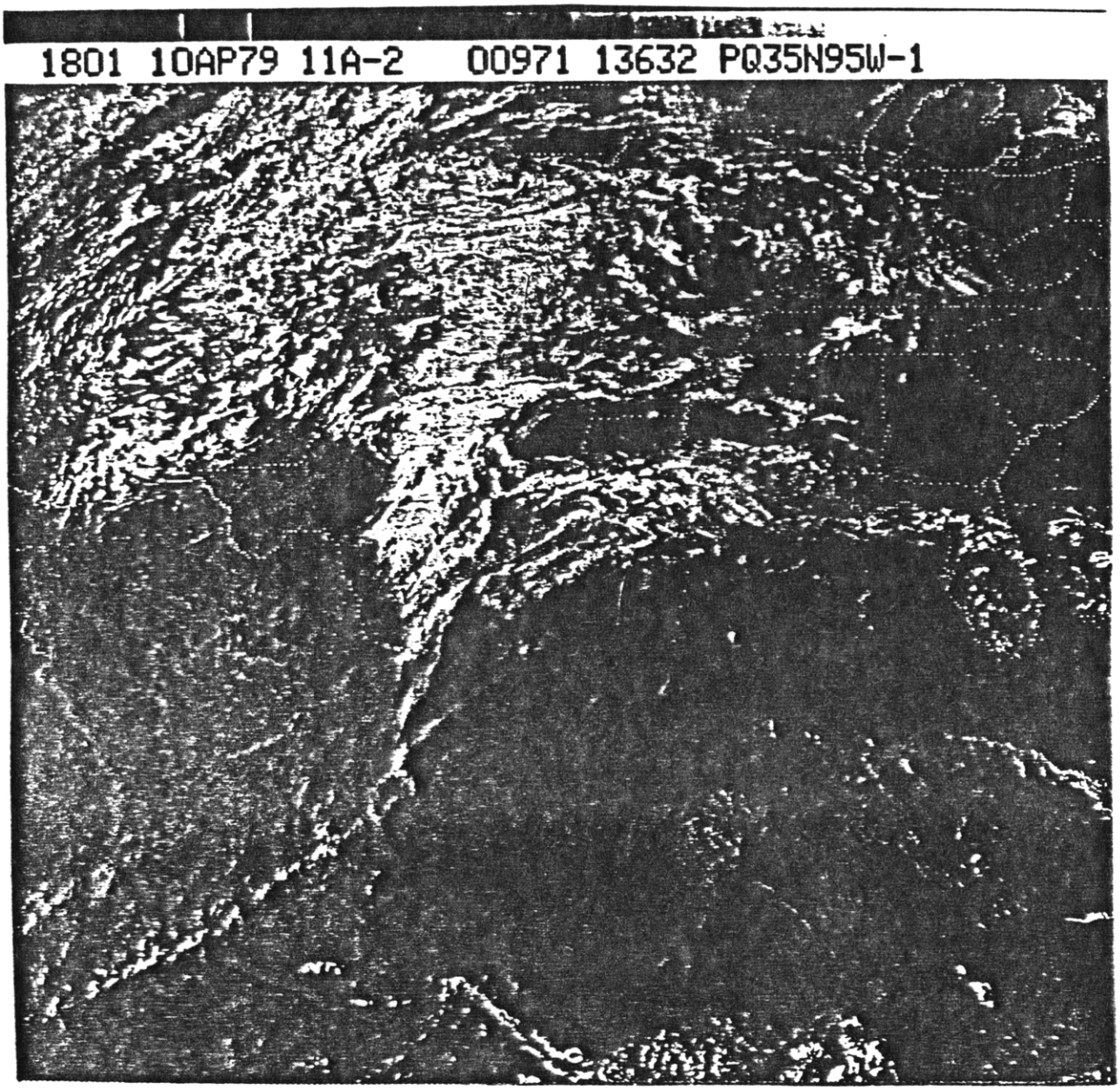


Figure 4.3.6. The visible satellite picture for 1801 GMT 10 April 1979.

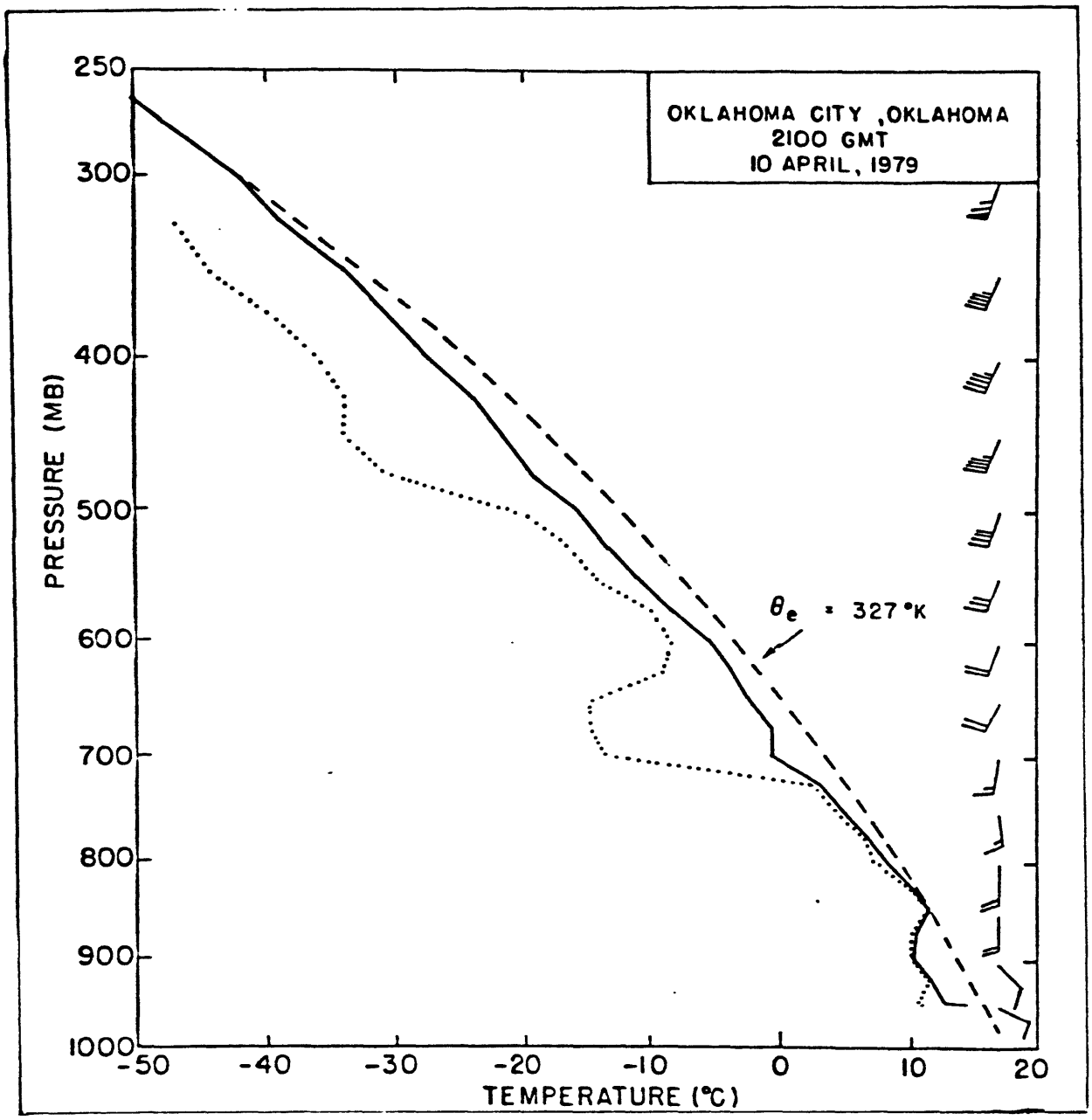


Figure 4.3.7. Radiosonde sounding for Oklahoma City at 2100 GMT 10 April 1979. The solid line is the temperature curve, and the dotted line the dew-point temperature curve. The wind (m/s) is plotted for each level using standard meteorological convention. The pseudo-adiabat for the 850-mb air (θ_e = 327°K) is also shown.

streak had extended northeastward over Oklahoma. The 850 mb winds had also increased from the south over Oklahoma, Arkansas and Louisiana. It was approximately 00 GMT 11 April when the devastating Wichita Falls tornado struck.

South of this convection, strong boundary layer winds continued to transport heat and moisture northward across Texas. The boundary layer over this region actually showed moderate to strong instability with the SLI's ranging between -4°C at SJT on the dry side of the dryline to -7°C at Brownsville, Texas (BRO). Deep convection was however inhibited by a strong inversion which was the result of hot dry air moving northeastward from the Mexican Plateau. This configuration has been recognized as being favorable for severe convection (Carlson and Ludlam, 1968). Figure 4.3.8 shows a cross section from El Paso, Texas (ELP) to Longview, Texas (GGG) for 00 GMT 11 April. The various airstreams involved are clearly evident. The warm moist Gulf of Mexico air moving northward on the south-southeasterly winds overlain by hot dry Mexican air is visible at SEP. The hot dry continental air is seen at the surface between the advancing cold front and the dryline. It will be shown later that although the capping inversion inhibits deep convection from the Gulf air, shallower convection below the cap plays an important role in priming the atmosphere for subsequent convection.

Elevated convection continued to spread northward and was reported more than 650 km north of the warm front at IRK at 0300 GMT 11 April.

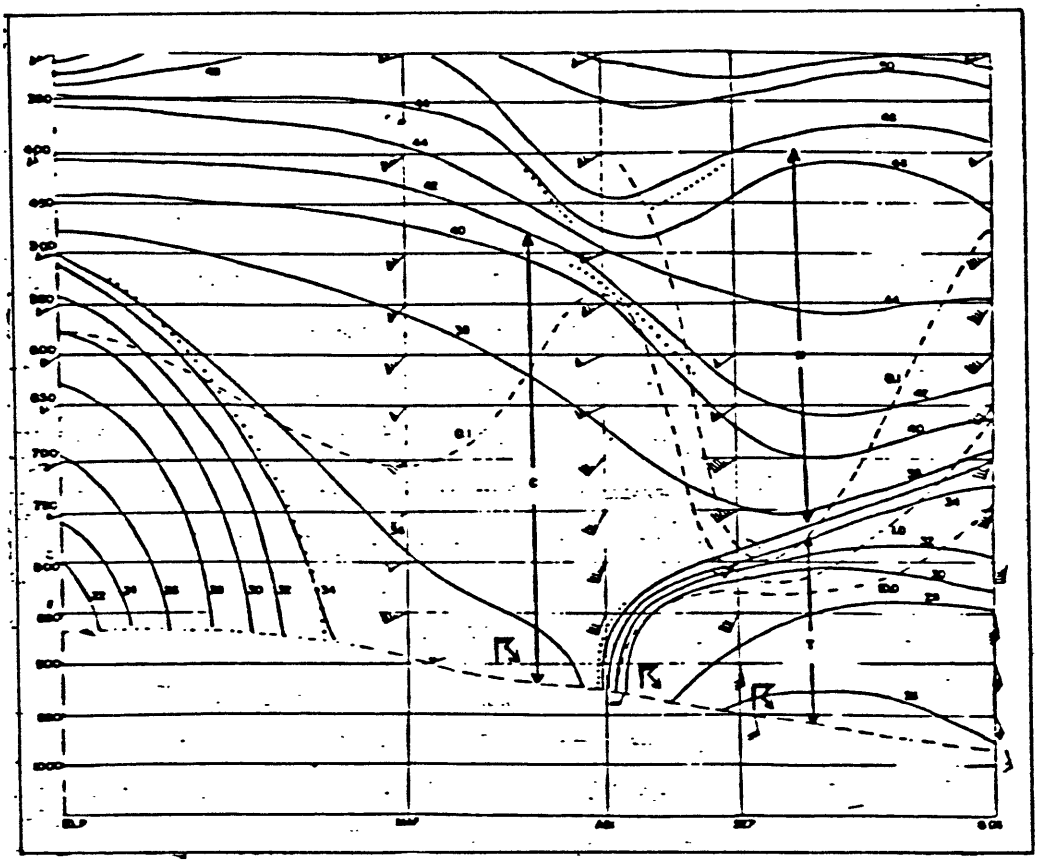


Figure 4.3.8. A cross section for the line from ELP to GGG for 0000 GMT 11 April 1979. Thin solid lines are isentropes and the dashed lines are isopleths of mixing ratio (g kg^{-1}). The segments labeled M, T, and C refer to the airstreams from Mexico, the Gulf of Mexico, and the Rocky Mountains, respectively. The dotted segments define the baroclinic zones. The wind is plotted in the conventional manner (Carlson et al., 1980). The positions of convective clouds are indicated with a ⌈ symbol.

The 0235 GMT 11 April radar summary (figure 4.3.9) shows the extensive precipitation area over Kansas and Missouri. The echo tops across this region were as high as 47,000 ft (in extreme southern Illinois). Other convective regions were located in Oklahoma and central Texas. The band in central Texas was positioned near the intersection of the advancing surface cold front and the dryline. This band was responsible for a second outbreak of severe weather. The convective regions were aligned along a strong gradient in the equivalent potential temperature at 850 mb (see Figure 4.3.10).

Elevated convection continued over the area through the night and into the next day. This prolonged activity was most likely related to the slow moving surface system and the maintenance of a cold boundary layer north of the warm front. The warm air at the surface did not advance northward, but instead appeared to have stalled across southern Oklahoma and central Arkansas. This position is related to the local topography (see figure 4.3.11) with the cold stable boundary layer being protected by the Ouchita, Boston and Ozark Mountains. The cold-frontal trough gradually swung across and northeast, so that by 21 GMT 11 April the only elevated convection being reported was in Missouri.

This extensive outbreak of elevated convection, which lasted more than 24 hours, was responsible for rainfall amounts over Missouri in excess of 4 inches (see Figure 4.1.2). The next section presents a detailed radar analysis that enabled the identification of individual convective elements. The mesoscale structure and lifetime characteristics are discussed.

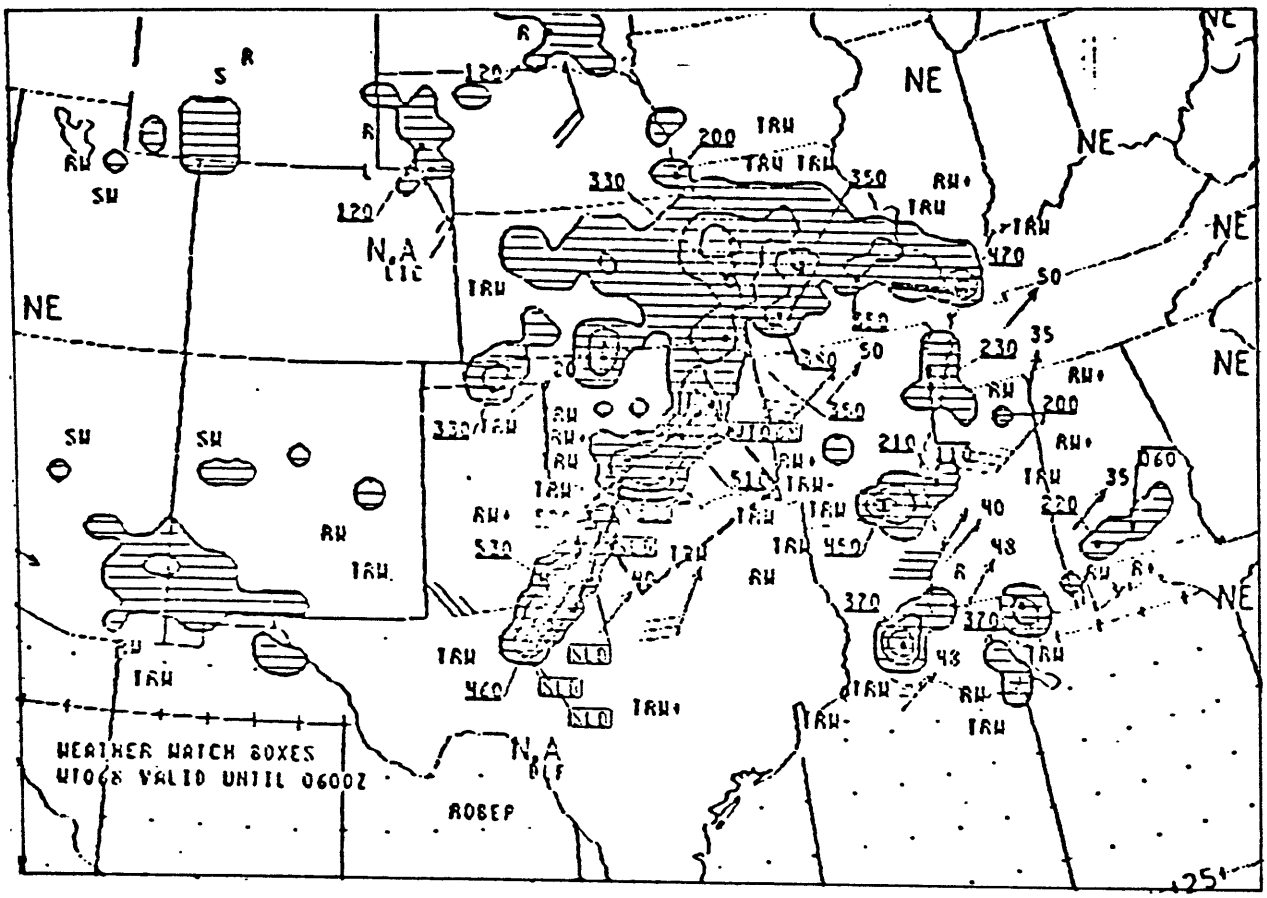


Figure 4.3.9. The 0235 GMT 11 April 1979 radar summary showing the areas of precipitation (shaded), cell tops in hundreds of feet, directional banks (group motion) and directional vectors (individual cell motion).

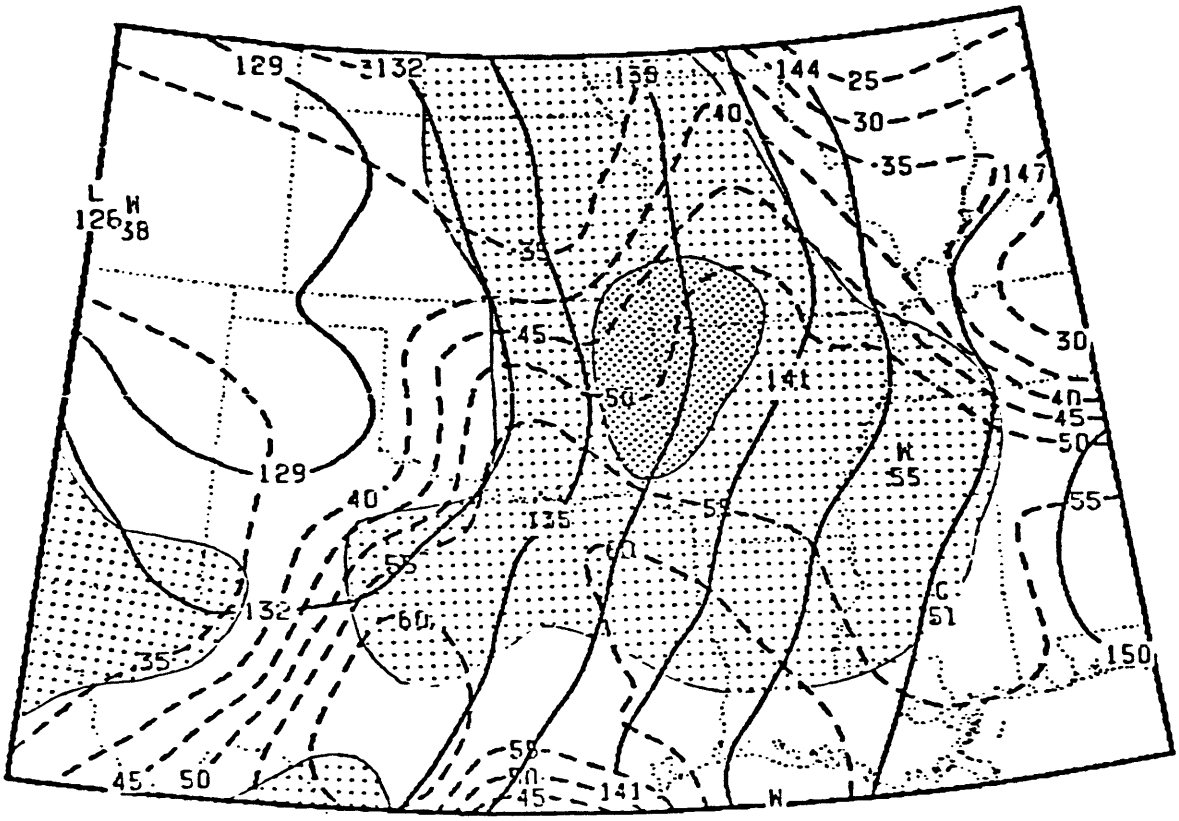


Figure 4.3.10. The 850-mb analysis for 03 GMT 11 April 1979. The solid lines are height contours (dm). The light shading is for wind speeds 20-29 m/s and dark shading for wind speeds 30-39 m/s. The dashed lines are isopleths of equivalent potential temperature (°C).

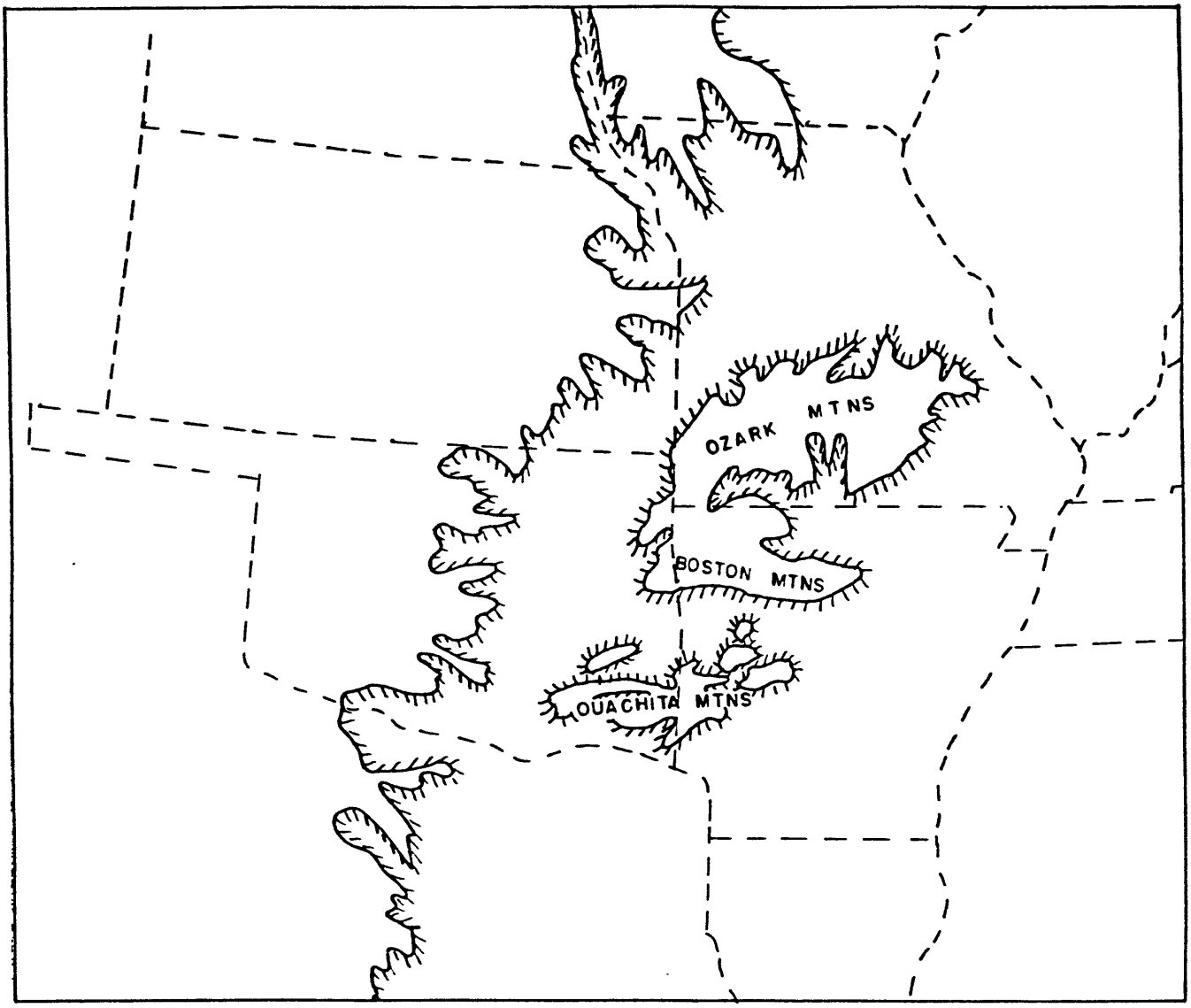


Figure 4.3.11. The 1000 foot elevation contour highlighting the regional topography. The hatching is on the downhill side of the contour.

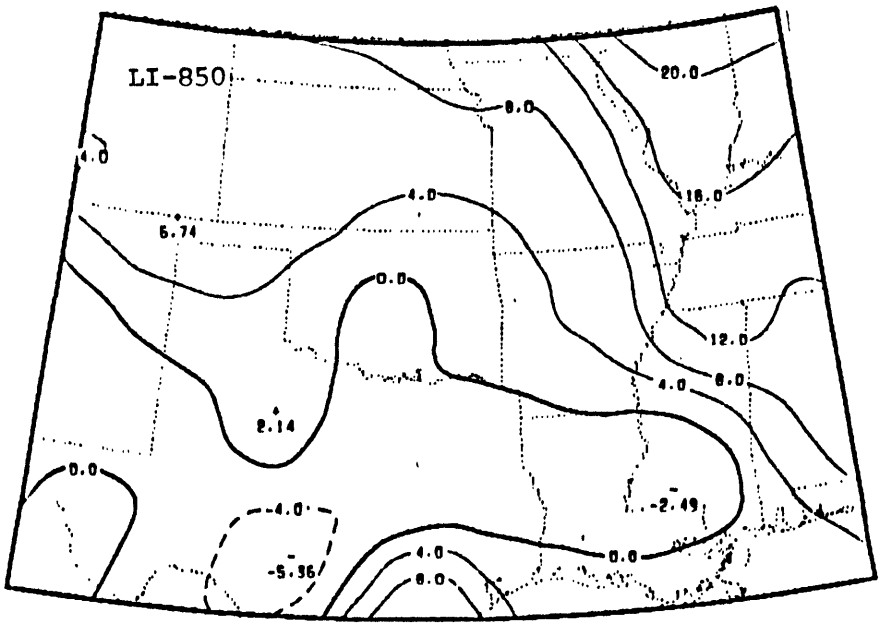
4.4 STABILITY ANALYSIS

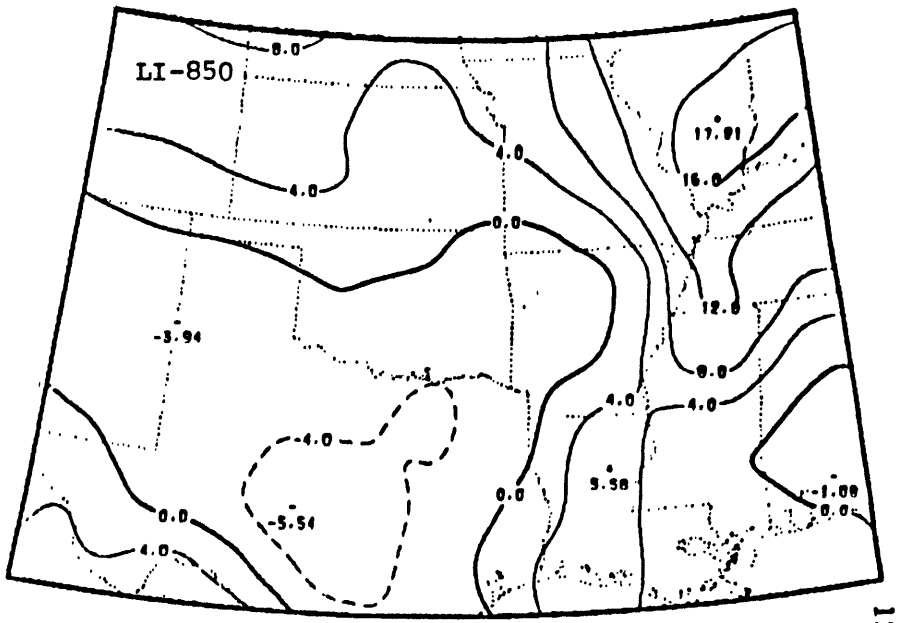
It is clear from the surface analyses in the preceding section that the majority of reported thunderstorms were on the cold side of the analyzed surface front. However, more important in defining an occurrence of elevated convection is to identify an increase of latent instability from the planetary boundary layer to an overriding layer. In this section, following the format of the climatology study, we will compare the SLI's and LI-850's for this case. The lifted indices were calculated using the temperature and relative humidity values from the grid point data set. Note that a result of gridding the data is a smoother field and extreme values that show up when individual observation are used (Sanders, 1983) should not be expected. Figure 4.4.1 contains the series of SLI and LI-850 analyses for the period from 15 GMT 10 April to 12 GMT 11 April.

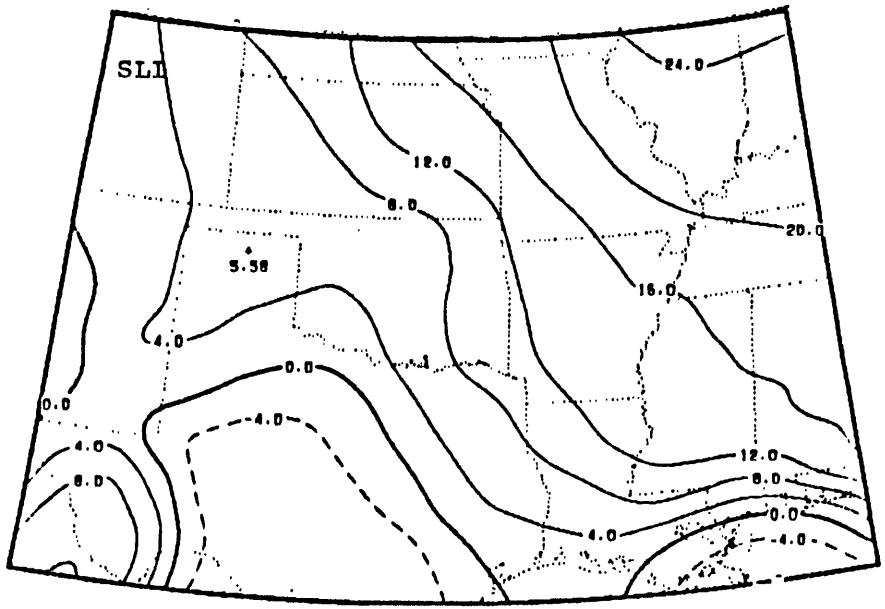
At 15 GMT the 0°C isopleth for the SLI's outlined an unstable region over central and southern Texas with minimum values less than -4°C, while the 0°C isopleth at 850 mb extends farther north, possibly indicating the beginning of an overrunning situation resulting from the strong southerly surface winds. However, with 15 GMT being morning in local time, it may just reflect the cooler nocturnal boundary layer.

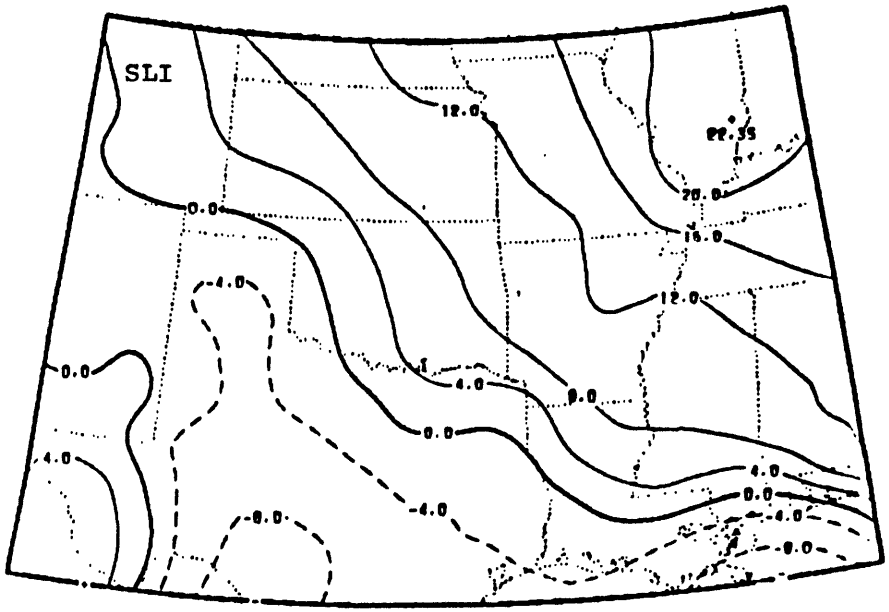
By 18 GMT the SLI values had decreased over Texas, particularly

Figure 4.4.1. The surface lifted indices (SLI) and the 850-mb lifted indices (LI-850) for the period from 1500 GMT 10 April 1979 to 1200 GMT 11 April 1979, every three hours. Units are in °C.



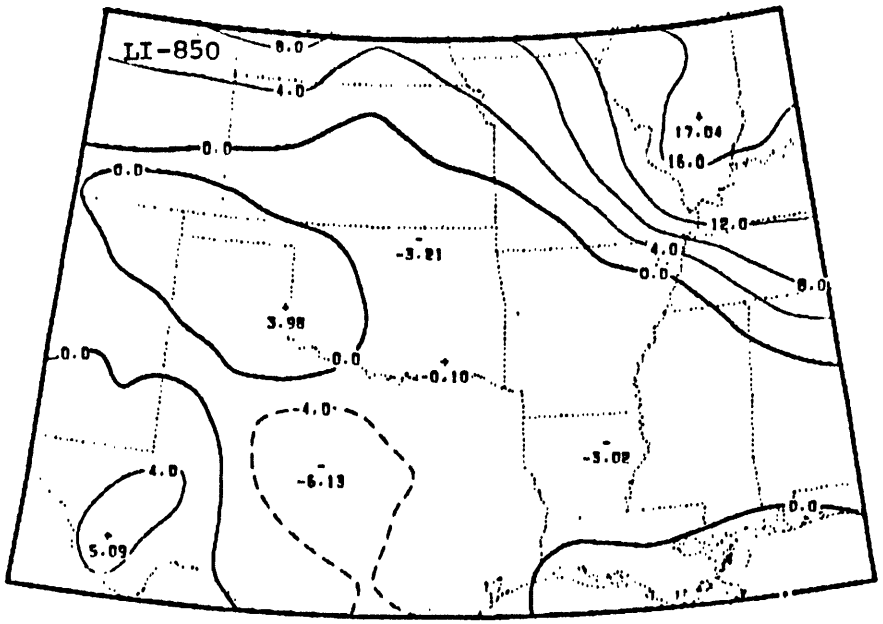


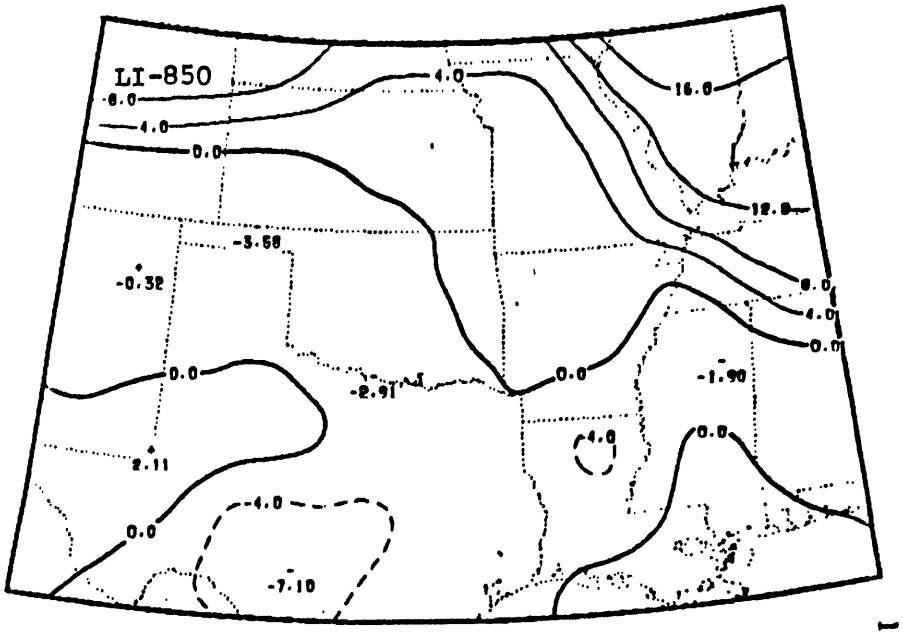


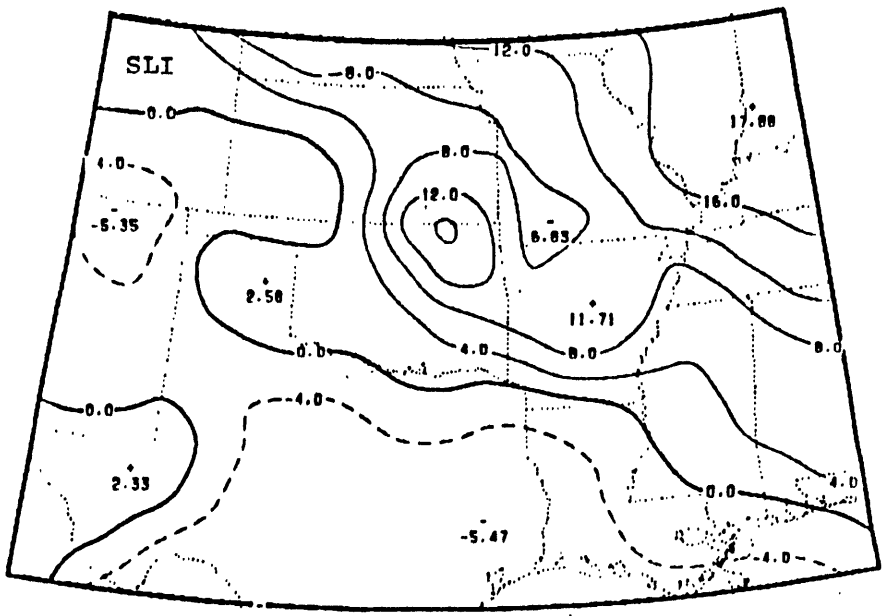


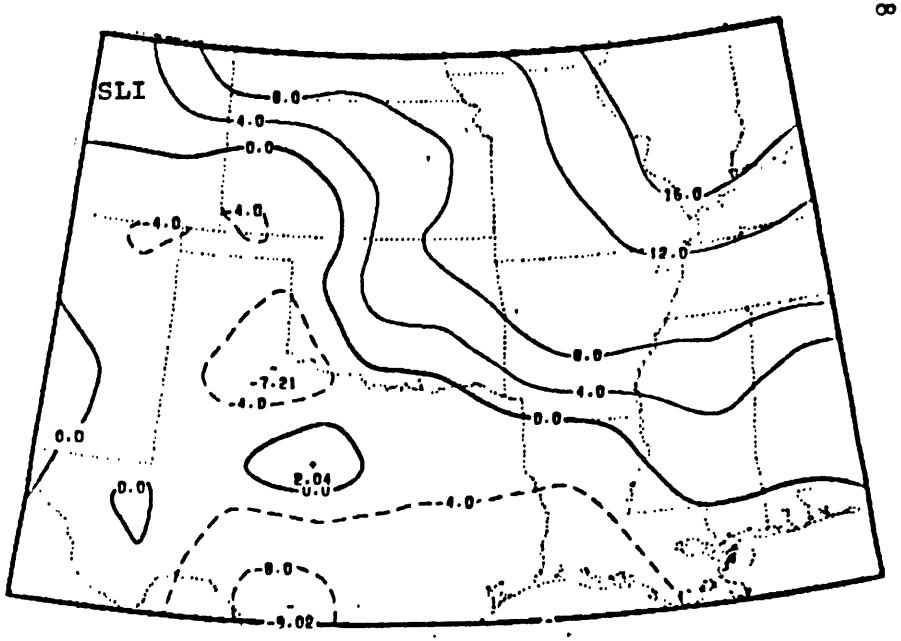
1500 GMT 10 April

1800 GMT 10 April



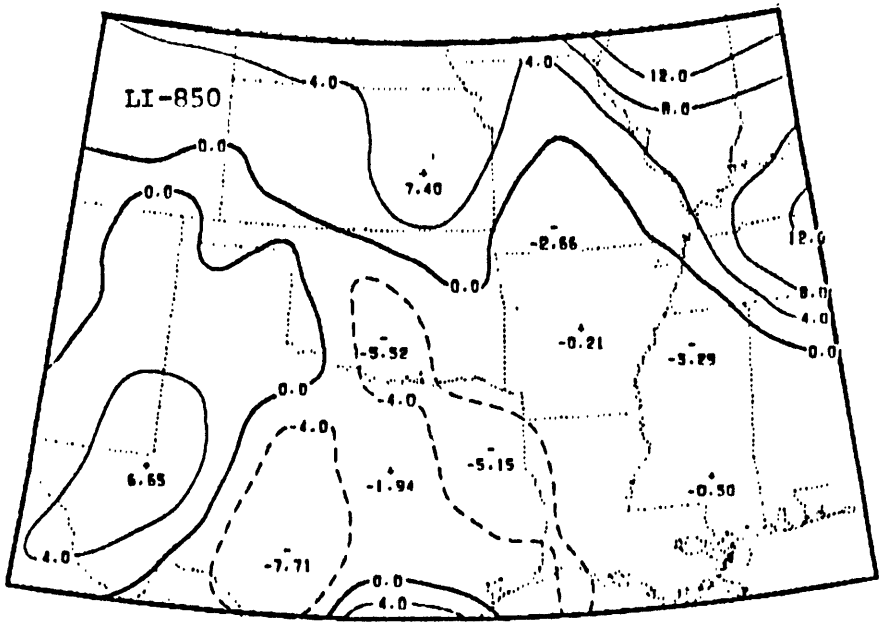


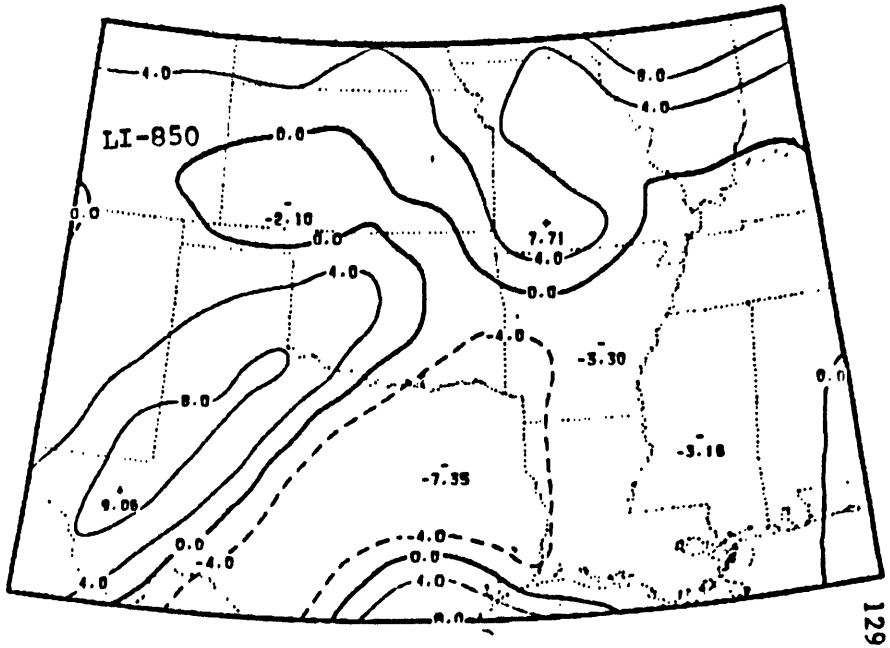


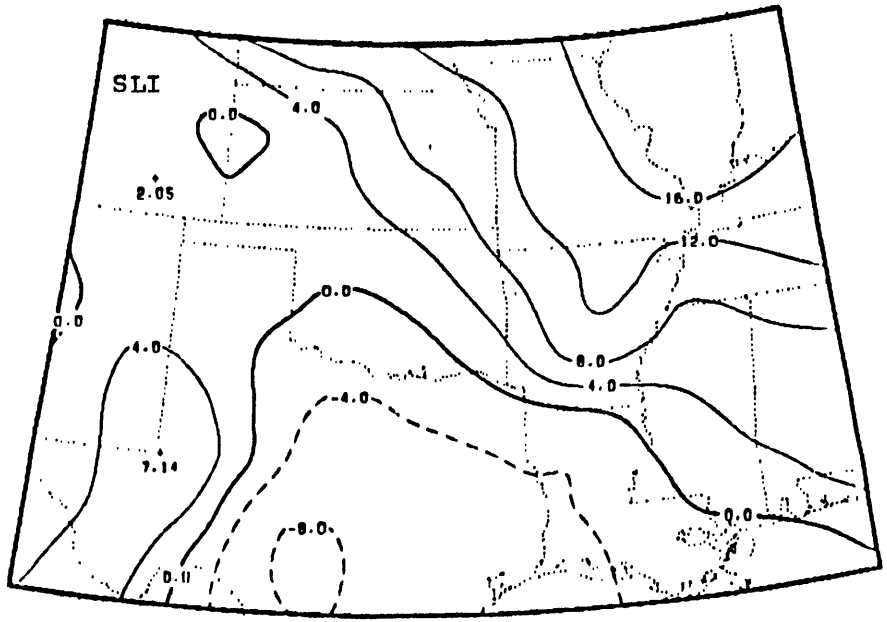


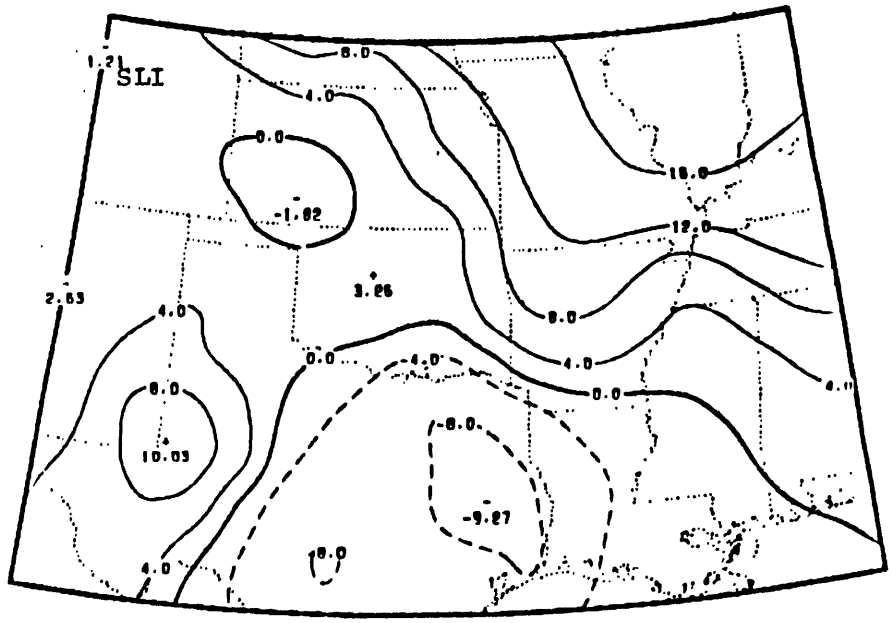
2100 GMT 10 April

0000 GMT 11 April



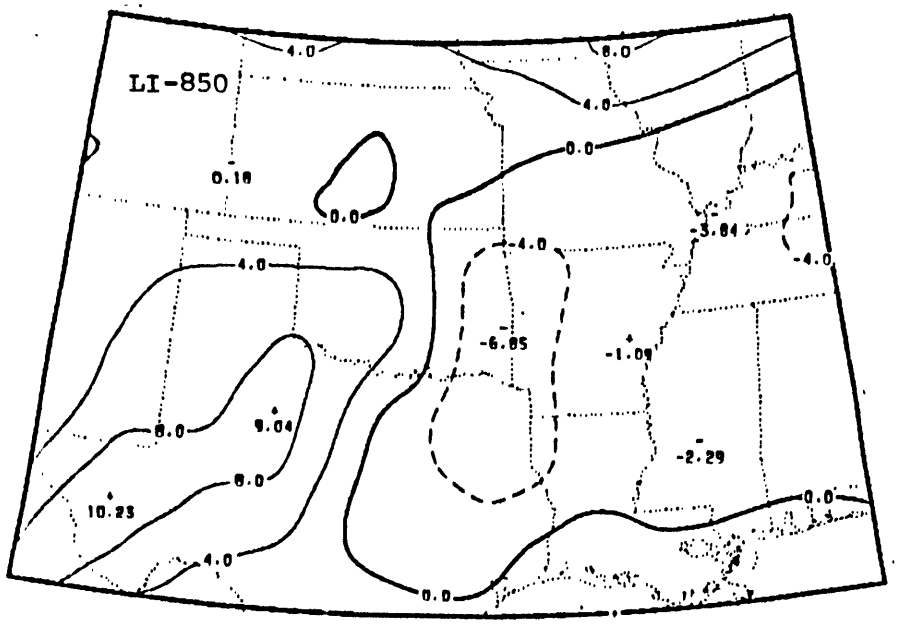


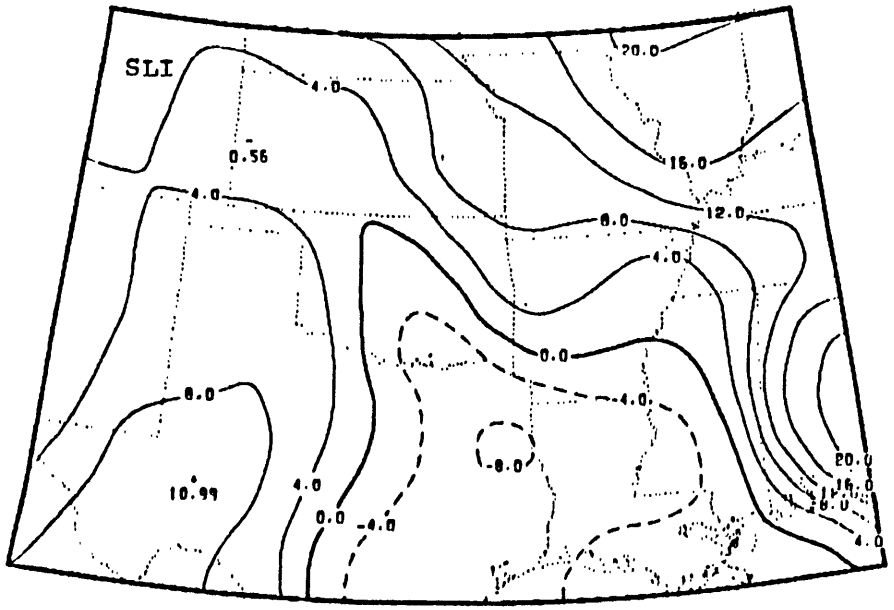




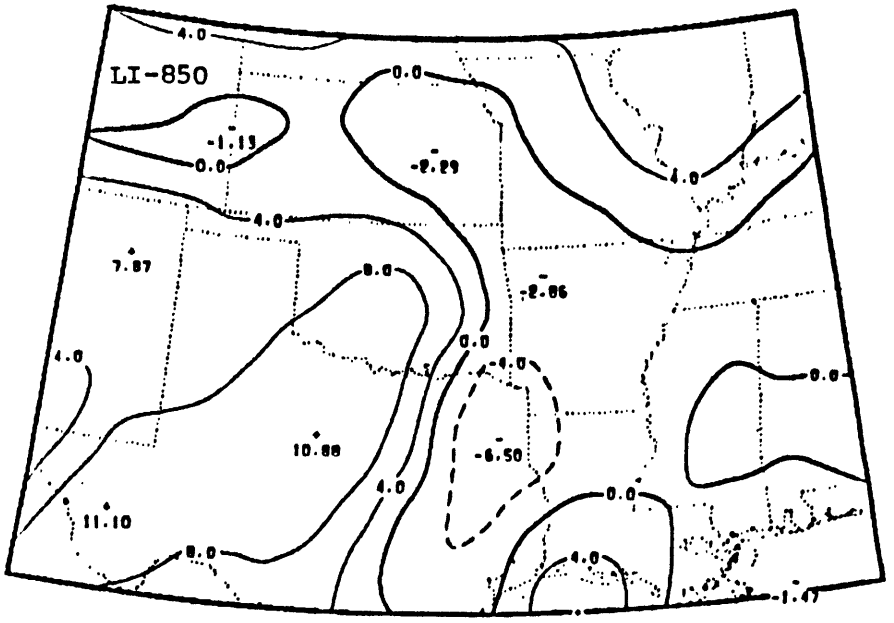
0300 GMT 11 April

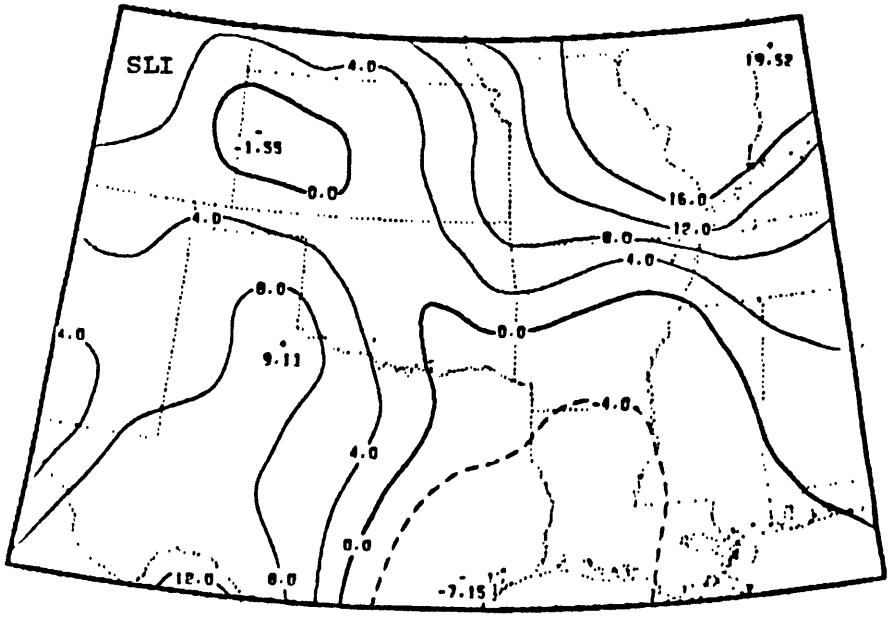
0600 GMT 11 April





0900 GMT 11 April





1200 GMT 11 April

over the panhandle where convection had broken out just prior to this time. The other convection developed over north central Texas in an area where the surface layer was neutral to slightly stable and the 850-mb layer was unstable. Between 18 GMT and 21 GMT, the 0°C SLI isopleth did not move northward substantially even with strong warm advection. The boundary layer over most of the area north of Texas remained very stable while the area of minus LI-850's expanded northward into Kansas. At 00 GMT 11 April, a time when the surface analysis showed an area of thunderstorms covering parts of Kansas, Missouri and Oklahoma, the SLI's ranged from near 0°C to 16°C, while the LI-850's were very close to 0°C. An interesting feature of the LI-850 analysis is the very flat gradient over the region of the active convection.

Between 21 GMT 10 April and 03 GMT 11 April, the elevated convection expanded northward into Nebraska, yet the 0°C LI-850 line moved slightly southward. This left a majority of the thunderstorms occurring in an environment with a strongly stable surface layer, and a nearly neutral 850-mb layer, which is in agreement with the climatology of elevated convection as shown previously. Topeka, Kansas (TOP) was reporting a thunderstorm at 03 GMT, yet an investigation of the sounding (not shown) showed no unstable air above the frontal inversion. The rather modest values of the LI-850's above the frontal surface are in sharp contrast to the very large negative values observed in both the SLI's and LI-850's in Texas.

The LI-850 analysis for 06 GMT shows an area of very stable

values over southwest Missouri. This is the effect of the cold boundary layer rising to above the 850-mb level at Monett, Missouri (UMN) as a mesoscale pressure wave propagated northeastward, and does not represent the air above the frontal inversion. By 09 GMT the SLI' and LI-850's both show an expanding area of stable air moving in from the west, while the LI-850's over extreme eastern Oklahoma approach -7°C. In this area, just north of the warm front, Fort Smith, Arkansas (FSM) was reporting a thunderstorm. At 12 GMT the only thunderstorms being reported were north of the front and once again in an area where little or no latent instability was observed.

4.5 RADAR ANALYSIS

Radar films consisting of photographs of the PPI scope for seven stations, obtained for NCC, were used for this study. The coverage of the stations is shown in Figure 4.5.1. The elevation angle of the WSR-57's was generally one degree. The compositing was done on an hourly basis by tracing all echoes that were of moderate intensity (VIP level 3; >48 dBZ) or higher for each station onto a common map. The analysis covered the time period from 17 GMT 10 April to 23 GMT 11 April. The radars at two stations, MKC and ICT, were operating at a range of 250 nautical miles and required an intermediate step to correct the scale before compositing.

Once all the films were composited, individual convective elements were identified. It was not possible to classify all areas

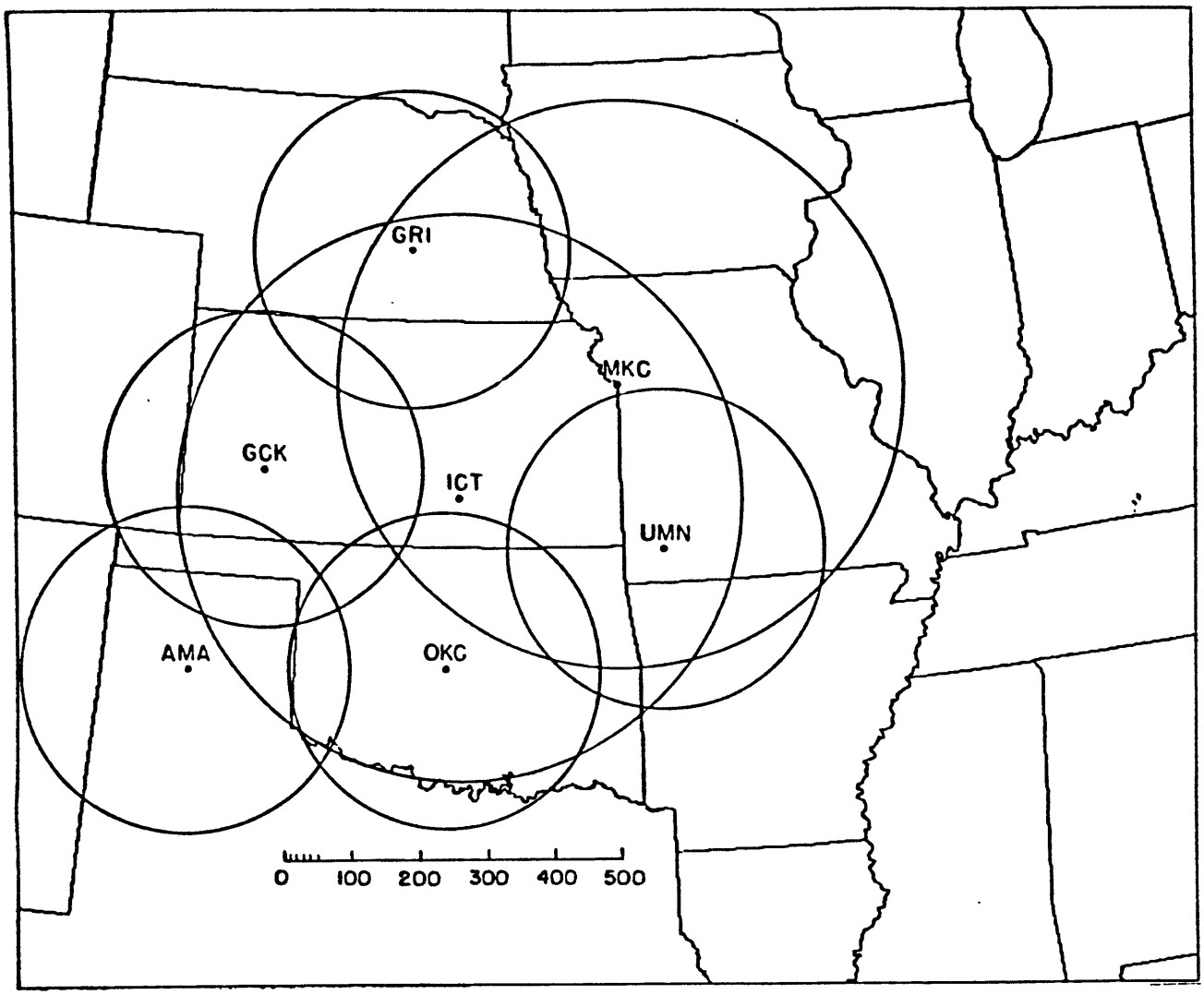
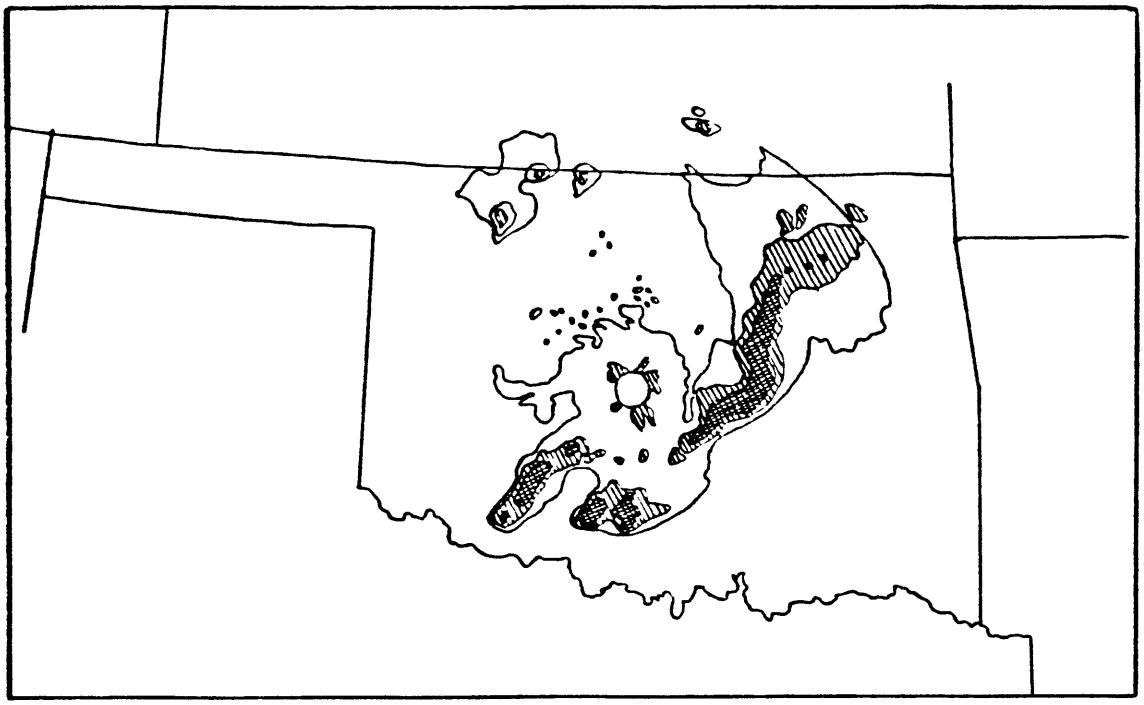


Figure 4.5.1. The combined radar coverage for the WSR-57 radars used in the analysis.

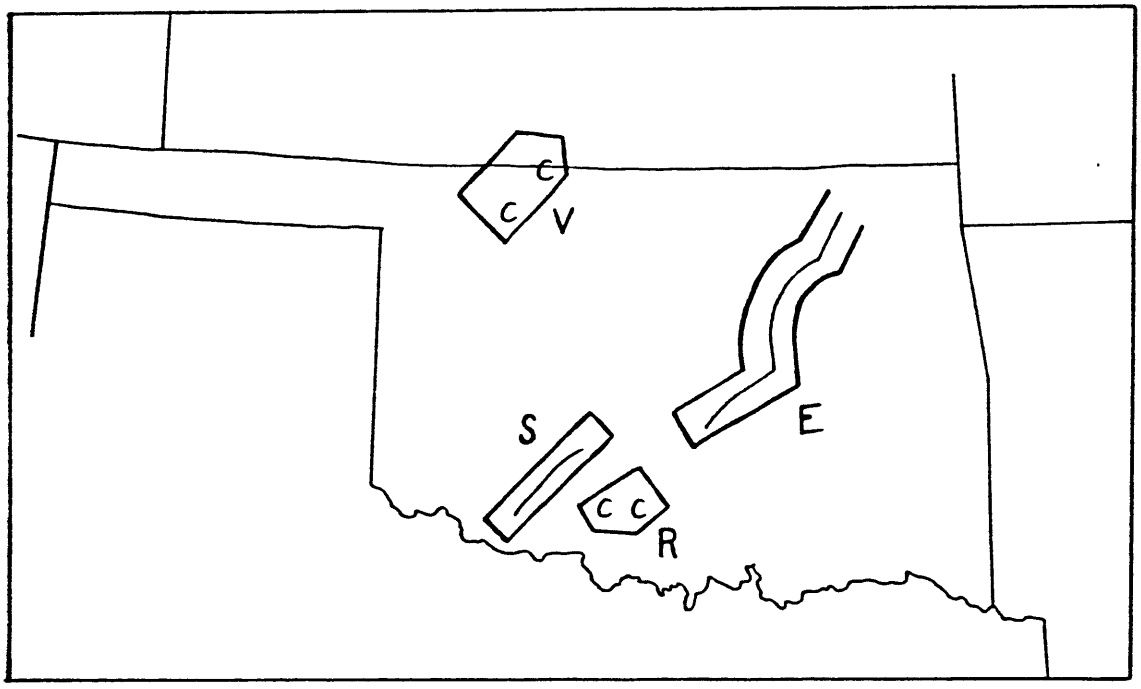
unambiguously and some degree of subjectivity was involved in selecting the individual elements and bands. However, great care was taken in selecting traceable and distinct echoes. Intermediate photographs, available at least every 5 minutes, were used to clarify any uncertainties in identity. An example of one of the traced PPI photographs, as well as the interpretation is shown in Figure 4.5.2. The hourly composites are shown in Figure 4.5.3.

Figure 4.5.4 shows the location and time that each element was first identified. A large number of positions are clustered in the southern part of the study region. This is likely the result of cells moving into the area of radar coverage fron the southwest. No attempt was made to determine whether the convective elements developed there or propagated into the region. The national radar summary maps received on DIFAX and satellite pictures were used to identify the starting location of larger convective regions and will be shown later.

Figure 4.5.5 shows the 'tracks' of the centers of convective areas, which are lines connecting the location of the initial identification with the location at which the convective area was last identified. From this figure it can be seen that the largest fraction of echoes moved along a path from Oklahoma northeastward into Missouri. Another group of thunderstorms moved north-northeastward from the Texas Panhandle. A comparison with Figure 4.1.2 shows that the pattern seen in the storm total precipitation strongly reflects these two paths. A minimum in precipitation amounts occurs between



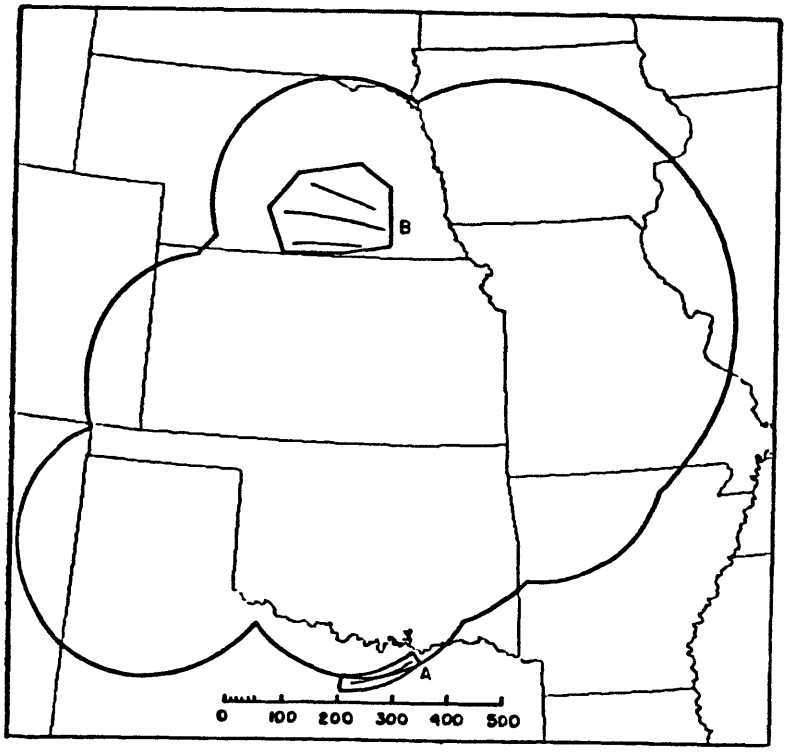
(a)



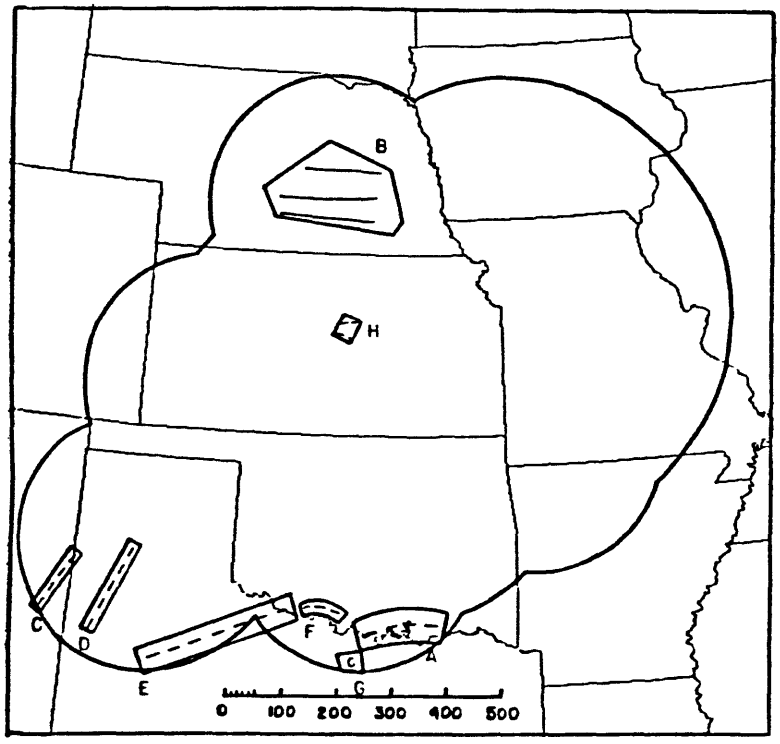
(b)

Figure 4.5.2. (a) The traced PPI scope for OKC at 0200 GMT 11 April 1979. (b) The interpretation of the scope in (a) as used in this study.

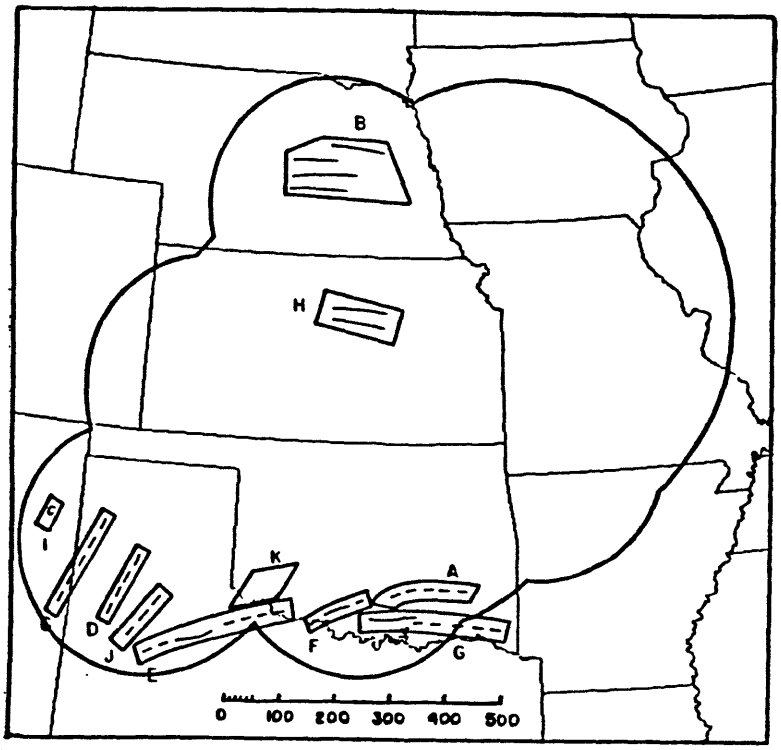
Figure 4.5.3. The interpreted radar composites for the period from 1700 GMT 10 April 1979 to 2300 GMT 11 April 1979. The outlined areas, each identified by a character, enclose echoes of VIP Level 3 or greater. Inside the areas, a solid line indicates a solid echo, a dashed line indicates a cellular line of echoes and a 'C' identifies an individual cell. A subscript identifies a fragment of a previously defined area.



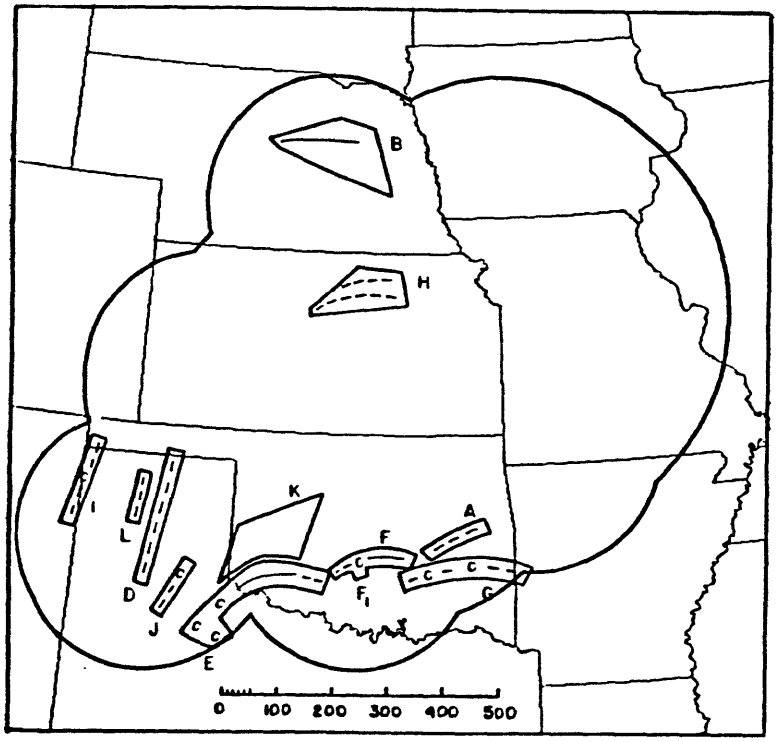
1700 GMT APRIL 10, 1979



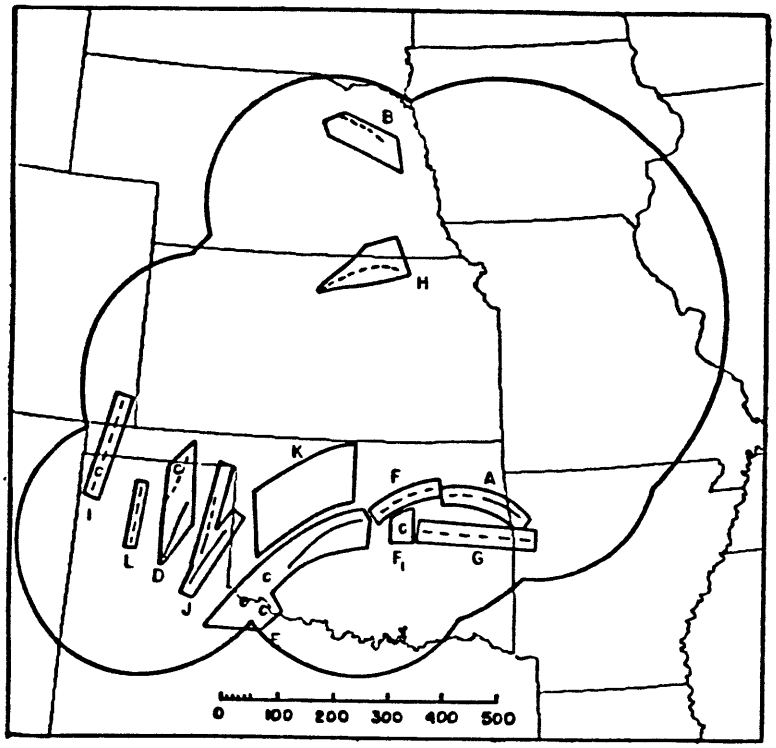
1800 GMT APRIL 10, 1979



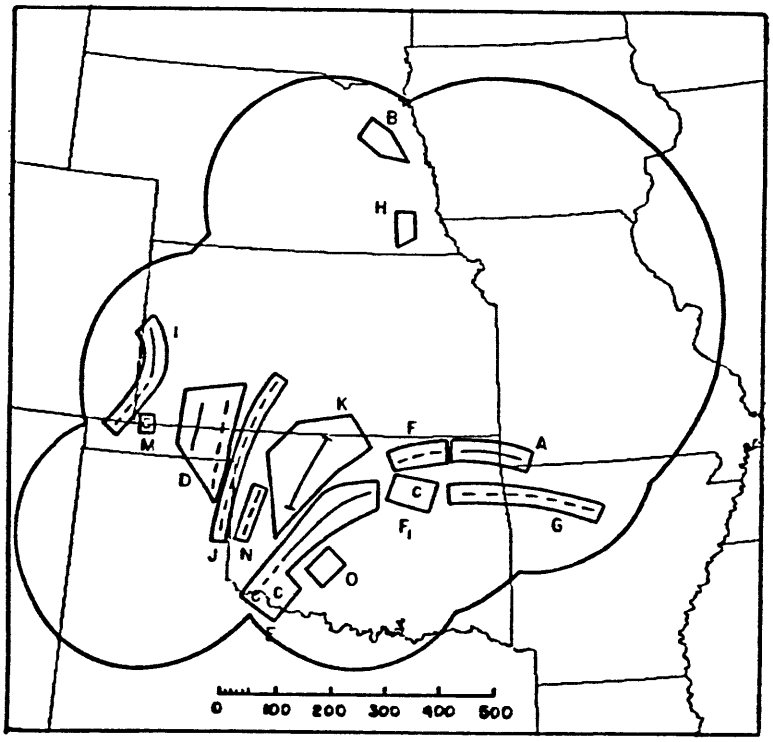
1900 GMT APRIL 10, 1979



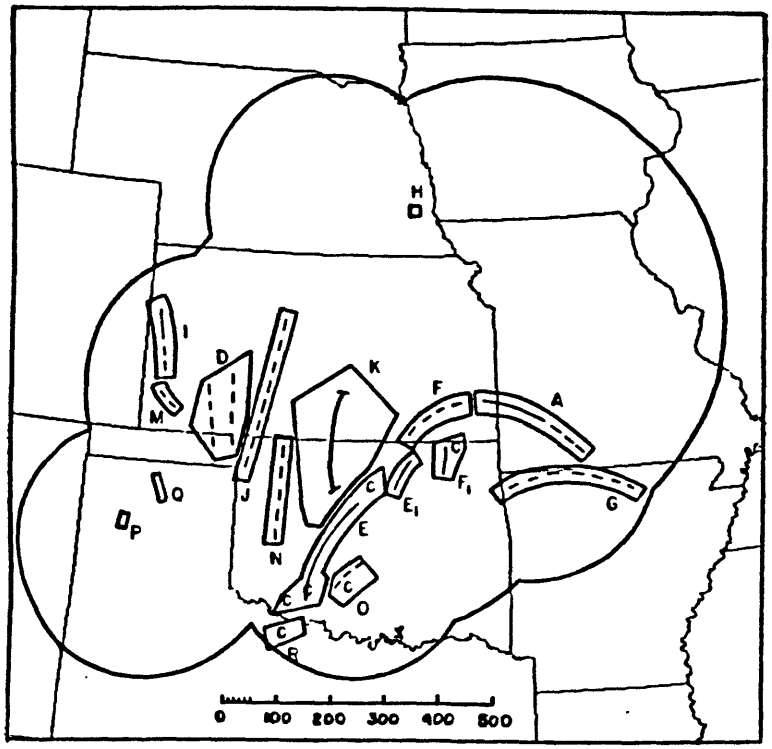
2000 GMT APRIL 10, 1979



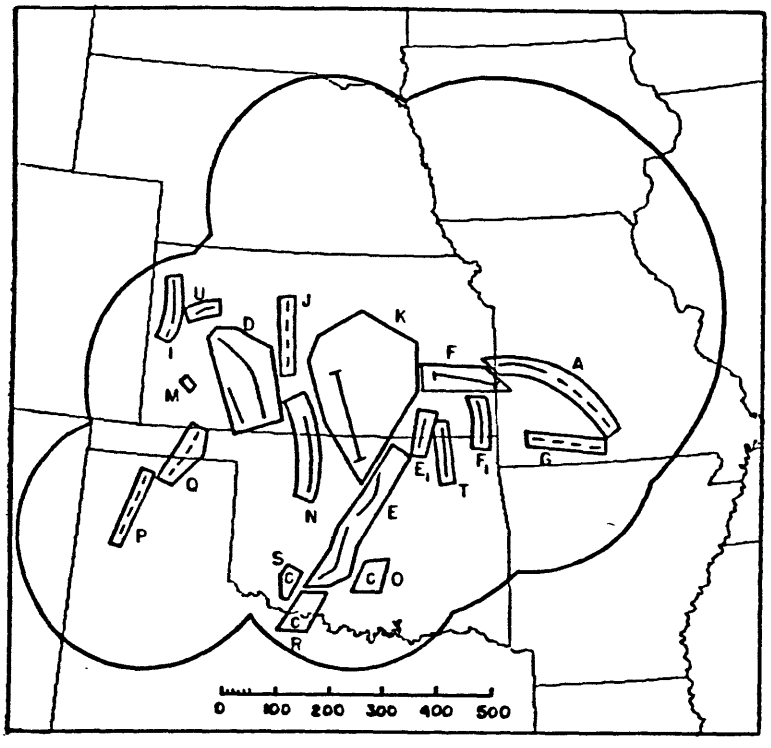
2100 GMT APRIL 10, 1979



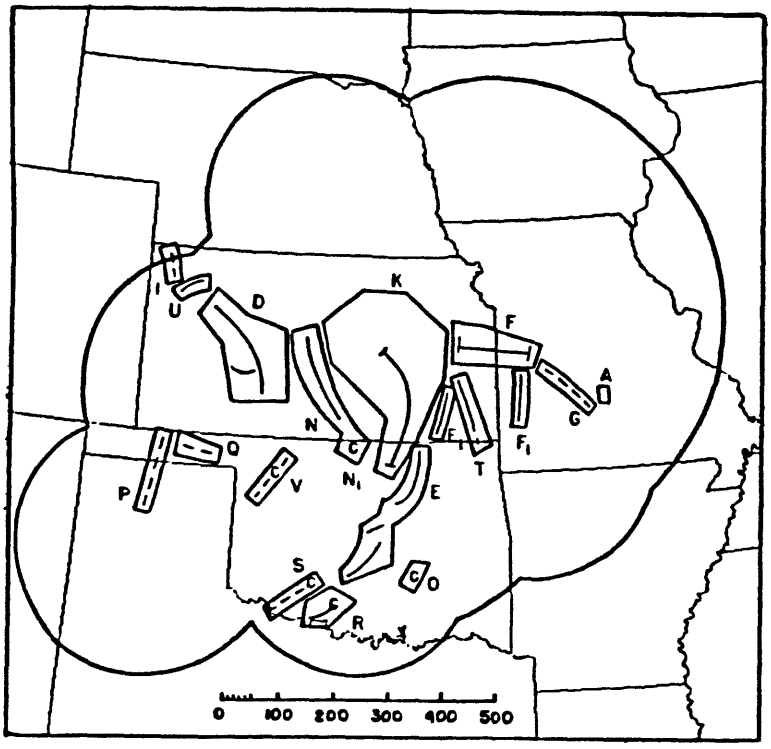
2200 GMT APRIL 10, 1979



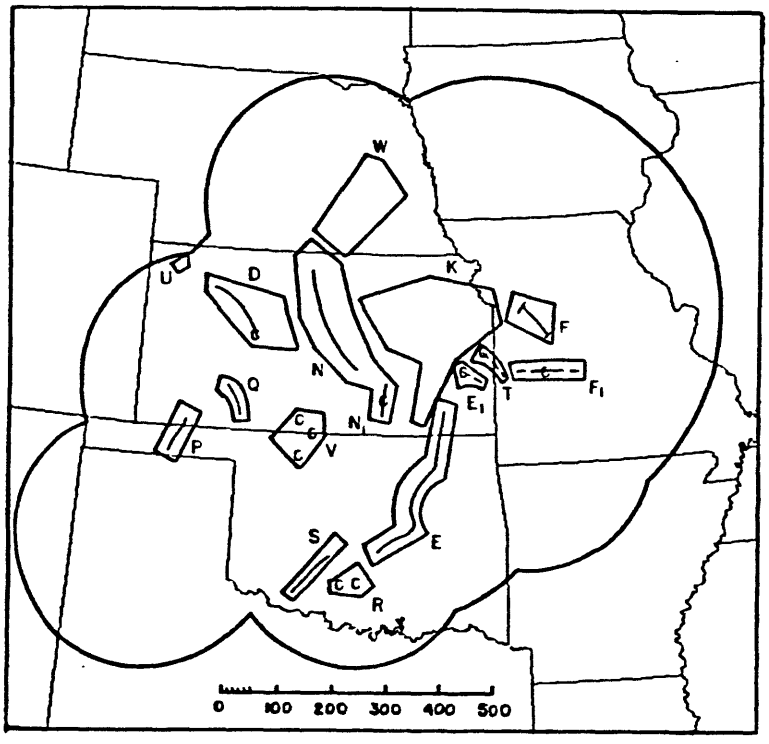
2300 GMT APRIL 10, 1979



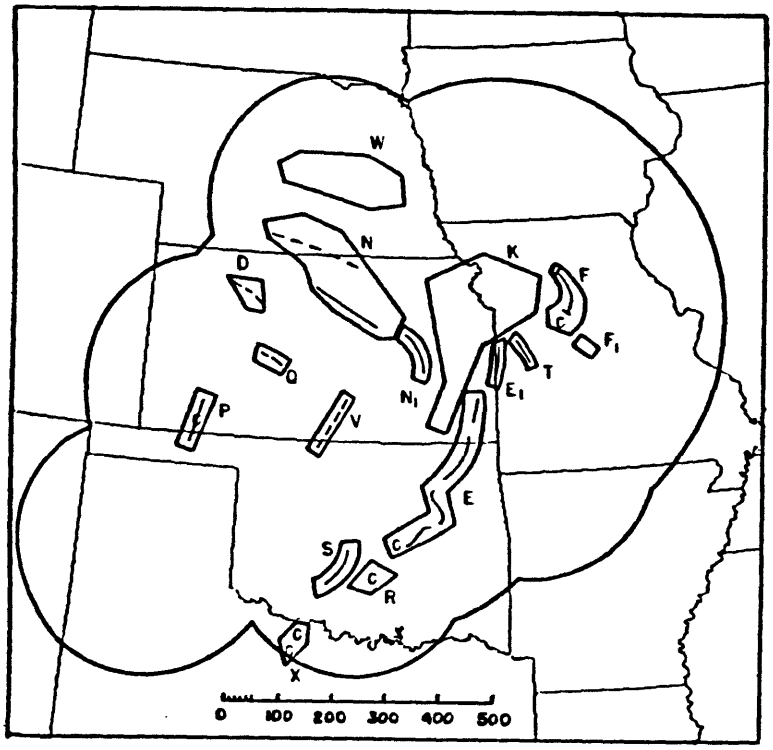
0000 GMT APRIL 11, 1979



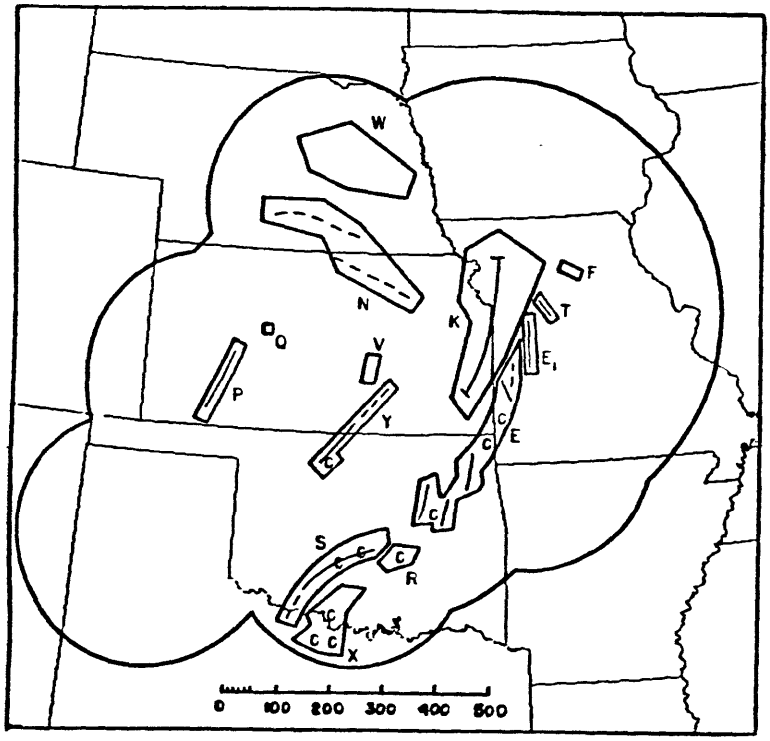
0100 GMT APRIL 11, 1979



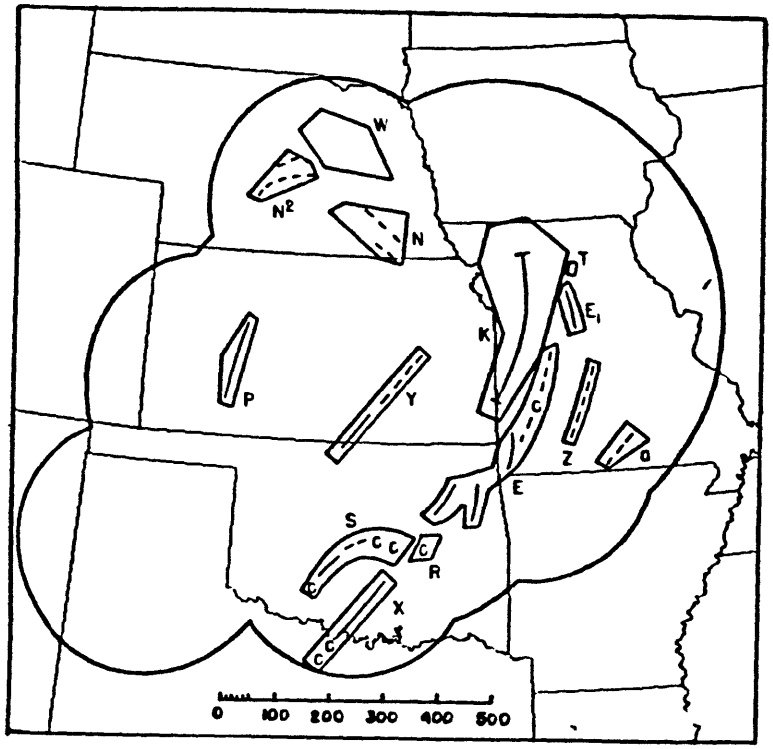
0200 GMT APRIL 11, 1979



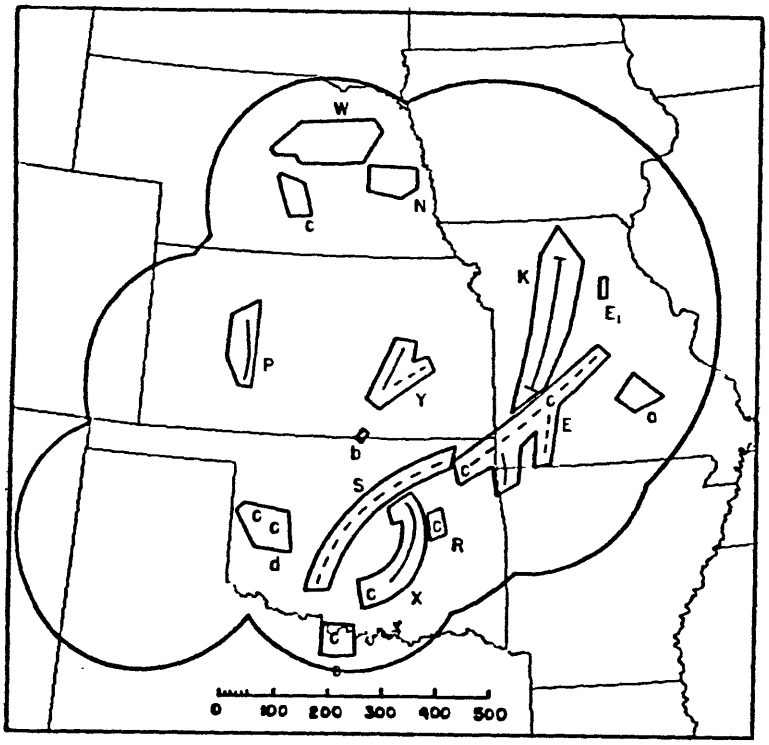
0300 GMT APRIL 11, 1979



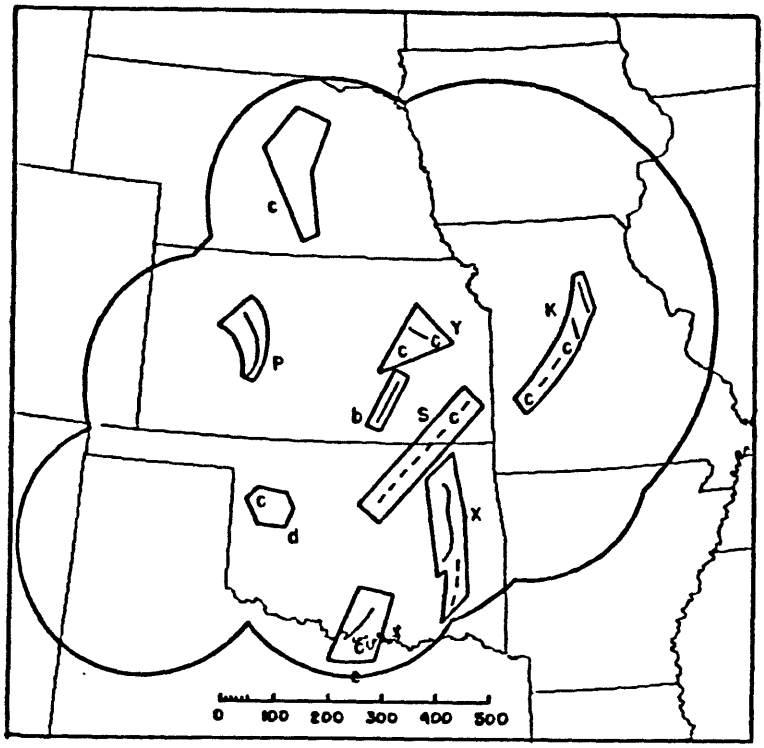
0400 GMT APRIL 11, 1979



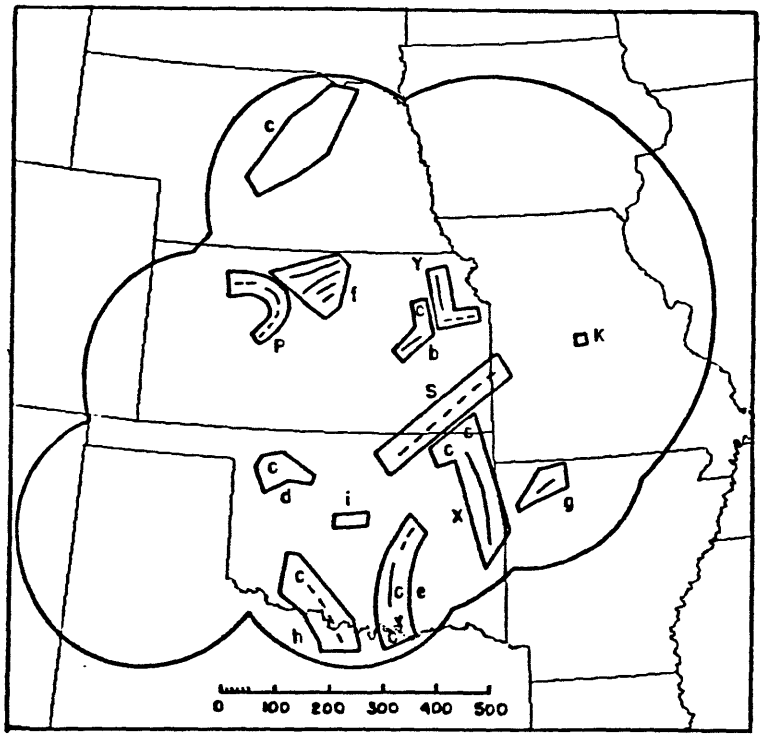
0500 GMT APRIL 11, 1979



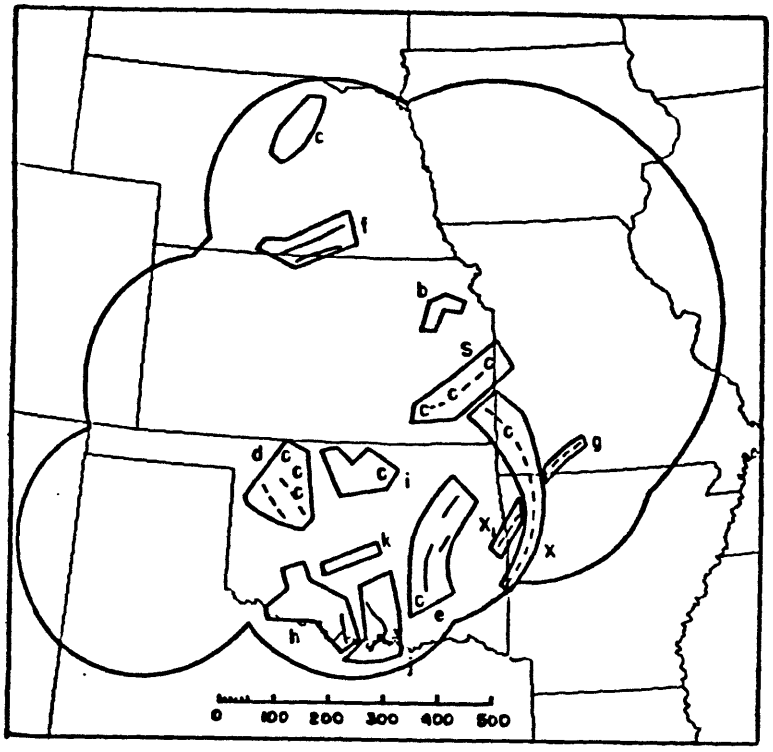
0600 GMT APRIL 11, 1979



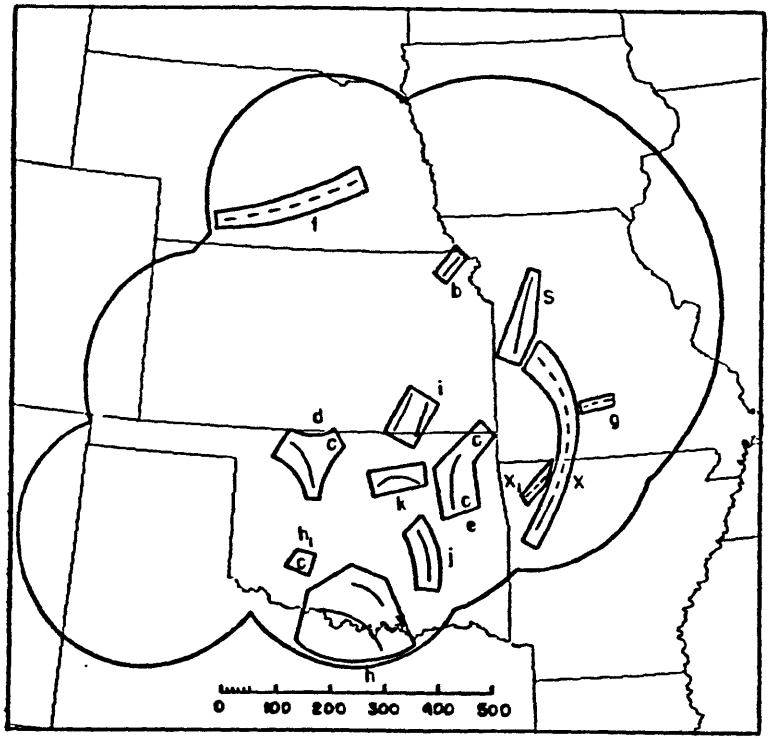
0700 GMT APRIL 11, 1979



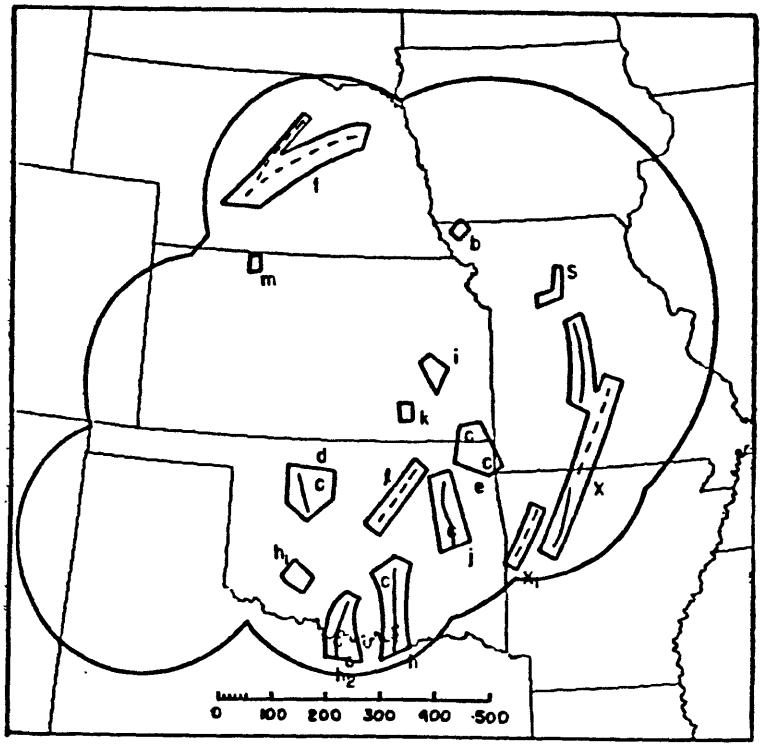
0800 GMT APRIL 11, 1979



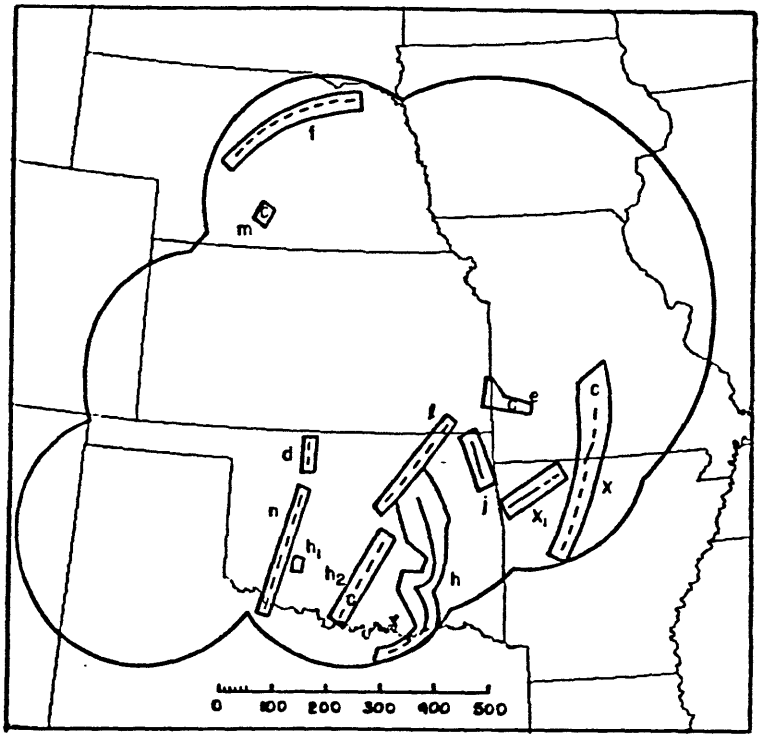
0900 GMT APRIL 11, 1979



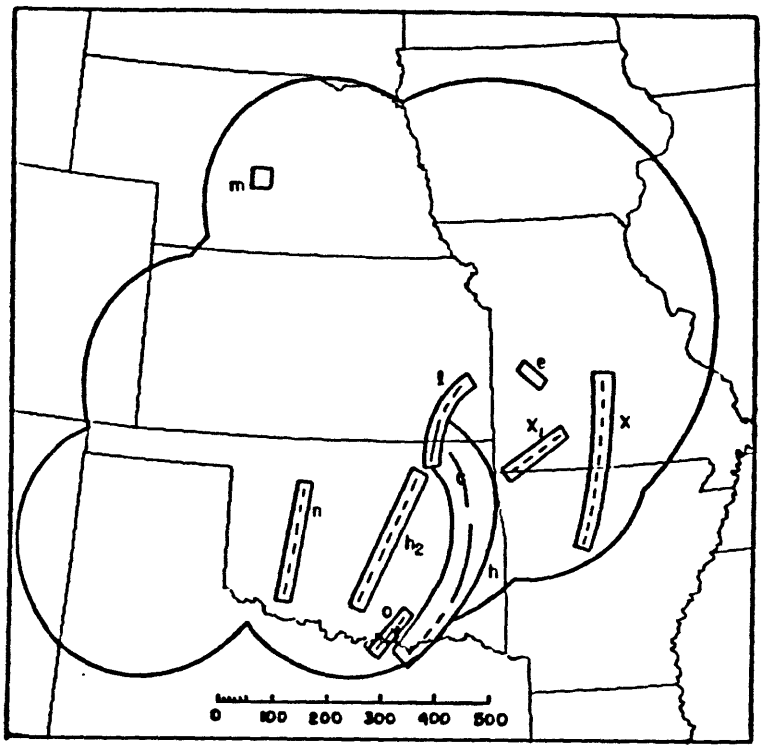
1000 GMT APRIL 11, 1979



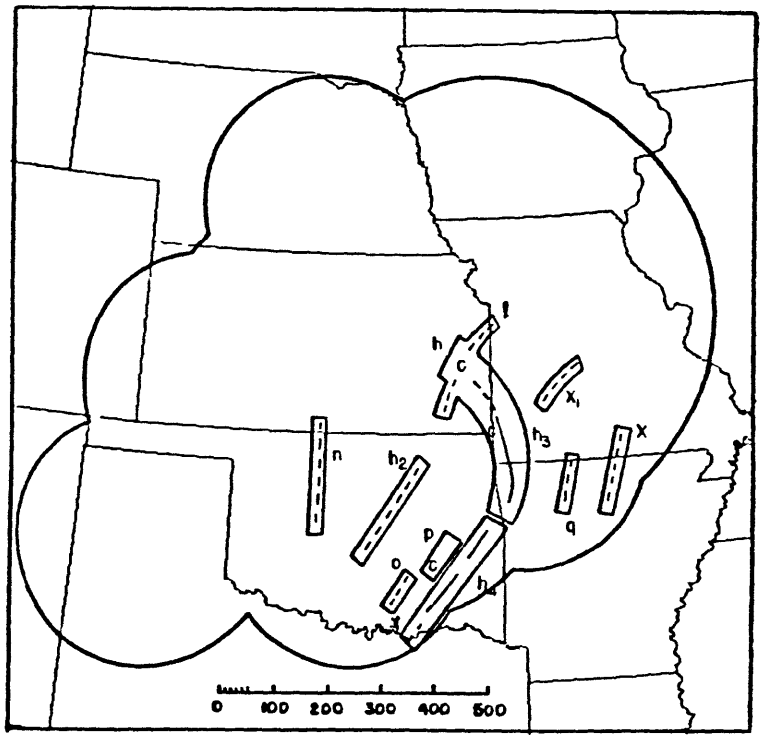
1100 GMT APRIL 11, 1979



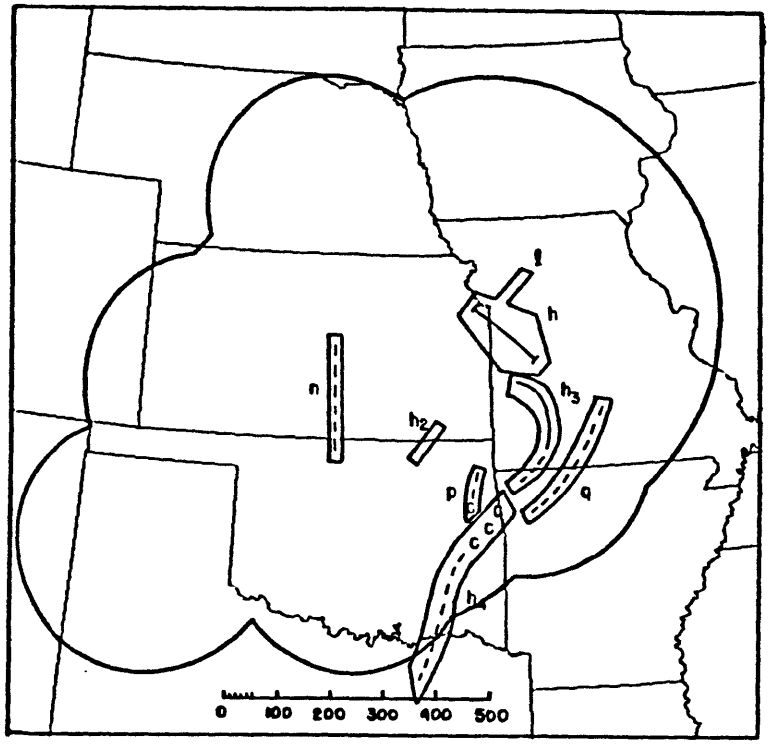
1200 GMT APRIL 11, 1979



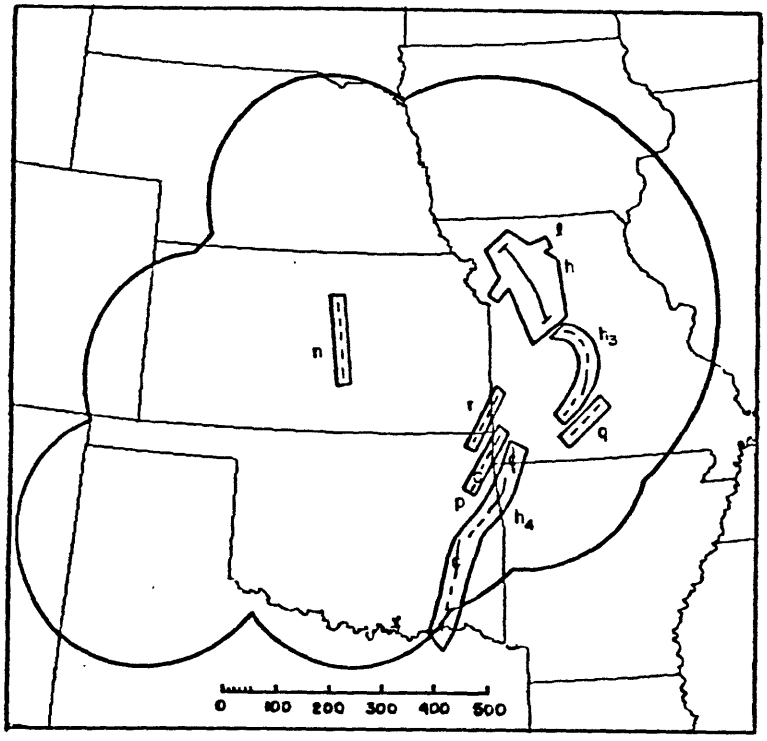
1300 GMT APRIL 11, 1979



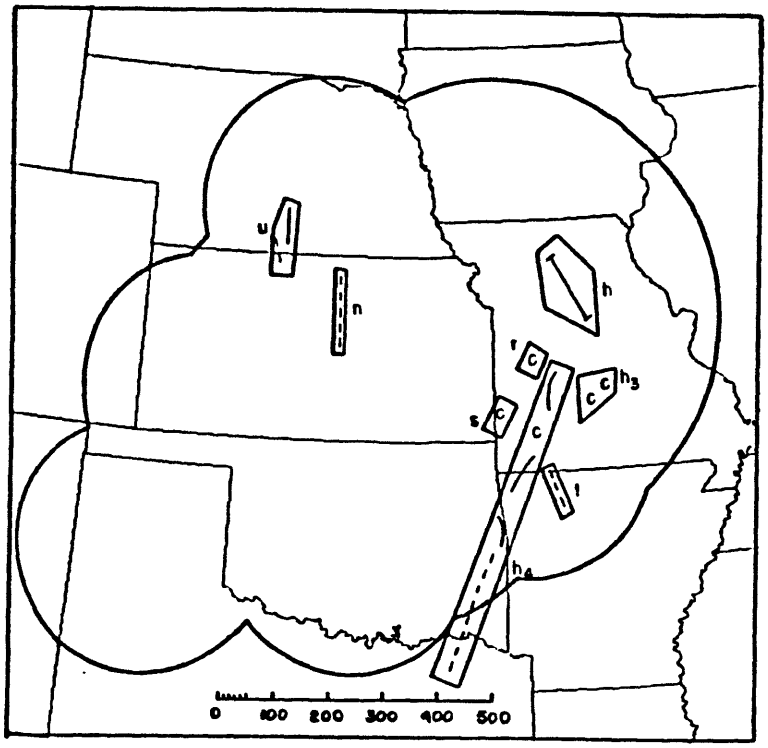
1400 GMT APRIL 11, 1979



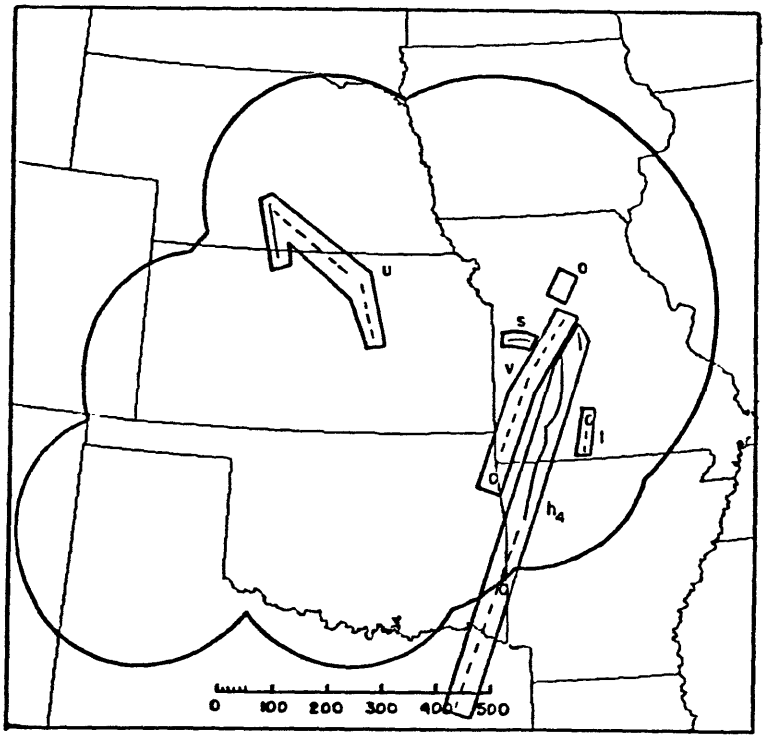
1500 GMT APRIL 11, 1979



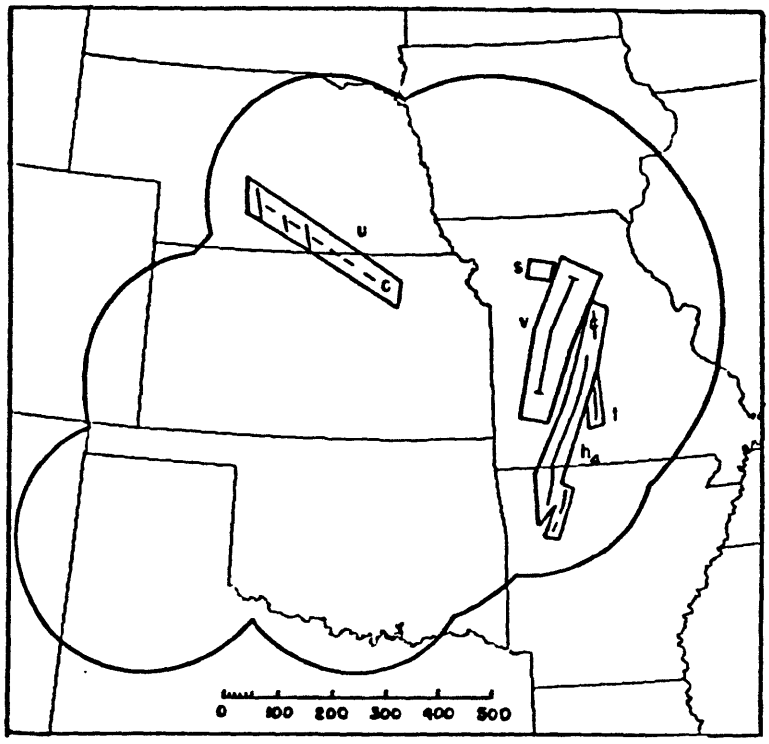
1600 GMT APRIL 11, 1979



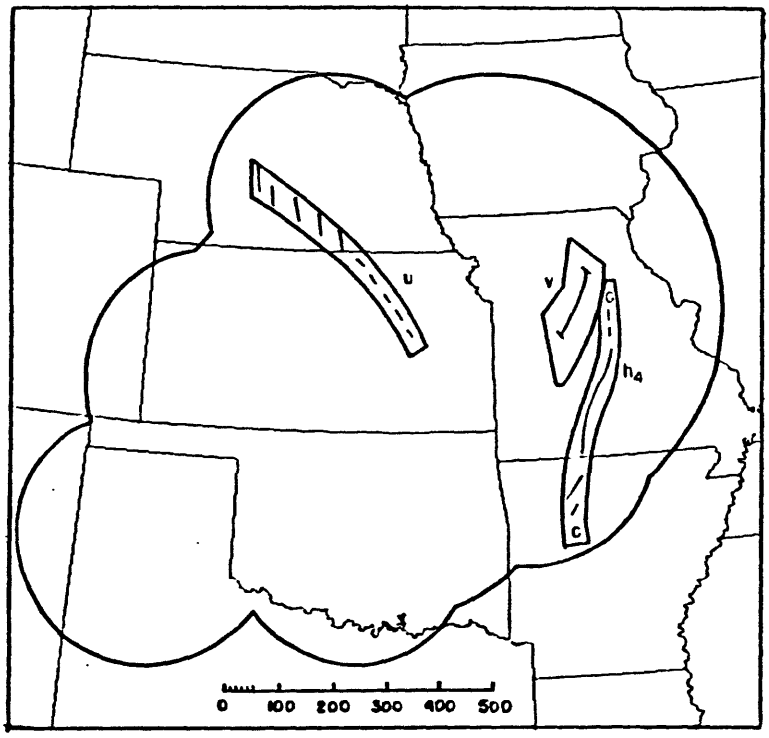
1700 GMT APRIL 11, 1979



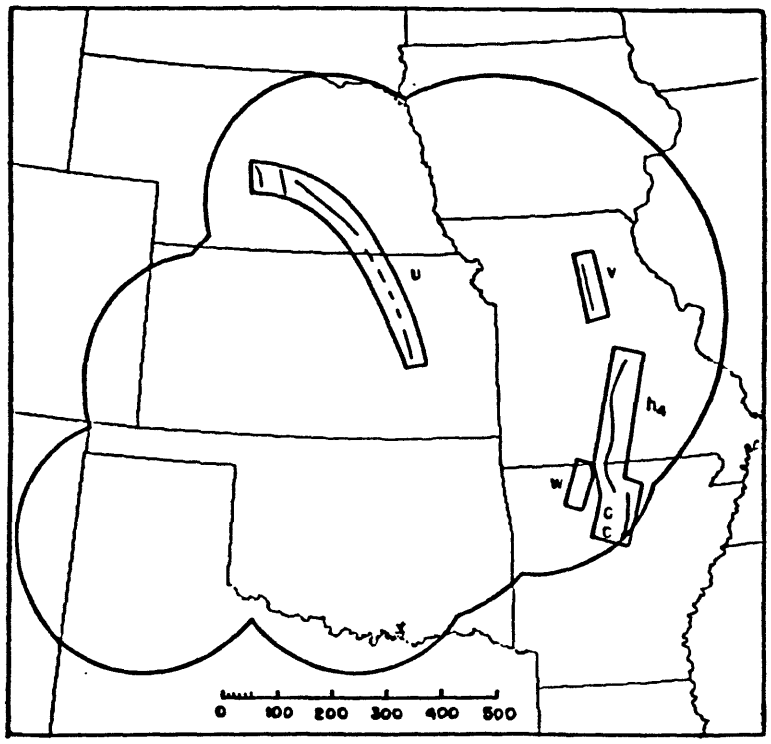
1800 GMT APRIL 11, 1979



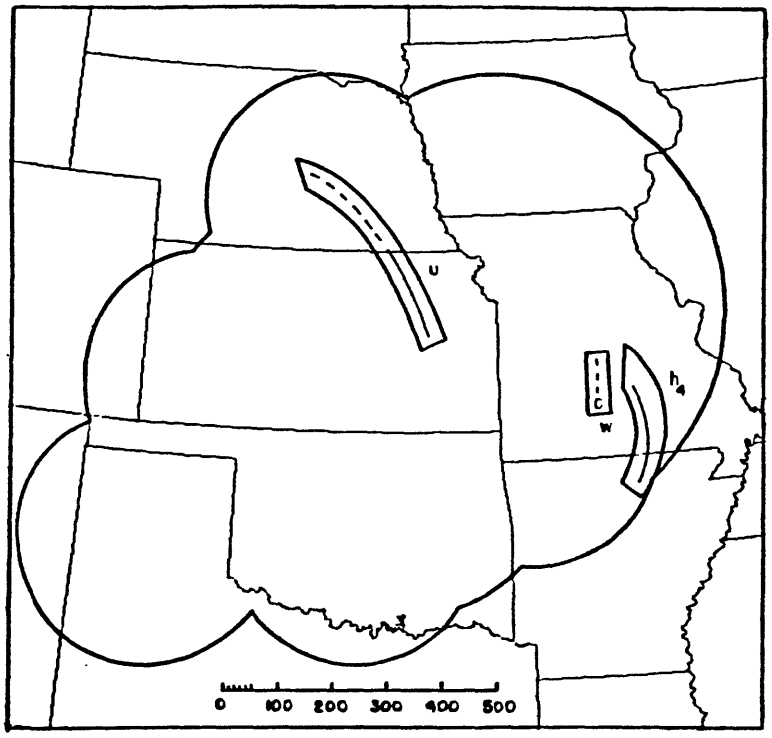
1900 GMT APRIL 11, 1979



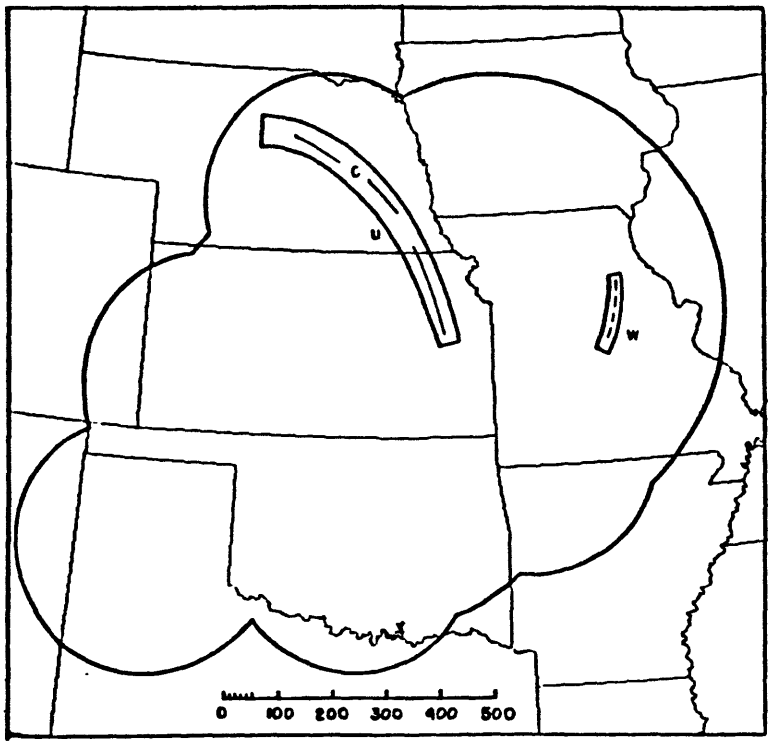
2000 GMT APRIL 11, 1979



2100 GMT APRIL 11, 1979



2200 GMT APRIL 11, 1979



2300 GMT APRIL 11, 1979



Figure 4.5.4. The location of the initial identification of each convective area. Each location is labeled with the area's identifying character followed by the day (10 or 11) and hour (00-23) the area was identified.

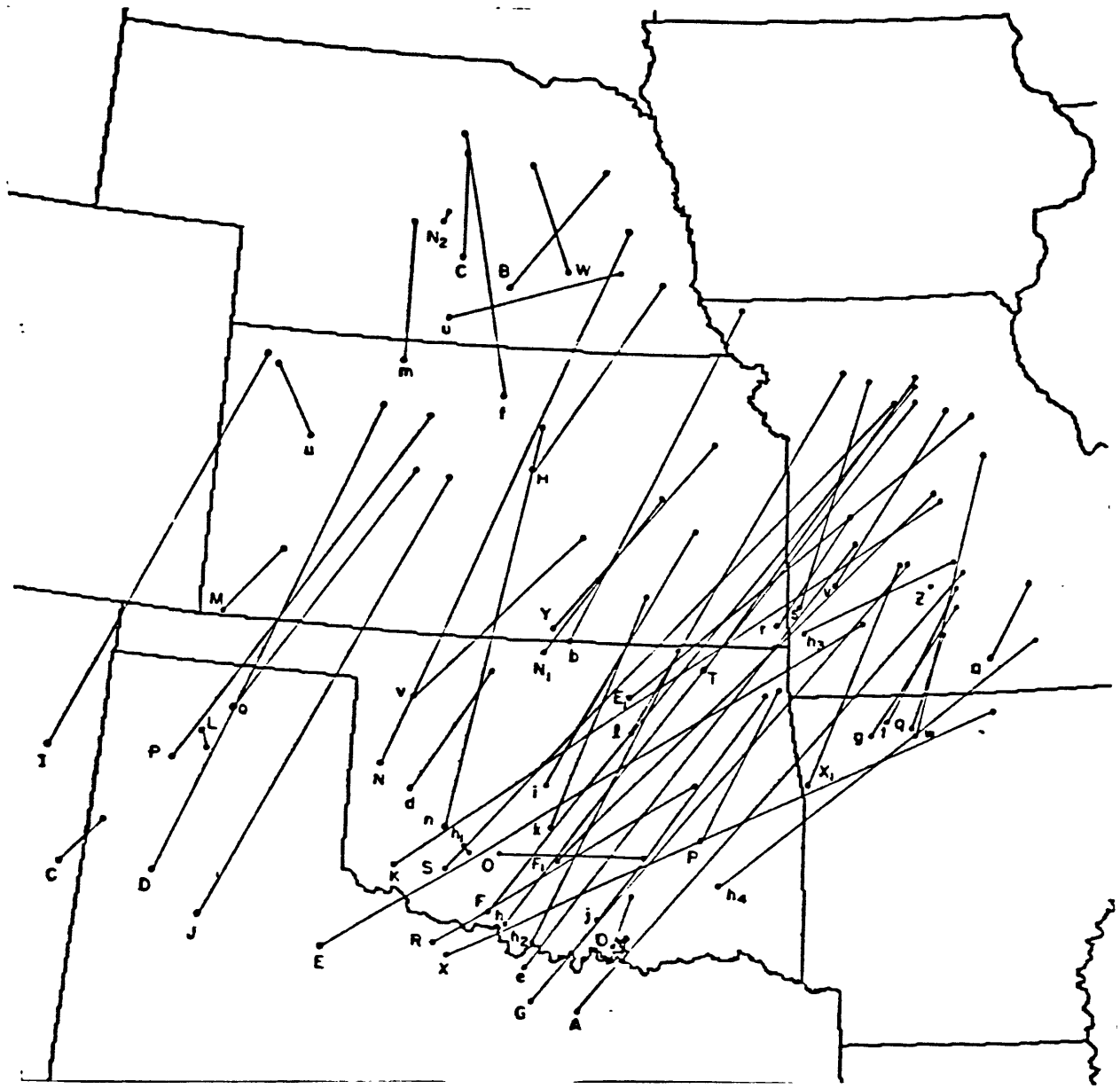


Figure 4.5.5. A composite of the 'tracks' of the centers of the convective areas. Each 'track' is labeled as to which convective area it represents.

them. Many stations through central Kansas into southeast Nebraska reported less than 1/4 of an inch total precipitation for the storm. Based on the radar surveillance, the average lifespan of the convective elements was 4.9 hours. This is longer than the lifespan of non-severe single-cell cumulonimbus, especially considering that many of the storms moved into the analysis area after development. The elements were generally banded, with an average length of nearly 200 km and a width of 39 km. For those bands that developed before 12 GMT 11 April it was possible to compare the orientation of the bands with the geostrophic shear (Figure 4.5.6). The bands were aligned along the shear with a slight counterclockwise rotation on the average, but with considerable scatter.

The first convection that developed over the Texas Panhandle is visible in the satellite picture for 18 GMT 10 April (Figure 4.3.6). These bands, C and D at 18 GMT and I and J at 19 GMT, were the bands that tracked north-northeastward. The clearly defined bands formed in a region ahead of the dryline with very strong vertical shear making them prime candidates for symmetric instability.

Emanuel (1983) showed that the potential for symmetric instability can be qualitatively assessed by comparing the slope of potential temperature contours (θ_e for a saturated environment) with the slope of lines of equal geostrophic angular momentum ($M=V + fx$, where V is the geostrophic wind speed, f the coriolis parameter and x the horizontal distance in the x-z plane which is selected perpendicular to the geostrophic shear vector). Simply stated, the

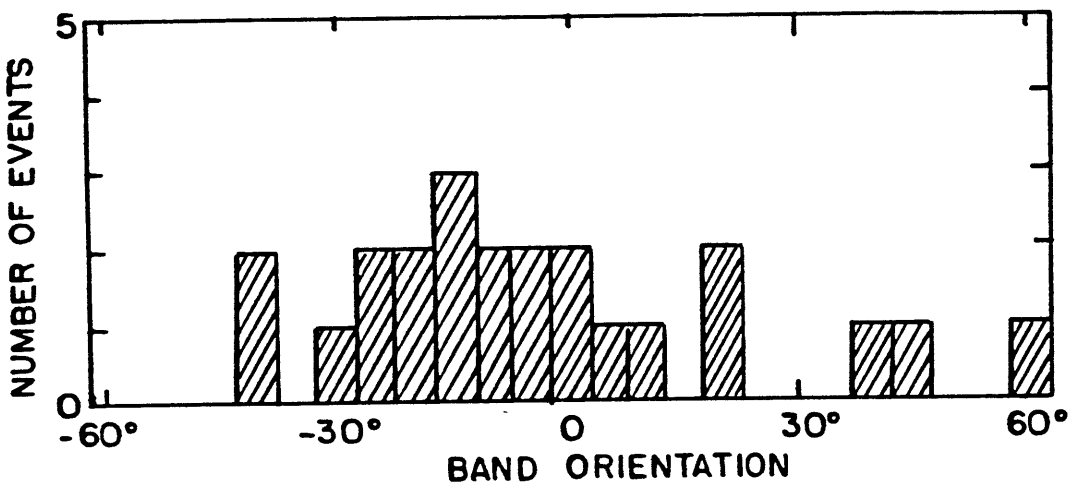


Figure 4.5.6. A histogram showing the orientation of the convective bands with respect to the geostrophic shear between 850 mb and 500 mb. A positive band orientation represents a clockwise rotation of the band.

atmosphere is symmetrically unstable in regions where the M surfaces are shallower than the θ surfaces.

Figure 4.5.7 shows that the boundary layer slightly northeast of where the bands formed was neutral with respect to dry symmetric instability. Apparently symmetric instability was manifest in the organization and triggering of the convection but was soon dominated by the gravitational instability of moist convection demonstrated by both reports of cumulonimbus from nearby stations and the observed negative SLI's. These storms moved through a region where the surface lifted indices were slightly negative and not much different from the 850-mb lifted indices. The surface elevations are relatively high across western Kansas with surface pressures of ≈900 mb. For these reasons we will not discuss these bands further.

Along the other track, the echoes appear to come in three surges. The first surge was characterized by bands A and E, which entered the surveillance area at 17 GMT and 18 GMT 10 April, respectively. A was the east to west oriented convective line across northern Texas mentioned in the preceding section, while band E tracked to the northeast as band A swung northward. Band E developed the line echo wave pattern (LEWP) (Nolen, 1959), characteristic of strong horizontal shear, beginning at 00 GMT 11 April and subsequently broke up into smaller fragments.

The second surge was represented by line X, initially identified at 03 GMT 11 April. This cluster of storms followed the same track as those associated with E. Finally, the third pulse of thunderstorms

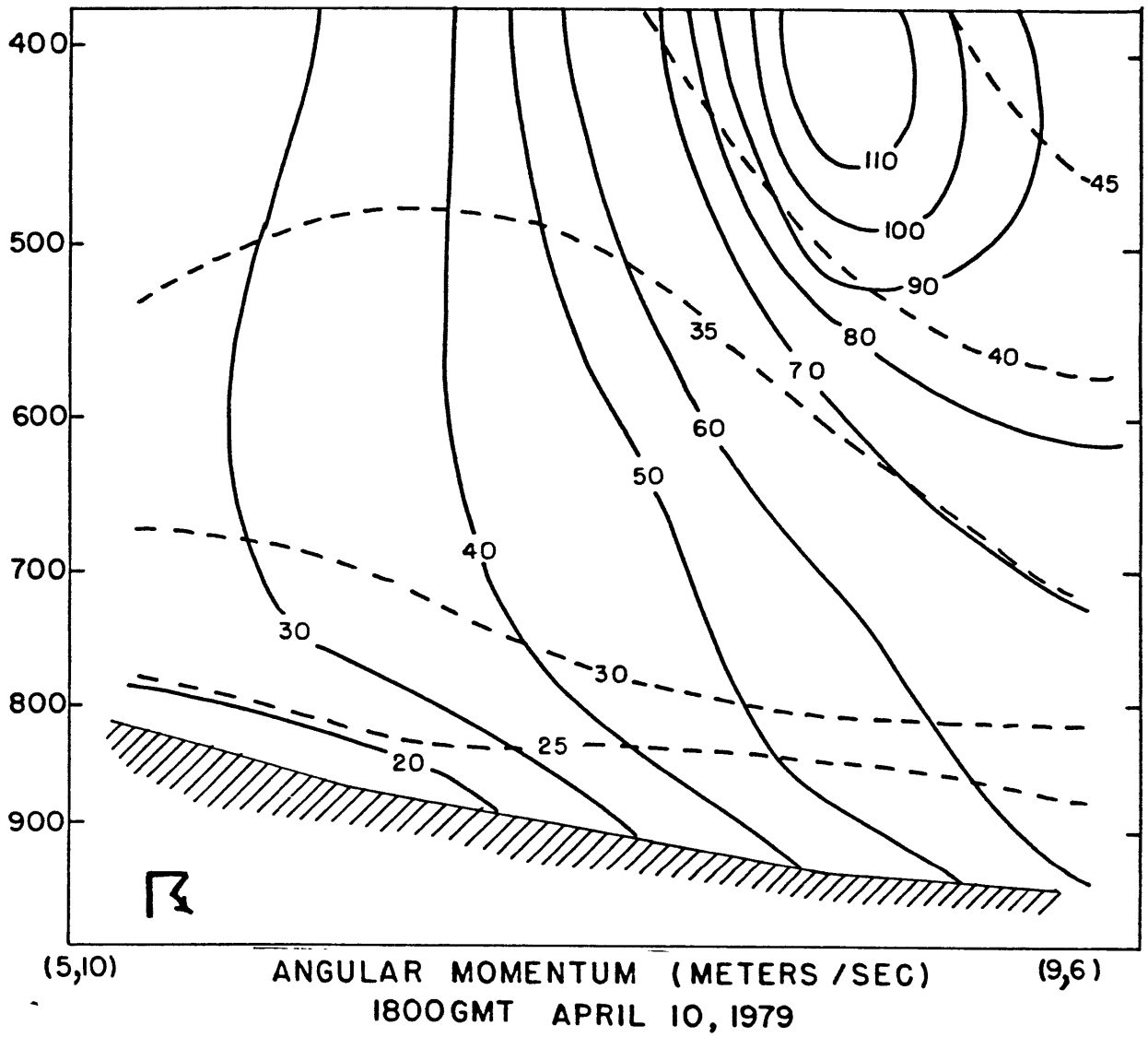


Figure 4.5.7. A vertical cross section along the line from (103°W, 37°N) to (99°W, 33°N) for 1800 GMT 10 April 1979. Refer to Figure 4.5.8 for the location. Solid lines are isopleths of constant geostrophic angular momentum (m/s). The dashed lines are isentropes (°C).

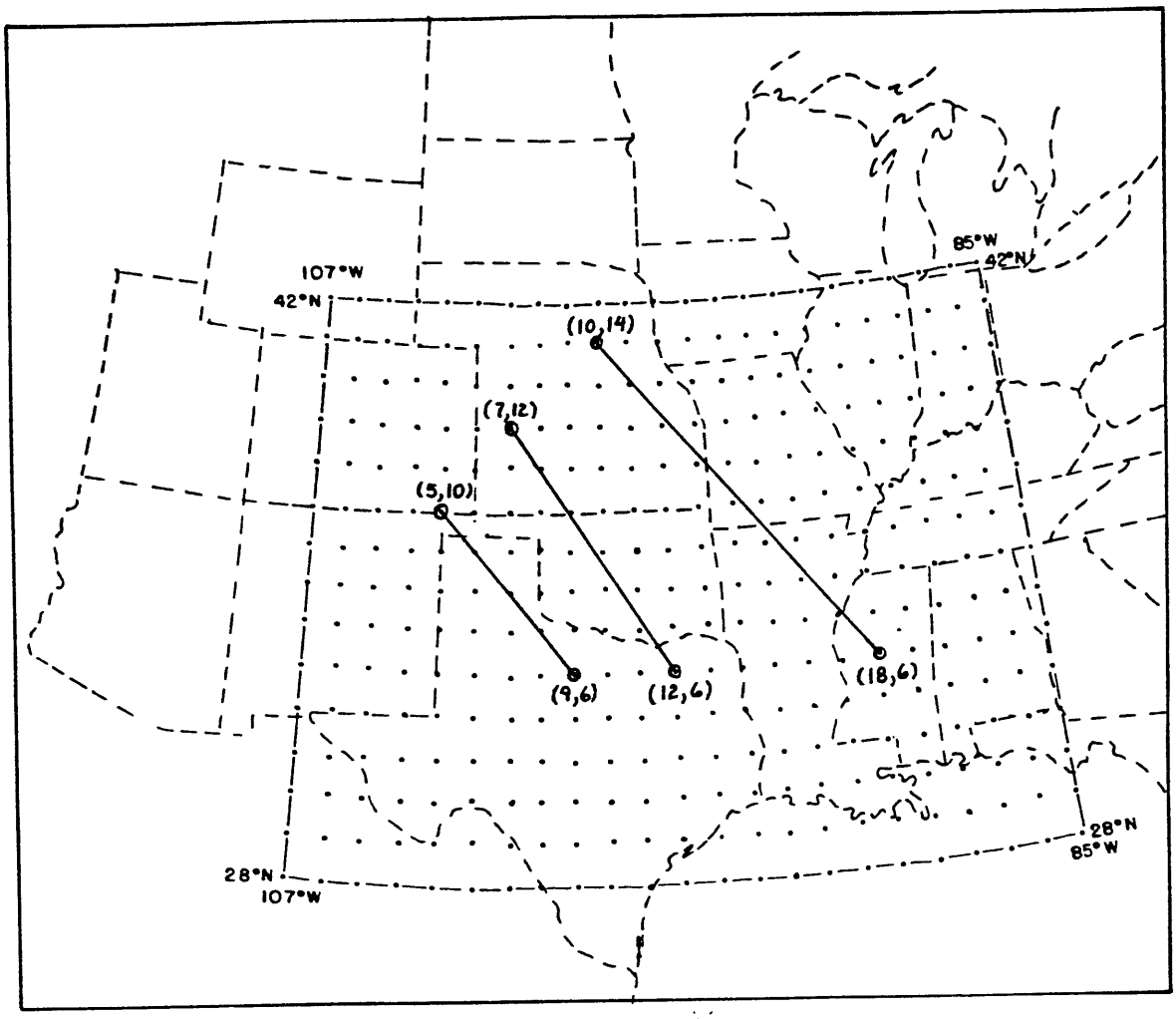


Figure 4.5.8. The orientation of cross sections that are identified by latitude/longitude coordinates.

arrived with band h at 08 GMT 11 April.

The three major bands, E, X, and h consisted of cells and solid lines and each showed continuity for more than ten hours. These three impulses will be investigated in detail in the next section.

4.6 MESOSCALE ANALYSIS OF CONVECTIVE IMPULSES

The first impulse of convection (Bands A and E) developed just prior to 17 GMT 10 April in north central Texas. The convection formed south of the surface warm front in a region with slight latent instability for the surface air as evidenced by the negative SLI's (see Figure 4.4.1).

Band A developed in an area of convergence across northern Texas which extended westward to include the area where band E developed (not shown). The associated kinematic vertical p-velocities at 700 mb (Figure 4.6.1) show weak ascent in a band extending across this region. This low-level convergence, although initially positioned near the weak surface warm front, seems best related to the advancing upper-level jet. At 21 GMT, the height falls identified on the isallohyptic chart for 850 mb (Figure 4.6.2) and the development of a low-level southerly jet (Figure 4.6.3) beneath the exit region of the 500-mb jet are consistent with a coupling between the upper-level jet and the lower-level jet through mass and momentum adjustment as suggested by Uccellini and Johnson (1979).

An inspection of the 15 GMT 850-mb analysis (Figure 4.6.4)

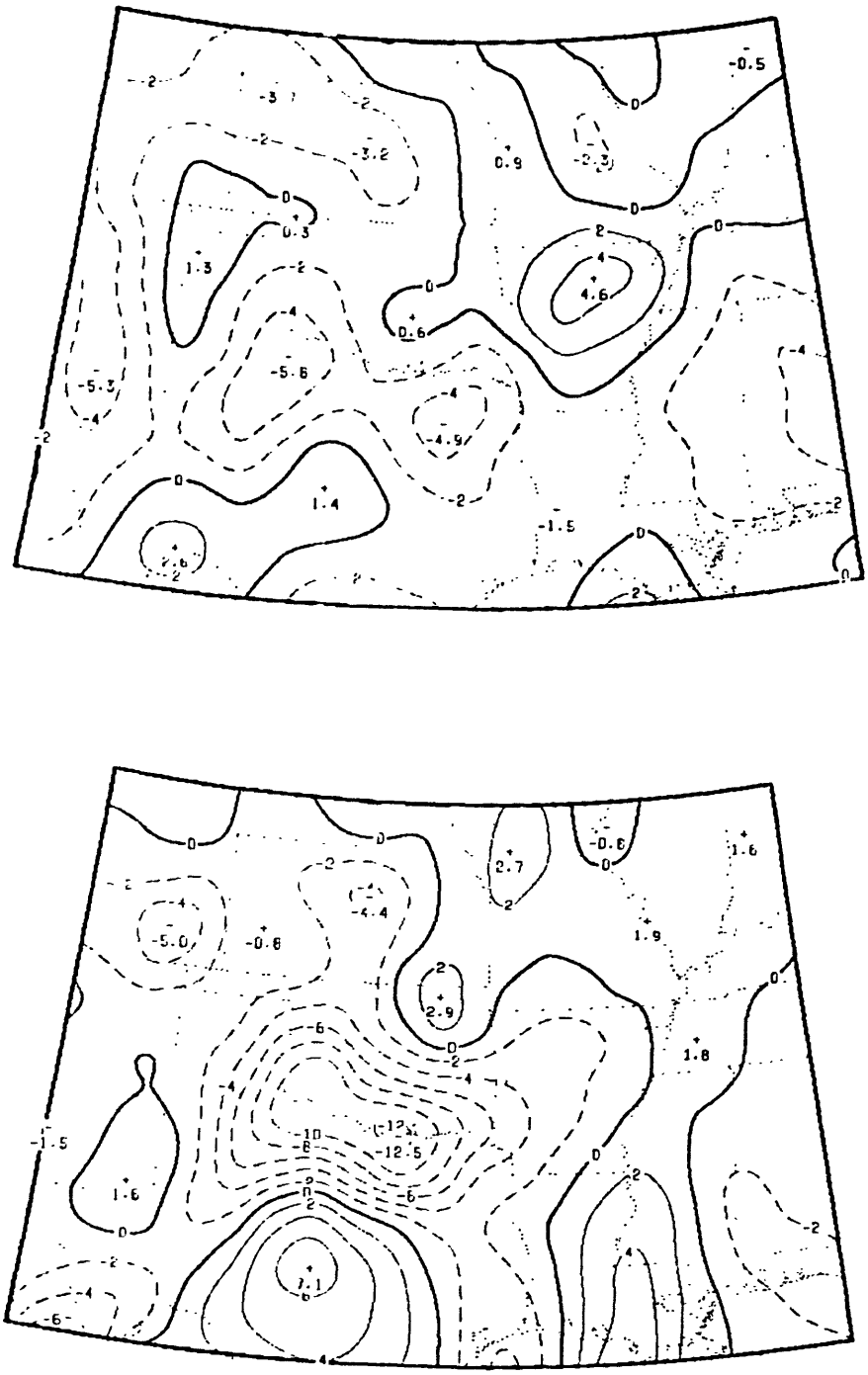


Figure 4.6.1. (a) The kinematically derived vertical p-velocity (μb/s) at 700 mb for 1800 GMT 10 April 1979. (b) The same as (a) except for 2100 GMT 10 April 1979.

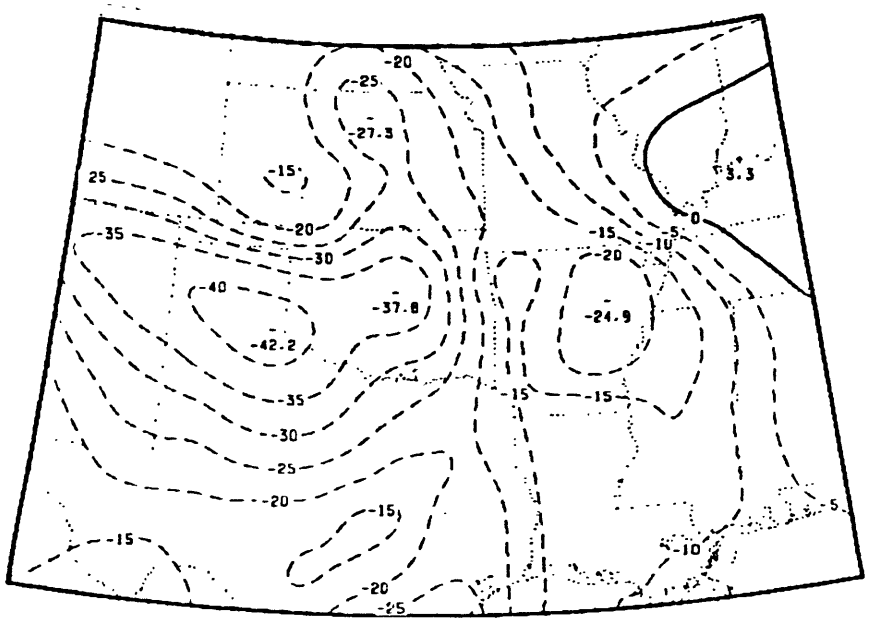
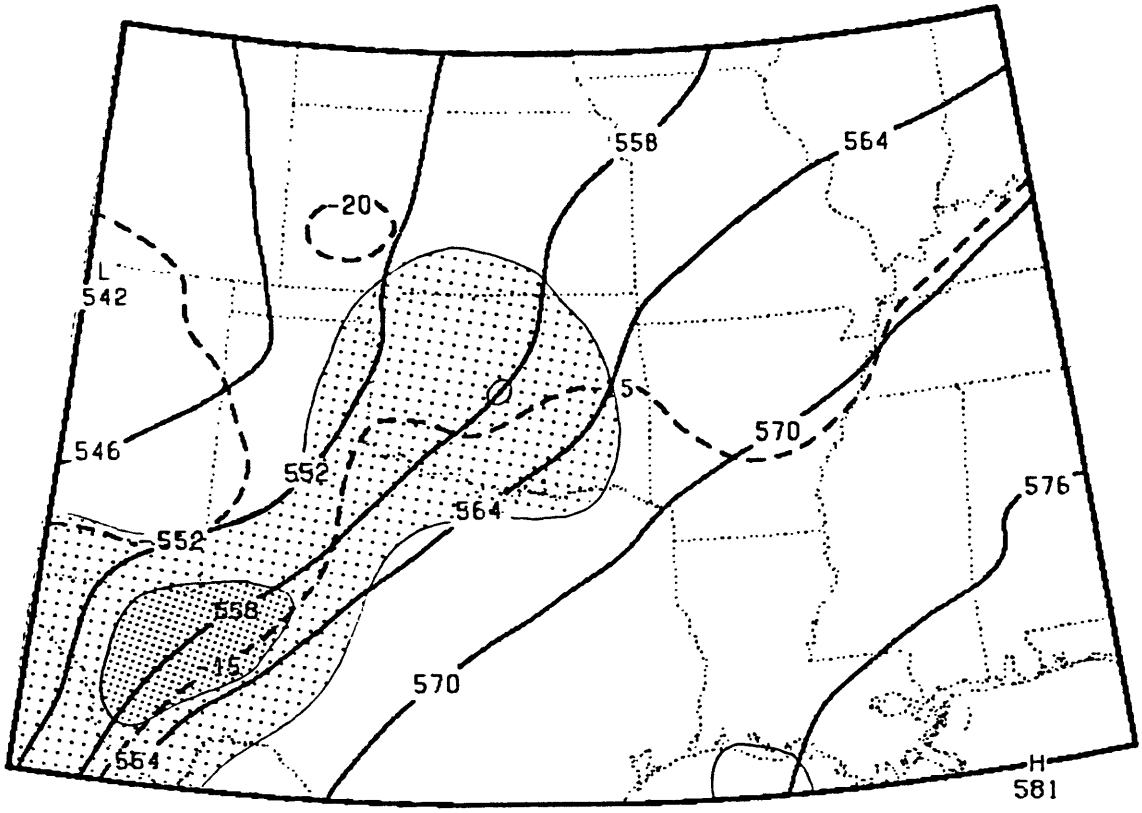
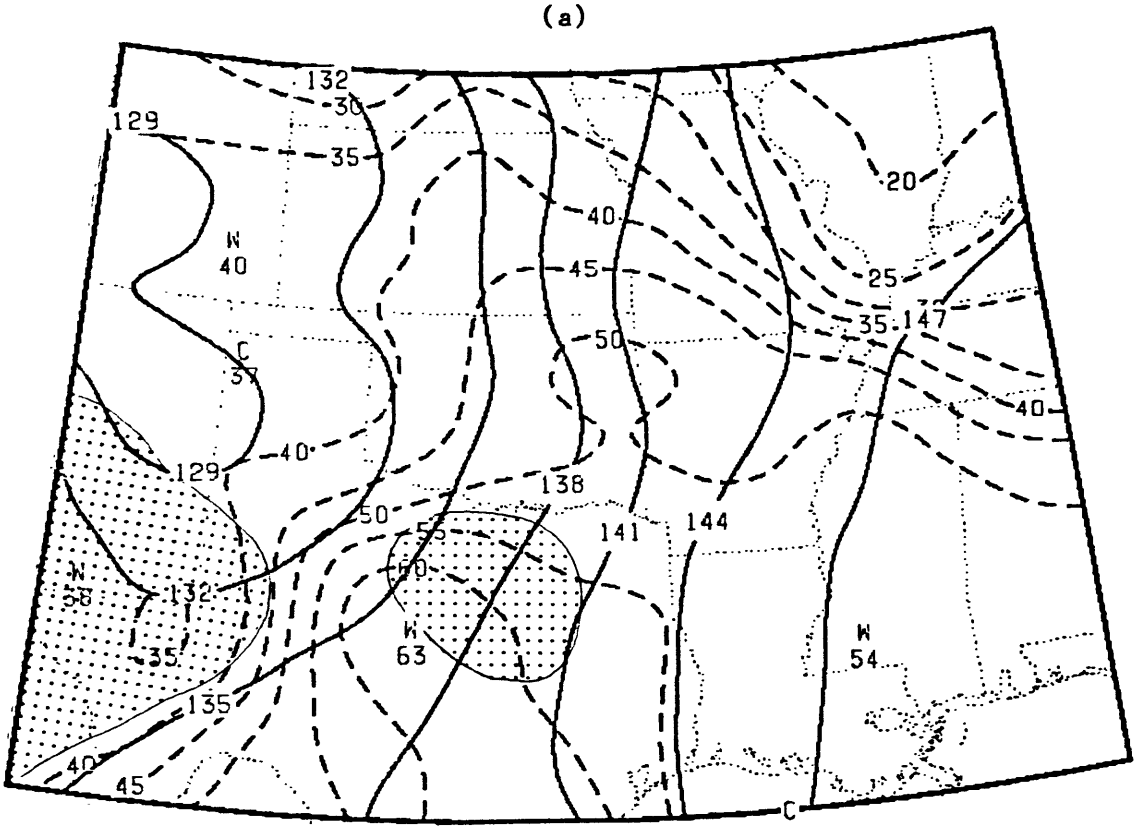


Figure 4.6.2. The 850-mb issallohypses (m) for the period 1500 GMT to 1800 GMT 10 April 1979.

Figure 4.6.3. (a) The 500-mb analysis for 2100 GMT 10 April 1979. The solid lines are height contours (dm). The light shading is for wind speeds 30-39 m/s and dark shading for wind speeds 40-49 m/s. Dashed lines are isotherms. (b) The 850-mb analysis for 2100 GMT 10 April 1979. The solid lines are height contours (dm). The light shading for wind speeds 30-39 m/s. Dashed lines are isopleths of equivalent potential temperature (°C).


558
564
20
L
542
5
570
546
552
576
564
552
558
15
570
564
H
581

(a)


132
30
129
35
20
40
W
40
45
25
35
147
C
50
40
40
129
138
50
55
141
144
60
W
58
132
W
63
W
54
35
135
40
45
C

(b)

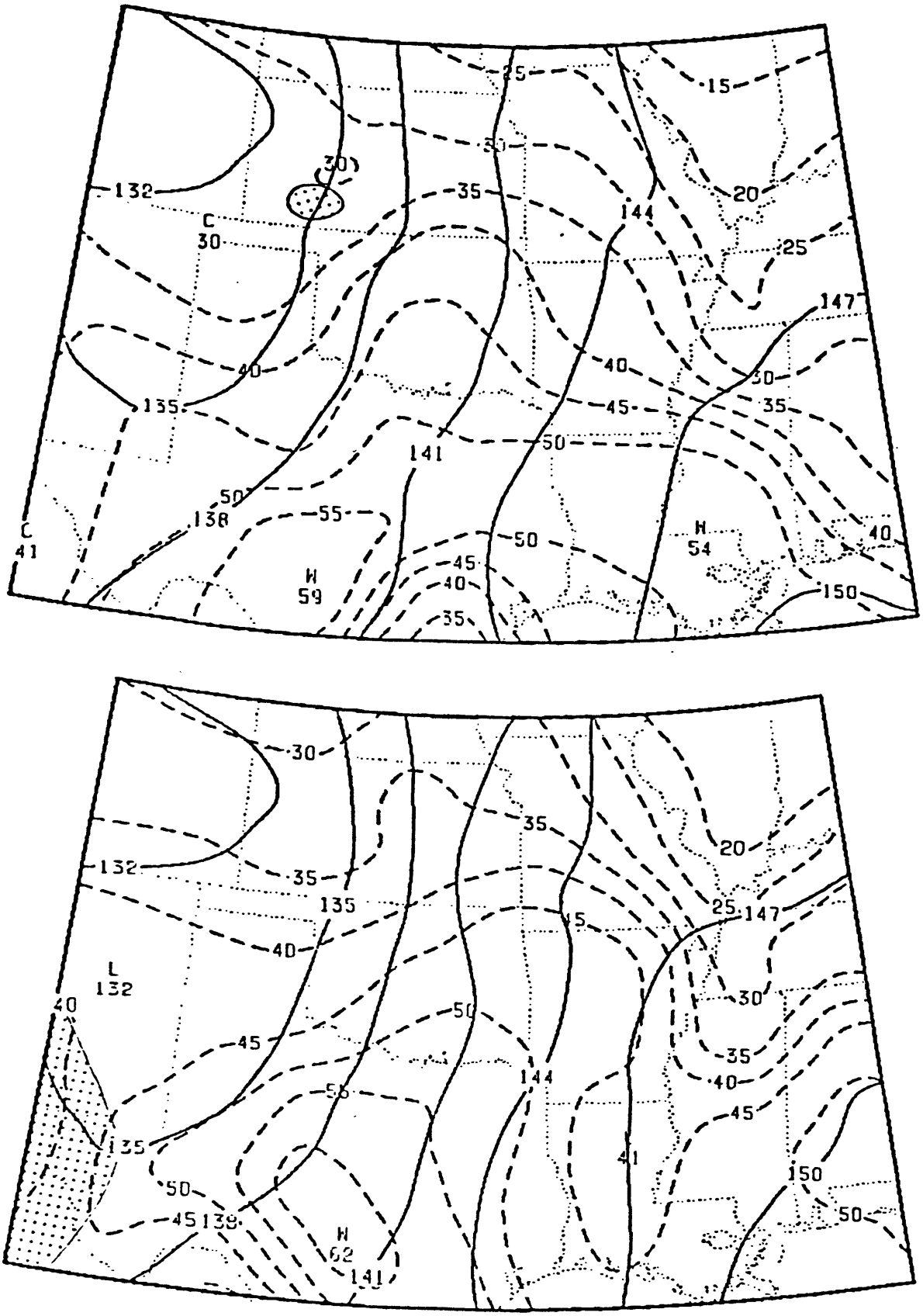


Figure 4.6.4. (a) The 850-mb analysis for 1500 GMT 10 April 1979. The solid lines are height contours (dm). The light shading is for wind speeds 20-29 m/s. The dashed lines are isopleths of equivalent potential temperature (°C). (b) The same as (a) except for 1800 GMT 10 April 1979.

reveals a bulge in the equivalent potential isotherms (θ_e) extending into Oklahoma. There was a minimum in the geostrophic advection of θ_e at 15 GMT southwest of Childress, Texas (CDS), however, by 18 GMT this minimum had been replaced by a relative maximum. The rotation of the θ_e isotherms to be positioned more east-west is explained by the ageostrophic response (see Figure 4.6.5) to the height falls in western Texas. This westward shift in high θ_e air is related to the development of E just prior to 18 GMT.

The structure of the boundary layer also seemed to be important in determining the development of band A. Figure 4.6.6 shows that the boundary layer, uniform near the surface, displayed strong variations in depth. The maximum in θ_e of 334.5°K at 800 mb at Junction, Texas (JCT) identifies a moisture ridge that is transported northward during the morning hours.

To get a better understanding of the convective potential for the lower part of the troposphere and not just the surface planetary boundary layer (PBL) we determined the cloud work function (Arakawa and Schubert, 1974) for multiple layers above the surface. The cloud work function is defined as

$$A(\lambda) = \int_{Z_B}^{Z_T(\lambda)} \frac{g}{C_p T(z)} \eta(z,\lambda) \left(S_{vc}(z,\lambda) - \bar{S}_v \right) dZ$$

C_p is the specific heat at constant pressure, Z_B is the cloud base height, Z_T is the cloud top height, S_{vc} and S_v are the

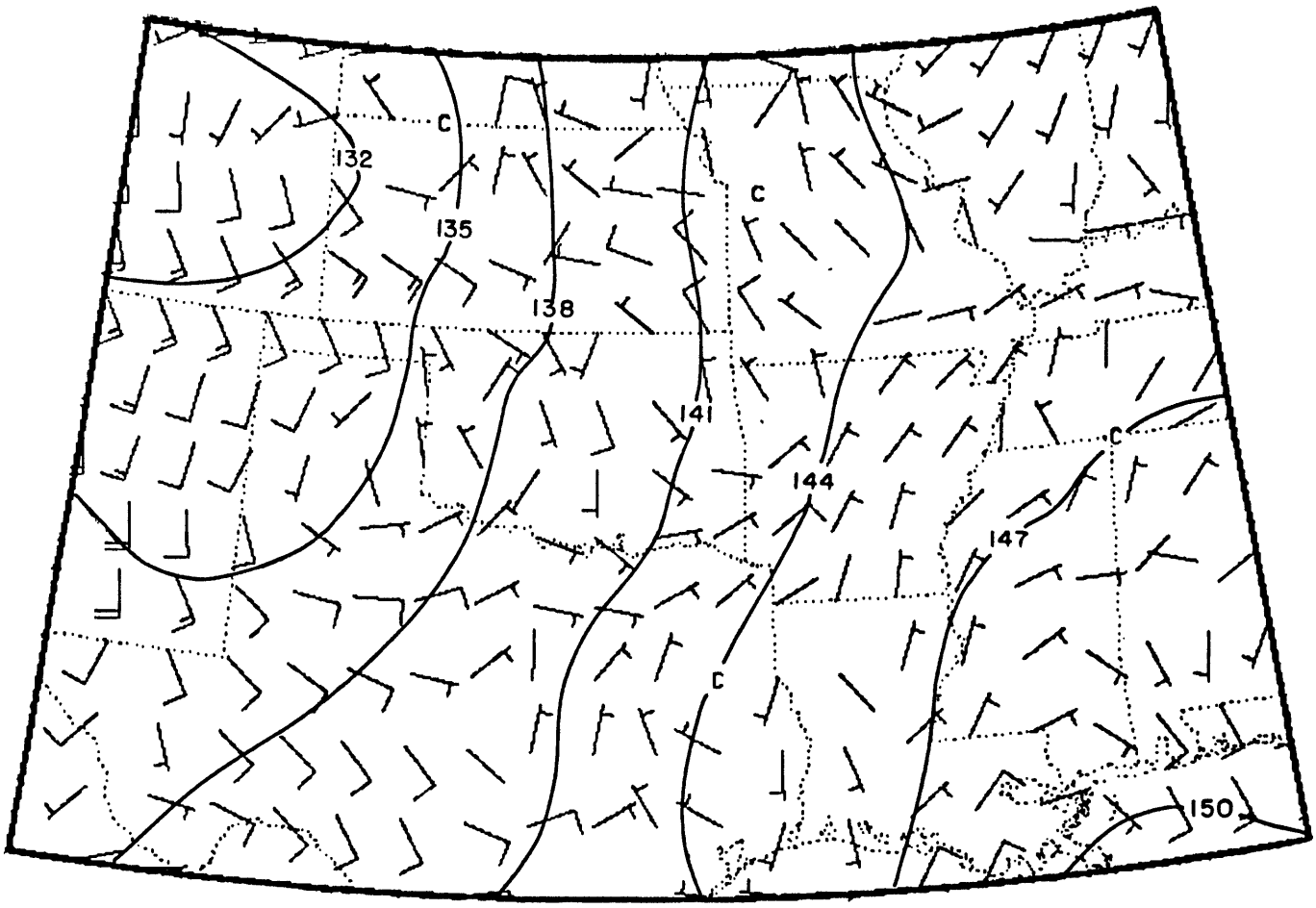
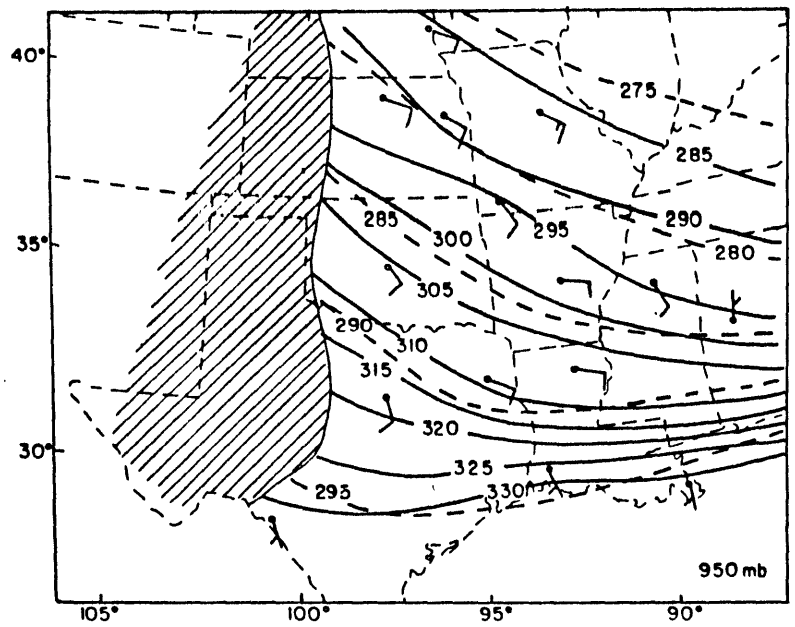
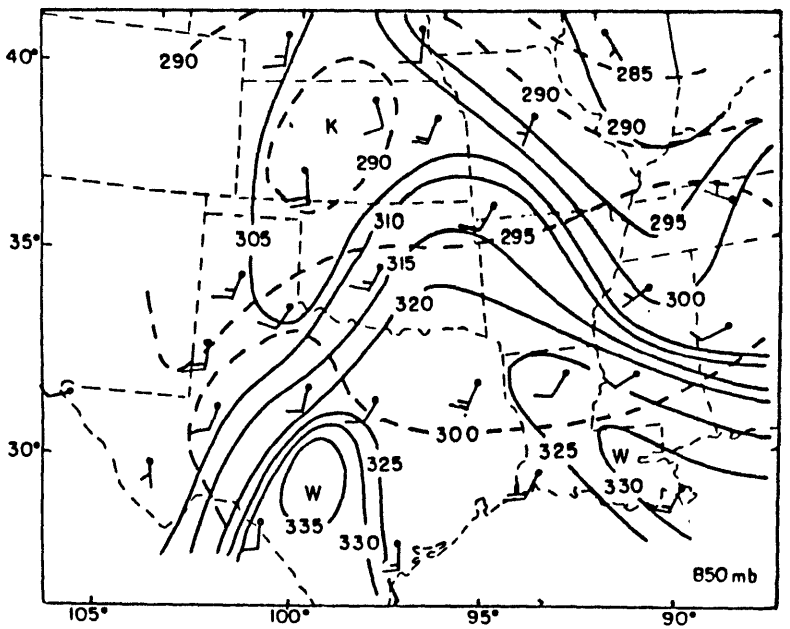
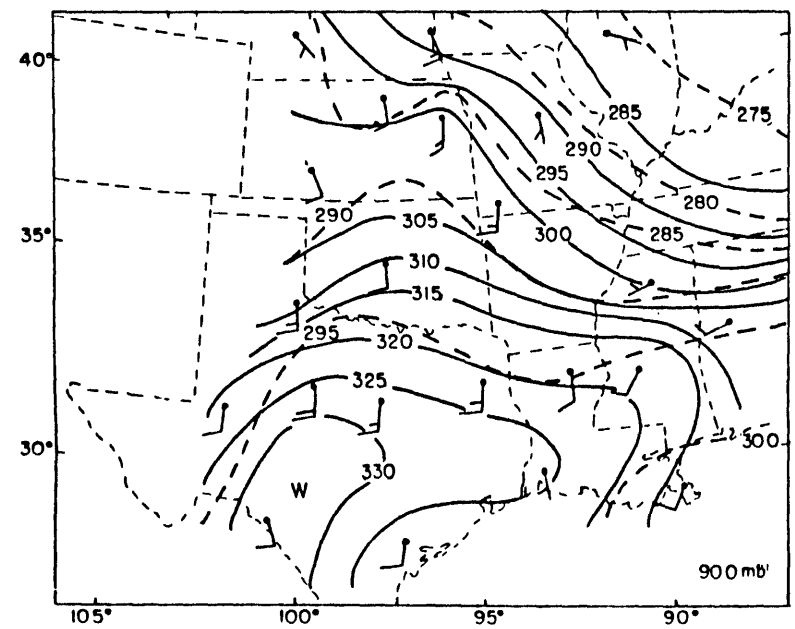


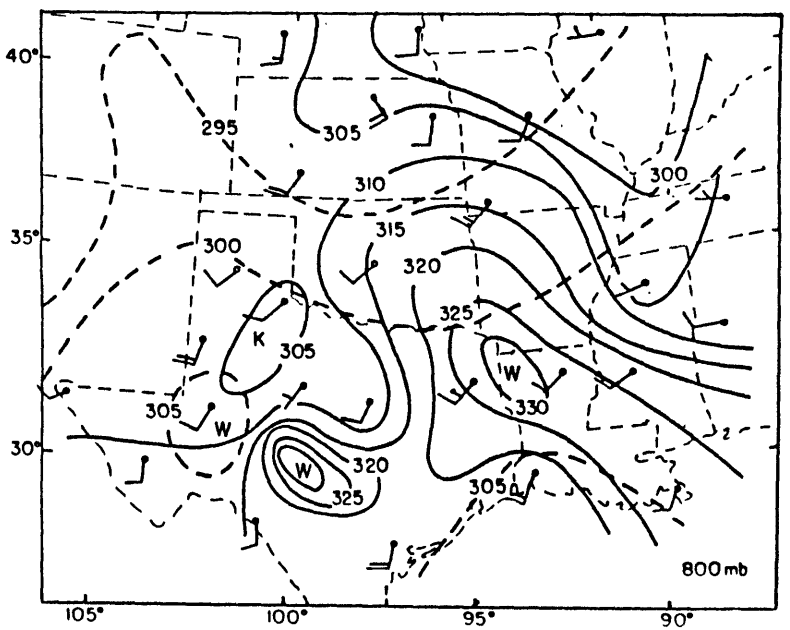
Figure 4.6.5. The ageostrophic wind component at 850 mb for 1500 GMT 10 April 1979. Plotting is done in the conventional manner (m/s). The solid lines are height contours (dm) for the same level.

Figure 4.6.6. Constant pressure analyses of potential temperature (dashed lines) and equivalent potential temperature (solid lines) in °C for a) 950 mb b) 900 mb c) 850 mb and d) 800 mb. Winds are plotted in the conventional manner (m/s).


40°
35°
30°
105°
100°
95°
90°
275
285
285
300
295
290
280
305
290
310
315
320
325
295
330
950 mb


40°
35°
30°
105°
100°
95°
90°
290
K
290
285
290
290
290
295
305
310
295
315
320
300
300
325
325
W
W
330
335
330
850 mb


40°
35°
30°
105°
100°
95°
90°
285
275
290
295
280
290
305
300
285
310
315
295
320
325
W
330
300
900 mb


40°
35°
30°
105°
100°
95°
90°
295
305
310
300
315
300
320
325
K
305
W
305
W
330
320
W
325
305
800 mb

virtual static energies of the cloud and the environment, respectively, and η is the normalized cloud base mass flux. λ is the fractional entrainment rate. The cloud work function is the rate of kinetic energy generation, by the buoyancy force, per unit mass. If λ is taken as zero, the cloud work function is equivalent to the integrated area on a thermodynamic diagram, as a parcel is lifted pseudo-adiabatically from its initial position to cloud top.

The cloud work function was calculated for each of the 10 lowest 25-mb layers in the soundings with λ set to zero. Lord (1974), using tropical data, estimated an equilibrium cloud work function for a cloud that reaches 150 mb at 1685 J/KG.

Figure 4.6.7 is a plot of the maximum cloud work function and at what level it occurred for 18 GMT. Stephenville, Texas (SEP) had one of the largest cloud work functions at the lowest pressure. Figure 4.6.8 shows the kinematically derived vertical p-velocity for this area at 18 GMT. The moisture ridge was deep enough that even though the low-level convergence was modest, it was strong enough to release the potential instability at 750 mb in less than one hour's time. This time is estimated by applying the vertical velocities for each level to the sounding and determining the amount of lift required for the 750-mb air to become neutral with respect to the 725-mb air, when both layers are lifted at the calculated rate for that level (see Figure 4.6.9).

For regions where the boundary layer moisture is shallower, much stronger convergence, or at least convergence on a smaller scale,

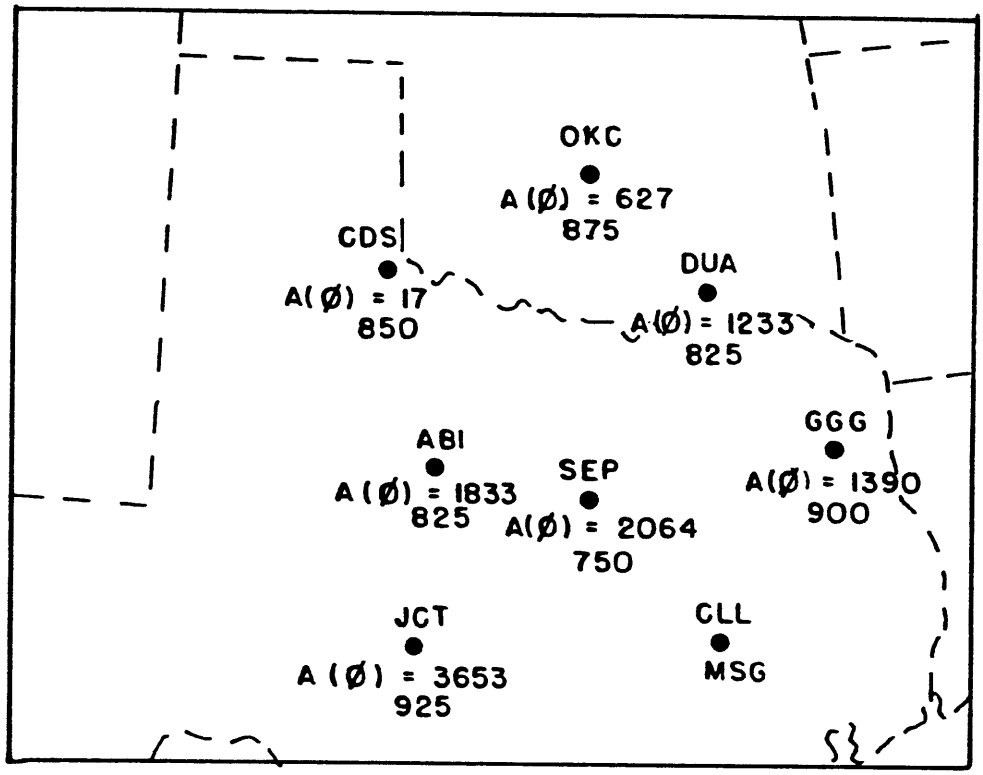


Figure 4.6.7. The maximum cloud work function (J/kg) for 1800 GMT 10 April 1979 calculated from a 25-mb layer in the lower 250 mb of the sounding with the subscript denoting the pressure of that layer.

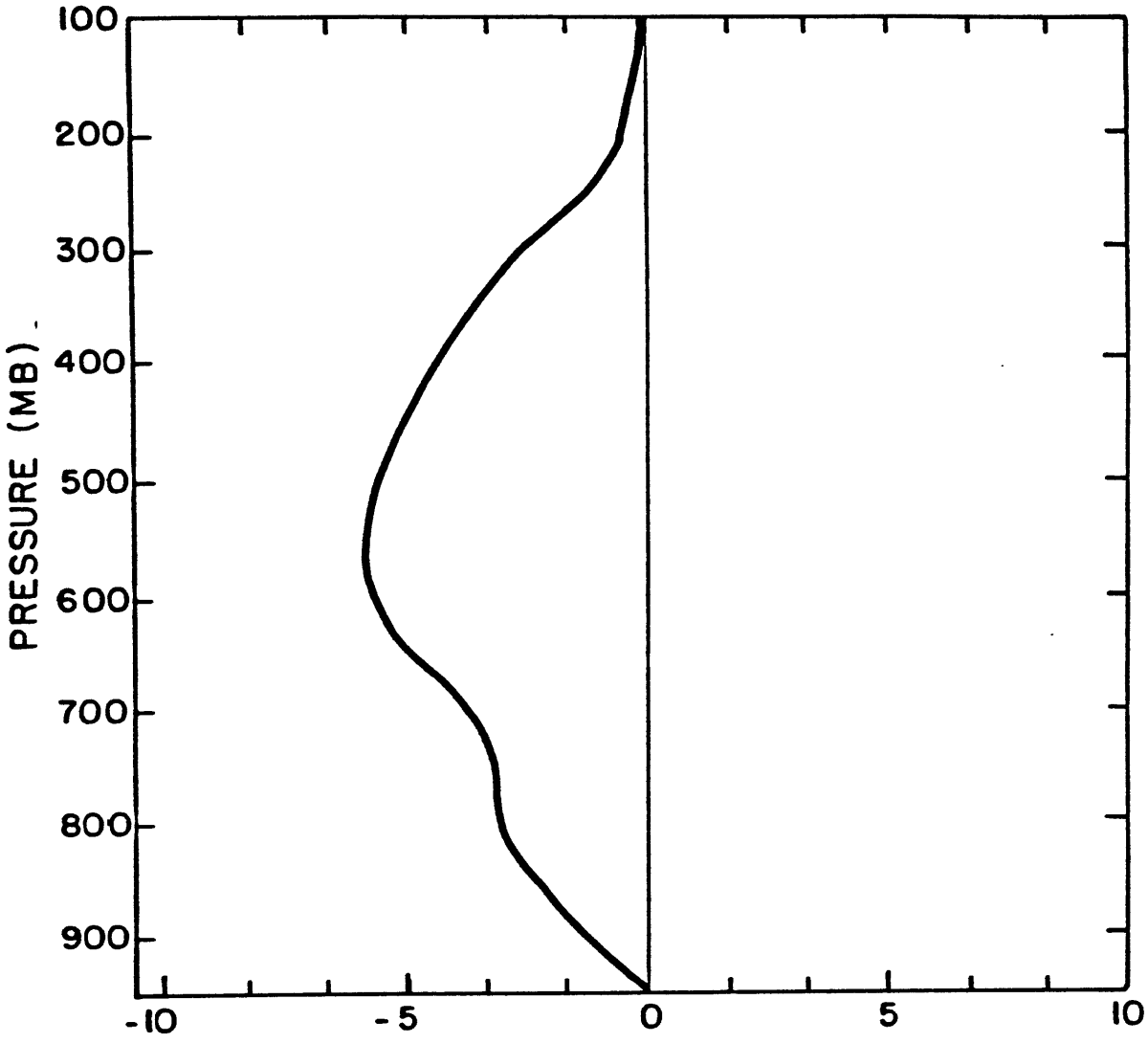


Figure 4.6.8. The vertical profile of the kinematically derived vertical p-velocity (μb/s) for 1800 GMT 10 April 1979 in the vicinity of SEP.

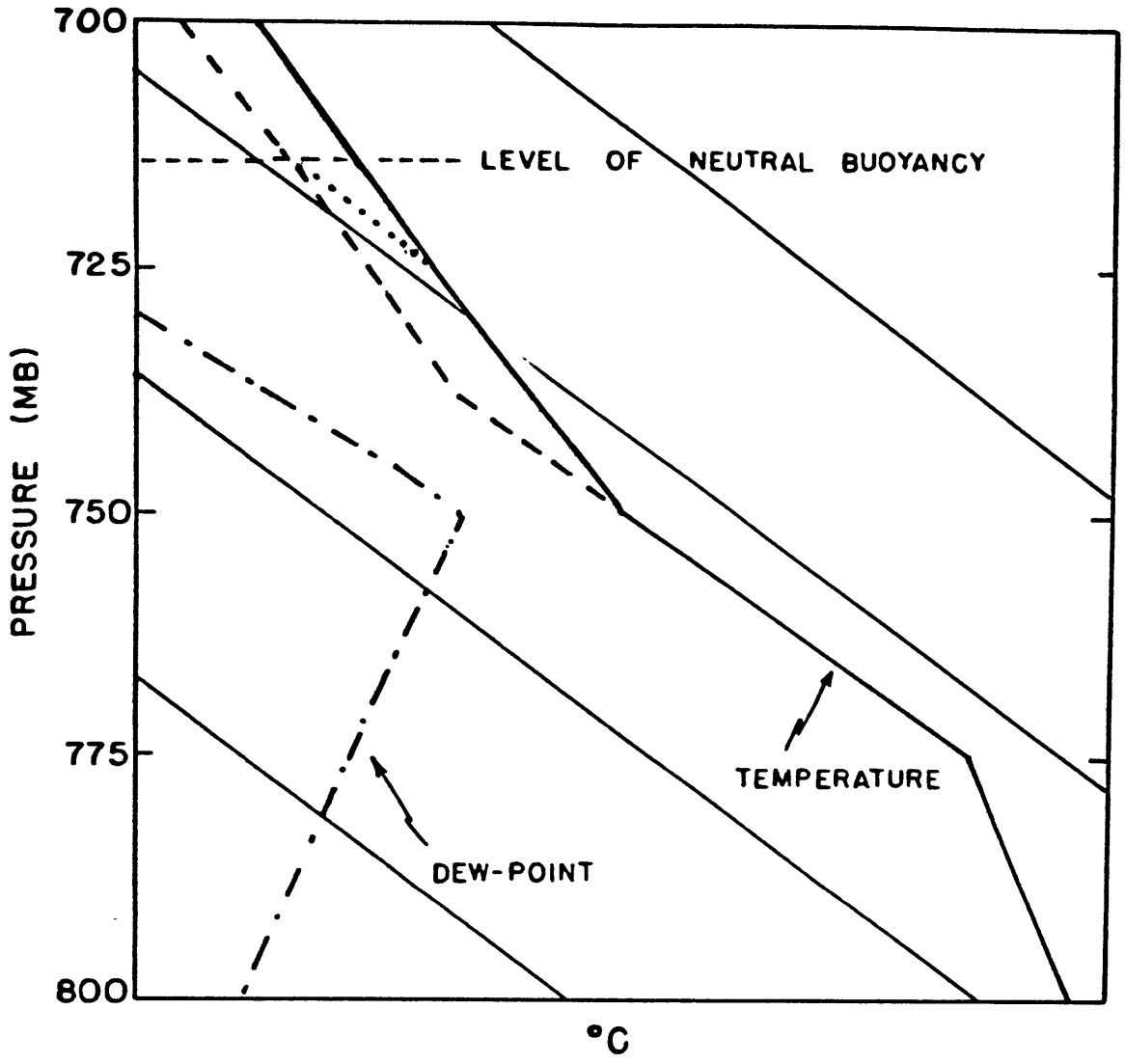


Figure 4.6.9. A schematic showing the method used on a pseudo-adiabatic diagram to determine the amount of lift required to destabilize the sounding when lift is applied to two layers. The sloping straight lines are isentropes. The state curves for the air at 750 mb and 725 mb are shown dashed and dotted, respectively.

would be necessary to release the potential instability.

Band A was aligned along the geostrophic shear. However, an investigation of the environment showed that is was not unstable to conditional symmetric instability.

As the bands associated with this first surge swung northeastward they overrode the frontal surface and became elevated. The mesoscale updraft associated with its initiation also moved north and more than doubled to a value of 12.5 μb/s at 700 mb by 21 GMT. Refer to Figure 4.6.1.

By 03 GMT 11 April the convective surge appeared to have developed into a quasi-steady mesoscale circulation. Figure 4.6.10 shows the mesoscale updraft and thermodynamic structure perpendicular to band E at 03 GMT. The low-level jet had increased to 35 m/s at Monett, Missouri (UMN) at 850 mb. The ageostrophic component (see Figure 4.6.11) accounts for more than half of this speed. There is a region above the frontal surface, just to the southeast of the band position, where the atmosphere approaches neutrality for dry symmetric instability (see Figure 4.6.12), possibly accelerating the low-level inflow of high θ air (compare with Figure 4.6.10). In the region of the band, the M surfaces become vertical indicating a barotropic environment in which the motion associated with an inertial circulation is vertical and comparable to upright convection.

Subsidence ahead of the band, which shows up in the kinematic p-velocities, agrees with Brown's (1979) finding that required low-level subsidence to maintain the convergence. This is also

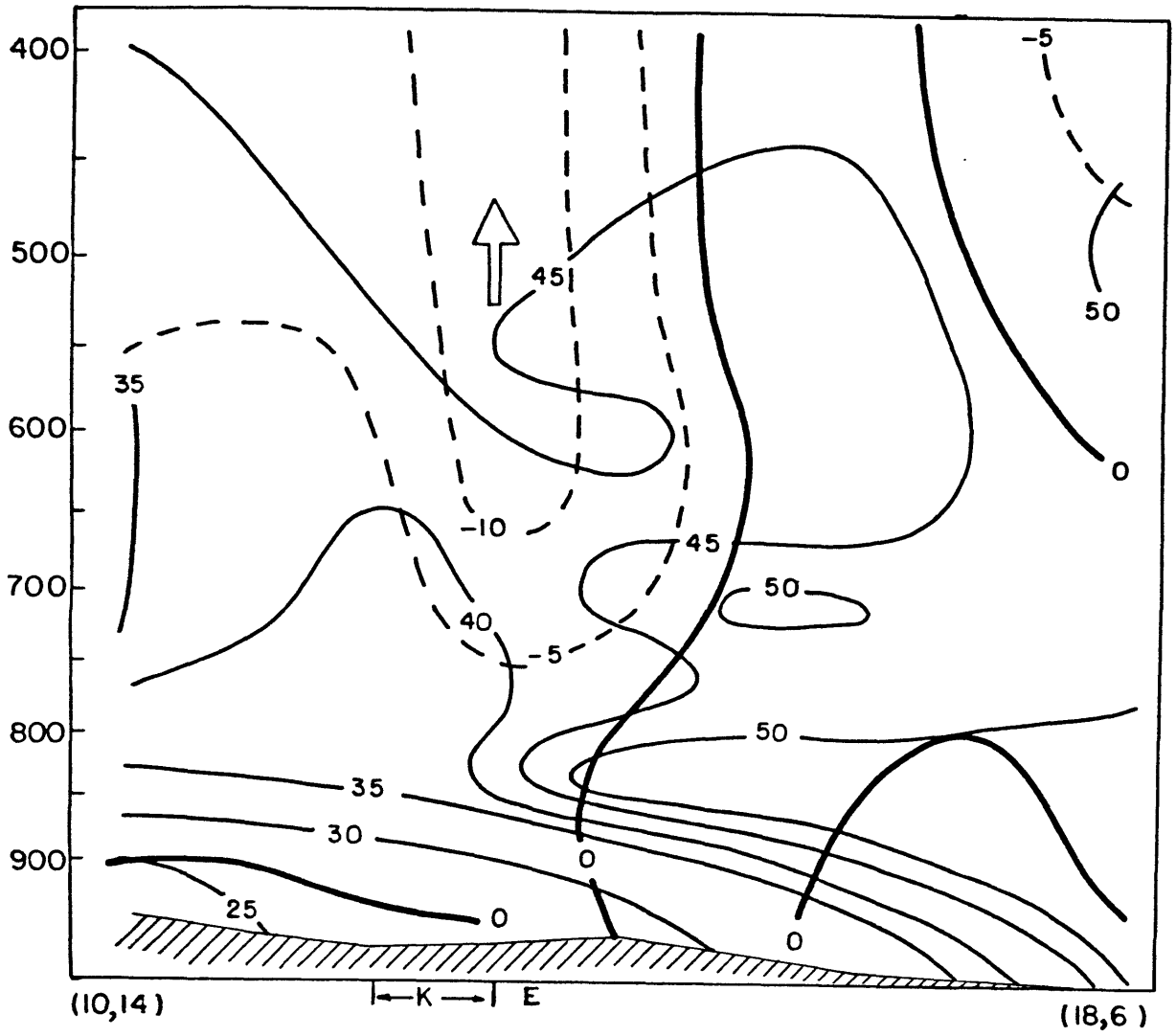


Figure 4.6.10. A vertical cross section along the line from (98°W, 41°N) to (90°W, 33°N) for 0300 GMT 11 April 1979. Refer to Figure 4.5.8 for location. The dashed lines are isopleths of equivalent potential temperature. The solid lines are contours of the vertical p-velocity in μb/s. Band positions are denoted by K and E.

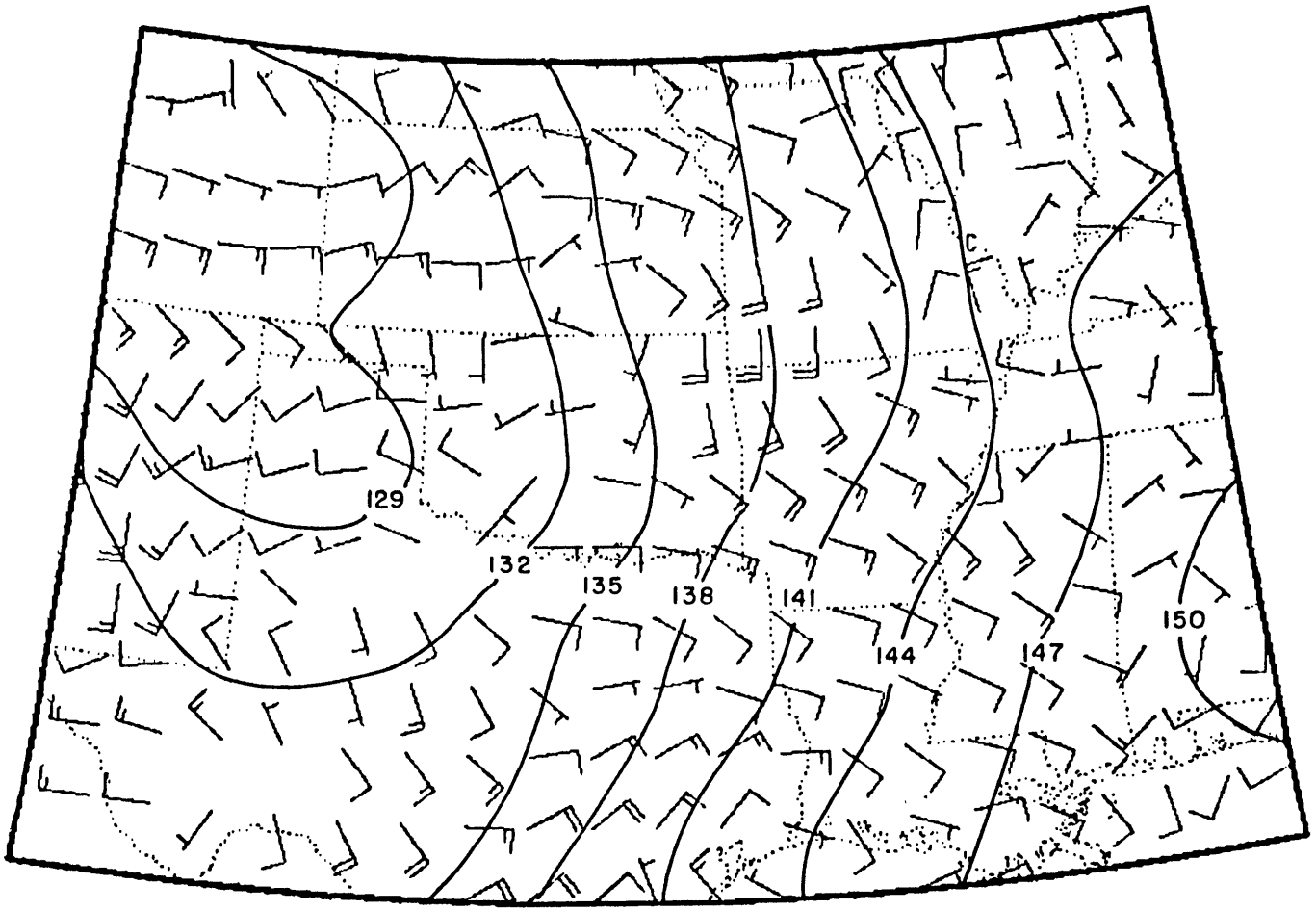


Figure 4.6.11. The ageostrophic wind component at 850 mb for 0300 GMT 11 April 1979. Plotting is done in the conventional manner (m/s). The solid lines are height contours for the same level (dm).

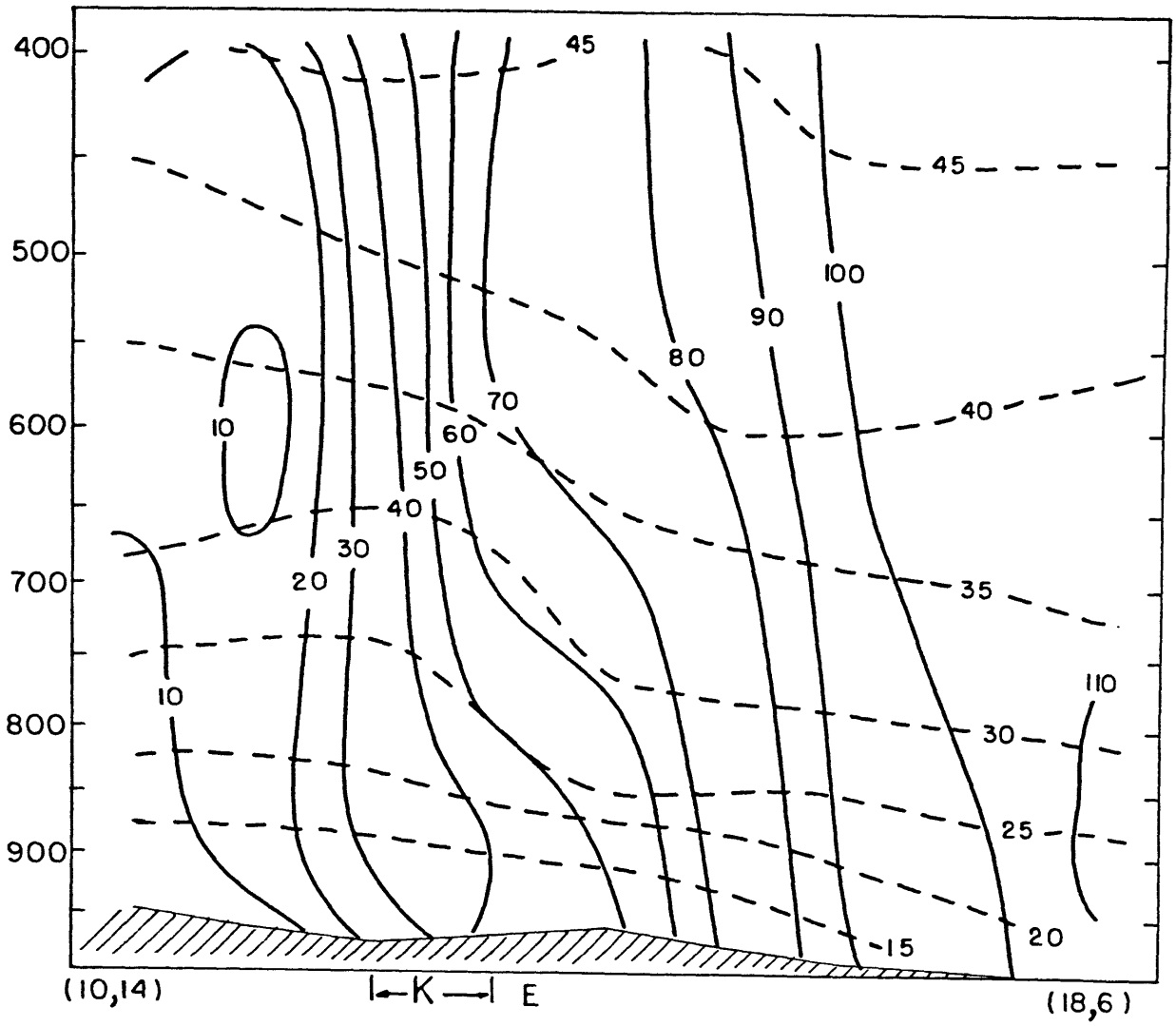


Figure 4.6.12. A vertical cross section along the line from (98°W, 41°N) to (90°W, 33°N) for 0300 GMT 11 April 1979. Refer to Figure 4.5.8 for location. Solid lines are isopleths of constant geostrophic angular momentum (m/s). The dashed lines are isentropes (°C). Band positions are denoted by K and E.

supported by the comparison of the UMN sounding with the Little Rock, Arkansas (LIT) sounding (not shown) which showed equal equivalent potential temperatures lower at UMN with a greater dew-point spread.

The second surge, characterized by band X and S, moved into the radar study area at 03 GMT 11 April. This convection developed in central Texas at about 23 GMT just to the east of the dryline. The line is clearly visible on the 23 GMT satellite picture south of Abilene, Texas (ABI) (see Figure 4.6.13). This development took place on the western edge of a moisture ridge which is visible on the 850-mb analysis for 21 GMT (Figure 4.6.3). Figure 4.6.14 shows the time-height cross section of the cloud work function for Del Rio, Texas (DRT). The air with the highest convective potential in the 11 GMT 10 April sounding was at 900 mb. 11 GMT is early morning and this maximum most likely represents the previous day's boundary layer that was not as affected by the surface nocturnal cooling as the near surface layer. This deep boundary layer, undoubtedly heated during the day, was transported northward into central Texas at the time band X was developing. The convection moved northeastward into Oklahoma along a track similar to band E.

At 03 GMT 11 April, the same time as when band E was located in northeast Oklahoma, the second surge of convection moved onto the frontal surface in southern Oklahoma. Figure 4.6.15 shows a cross section which helps define the moisture impulses associated with the first two convective surges. The orientation of the cross section is shown in Figure 4.6.16. The cross section, parallel to bands E and

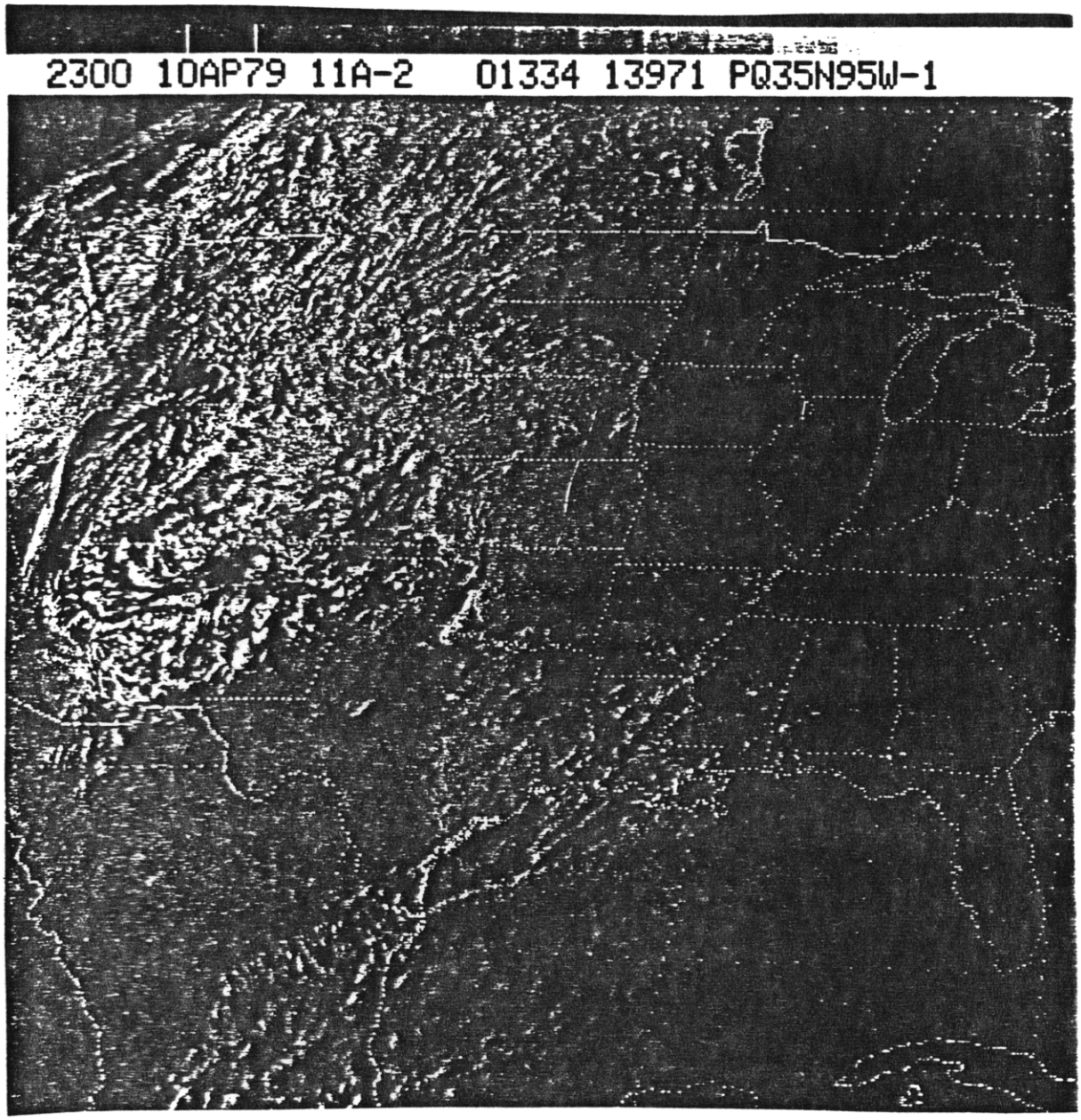


Figure 4.6.13. The visible satellite picture for 2300 GMT 10 April 1979.

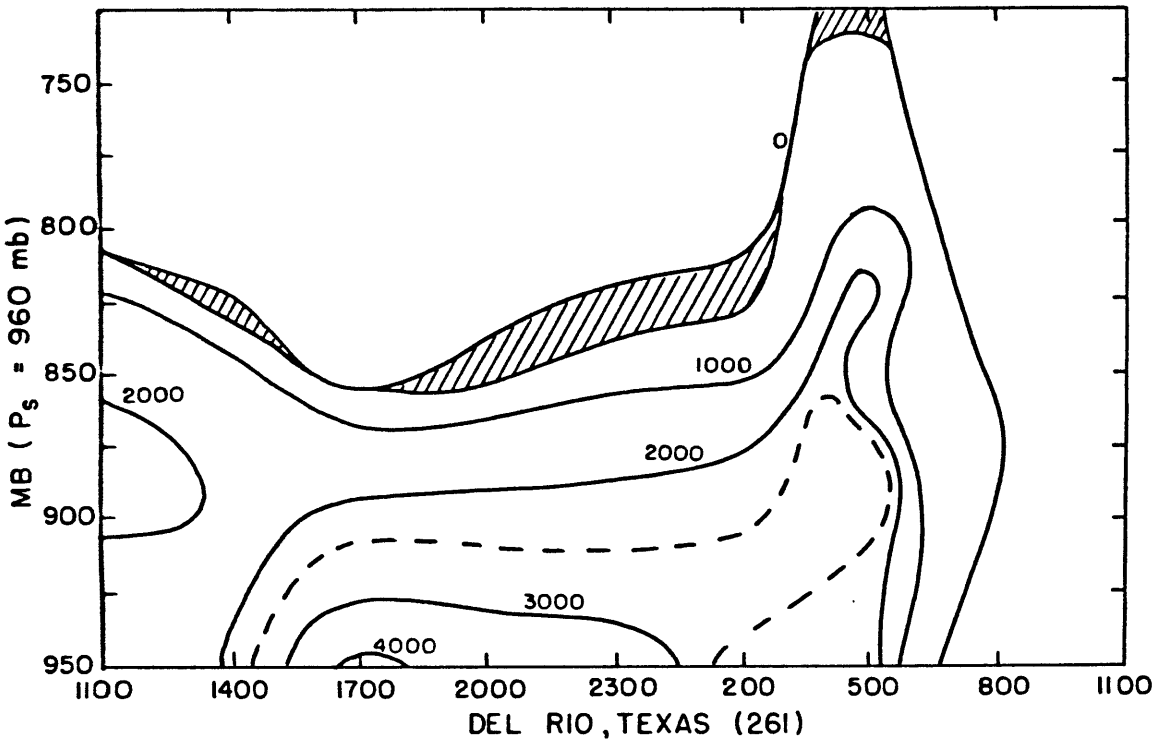


Figure 4.6.14. The time-height cross section of the cloud work function (J/kg) for Del Rio, Texas.

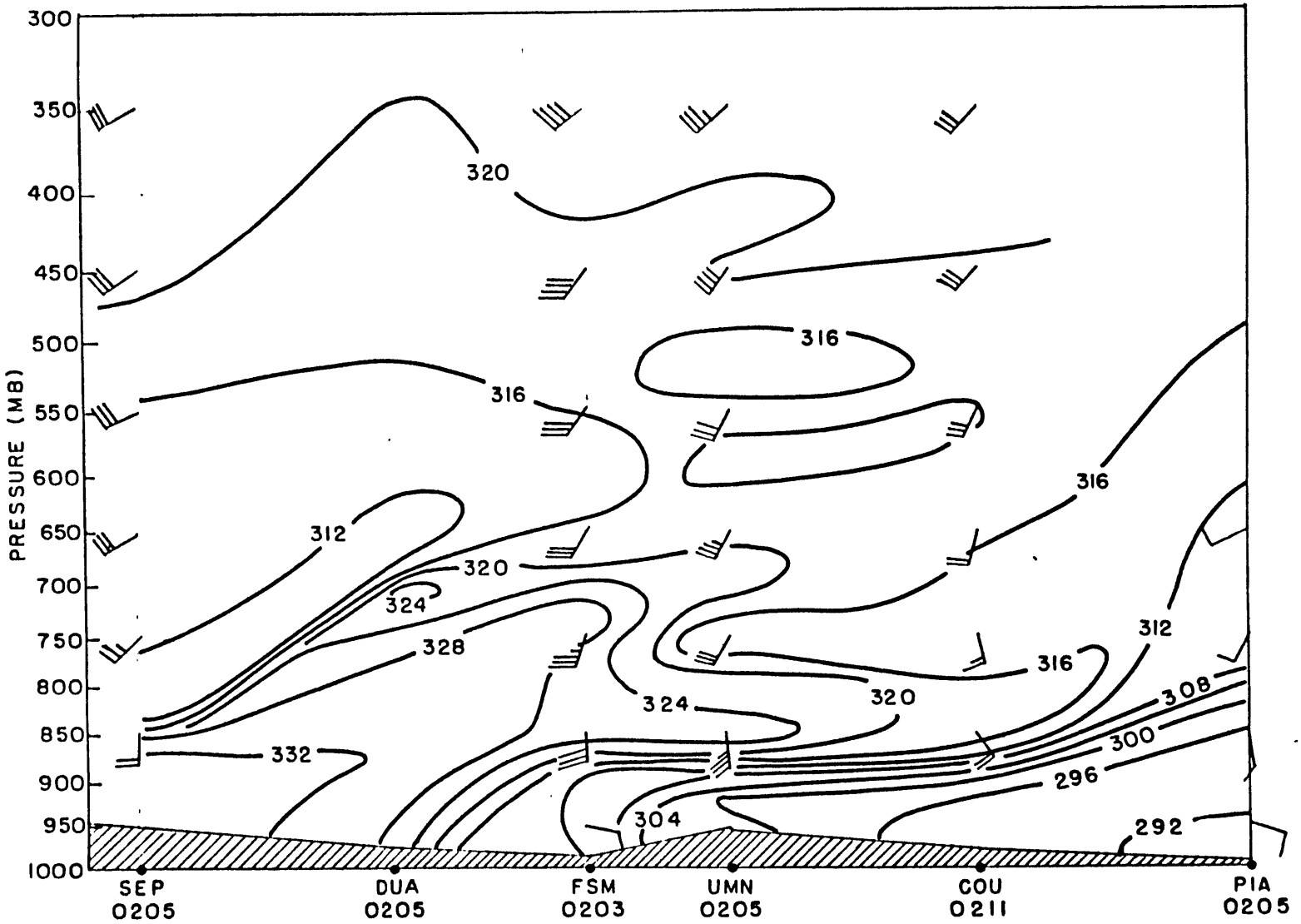


Figure 4.6.15. A cross section for the line from SEP to PIA for 0300 GMT 11 April 1979. The solid lines are isopleths of equivalent potential temperature (^{o}C). Winds are plotted in the conventional manner (m/s).

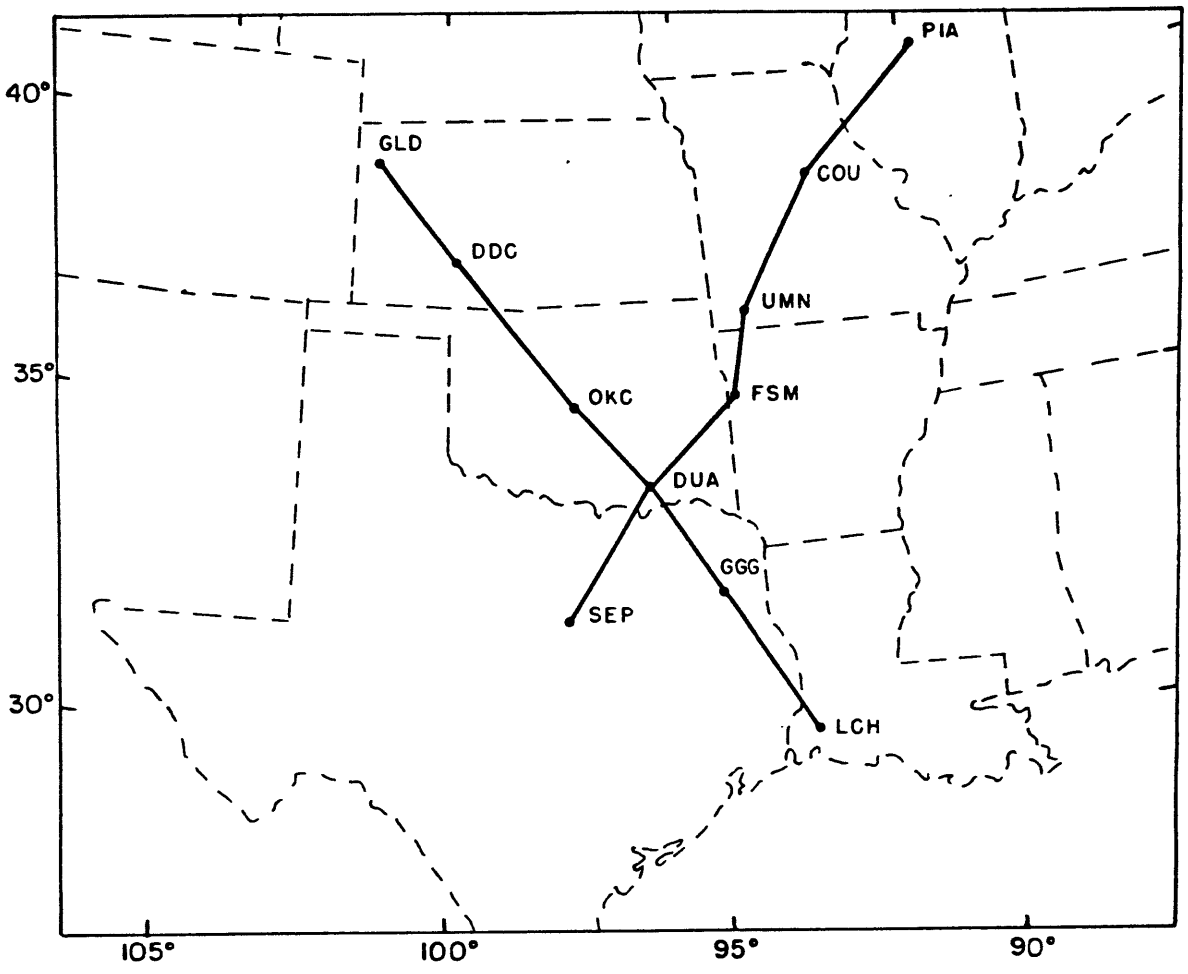


Figure 4.6.16. The orientation of cross sections that are identified by 3-letter station identifiers.

X/S, shows the new impulse of high θ air overriding the front. The shallower 'baroclinic leaf' extending farther northeast to COU was the impulse associated with E and A. Figure 4.6.17 shows the cross section that runs from Goodland, Kansas (GLD) to Lake Charles, Lousiana (LCH). The convective bands are positioned very close to the right flank of the sharply defined moisture impulse.

Finally, the third impulse of convection moved into the radar study area with band h at 08 GMT 11 April. Without satellite pictures or radar summaries for the period when this impulse was triggered, we can only speculate that it was rooted in the boundary layer ahead of the cold front.

At 09 GMT band h was positioned just east of the triple-point in the frontal analysis. A third moisture surge is outlined by the θ_e isotherms on the 850-mb analysis for 09 GMT in northern Texas (Figure 4.6.18). By 12 GMT the band had moved over the warm-frontal surface. The radar analysis for 12 GMT displays the LEWP in band h that was seen with band E. Band h displayed slightly different characteristics from the other two discussed. An initial surge moved northeastward above the frontal surface along a similar path to the previous elevated convection. However, the band was more intimately associated with the cold front and the remaining band developed into an elongated line of echoes positioned north-south just ahead of the cold front. The AVE-SESAME I experiment stopped at 12 GMT making it difficult to determine the characteristics of this band. An inspection of the surface analyses and radar analyses for 21 GMT (see Figures 4.3.4 and

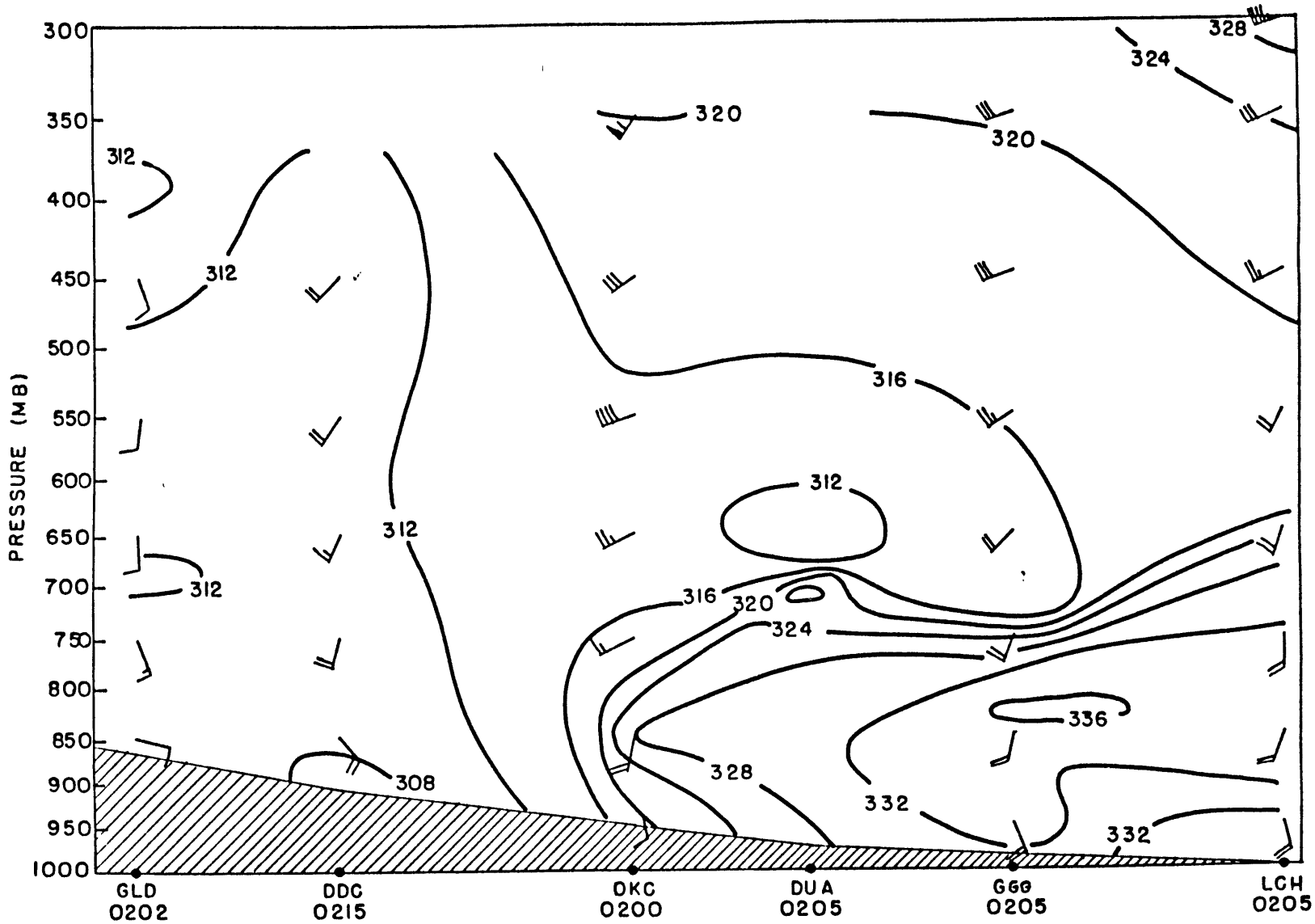


Figure 4.6.17. The same as Figure 4.6.15 except that it is for the line from GLD to LCH.

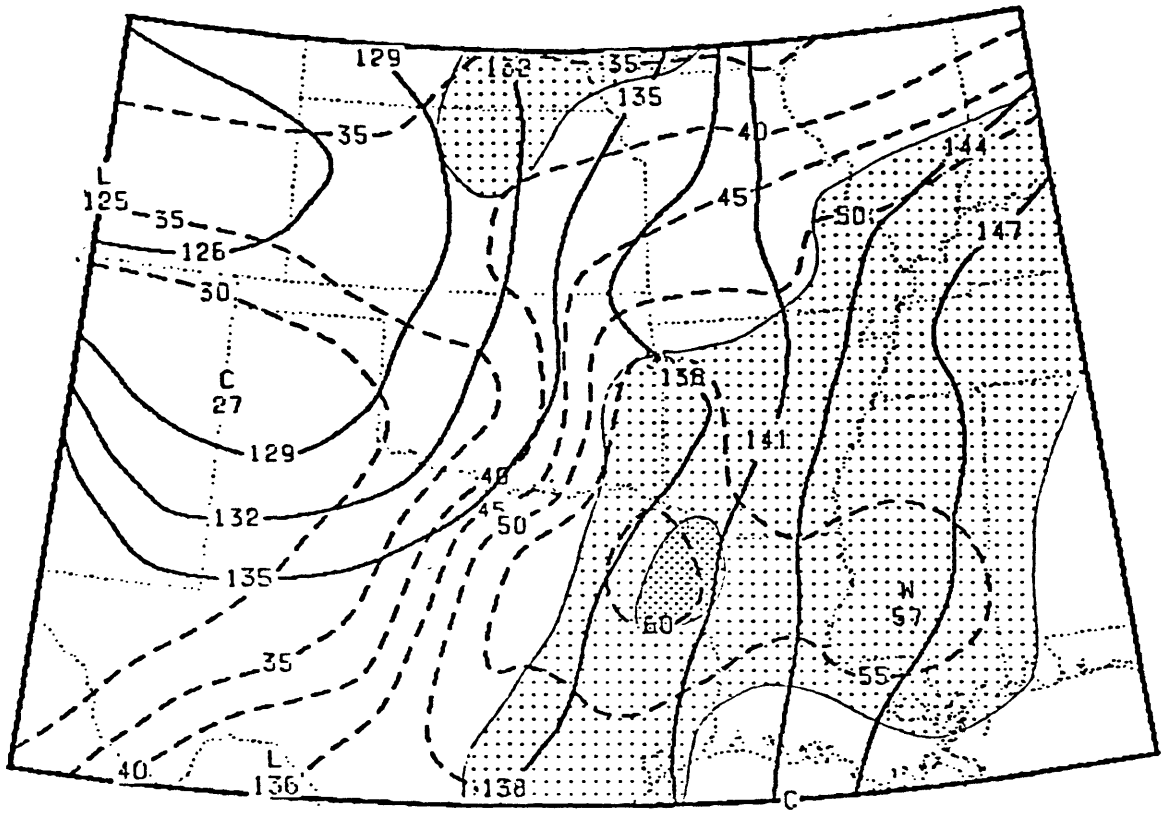


Figure 4.6.18. The 850-mb analysis for 0900 GMT 11 April 1979. The solid lines are height contours (dm). The light shading is for wind speeds 20-29 m/s and dark shading for wind speeds 30-39 m/s. The dashed lines are isopleths of equivalent potential temperature (°C).

4.5.3) suggest that the band was rooted in the boundary layer over Arkansas and extended north over the front into Missouri. It was oriented parallel to the cold front and the extension of the cold front above the warm-frontal surface. This is similar to the findings of Kreitzberg and Brown (1970) where the final bands in their case were oriented parallel to the cold-frontal baroclinic zone and wind shear.

The three main impulses of convection have been shown to be associated with convection that originated in the boundary layer and then propagated onto the frontal surface. We will now discuss a band that developed over the frontal surface. Band Y was first analyzed on the 04 GMT 11 April radar composite over southern Kansas more than 200 km north of the surface warm front. A cross section for 03 GMT, just prior to the development of Y, is shown in Figure 4.6.19. The convection developed in a region where there was very little potential instability. The higher convective potential air was positioned just to the southeast. A comparison of the geostrophic angular momentum surfaces with the potential temperature surfaces shows a region neutral to dry symmetric instability. Figure 4.6.20 shows a sounding taken along the M=40 surface. The 800-mb air, at the base of the neutral region, shows a LI of -2°C and essentially no negative area. The 850-mb air, after overcoming a stable layer, would be 6°C positively buoyant at 500 mb.

Emanuel (1983) showed that local conditional symmetric instability results in parcel motion along a surface, which he called

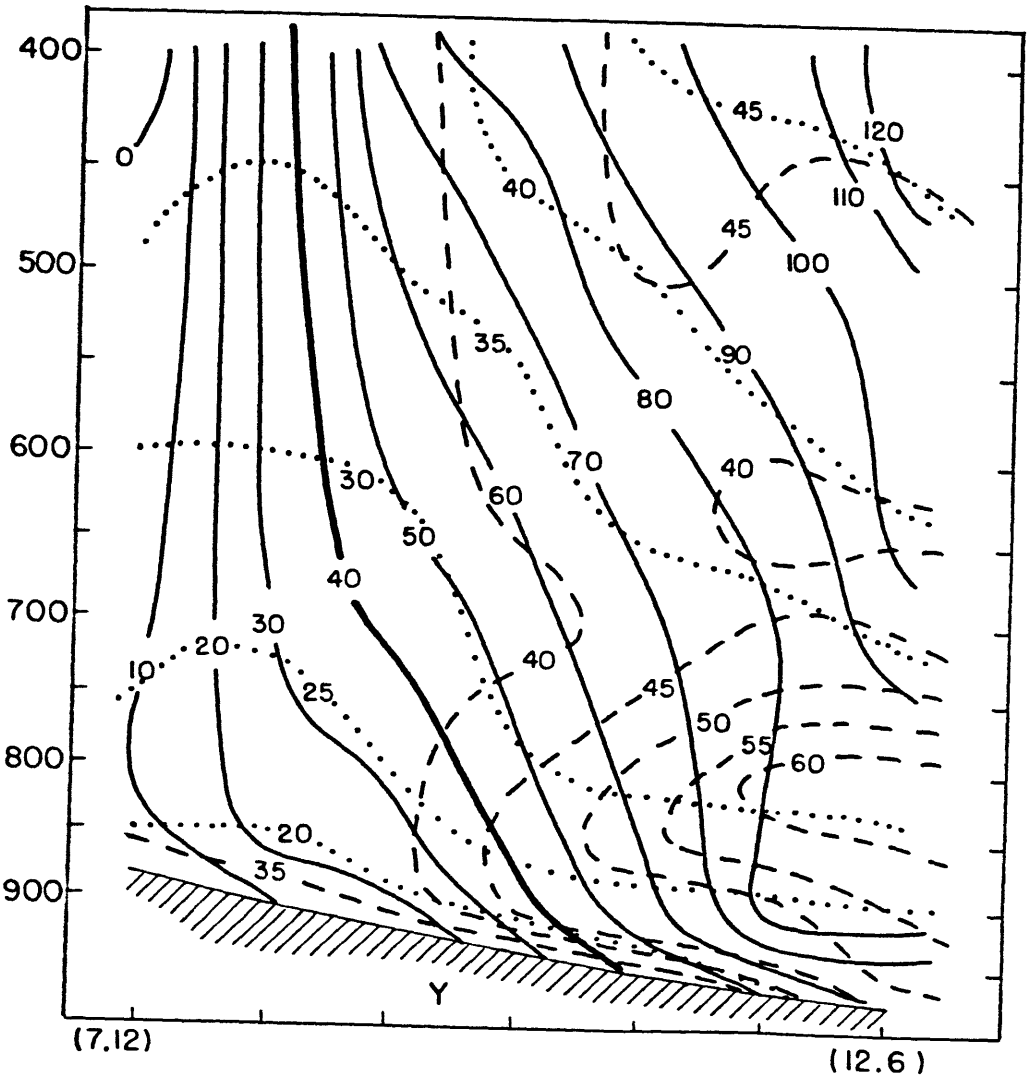


Figure 4.6.19. A vertical cross section along the line from (101°W, 39°N) to (96°W, 33°N) for 0300 GMT 11 April 1979. Refer to Figure 4.5.8 for location. Solid lines are isopleths of constant geostrophic angular momentum (m/s). Dashed lines are isopleths of equivalent potential temperature (°C), and dotted lines are isentropes (°C).

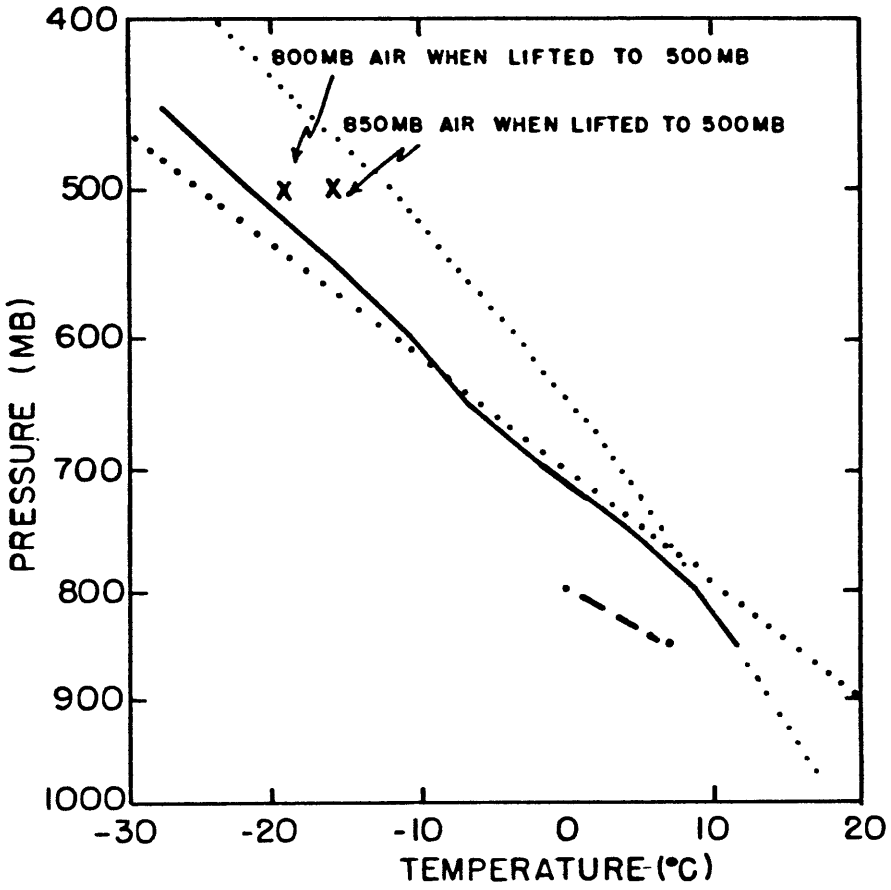


Figure 4.6.20. Sounding along the M = 40 surface [Figure 4.6.19]. Solid line is the temperature curve and the dashed line the dew-point temperature curve. The dotted lines are reference moist and dry adiabats.

an S surface, that allows it to remain neutrally buoyant with respect to the environment. For a totally dry environment, these S surfaces are potential temperature surfaces and for saturated environments they are virtual equivalent potential surfaces. To determine the stability of the atmosphere to slantwise displacements the slopes of the S and M surfaces are compared. Recall that for dry symmetric instability the M surface had to have a shallower slope than the θ surface. Since the θ surface is an S surface, the same comparison holds for all S surfaces. Figure 4.6.21 shows the S surface for the air at 800 mb from the M=40 surface. Initially the air is neutral to slantwise displacements, but then becomes unstable between 750 mb and 700 mb. The parcel would accelerate along the S surface until the S surface folds over. At that point ($\approx$700mb) a vertical displacement away from the S surface would result in the parcel becoming positively buoyant and upright convection would result.

Further evidence that this band is organized by inertial processes is found when the geostrophic shear at 06 GMT (Figure 4.6.22) is compared with the echo configuration for the same time. The band bifurcates over eastern Kansas as it enters an area where the thermal wind is strongly diffluent. The band is never able to get reorganized and soon dissipates.

4.7 GRAVITY WAVE ANALYSIS

A mesoscale analysis of the surface pressure and its relation to

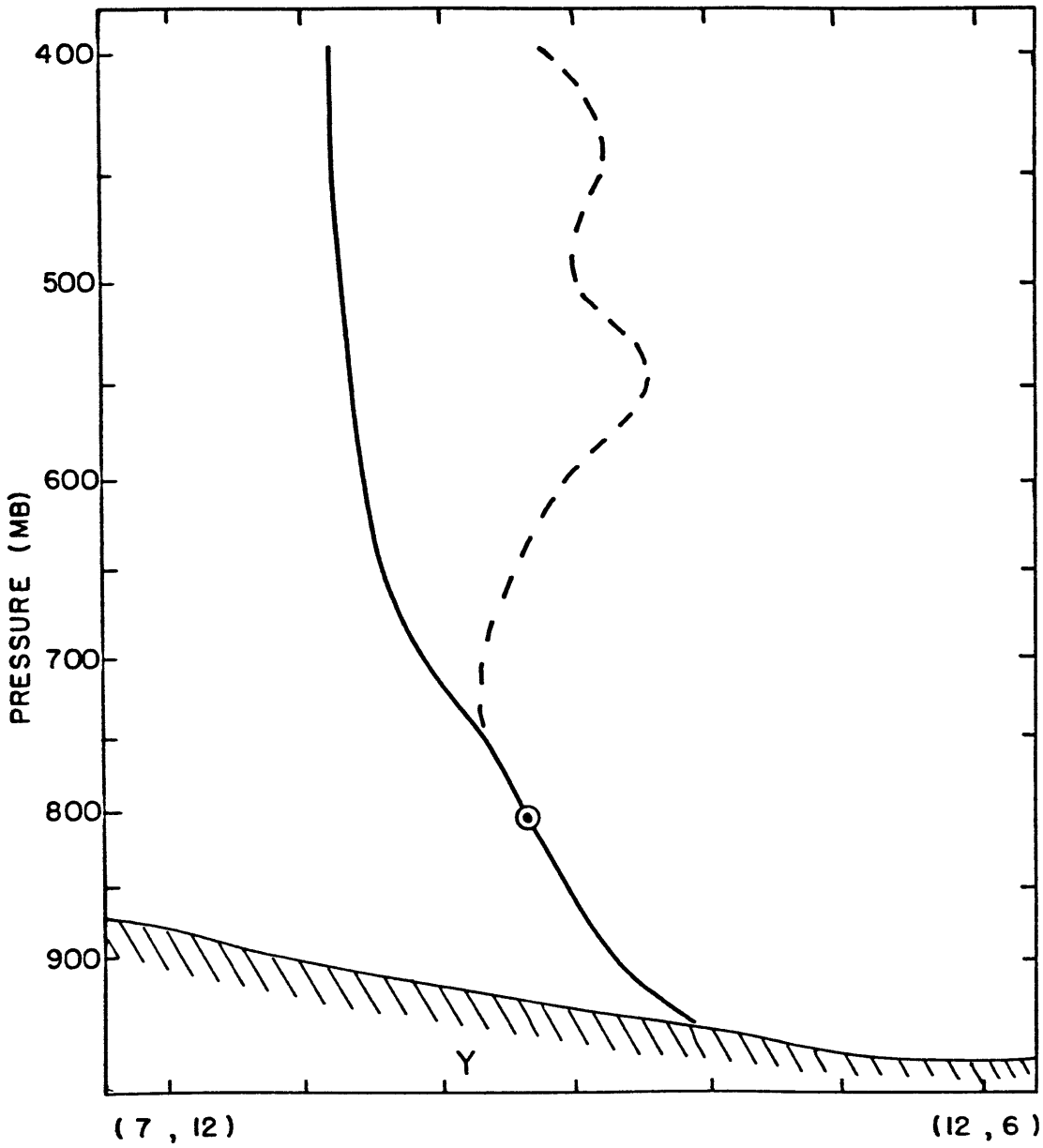


Figure 4.6.21. The M = 40 surface (solid) and the S surface (dashed) for the parcel at 850 mb (circled) on the M = 40 surface for the vertical cross section along the line from (101°W, 39°N) to (96°W, 33°N) for 0300 GMT 11 April 1979.

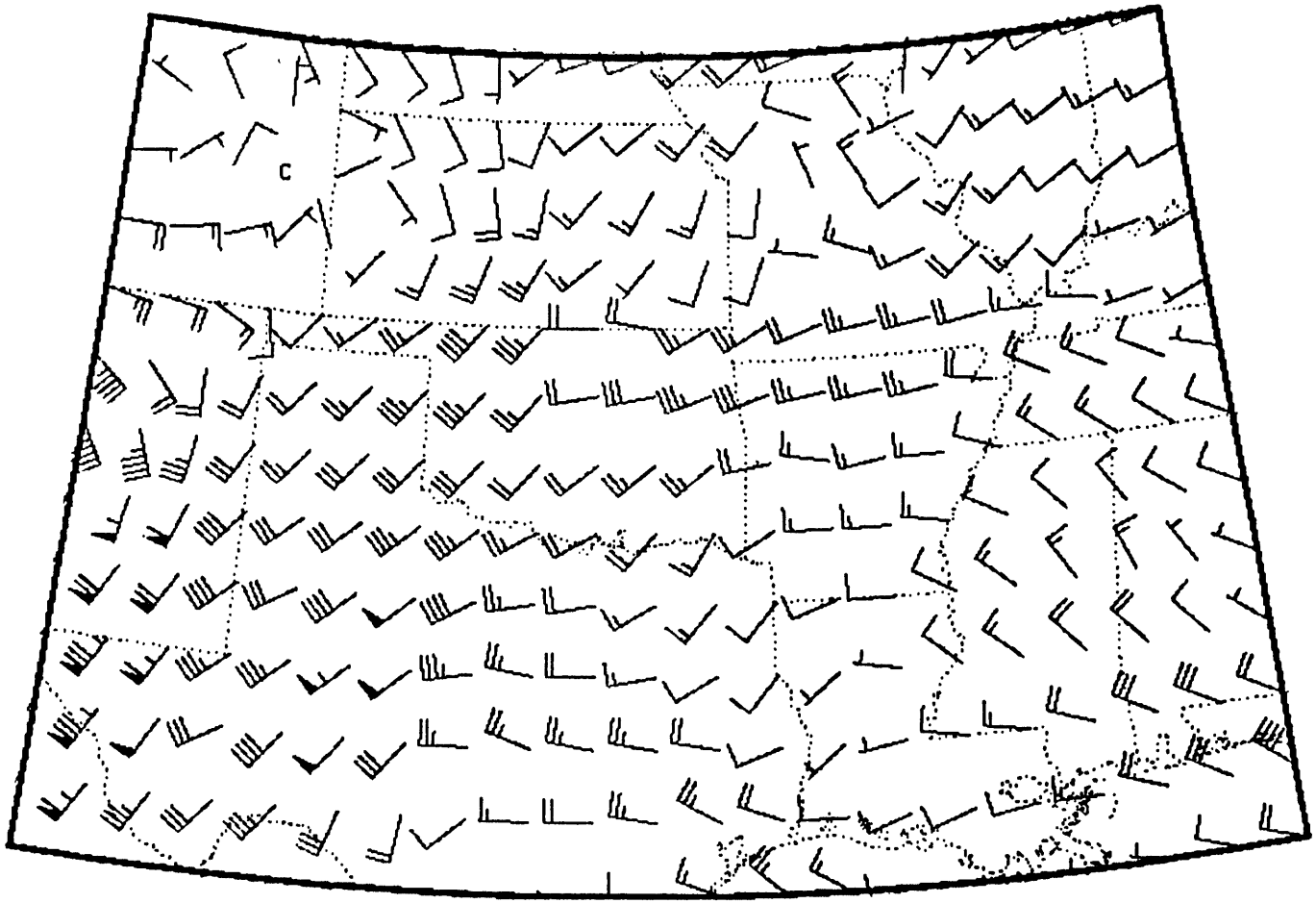


Figure 4.6.22. The geostrophic shear between 850 mb and 500 mb for 0600 GMT 11 April. Plotting is done in the conventional manner (m/s).

precipitation patterns has already been presented for this case by Vincent and Homan (1983). They identified three pressure waves that had propagated northeast across Oklahoma and Missouri and found, as did Miller and Sanders (1980), that thunderstorms and the occurrence of heavy precipitation were well correlated with the passage of high pressure ridges. The thunderstorms they related to the pressure waves were elevated, occurring in an area with a stable boundary layer overlain by potentially warmer air. This stratification, as already discussed in chapter 2, is similar to that required to duct gravity waves (Lindzen and Tung, 1976).

This relationship between gravity waves and elevated thunderstorms is not surprising, however, the unanswered question is what role can the gravity waves play in the triggering of these storms. Uccellini (1975) utilized a three-layer linear model derived by Eom (1972) to test this role. In Eom's model, the surface layer had a depth of 3 km. The maximum vertical displacement was realized at the interface between the bottom two layers, with a linear decrease above and below. Uccellini (1975) applied the pressure-wave characteristics observed in his case to Eom's model without adjusting for a much shallower stable boundary layer. In his case the stable layer was approximately 500 m deep compared with Eom's 3 km. Using the shallower depth for the first layer and recalculating the wave characteristics, the maximum vertical displacement becomes 172 m at 0.5 km compared with 962 m at 3 km used by Uccellini. For the sounding used by Uccellini, this shallower vertical velocity profile

appears to be insufficient in removing a capping inversion and lifting the air to its level of free convection.

In the non-linear model (Lindzen and Tung, 1976) the damping of the vertical velocity in the unstable layer is considerable and further raises the question of whether or not the effect of the gravity wave can generally be 'felt' by the overriding air enough to trigger a thunderstorm.

In this study, six nearly parallel time-cross sections were analyzed. One of these is shown in Figure 4.7.1. Inspection reveals that the strongest pressure waves occurred in the stable region on the cold side of the warm front. It is also clear that they occur with or near thunderstorms.

The time-cross sections were used to compare the time and location of the initial identification of convection with the passage of pressure waves. There was no apparent preference to develop with either the passage of troughs or ridges. There is an apparent increase in amplitude of both the pressure wave and the convection when they became in phase. Notice how F first appears at SPS at 19 GMT 10 April as light rain with rapidly falling pressure but then later reappears in this time-cross section as F , at TUL and F at ONU associated with a strong pressure ridge. This modulation of convection has already been discussed by Sanders and Miller (1980). Another example would be S, initially a rainshower at OKC at 03 GMT 11 April but later a thunderstorm and associated strong pressure ridge at TUL and ONU.

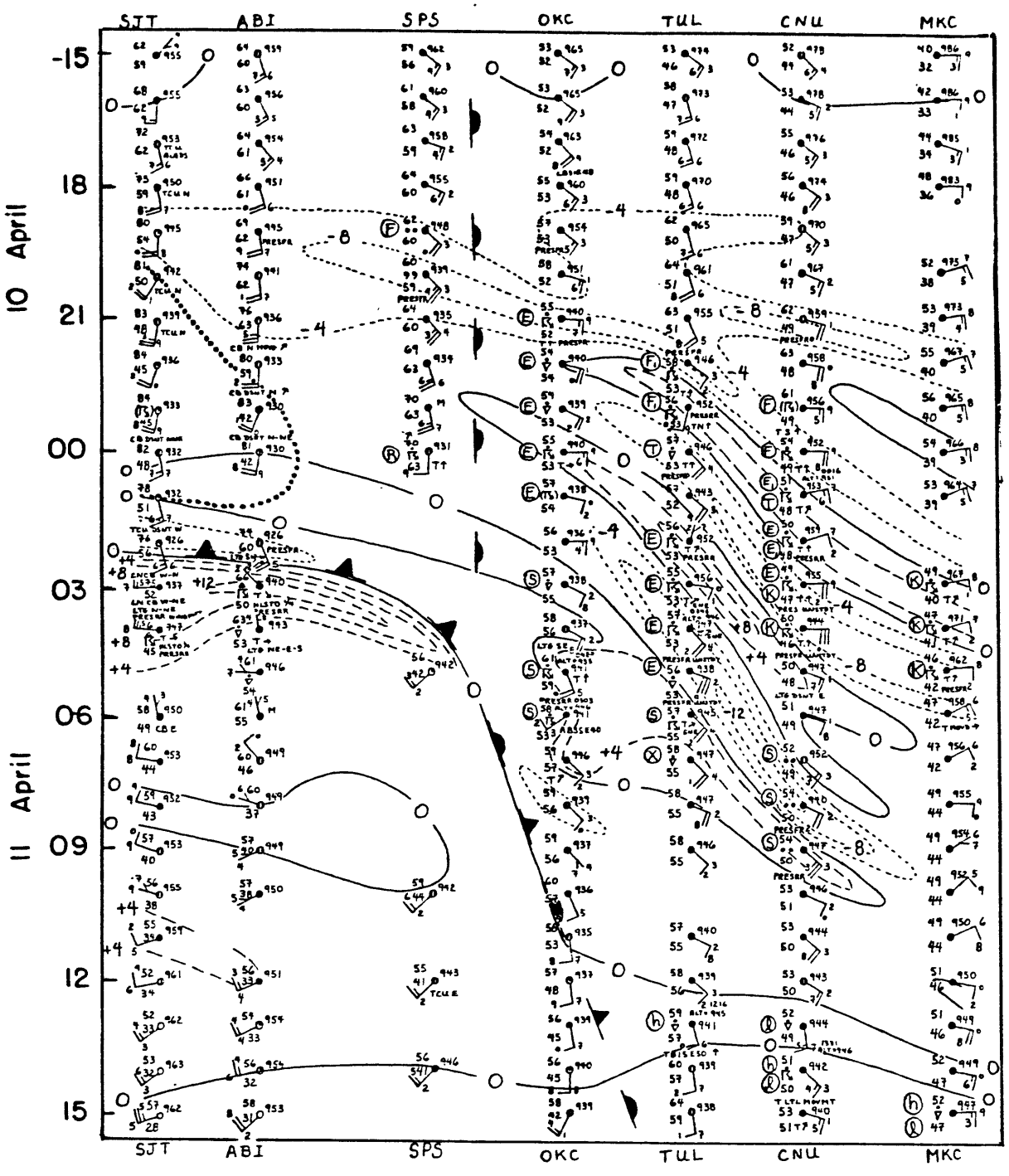


Figure 4.7.1. Time cross section analysis of the 1-hour change in the altimeter setting. The station plots are conventional with wind speed in knots, temperature in °F. For all observations with precipitation, the associated convective area is noted to the left of the observation and circled. Frontal positions are also shown.

It is clear that the ducted gravity waves in the stable planetary boundary layer and the elevated convection are intimately related. However, from this study it does not appear that the gravity waves were important in triggering the elevated storms.

4.8 DISCUSSION

An investigation of elevated convection in AVE-SESAME I has been presented. The outbreak of elevated convection has been shown to be extensive in both area affected and duration. The date, 10 and 11 April, 1979, places the case study at the peak in the annual frequency distribution and the region of study very near the area of greatest occurrence observed in the climatology study.

The accumulated precipitation amounts observed during the passage of the synoptic-scale system showed a very strong signature from the elevated convection. Hence, even though no severe events were recorded from clearly elevated storms, it is important to understand the mechanisms of the elevated thunderstorms and their relation to the larger scale systems.

A mesoscale analysis revealed that the thunderstorms developed in a strong low-level southerly flow ahead of a slowly moving and intensifying low pressure center. After the first storms were observed, about midday on the 10 , they spread rapidly north and east and continued to be observed for more than 24 hours. The SLI's in the area of elevated convection were characteristically very stable.

Interesting, and consistent with the climatology, was the fact that even with very low SLI's south of the warm front the LI-850's were not very impressive. Many of the elevated storms were observed in areas where there was no apparent latent instability.

It was suggested that one of the reasons that the event was able to persist so long was that a series of small mountains was able to protect the cold surface boundary layer by deflecting the southerly flow up and over the cold layer. The effect was to keep the warm front stationary and allow the elevated thunderstorms to continue until the passage of the surface trough from the west. The characteristics of the thunderstorms were investigated utilizing a detailed radar analysis consisting of hourly composites of seven radar sites. The convection occurred in three impulses, each of which was characterized by a convective band that developed south of the warm front and propagated northeastward. Each of these original bands developed through a slightly different scenario. One characteristic that was found to play a role in the timing and position of the initial developments was the depth of the boundary layer. In an area where the air with strong latent instability extends to a higher level it can be more easily destabilized by mesoscale convergence in the boundary layer. This variation in the depth of the boundary layer appeared to be related to the diurnal variation in vertical mixing over southern Texas.

As these convective impulses moved onto the frontal surface they displayed characteristics similar to warm sector convection. One band

developed a clear LEWP and broke up into several fragments. The convection was banded and generally aligned along the geostropic shear. Near the beginning of the outbreak the convection was positioned downstream and on the cyclonic side of the 500-mb jet maximum. However, as the storm progressed they gradually switched to occur almost exclusively on the anticyclonic side but still downstream or near the maximum.

The three main impulses were identifiable for more than 10 hours as they passed through the radar coverage area. The kinematic p-velocities revealed the development of strong mesoscale updrafts in association with these main impulses. Also, a very strong ageostrophic low-level jet was observed with the first impulse.

There were many pressure waves observed over the region with an association between the passage of pressure ridges and the occurrence of an elevated thunderstorm. However, an attempt to associate these waves with the triggering of those elements that formed above the warm-frontal surface failed. It was suggested that possibly the wave amplitude is generally too quickly damped above the frontal inversion to be able to lift the latently unstable air to its LFC.

One of the bands that developed above the warm-frontal surface formed in an area that showed very little latent instability. A cross section revealed that it developed at the edge of a tongue of high θ_e air in a region that was close to being inertially unstable. Further investigation showed that the development process could be twofold, with an initial part where the parcel was inertially unstable

to a point where the parcel became convectively buoyant and developed into upright convection.

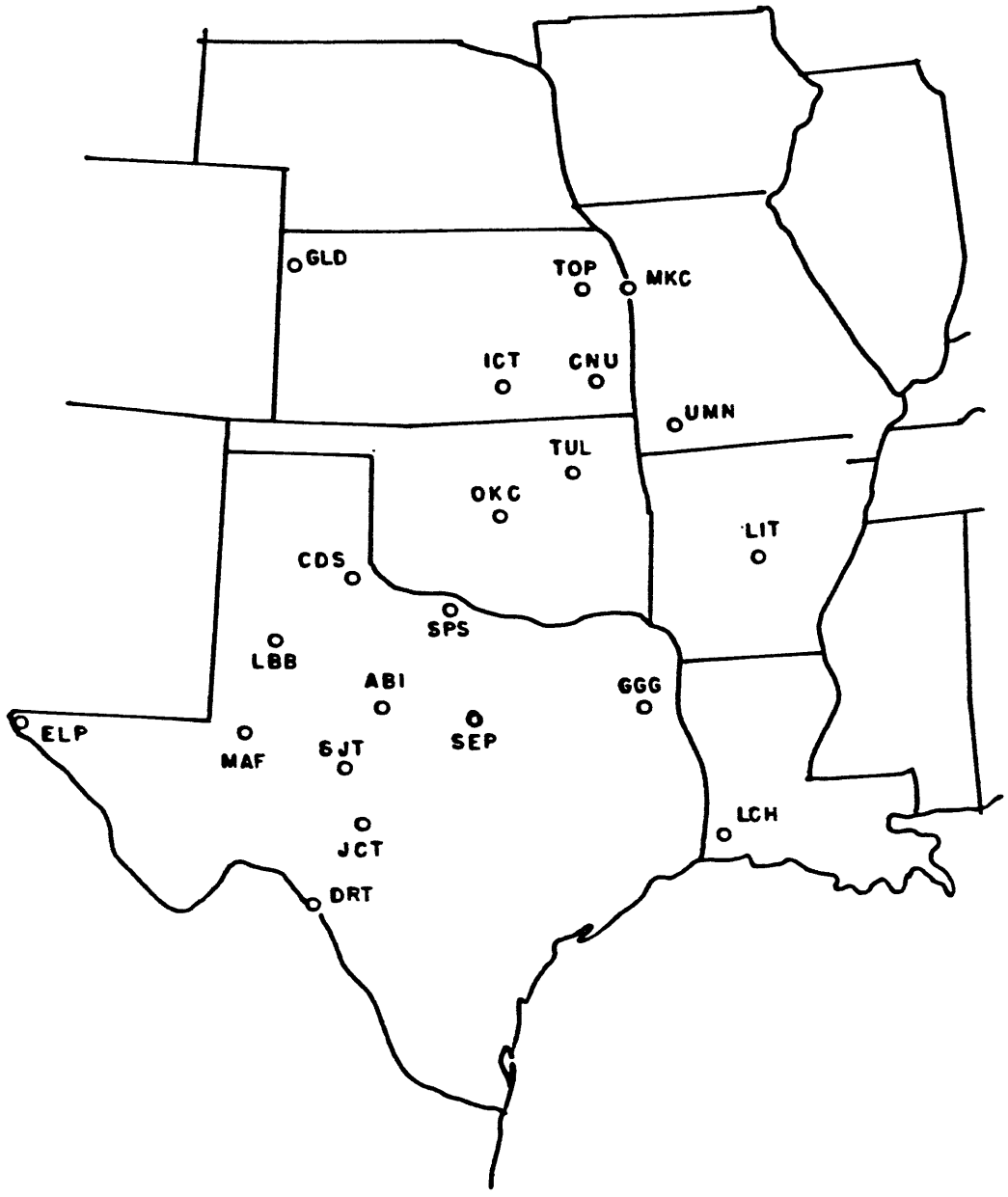


Figure 4.8.1. The locations of all stations referenced in chapter 4 identified by their 3-letter identifiers.

CHAPTER 5: CONCLUSIONS

The goal of this dissertation has been to define and investigate the climatology and mesoscale dynamics of elevated convection occurring in association with midlatitude cyclones. Initially we defined elevated convection as thunderstorm activity that occurs in an environment that is characterized by having a gravitationally stable planetary boundary layer overlain by a layer that is less stable. We made no *a priori* assumption about the actual process responsible for the convection, however, we did assume that the overlying air had existed as a surface boundary layer prior to being lifted over the frontal surface.

The first part of this dissertation established a comprehensive climatology of the seasonal, diurnal and geographical variation of elevated convection for the United States. By utilizing a routinely reported phenomenon, namely lightning, as the identifying characteristic, we were not restricted to a particular region by the use of radar or precipitation gauge networks as in previous studies that have investigated mesoscale structure above frontal inversions.

To complete the climatology, we collected a number of surface observations reporting thunder that were positioned on the 'cold' side of an analyzed synoptic-scale surface front as well as the corresponding data for the 850-mb and 500-mb levels. These surface observations were then filtered to eliminate the storms that did not show the required vertical stratification, resulting in a final set of

observations containing 1093 cases covering a four-year period from September, 1978 to August, 1982.

The second part of this dissertation presented a detailed case study of elevated convection occurring during the AVE-SESAME I experiment on 10, 11 April 1979. In this case, the outbreak of elevated convection was extensive and long-lasting. Although there were not any observed severe events associated with these storms, they were still found to be an important aspect of the storm. The study was built upon a detailed radar analysis that was composited from a network of seven WSR-57 radars. This analysis made it possible to identify and track many convective areas from their initial development to their decay.

The elevated convection occurred in three major impulses, each of which contained convective areas which lasted for more than ten hours. Excessive rainfall amounts (>4 inches) were recorded along a swath where the majority of elevated thunderstorms occurred and actually dominated the character of the storm total precipitation. The findings of this case study were useful in answering some of the questions raised by the results of the climatology study.

The results of the case study showed that the precipitation resulting from this storm was dominated by smale-scale processes associated with elevated convection. This suggests that it is important to parameterize this phenomenon in numerical models. For convective parameterization schemes that passively define the boundary layer (e.g., Arakawa and Schubert's), however, most elevated

convection would be missed and probably result in grid point instabilities. It is therefore important that any scheme used allow for multiple cloud sources in the vertical if the 'cloud' is to be explicitly defined. A moist adiabatic adjustment scheme does not have this problem since there is a direct comparison between the different layers.

In carrying out the climatology study, we found that there are several differences between the climatology of elevated convection and that of all thunderstorms. First, we found that the annual maximum concentration of elevated convection extends farther north into the Mississippi and Ohio River Valleys. It was suggested that this is the result of the northward retreat of the storm tracks, and the associated elevated convection, during the warm season,while convection rooted in the boundary layer still occurs in high concentration across the South. Second, and perhaps most striking, is that over the Florida Peninsula, the area of maximum frequency for all thunderstorms, there were no elevated thunderstorms observed, showing that the convection there is exclusively ground based. in contrast to this result, we were able to show that winter season (December through February) convection over the remainder of the United States, east of the Rocky Mountains, is almost exclusively elevated.

The annual frequency distribution of elevated convection was found to be bimodal with a primary peak in April, and a secondary peak in September. The associated minima occur in July and November. We proposed that this distribution is the result of the combination of a

winter maximum in extratropical cyclones and a late spring maximum in thermodynamic instability. The primary peak in April occurs when there is strong thermodynamic instability present, resulting from intense insolational heating of the boundary layer and very cold mid and upper levels, and frequent cyclonic activity.

As cyclonic activity increases across the Great Lakes in September, the frequency of elevated convection increases from the minimum in July to the secondary maximum. In the fall, another preferred region develops associated with a southern storm track across the Gulf Coast. This mid-winter activity is partly the result of a continued warm moist air supply off the Gulf of Mexico and a contrasting cold boundary layer over the land.

Year-to-year variations in the location and frequency of elevated convection occurred in association with changes in the observed large scale flow. A comparision of the observed elevated convection with the monthly mean flow for individual months showed that the convection tends to occur downstream from the mean 700-mb trough position, and generally on the cyclonic side of the mean 700-mb jet.

In studying the relationship to frontal type we found that nearly half of all elevated convection is associated with warm fronts, about a third with stationary fronts, and slightly less than a quarter with cold fronts. The warm-frontal frequency is slightly higher from January through April, presumably this is associated with the increased overrunning along the Gulf Coast. Elevated convection associated with stationary fronts accounts for a higher than average

percentage from May through August, a result of an increased frequency of trailing fronts and generally more stagnant conditions.

When we investigated the diurnal variation of elevated convection we found that the frontal type is important. Elevated thunderstorms that occur above warm-frontal and stationary-frontal inversions are more likely to occur at 12 GMT while those above cold-frontal inversions are more likely to occur at 00 GMT. Aside from this frontal dependence we found no other detectable difference in wind speed, cross-frontal component or travel time between the cases that occurred at 00 GMT and 12 GMT.

The frontal dependence can best be accounted for by considering the position of the convection with respect to the surface frontal boundary. For the warm-frontal and stationary-frontal cases the mean distances from the surface front were found to be 2.3 and 2.0 degrees of latitude, respectively, while those associated with cold fronts were only displaced 1.4 degrees of latitude, on the average. The difference would most likely have been even greater if frontal motion had been considered. This difference would have considerable effect on the time required for the air to travel across the frontal inversion. The median of this travel time above the frontal surface for all cases with a cross frontal component at 850 mb was nearly eight hours. With the observed differences in mind and recalling that we had assumed the involved air had previously existed as a surface boundary layer, the following sequence was proposed. The surface boundary layer in the warm sector is heated and moistened during the

day, reaching a maximum in latent energy in the mid to late afternoon. The air is subsequently transported onto the frontal surface where the energy is then released as elevated convection, delayed by the travel time of the source air. For those cases where the convection originates in the warm sector and then propagates onto the frontal surface (e.g., the three main impuses in the case study), it would be expected that the convection would develop during the late afternoon (generally the time of maximum instability), then become elevated during the evening as it travels onto the frontal surface. This was true for the three main impulses of convection identified in the case study, which after propagating onto the frontal surface, remained active throughout the night.

Following this scenario, we suggested that elevated convection would have a late night to early morning maximum and a late morning minimum. However we were not able to verify this, since we were limited by the twice-daily upper-air soundings. Wallace's (1975) work substantiates this for the winter season, when the convection is mostly elevated and does not require the identification of type. Further work could be done along this line for the summer season if a reliable way to identify elevated storms was developed which did not require upper-air observations. Another interesting question relating to summer season convection is what association elevated convection has with mesoscale convective complexes (MCC's) (Maddox, 1981). It has been shown that MCC's are nocturnal phenomena and frequently occur with a stable planetary boundary layer. It is possible that they

develop as a result of classical convection during the day that then becomes elevated convection above the outflow air at night.

Characteristics of the environment in which elevated thunderstorms occur were compiled from the collected data. The typical elevated thunderstorm occurs to the northeast of an associated surface low pressure center and north of a warm front in a region with northeasterly surface winds. The 850-mb flow is cyclonic and the elevated thunderstorm occurs in the left exit region of a low-level wind maximum in a south-southwesterly flow with strong warm advection, frequently flanked by an area of strong deformation. In relation to the upper levels, the event occurs near the inflection point in a southwesterly 500-mb flow and in the right exit region of the associated wind maximum.

On 10, 11 April 1979, the elevated thunderstorms occurred in a situation very similar to the typical case just described. The exceptions were, first, there was not an area of strong deformation at 850 mb, and second, the first storms occurred on the cyclonic side of the 500-mb jet instead of the anticyclonic side (however, later storms did occur on the anticyclonic side).

The surface lifted indices (SLI) were determined from the climatological data set in order to allow us to investigate the thermodynamic stability of the boundary layer. A similar calculation was done using the 850-mb temperature and dew-point temperature values to determine the stability of the air above the frontal inversion (LI-850). The results showed that the boundary layer was very stable

both with respect to the 500-mb and 850-mb air. It was suggested that this strong stability would better enable a more complete decoupling between the layers and allow for a more efficient convective process above the inversion.

The gravitational stability of the 850-mb air with respect to the 500-mb air was found to be neutral in the mean. There were some cases where the LI-850 was less the -5°C suggesting upright convection as the acting mechanism, however, these were more the exception. The same results were found in the case study, with many of the elevated thunderstorms occurring in an environment with no apparent latent instability. The SLI's and LI-850's south of the warm front were frequently less than -5°C yet, even with a strong southerly flow, these low values never advanced very far over the front. The gradient of the LI-850 was found to be very flat in the area where the elevated thunderstorms were occurring. The 0°C isopleth was found to actually move against the flow at times. Thus, elevated convection is an apparent sink for the latent energy transported onto the frontal surface.

An investigation into the possibility of conditional symmetric instability accounting for elevated convection did not show convincing evidence for this mechanism. In the regions of development, we did not find any deep layers that were symmetrically unstable. Also in the vicinity of mature elevated thunderstorms, the atmosphere was found to be essentially barotropic through a large part of the troposphere, which would make the two processes equivalent.

Mesoscale updrafts were observed to develop in association with each of the three main impulses of convection. There was also the development of a very strong ageostrophic jet that fed into the system.

From these observations we were able to suggest the following mechanism. Initially cumulus convection develops from latent instability either above the front, in which case the latent instability is from the air overlying the frontal inversion, or in the boundary layer and subsequently propagates onto the frontal surface. In association with the strong convective heating, a mesoscale updraft develops above the frontal inversion. The latent instability is soon exhausted, yet the latent heating from the updraft is strong enough to develop a steady state mesoscale circulation system with a continual moisture supply being drawn into the system above the frontal surface unencumbered by surface friction. This system is similar to the one documented by Sanders and Paine (1975) and modeled by Brown (1979).

It was shown that the depth of the boundary layer was important in the development of band A. The boundary layer over southern Texas, although capped for deep convection, had developed a well mixed layer to above 800 mb during the previous day's heating. This area of very high θ_e air was transported northward during the night to a position over northern Texas at about midday on the 10^{th}. Also at that time, in response to an advancing upper level jet streak, an area of weak convergence developed across northern Texas. As a result of the greater depth of the boundary layer, the vertical velocities resulting

from the convergence were able to more efficiently trigger the convection. We found that even though pressure waves occur concomitantly with elevated thunderstorms, they are apparently not important in their development. It has been suggested that the vertical velocities associated with a ducted gravity wave in the cold underlying layer decay too quickly above the inversion to be able to lift the air to its LFC.

The development of one of the bands that formed above the frontal inversion appeared to take place through a two step process. The environment where the elevated thunderstorm developed had no latent instability. However, just to the south there was a tongue of very high θ_e air above the frontal inversion. An analysis of the environment showed that there was an area at the boundary of this 'baroclinic leaf' that was neutral to dry symmetric instability. The construction of the S surface for a parcel in this region showed that the parcel was initially stable to vertical displacements but neutral (then becoming unstable) to displacements along the surface of constant geostrophic angular momentum. There was then a transition (at the point where the S surface folded over) from the region where the parcel was inertially unstable, to one where the parcel was unstable to vertical displacements. At that point, the resulting convection was upright and indistinguishable from classical convection. This process is appealing in several ways. First, it provides a mechanism to transport high θ_e air farther onto the frontal surface, and second, it allows the release of the latent

instability of that air as upright convection without requiring a mechanism to lift it to its LFC. Further investigation is necessary to determine to what extent this is a viable mechanism for the triggering of elevated convection.

REFERENCES

Alexander, W.H., 1935: Distribution of thunderstorms in the United States. Mon. Wea. Rev., 63, 157-158.

Austin, P.M. and R.A. Houze, Jr., 1970: Analysis of meso-scale precipitation areas. Preprints 14th Weather Radar Conf., 329-334.

Bennetts, D.A. and J.C. Sharp, 1982: The relevance of conditional symmetric instability to the prediction of mesoscale frontal rainbands. Quart. J. Roy. Meteor. Soc., 108, 595-602.

Bennetts, D.A. and B.J. Hoskins, 1979: Conditional symmetric instability--a possible explanation for frontal rainbands. Quart. J. Roy. Meteor. Soc., 105, 945-962.

Bjerknes, J., 1919: On the structure of moving cyclones, Geofysiske Publikationer, Vol. I, No.2.

Bonner, W.D., 1968: Climatology of the low-level jet. Mon. Wea. Rev., 96, 833-850.

Bosart, L.F. and J.P. Cussens, 1973: Gravity wave phenomena accompanying East Coast cyclogensis. Mon. Wea. Rev., 101, 446-454.

Bosart, L.F., C.J. Vauds, and J.H. Helsdon, Jr., 1972: Coastal frontogenesis. J. Appl. Meteor., 11, 1236-1258.

Brown, J.M., 1979: Mesoscale unsaturated downdrafts driven by rainfall evaporation: A numerical study. J. Atmos. Sci., 36, 313-338.

Carlson, T.N., R.A. Anthes, M. Schwartz, S.G. Benjamin, and D.G. Baldwin, 1980: Analysis and prediction of Severe Storms Environment. Bull. Amer. Meteor. Soc., 61, 1018-1032.

Carlson, T.N. and F.H. Ludlam, 1968: Conditions for the formation of severe local storms. Tellus, 20, 203-226.

Charney, J.G., 1947: The dynamics of lone waves in a baroclinic westerly current. J. Meteor., 4, 135-162.

Colby, F.P., 1983: The development of convective instability during SESAME, 1979. Ph.D. thesis, Mass. Inst. Tech., Dept. of Meteorology. 312 pp.

Court, A. and J.F. Griffiths, 1982: Thunderstorm climatology. Thunderstorms: Vol. 2: Thunderstorm Morphology and Dynamics. Feb. 1982, E. Kessler (editor), U.S. Dept. of Commerce, NOAA.

Darkow, G.L., 1982: Thunderstorm Energetics. Thunderstorms: Vol. 2: Thunderstorm Morphology and Dynamics. Feb. 1982, E. Kessler (editor), U.S. Dept. of Commerce, NOAA.

Dexter, R.V., 1944: The diurnal variation of warm-frontal precipitation and thunderstorms. Quart. J. Roy. Meteor. Soc., 70, 129-137.

Eady, E.T., 1949: Long waves and cyclone waves. Tellus, 1, 32-52.

Elliot, R.D. and E.L. Hovind, 1965: Heat, water and vorticity balance in frontal zones. J. Appl. Meteor., 4, 196-211.

Emanuel, K.A., 1979: Inertial instability and mesoscale convective systems, Part I: Linear theory of inertial instability in rotating viscous fluids. J. Atmos. Sci., 36, 2425-2449.

Emanuel, K.A., 1983: The Lagrangian parcel dynamics of moist symmetric instability. J. Atmos. Sci., 40, 2368-2376.

Eom, J., 1975: Analysis of the internal gravity wave occurrence of April 19, 1970 in the Midwest. Mon. Wea. Rev., 103, 217-226.

Fawbush, E.J., R.C. Miller, and L.G. Starrett, 1951: An empirical method of forecasting tornado development. Bull. Amer. Meteor. Soc., 46, 4-15.

Ferguson, H.L., 1967: Mathematical and Synoptic Aspects of a small-scale wave disturbance over the Lower Great Lakes area. J. Appl. Meteor., 6, 523-529.

Fujita, T.T., 1963: Analytical mesometeorology: A review. Meteor. Monogr., No. 27, 77-125.

Gunn, K.L.S., M.P. Langleben, and A.S. Dennis: Radar evidence of a generating level for snow. J. Meteor., 11, 20-26.

Harrold, T.W., 1973: Mechanisms influencing the distribution of precipitation within baroclinic disturbances. Quart. J. Roy. Meteor. Soc., 99, 232-251.

Herzegh, P.H. and P.V. Hobbs, 1980: The mesoscale and microscale structure and organization of clouds and precipitation in mid-latitude cyclones. II. Warm-frontal clouds. J. Atmos. Sci., 37 597-611.

Hewson, E.W., 1937: The application of wet-bulb potential temperature to air mass analysis. III. Rainfall in depressions. Quart. J. Roy. Meteor. Soc., 63, 323-335.

Hobbs, P.V., T.J. Matejka, P.H. Herzegh, J.D. Locatelli, and R.A. Houze, Jr., 1980: The mesoscale and microscale structure and organization of clouds and precipitation in midlatitude cyclones. I: A case study of a cold front. J. Atmos. Sci., 37, 568-596.

Hsu, S.A., 1981: Relationship between monthly frontal overrunning and offshore-onshore temperature differences across the Central Gulf Coast. J. Appl. Meteor., 20, 1479-1482.

Johns, R.H., 1982: A synoptic climatology of northwest flow severe weather outbreaks. Part I: Nature and Significance. Mon. Wea. Rev., 110, 1653-1663.

Koch, S.E. and J. McCarthy, 1982: The evolution of an Oklahoma dryline. Part II. Boundary-layer forcing of mesoconvective systems. J. Atmos. Sci., 39, 237-257.

Kreitzberg, C.W. and H.A. Brown, 1970: Mesoscale weather systems within an occlusion. J. Appl. Meteor., 9, 417-432.

Kreitzberg, C.W. and D.J. Perkey, 1976: Release of potential instability: Part I. A sequential plume model within a hydrostatic primitive equation model. J. Atmos. Sci., 33, 456-475.

Kreitzberg, C.W. and D.J. Perkey, 1977: Release of potential instability: Part II. The mechanism of convection/mesoscale interaction. J. Atmos. Sci., 34, 1569-1595.

Lindzen, R.S., 1974: Wave-CISK in the tropics. J. Atmos. Sci., 31, 156-179.

Lindzen, R.S. and K.K. Tung, 1976: Banded convective activity and ducted gravity waves. Mon. Wea. Rev., 104, 1602-1617.

Maddox, R.A., 1981: The structure and lifecycle of midlatitude mesoscale convective complexes. Doctoral thesis, Colorado State University, 311 pp.

Marshall, J.S., 1953: Precipitation trajectories and patterns. J. Meteor., 10, 25-29.

Matejka, T.J., R.A. Houze, Jr., and P.V. Hobbs, 1980: Microphysics and dynamics of clouds associated with mesoscale rainbands in extratropical cyclones. Quart. J. Roy. Meteor. Soc., 106, 29-56.

Means, L.L., 1944: The nocturnal maximum occurrence of thunderstorms in the midwestern states. Miscellaneous Reports, No. 16, University of Chicago Press.

Miller, D.A. and F. Sander, 1980: Mesoscale conditions for the severe convection of 3 April 1974 in the East-Central United States. J. Atmos. Sci., 37, 1041-1055.

Muller, R.A., 1977: A synoptic climatology for environmental baseline analysis: New Orleans. J. Appl. Meteor., 16, 20-33.

Orville, R.E., 1982: Personal Communication.

Pitchford, K.L., and J. London, 1962. The low-level jet as related to nocturnal thunderstorms over Midwest United States. J. Appl. Meteor., 1, 43-47.

Rex, D.B., 1950: Blocking action in the middle troposphere and its effect on regional climate. I. Aerological study of blocking. Tellus, 2, 196-211.

Sanders, F., 1971: Analytic solution of the nonlinear omega and vorticity equations for a structurally simple model of disturbances in the baroclinic westerlies. Mon. Wea. Rev., 99, 393-407.

Sanders, F., and J.R. Gyakum, 1980: Synoptic-Dynamic Climatology of the "bomb". Mon. Wea. Rev., 108, 1589-1606.

Sanders, F., and R.J. Paine, 1975: The structure and thermodynamics of an intense mesoscale convective storm in Oklahoma. J. Atmos. Sci., 32, 1563-1579.

Saucier, W.J., 1955: Principles of Meteorological Analysis. University of Chicago Press, Chicage. 438 pp.

Schaefer, J.T., 1973: The motion and morphology of the dryline. NOAA Technical Memorandum, ERL NSSL-66.

Shands, A.L., 1948: Thunderstorm Probabilities in the United States. Bull. Amer. Meteor. Soc., 29, 270-274.

Sun, W.Y., and Y. Ogura, 1979: Boundary-layer forcing as a possible trigger to a squall-line formation. J. Atmos. Sci., 36, 235-254.

Uccellini, L.W., 1975: A case study of apparent gravity wave initiation of severe convective storms. Mon. Wea. Rev., 103, 497-513.

U.S. Department of Commerce, NOAA, EDIS, 1979. Daily Weather Maps (Week including April 10, 1979).

United States Weather Bureau, 1946: Airway Meteorological Atlas of the United States. Leslie Smith (supervisor), 140 pp.

United States Weather Bureau, 1957. Technical Paper No. 40.

Wallace, J.M., 1975: Diurnal variations in precipitation and thunderstorm frequency over the conterminous United States. Mon. Wea. Rev., 103, 406-419.

Weber, E.M. and S. Wilderotter, 1981: Satellite interpretation note. Dept. of the Air Force, 3WW/TN-81/001. 108 pp.

ADDITIONAL REFERENCES

Alberty, R.L., D.W. Burgess, C.E. Hane, and J.F. Weaver, 1979: Sesame 1979 Operations Summary. NOAA/ERL, Boulder, Colorado.

Arakawa, A. and W.H. Schubert, 1974: Interaction of a cumulus cloud ensemble with the large-scale environment, Part I. J. Atmos. Sci., 31, 674-701.

Barnes, S.L., 1964: A technique for maximizing detail in numerical weather map analysis. J. Appl. Meteor., 3, 396-409.

Barnes, S.L., 1973: Mesoscale objective map analysis using weighted time series observations. NOAA Tech. Memo. ERL NSSL-62, National Severe Storms Laboratory, Norman, OK. 60 pp.

Gerhard, M.L., H.E. Fuelberg, S.F. Williams, and R.E. Turner, 1979: AVE-SESAME I: 25-mb Sounding Data. NASA TM-78256, December 1979.

O'Brien, J.J., 1970: Alternate solutions to the classical vertical velocity problem. J. Appl. Meteor., 9, 197-203.

Sanders, F., 1983: The Initiation of Severe Convection on 10 April 1979. Sesame Newsletter, Vol. 1, No. 2, September, 1983.

Vincent, D.G., T.Q. Carney, J.H. Homan, and R. Fulton, 1979: Mesoscale Data Sets for 10-11 April 1979, Sesame Newsletter, Vol 1, No. 1.

APPENDIX I: UPPER-AIR SOUNDINGS FROM AVE-SESAME I

The upper-air soundings were initially processed at St. Louis University, with the complete soundings computed at Texas A and M University. Several error checks were used on the punched data to ensure the best possible products. Centered differences were calculated and compared to the input data as well as to constant pressure analyses for 850 mb, 500 mb, and 200 mb at all release times. Time series for each station were also checked for continuity. Any suspected errors were compared with the original strip charts and any appropriate corrections made. The final set consisted of data at 25-mb intervals. Figure I shows the location of the rawinsonde stations available for the experiment.

The accuracy for the processed soundings is estimated at approximate RMS errors of 0.5°C for the temperature and 10% for the humidity. The RMS error for the pressure ranges from 1.3 mb for the layer from the surface to 400 mb, to 0.7 mb between 100 and 10 mb. The RMS error of the pressure altitude varies from 10 gpm at 500 mb to 50 gpm at 50 mb. The RMS error for the wind, although more difficult to estimate because of its dependence on balloon position, is better than 0.8 ms^{-1} and 1.8 degrees at 500mb with an elevation angle of 40° (NASA, 1979).

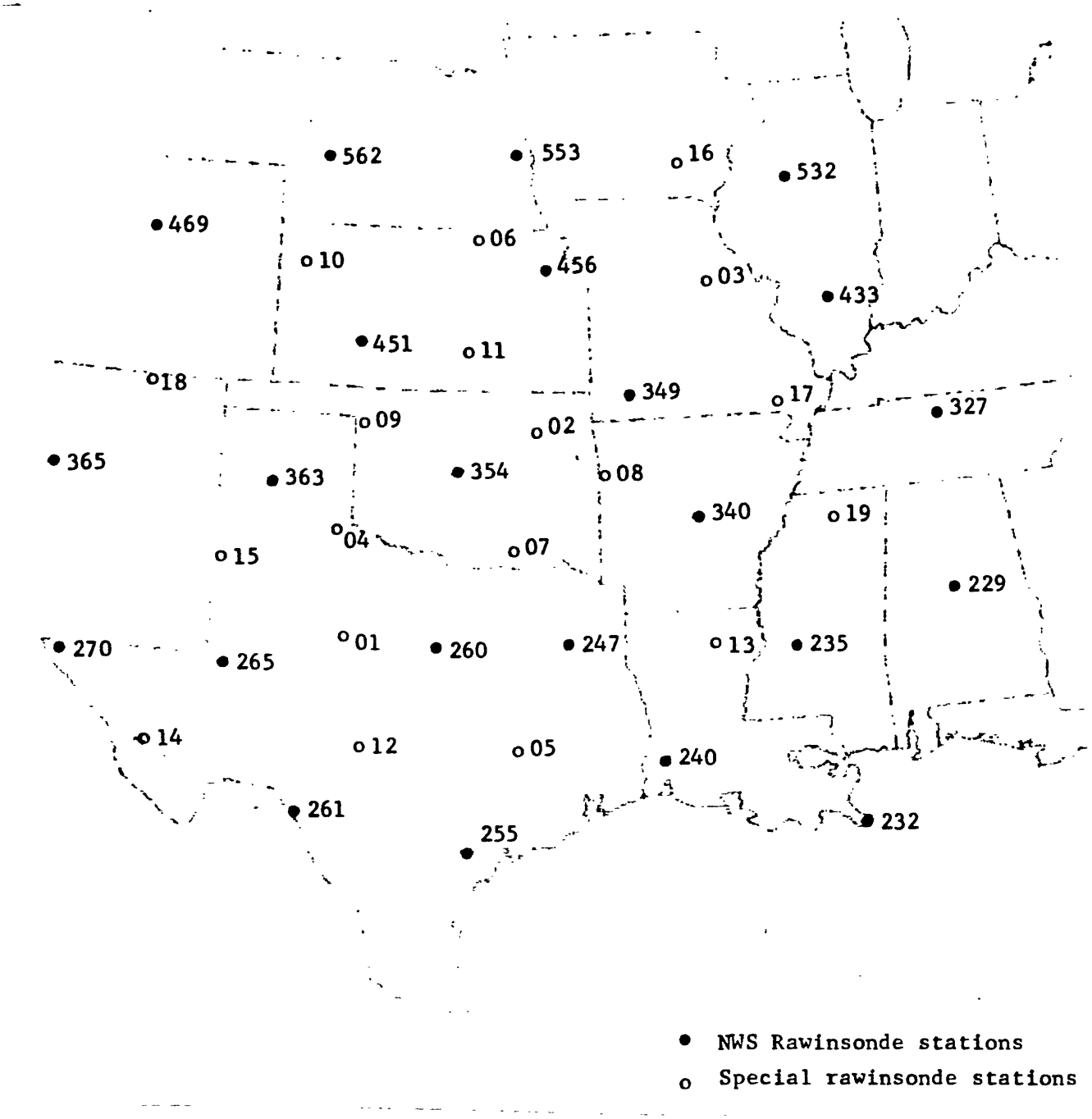


Figure I. Location of rawinsonde stations participating in the AVE-SESAME I experiment (NASA, 1979).

APPENDIX II: AVE-SESAME I GRID-POINT DATA SET

The grid-point data set obtained was from Purdue University. The research group at Purdue used an objective analysis technique devised by Barnes (1964, 1973) to grid the data at horizontal increments of one degree and vertical increments of 25 mb. Extensive hand analysis was also performed by the Purdue group on each of the elements at the mandatory levels. This subjective analysis technique was used to implicitly allow for balloon drift and variations in release time (personal communication). After making these corrections, the objective analysis was completed. The weighting scheme used in the analysis took the eight nearest soundings to the grid point. If any data was missing, the next closest sounding was used. No attempt was made to interpolate in time or space for missing data.

The domain and grid spacing is shown in Figure II. The domain is bounded by 42°N, 85°W, 28°N and 107°W. The data set was smoothed in the vertical to 50 mb increments using a 3 pt. quarter-weight smoother. The surface, 950-mb and 100-mb levels were not smoothed. An exponential weighting scheme was used in the gridding that allowed for 99% recovery of features with wavelengths at 1500 km, 95% at 1000 km, and 63% at 500 km (Vincent, et al., 1983). The data set contained geopotential, u-velocity, v-velocity, temperature, relative humidity and pressure-velocity. The pressure-velocity was calculated kinematically using an O'Brien (1970) -type mass adjustment scheme with the velocity equal to zero at the surface and 100 mb.

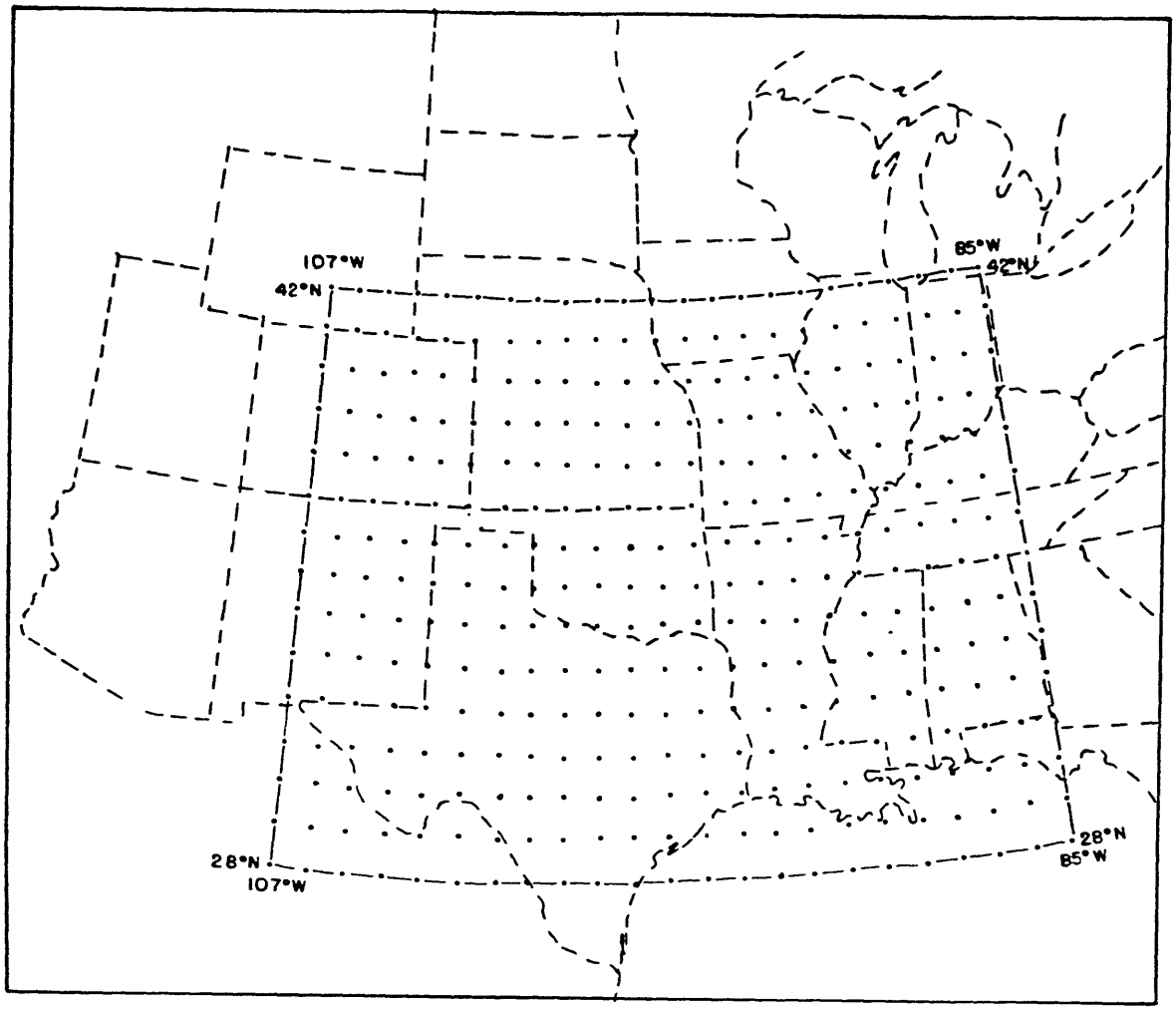
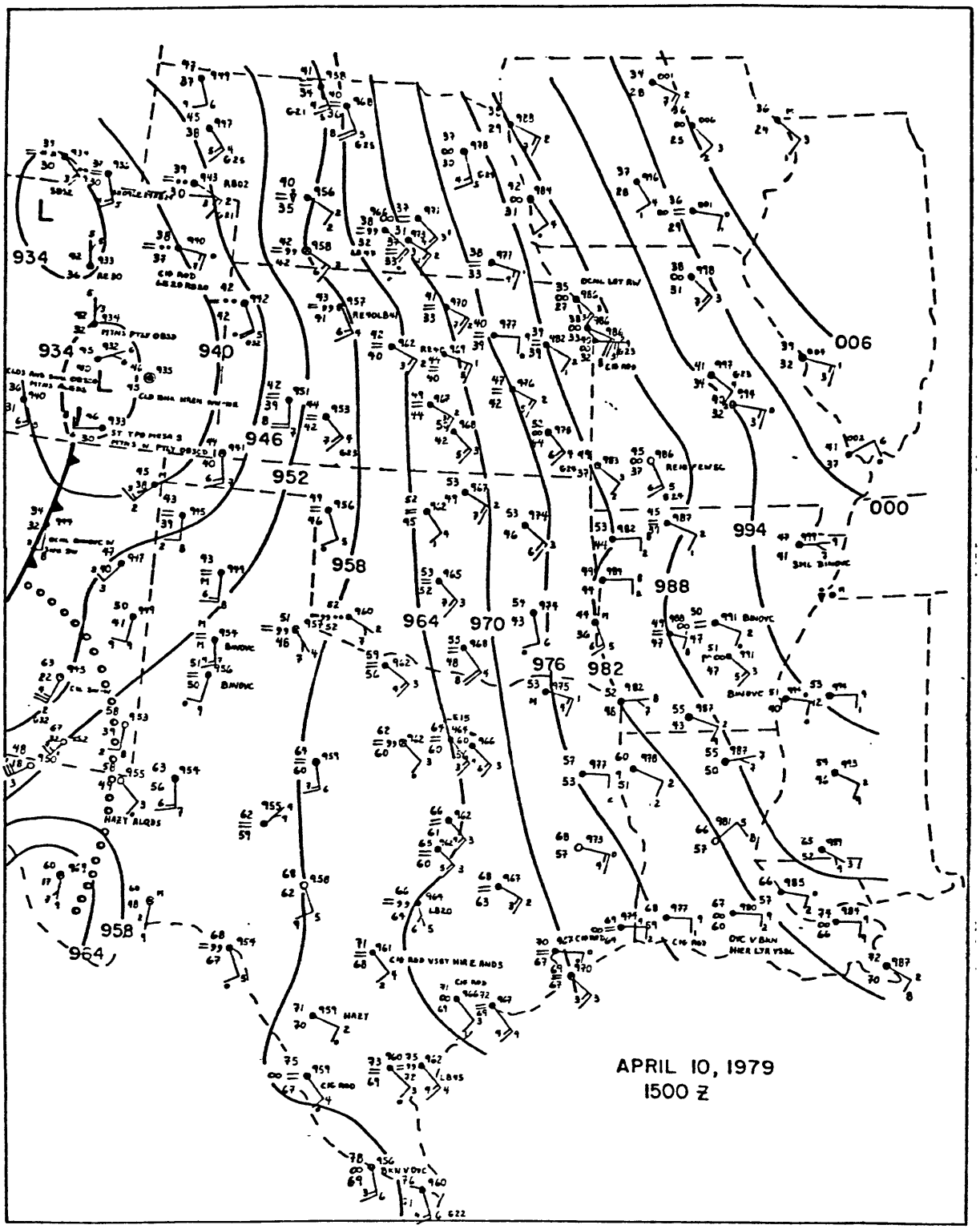
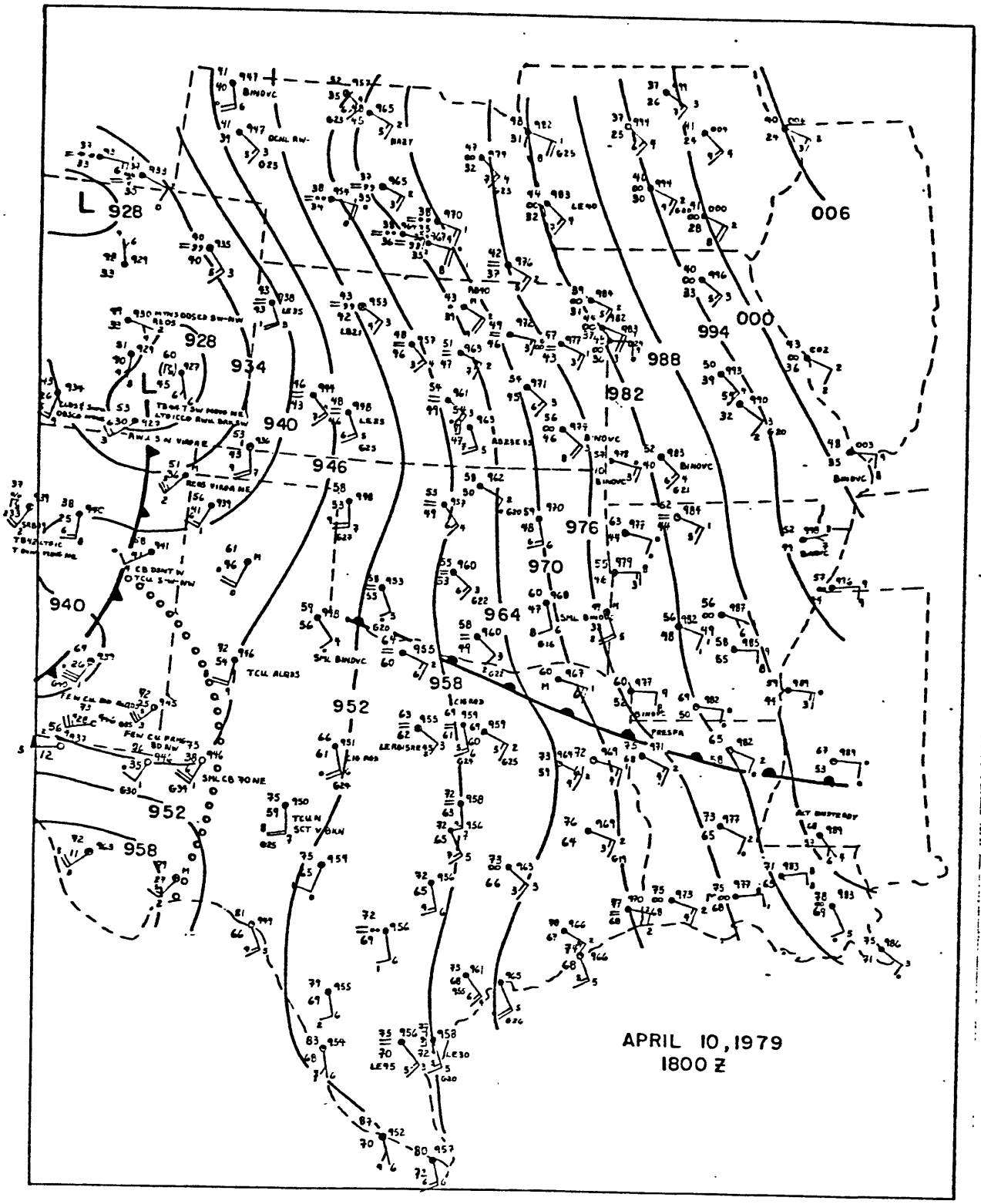


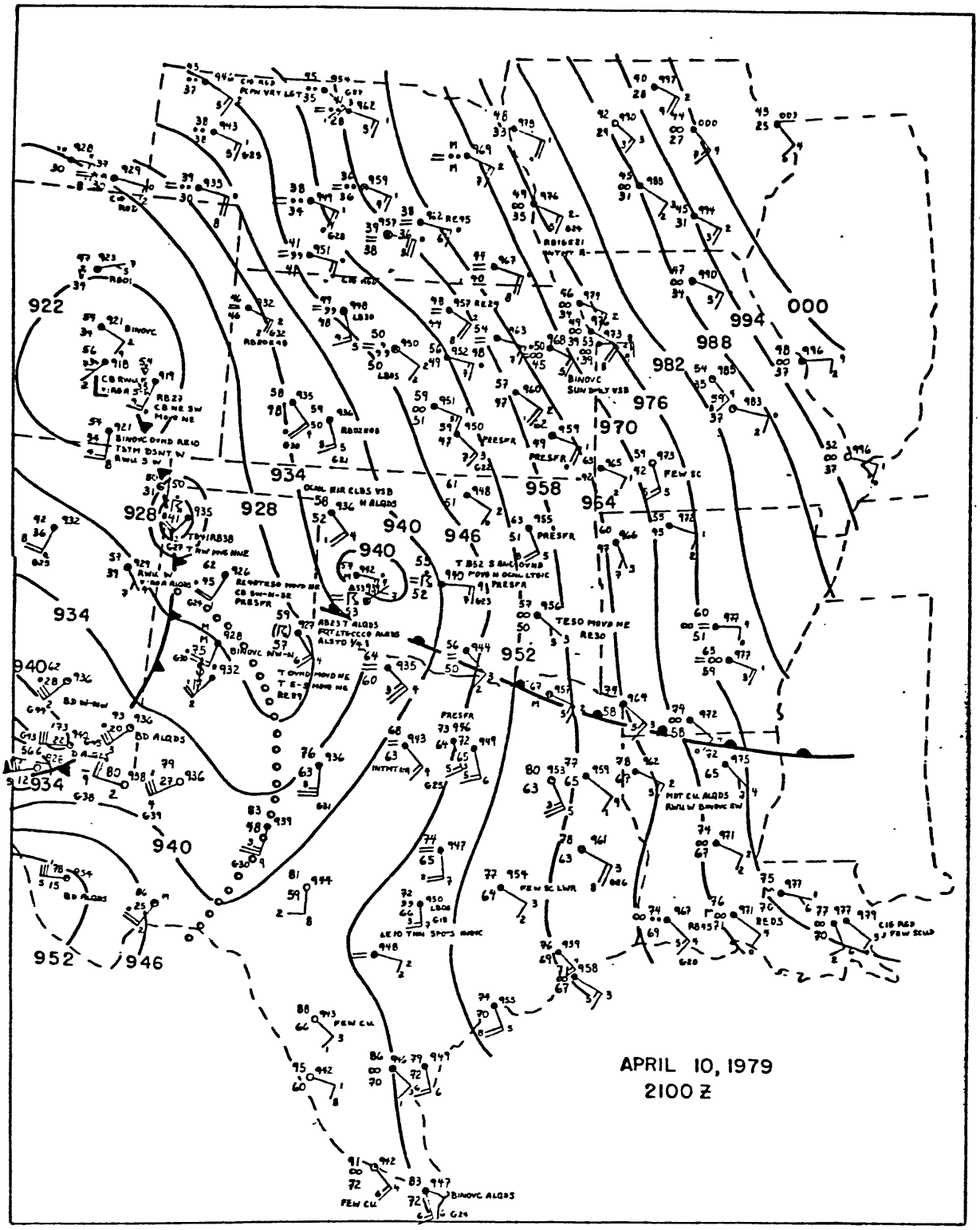
Figure II. The domain of the Grid-Point data set.

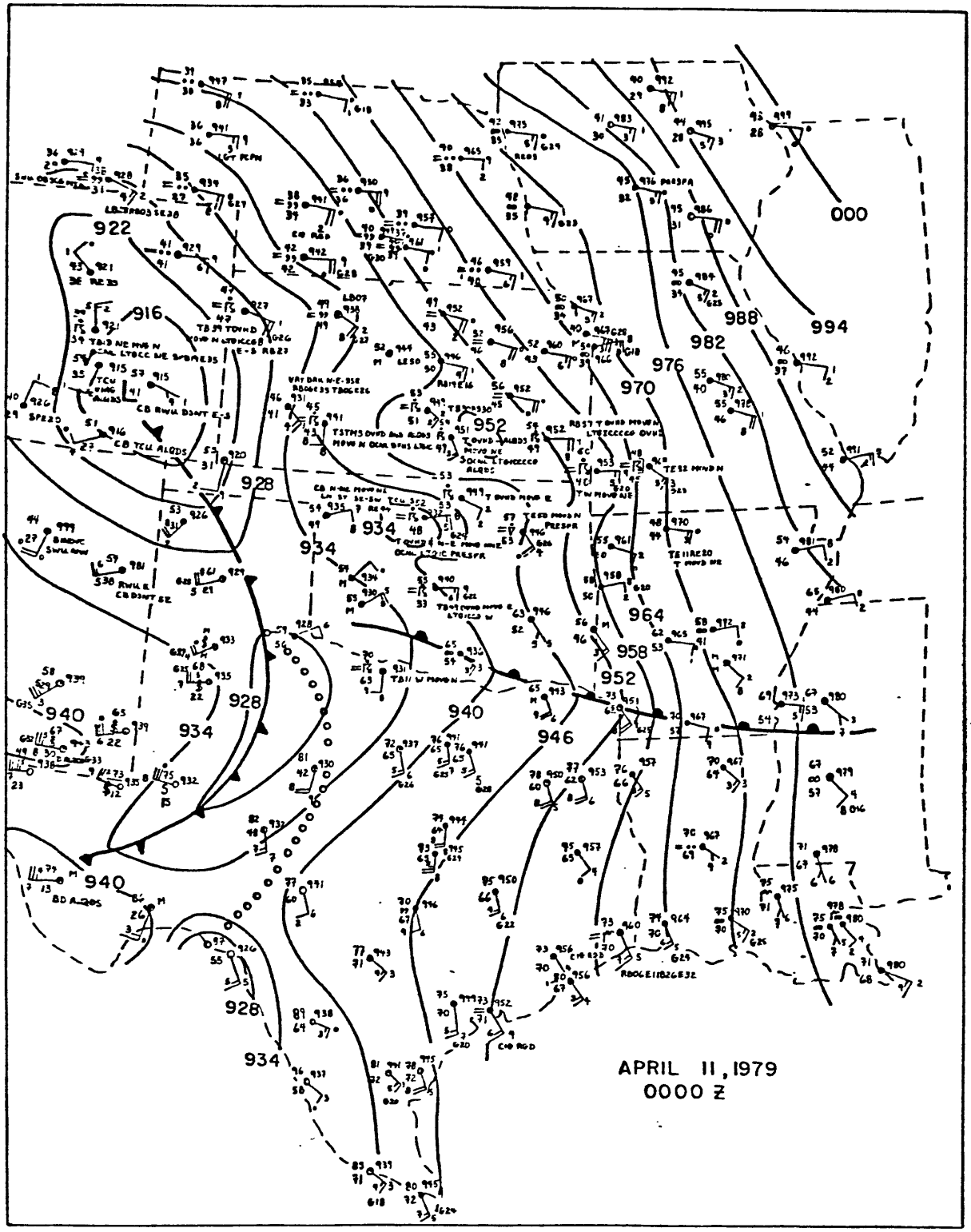
APPENDIX III: COMPLETE SET OF MESOSCALE SURFACE ANALYSES

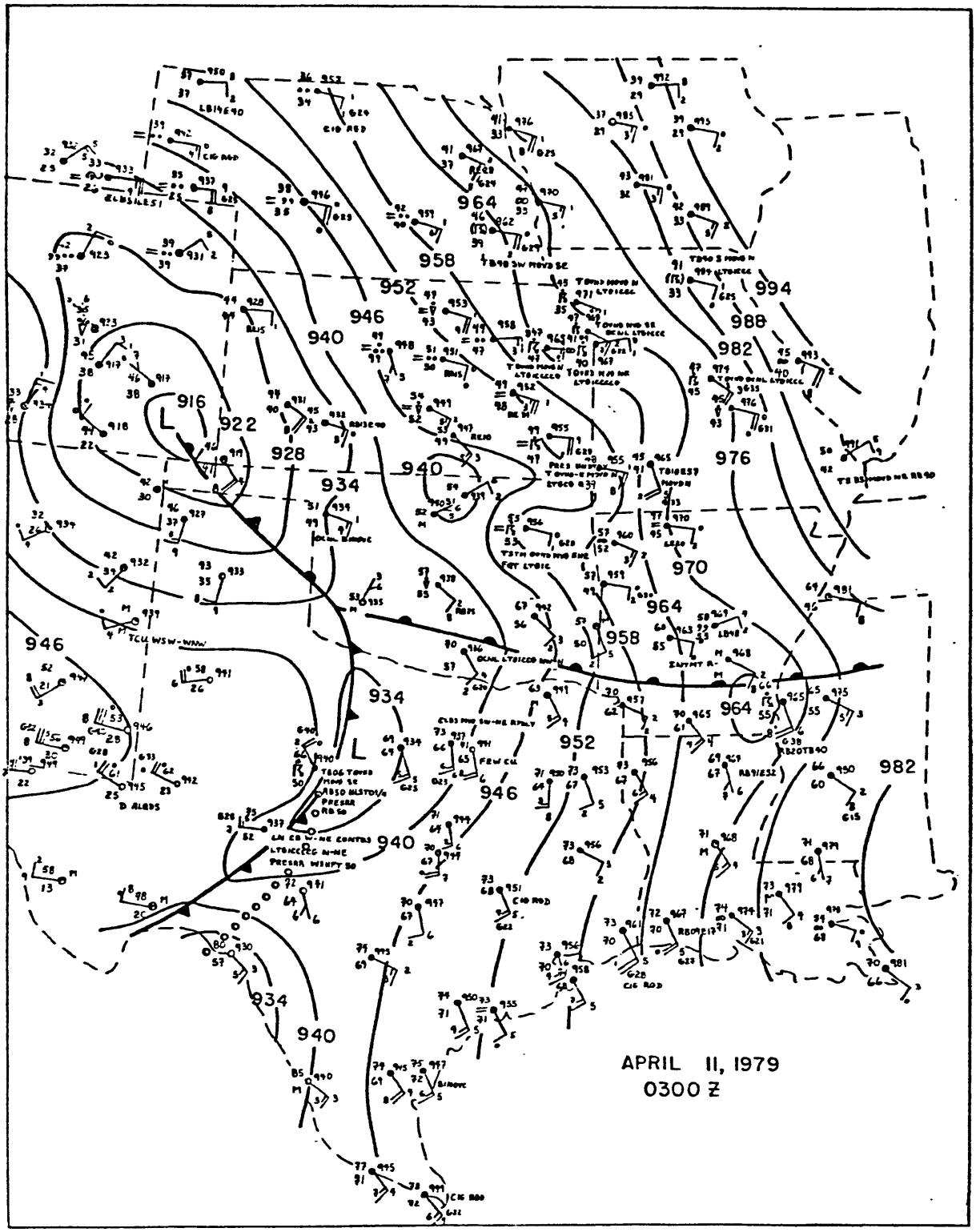
The Mesoscale Surface Analyses for the period from 1500 GMT 10 April 1979 to 2100 GMT 11 April 1979 (every 3 hours). The solid lines are isopleths of altimeter setting (970 = 29.70" of Hg). The station model is conventional, with temperatures in °F and wind in kts. The position of the dry line is marked with a line of circles.

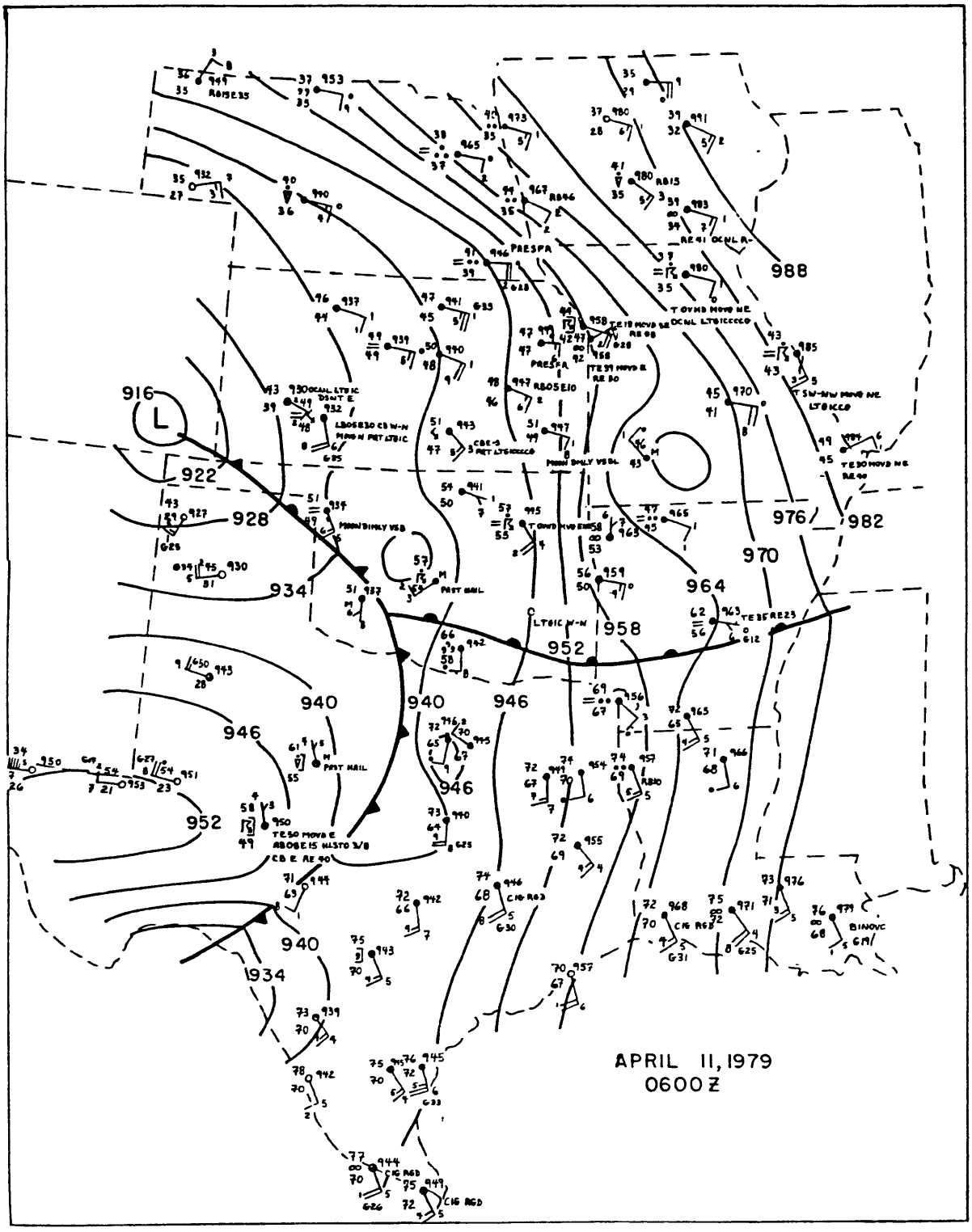

934
940
946
952
958
964
970
976
982
988
994
000
006
L
APRIL 10, 1979
1500 Z

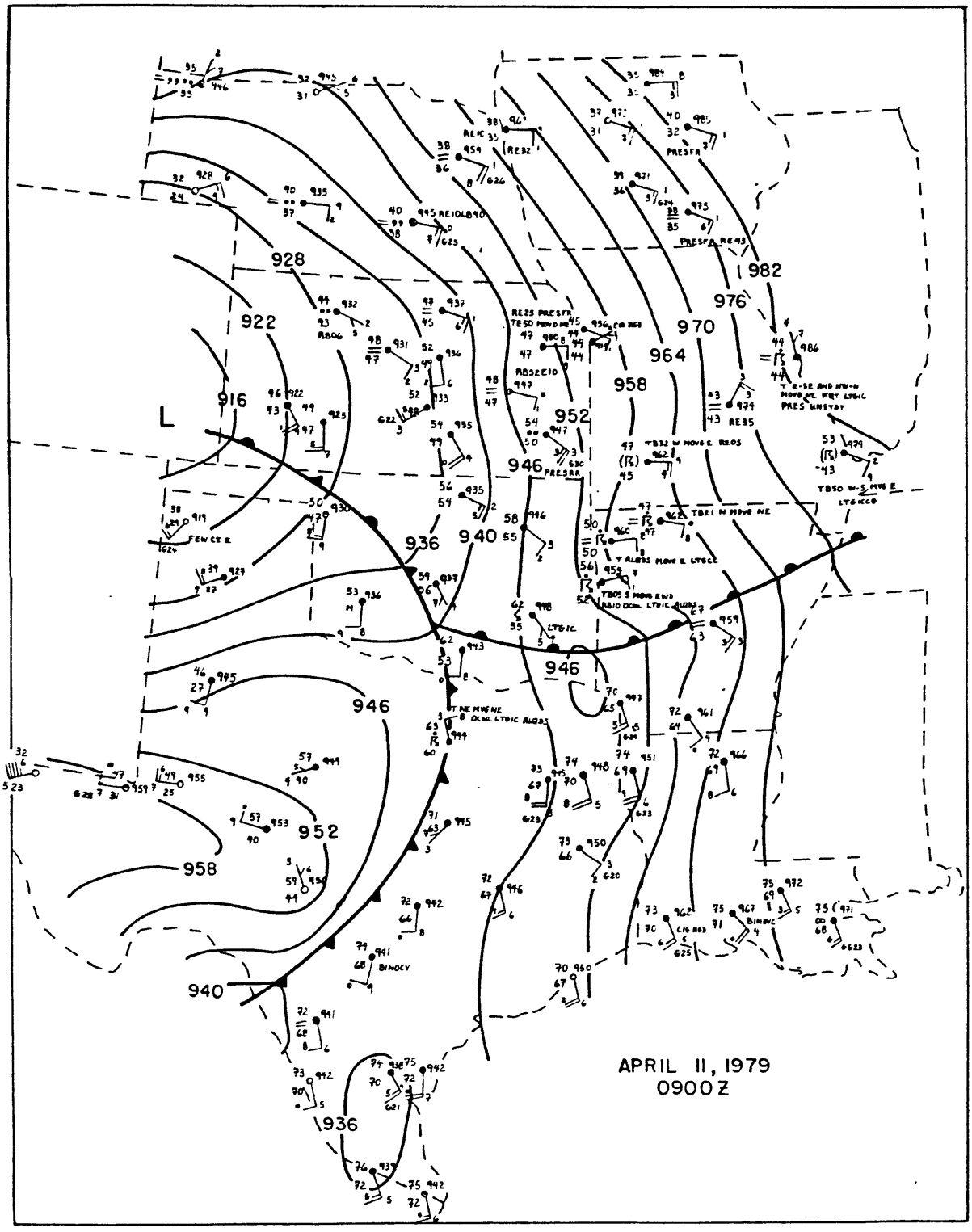

APRIL 10, 1979
1800 Z

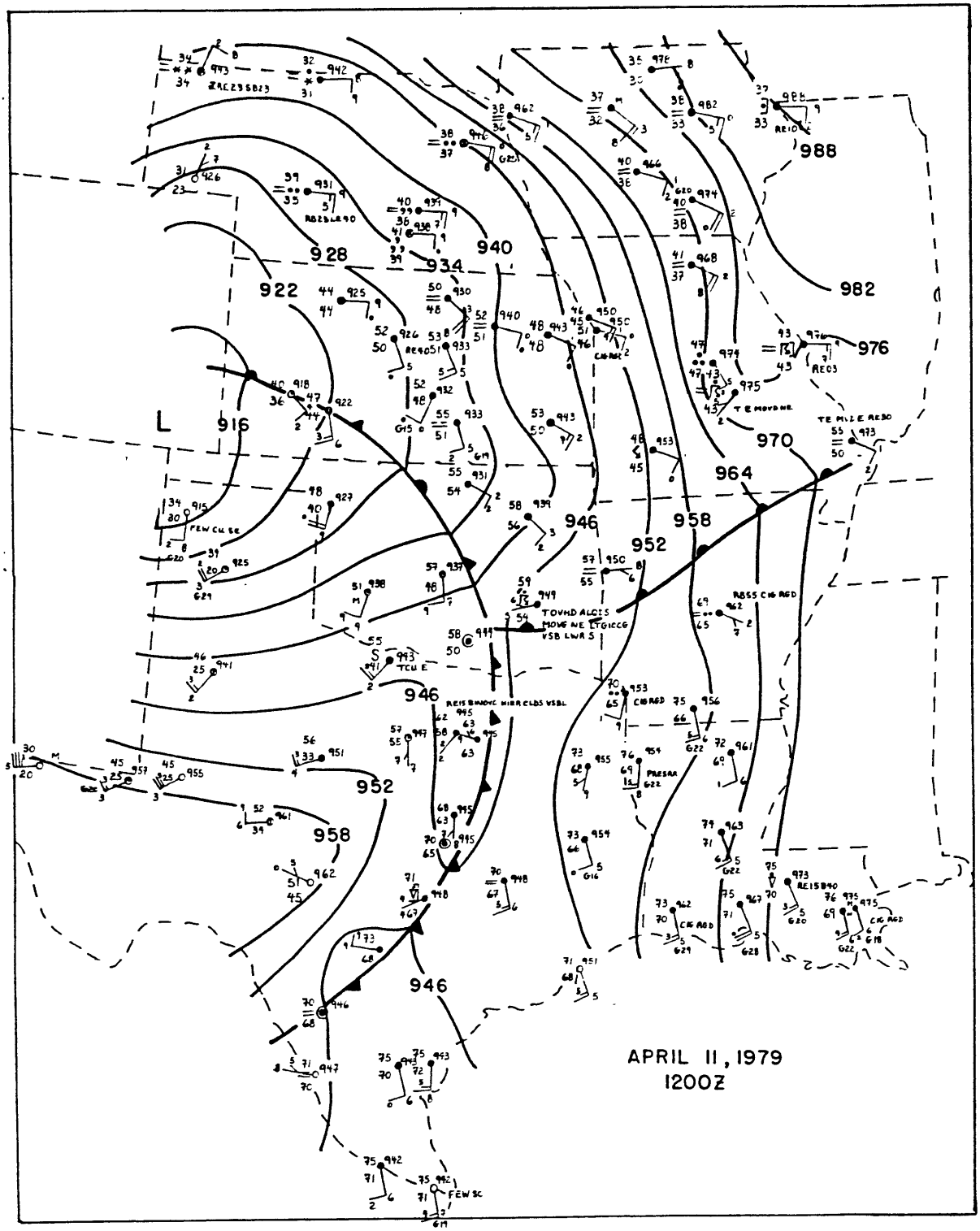

APRIL 10, 1979
2100 Z

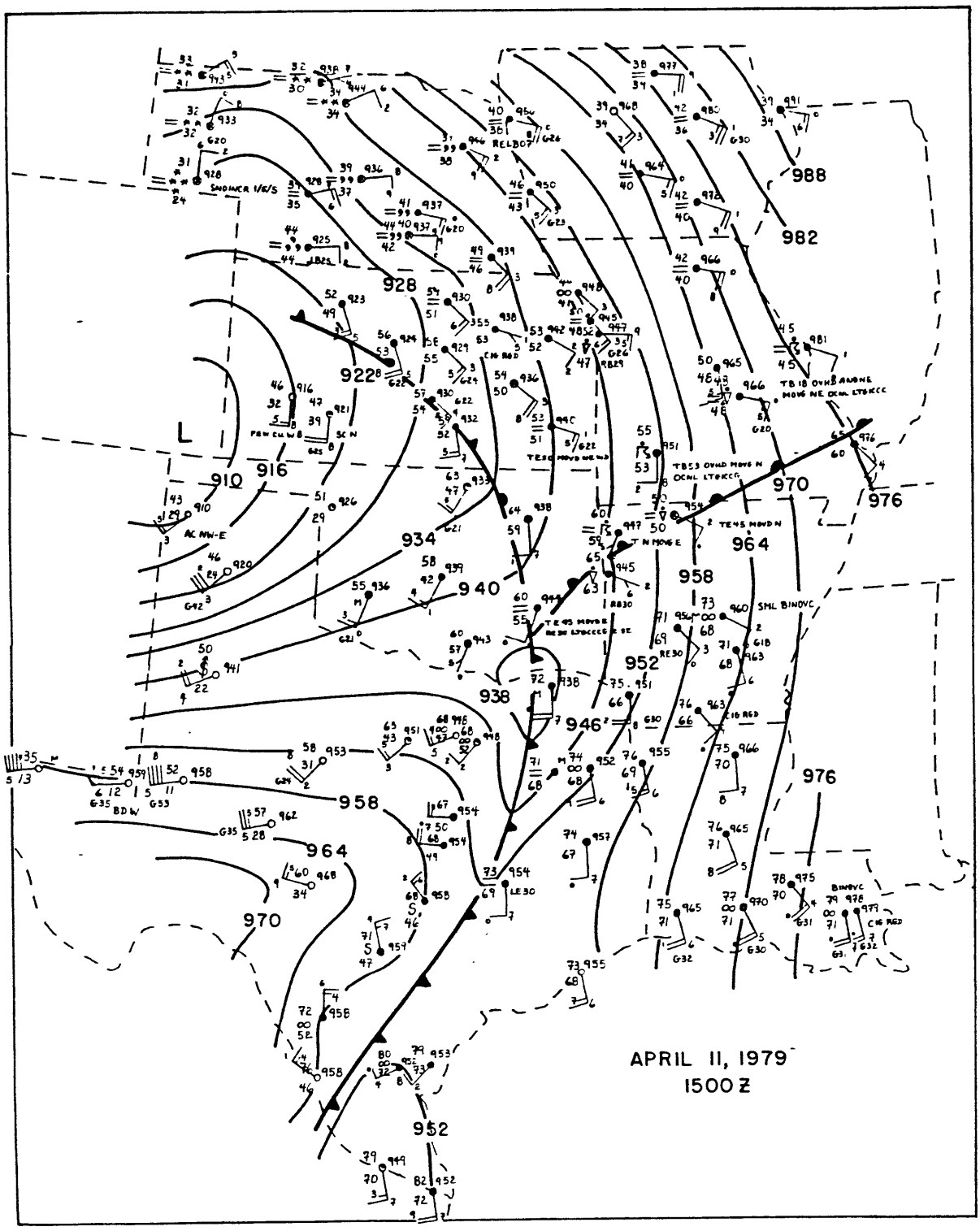

APRIL 11, 1979
0000 Z

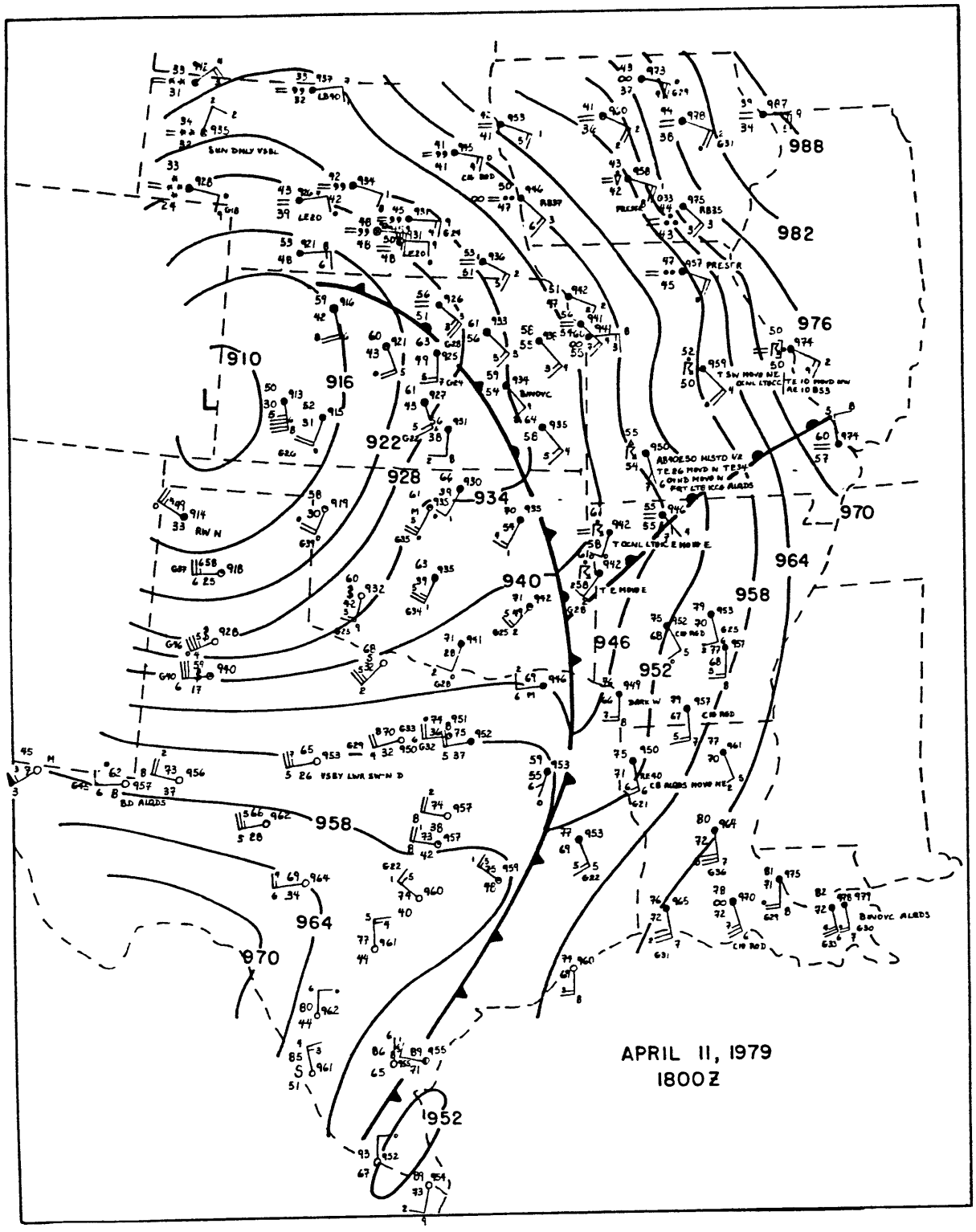

APRIL 11, 1979
0300 Z

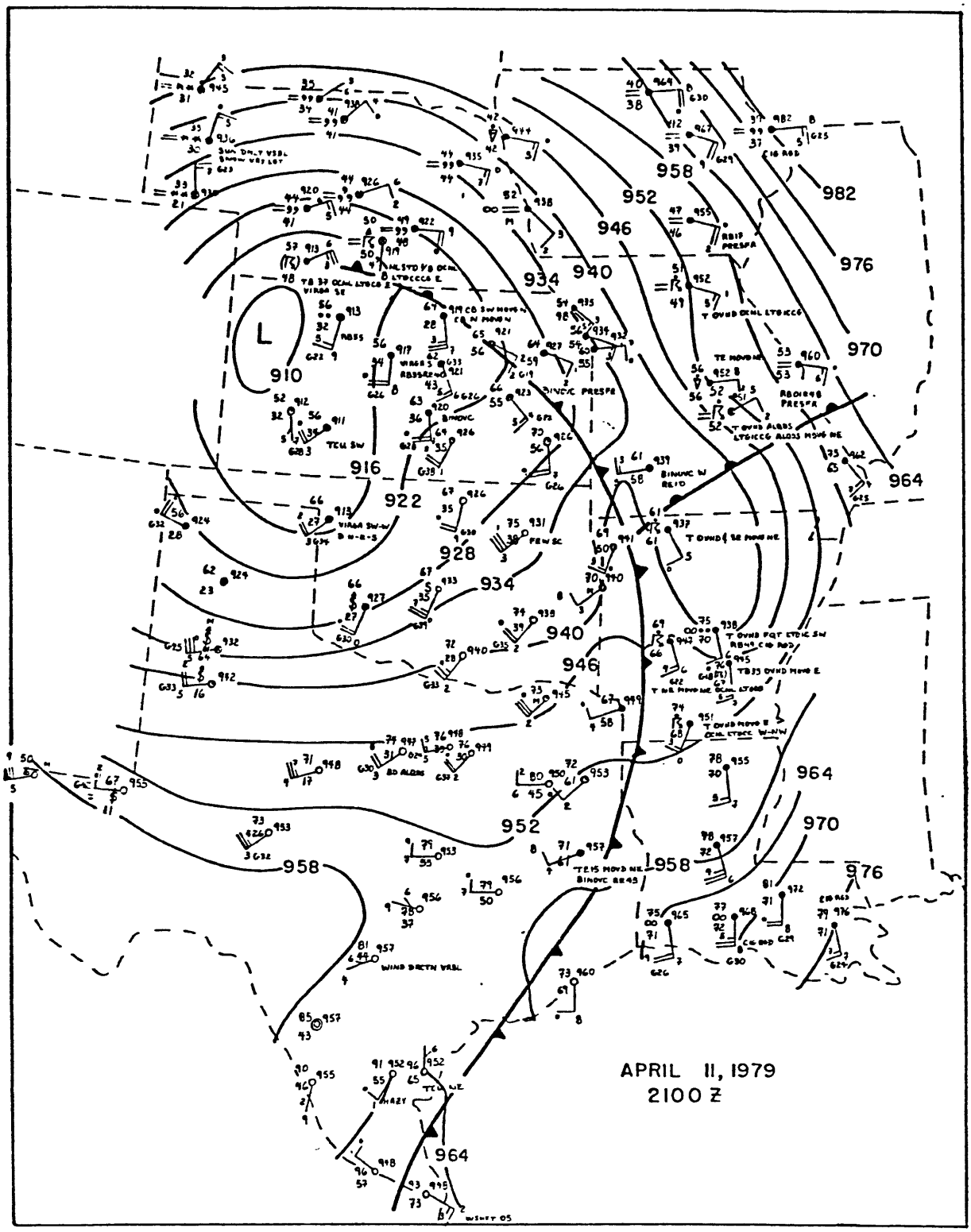

916
922
928
934
940
946
952
958
964
970
976
982
988
APRIL 11, 1979
0600 Z


928
922
916
L
936
940
946
952
958
964
970
976
982
APRIL 11, 1979
0900Z


L
916
922
928
934
940
946
952
958
964
970
976
982
988
APRIL 11, 1979
1200Z

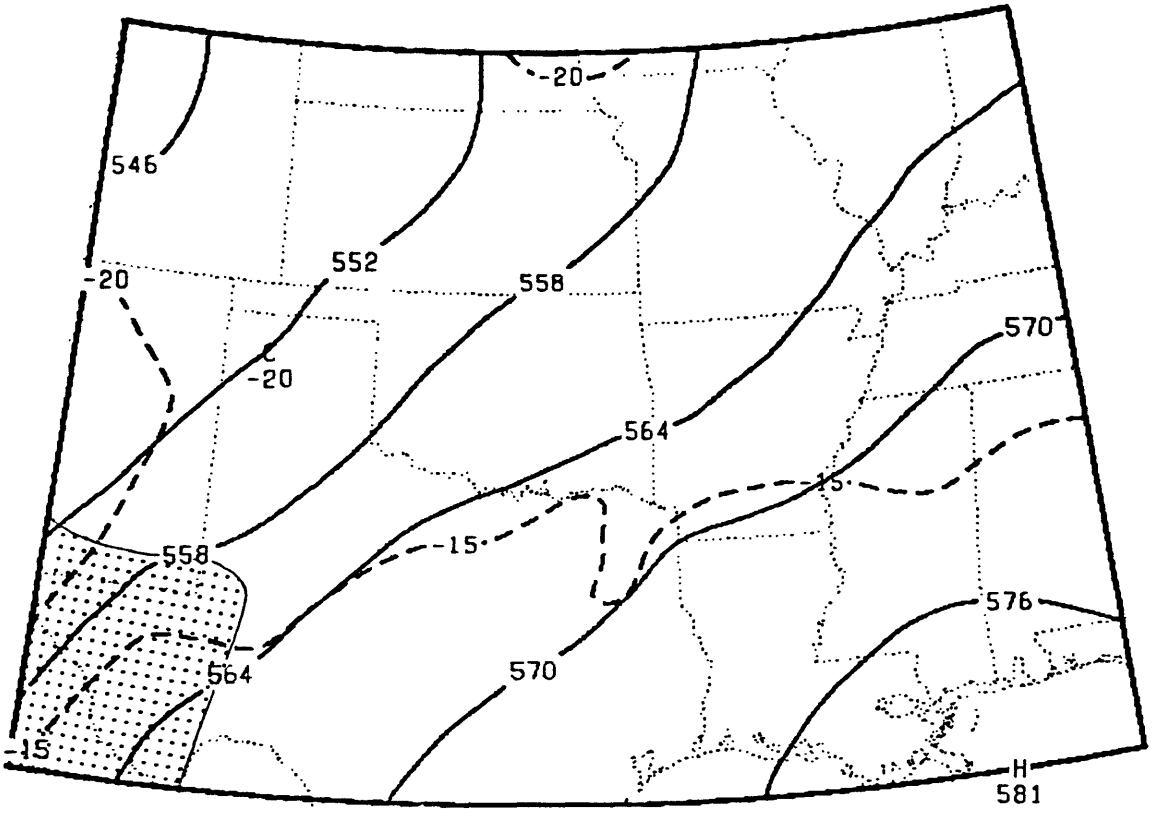

L
910
916
928
922
934
940
938
946
952
958
964
970
976
982
988
APRIL 11, 1979
1500 Z

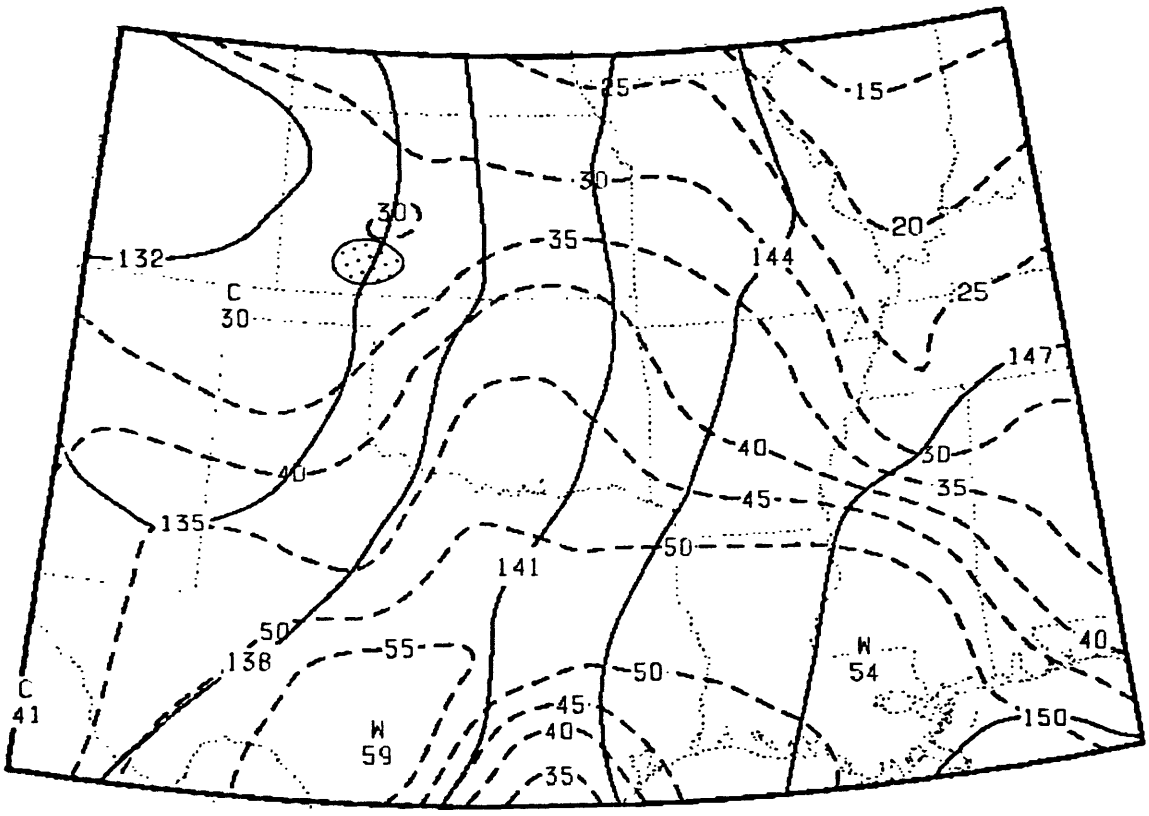

910
916
922
928
934
940
946
952
958
964
970
976
982
988
APRIL 11, 1979
1800Z


L
910
916
922
928
934
940
946
952
958
964
970
976
982
APRIL 11, 1979
2100 Z

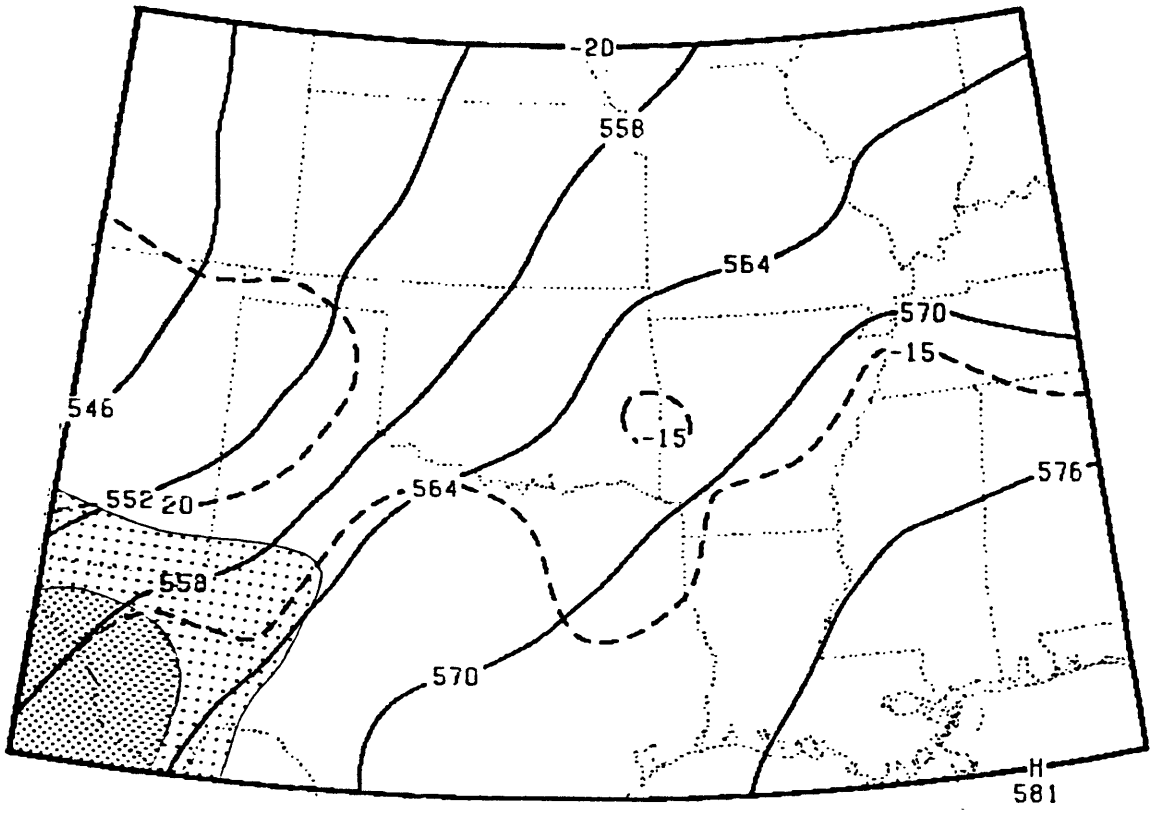
APPENDIX IV: COMPLETE SET OF 850-MB AND 500-MB ANALYSES

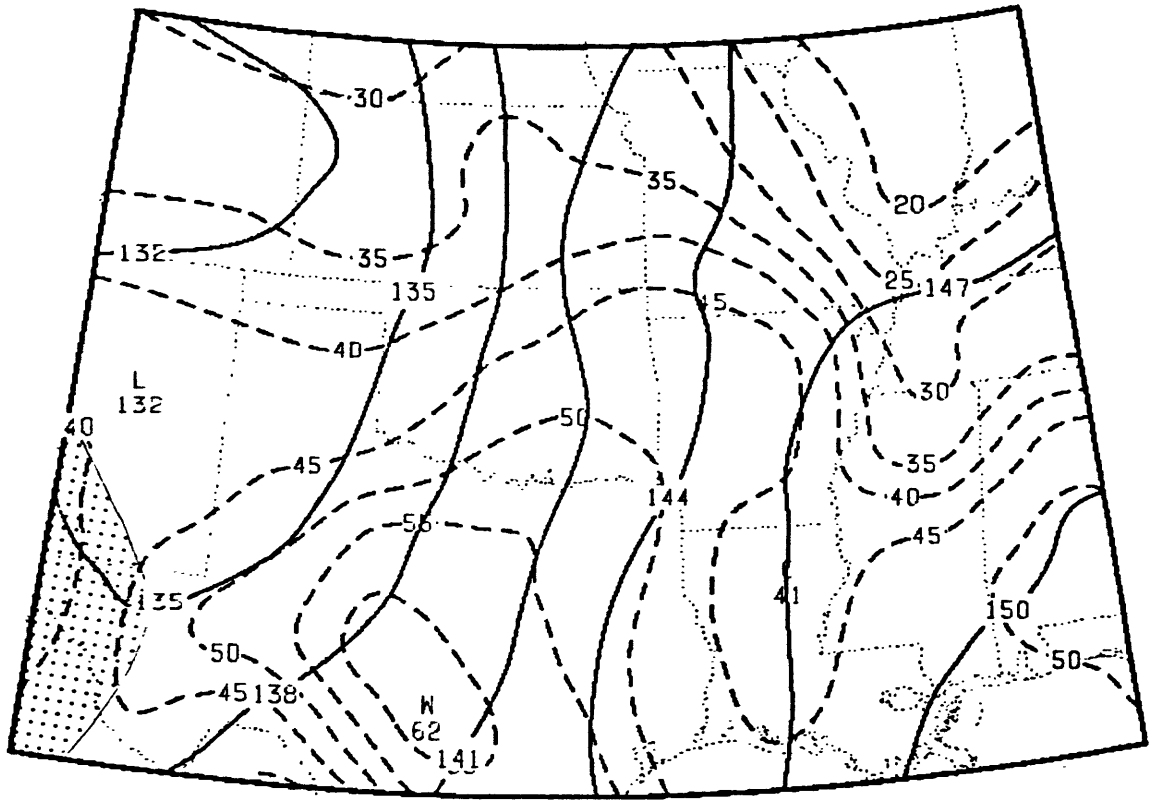
The 850-mb and 500-mb upper-air analyses for the period from 1500 GMT 10 April 1979 to 1200 GMT 11 April 1979 (every 3 hours). TOP. The 500-mb analysis. The solid lines are height contours (dm). The light shading is for wind speeds 30-39 m/s, medium shading for wind speeds 40-49 m/s, and dark shading for wind speeds ≥50 m/s. Dashed lines are isotherms (°C). BOTTOM. The 850-mb analysis. The solid lines are height contours (dm). The light shading for wind speeds 20-29 m/s, medium shading for wind speeds 30-39 m/s, and dark shading for wind speeds ≥40 m/s. Dashed lines are isopleths of equivalent potential temperature (°C).



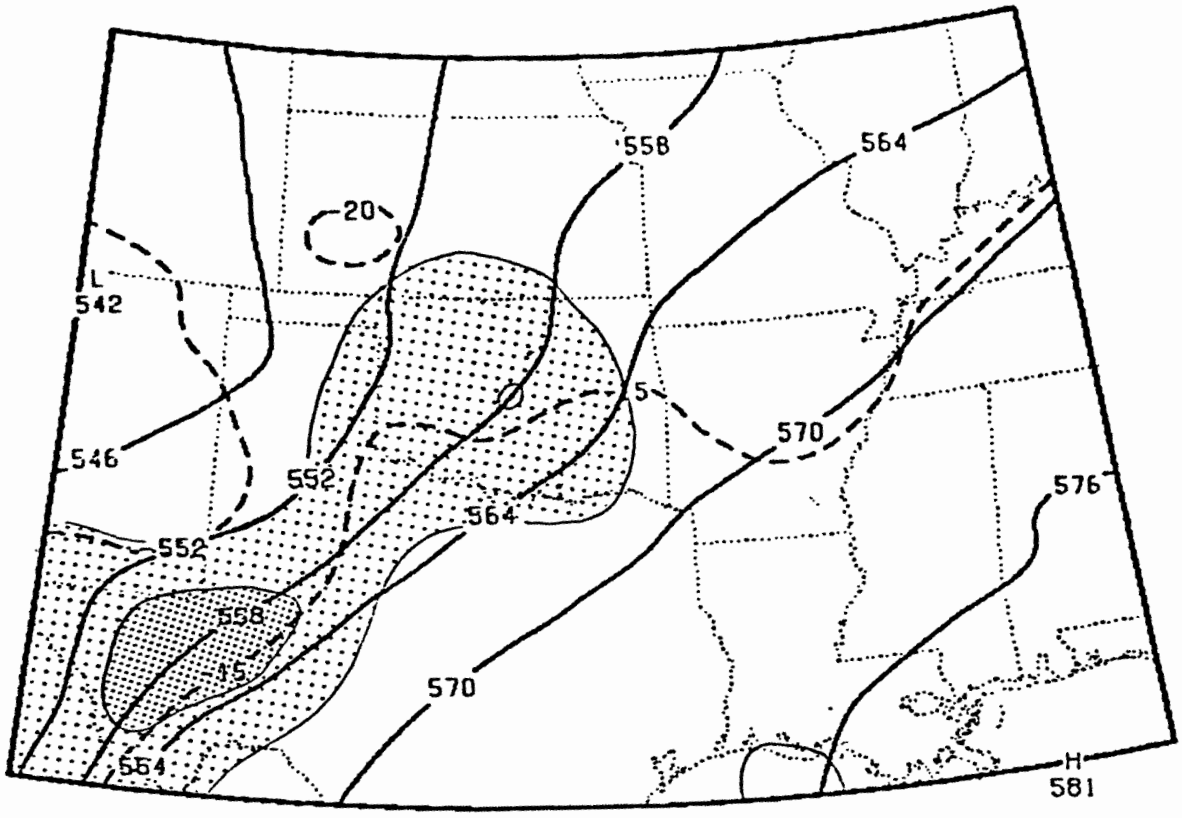


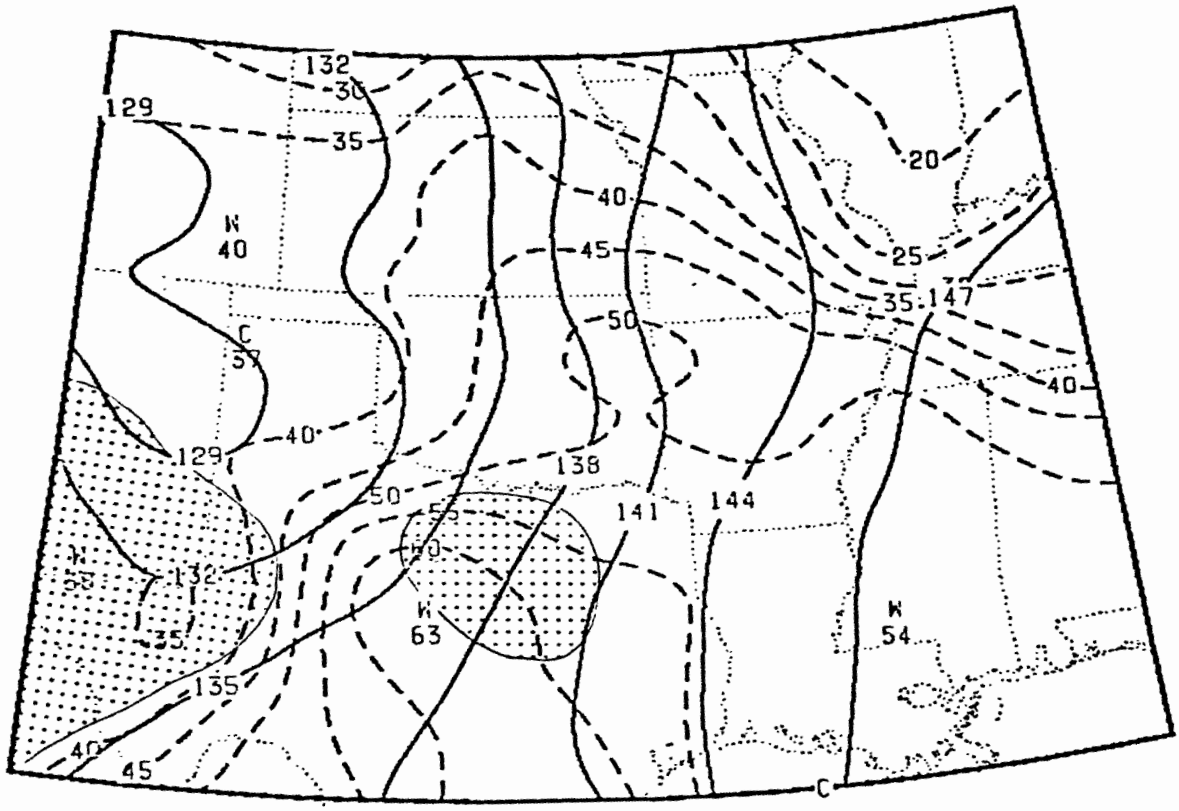
1500 GMT 10 April 1979



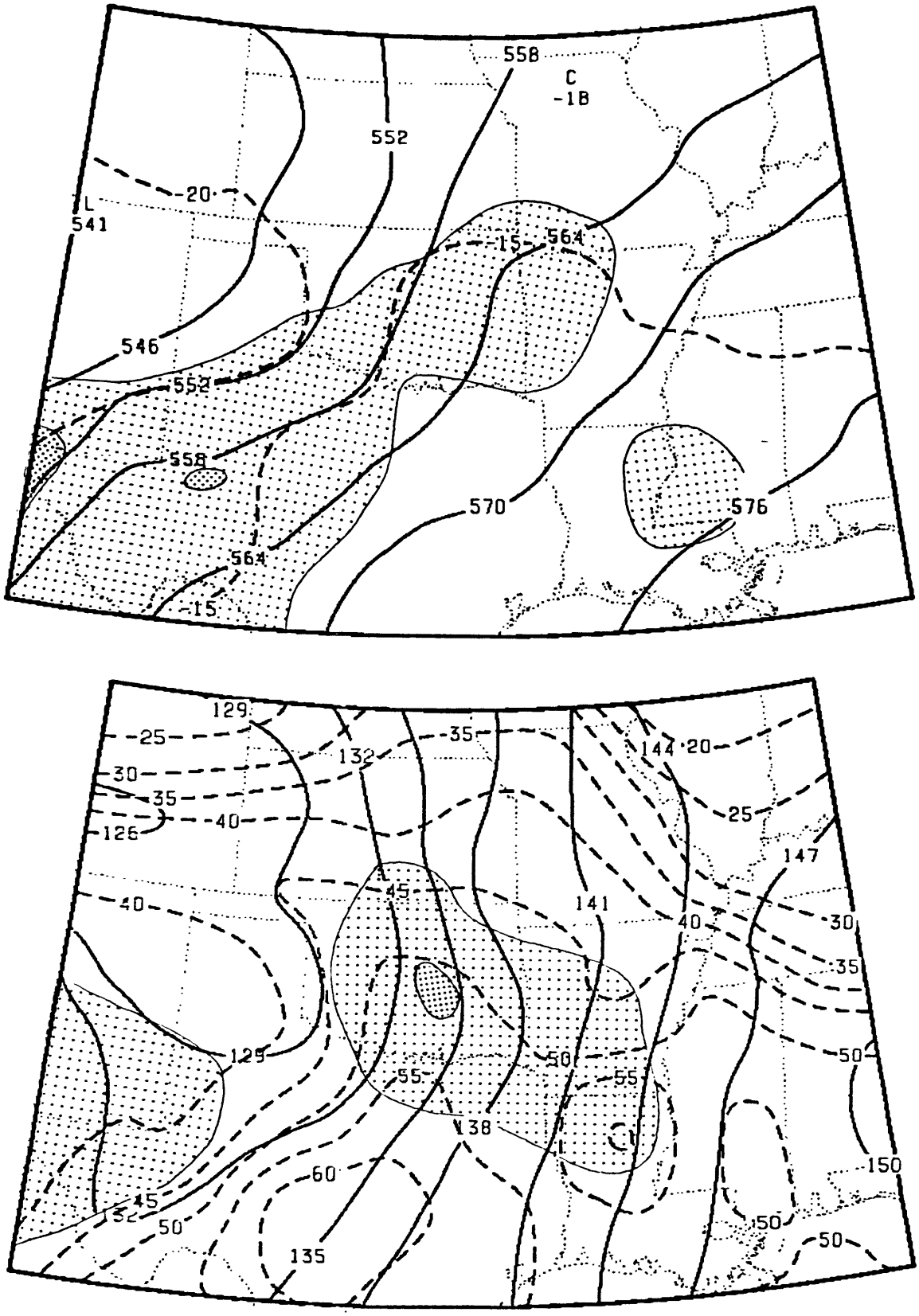


1800 GMT 10 April 1979

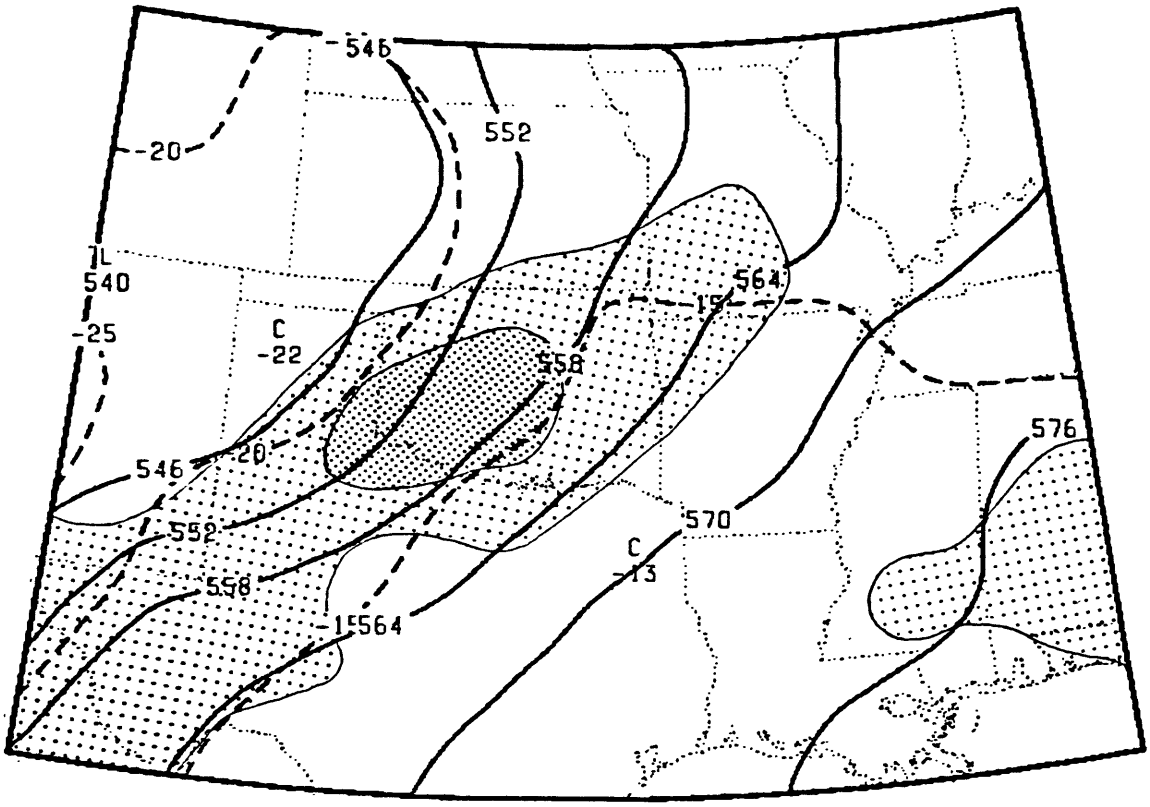


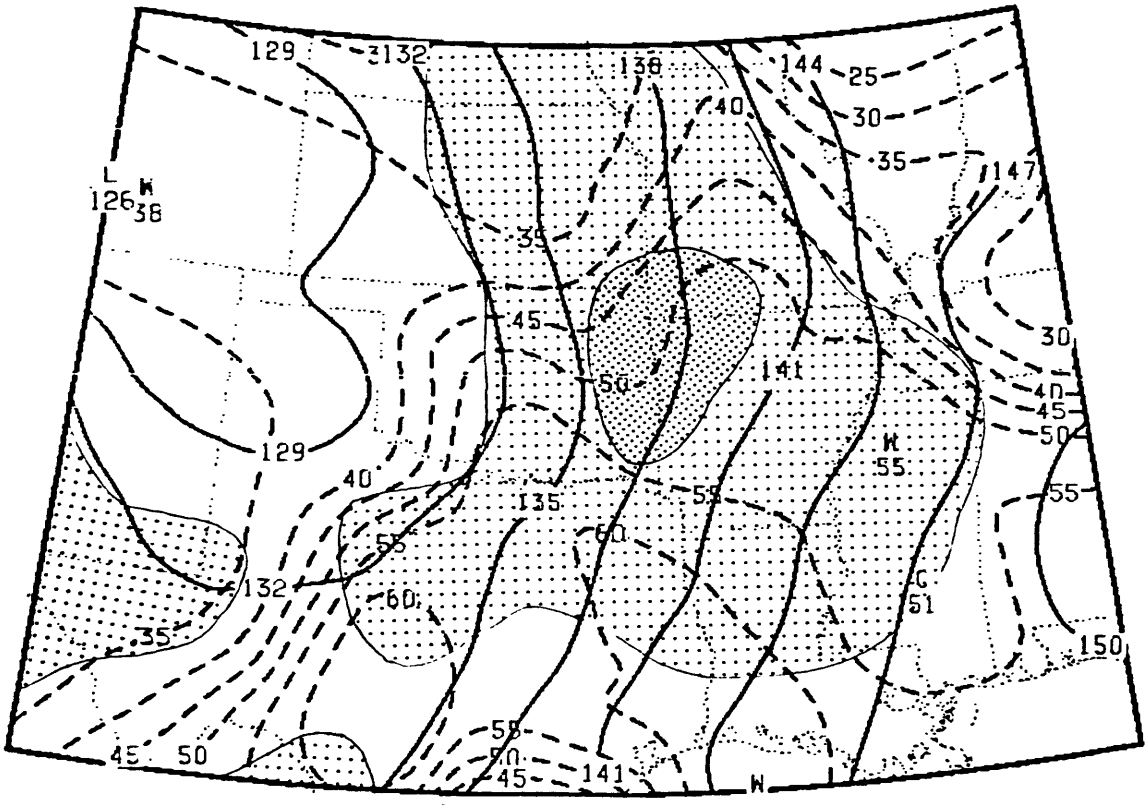


2100 GMT 10 April 1979

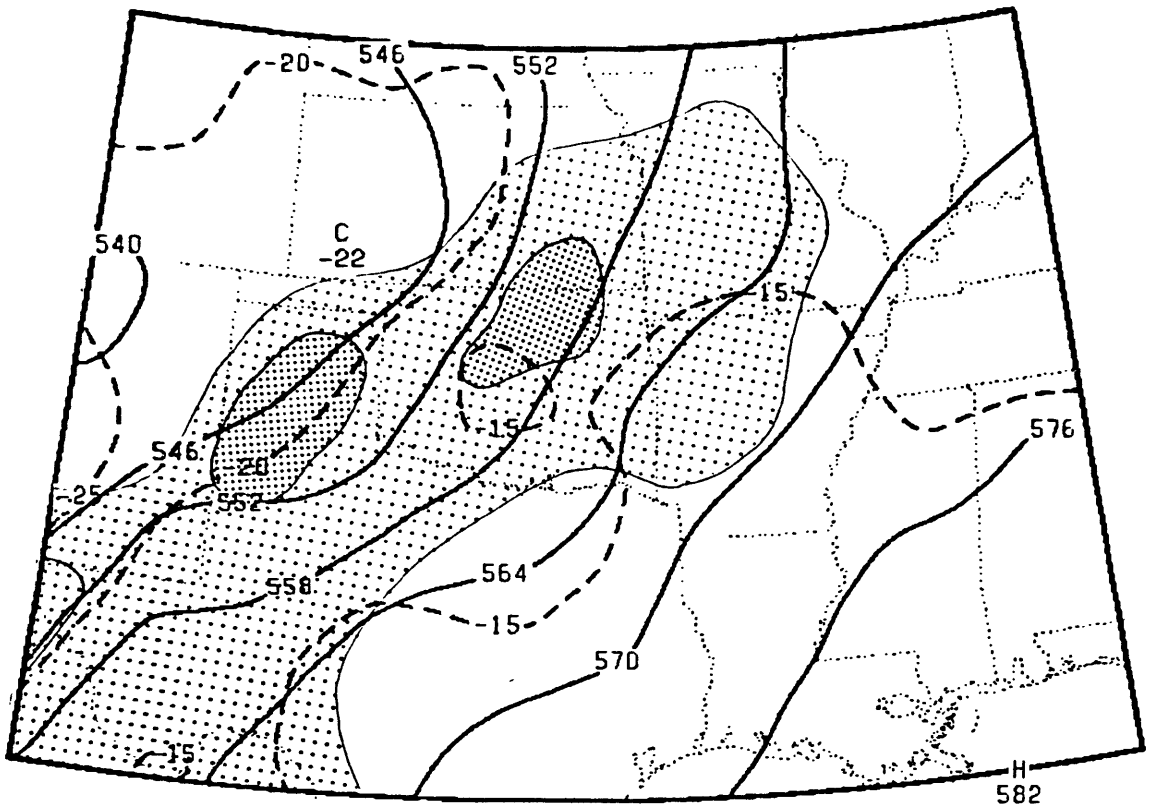


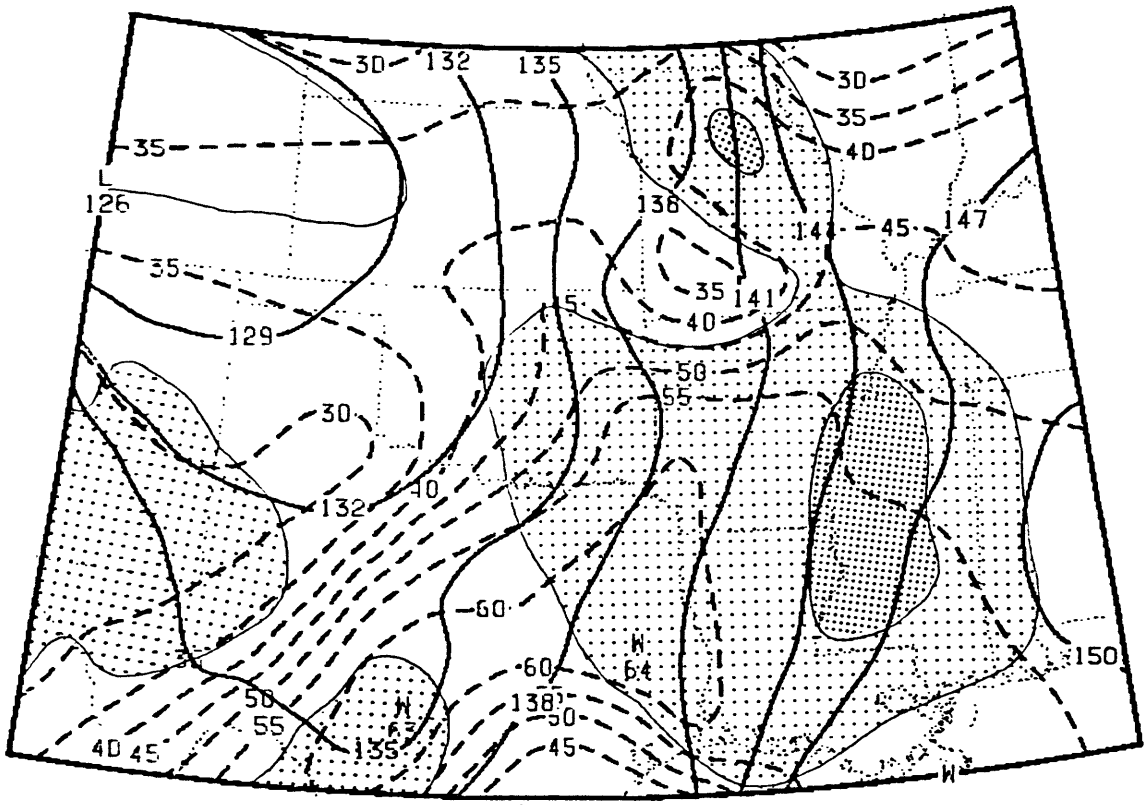
0000 GMT 11 April 1979



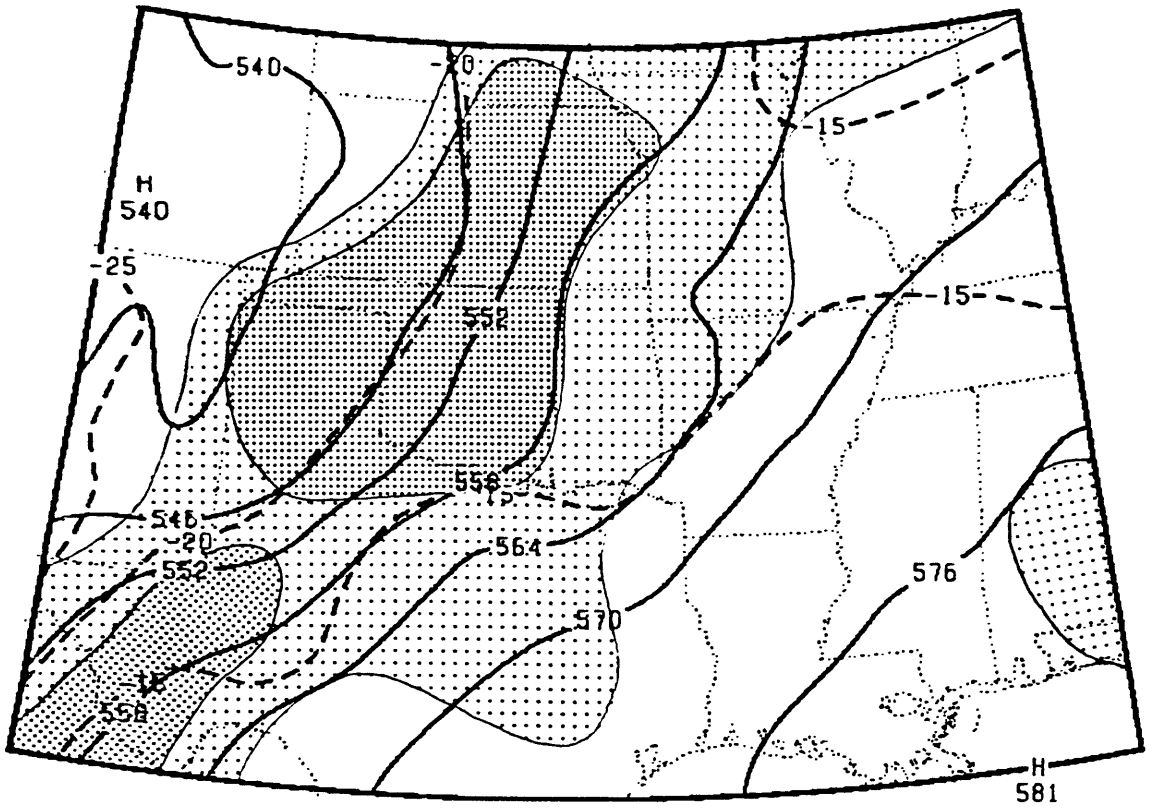


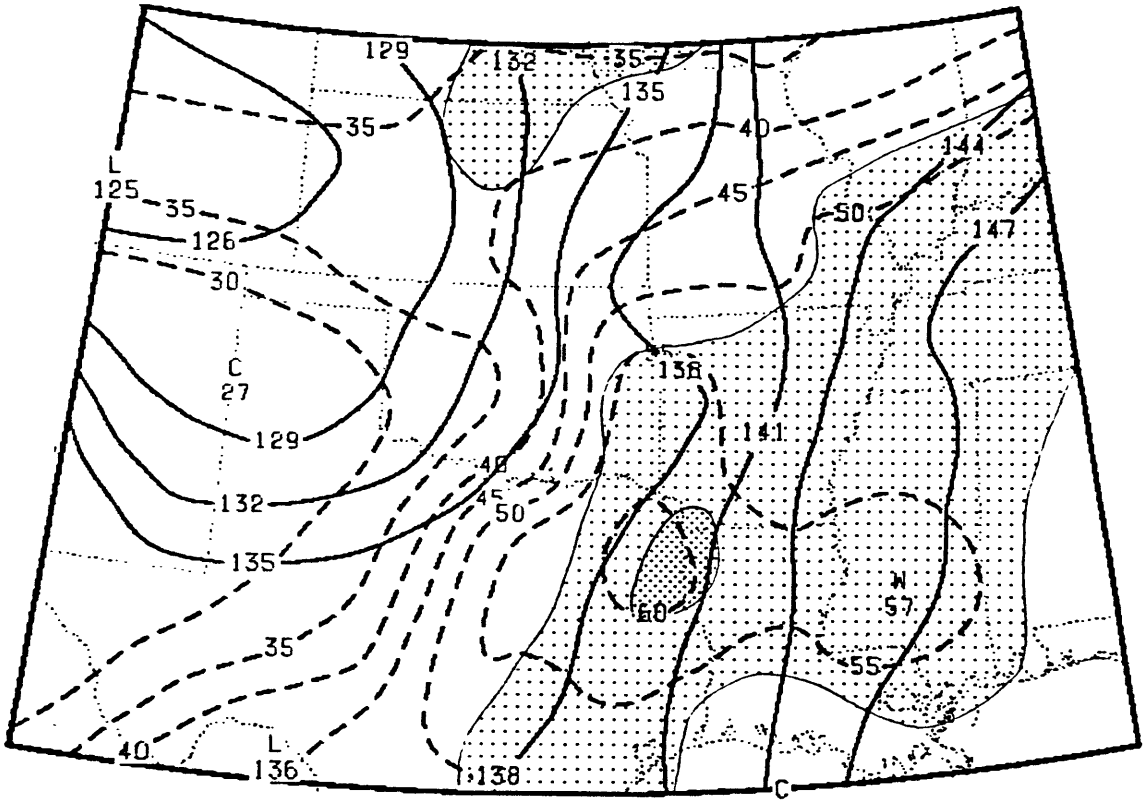
0300 GMT 11 April 1979



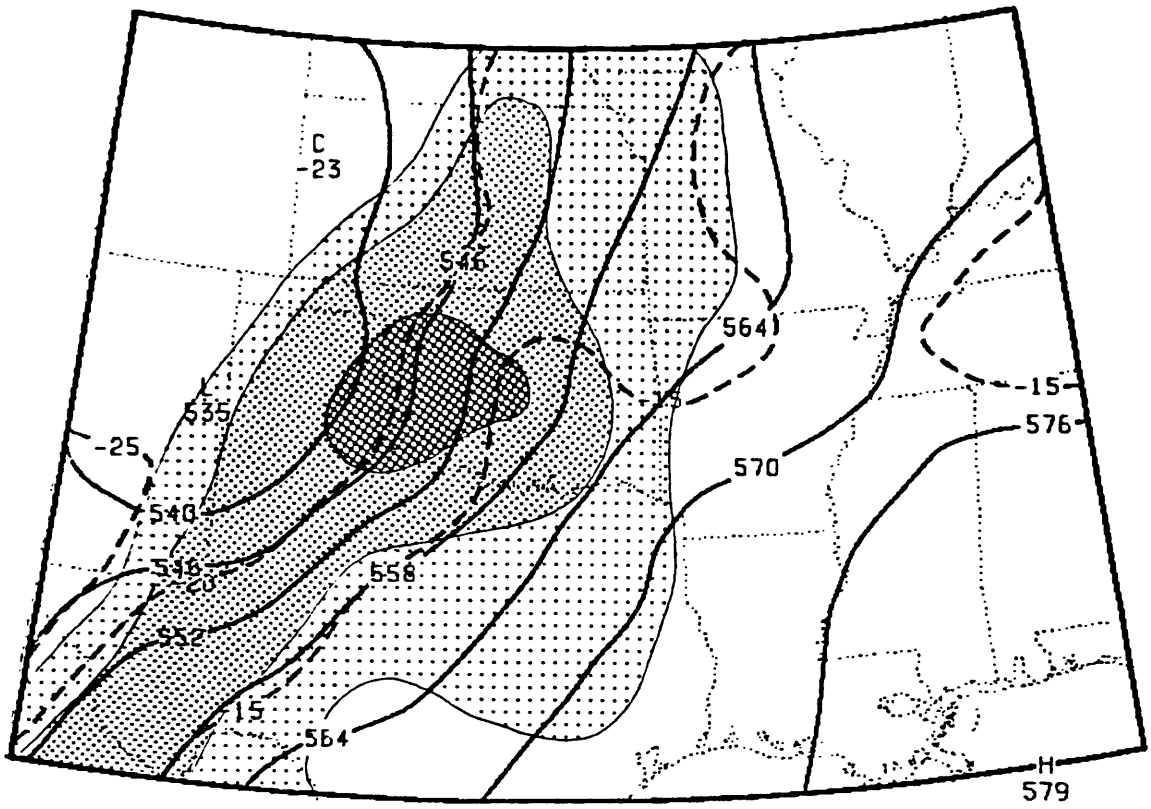


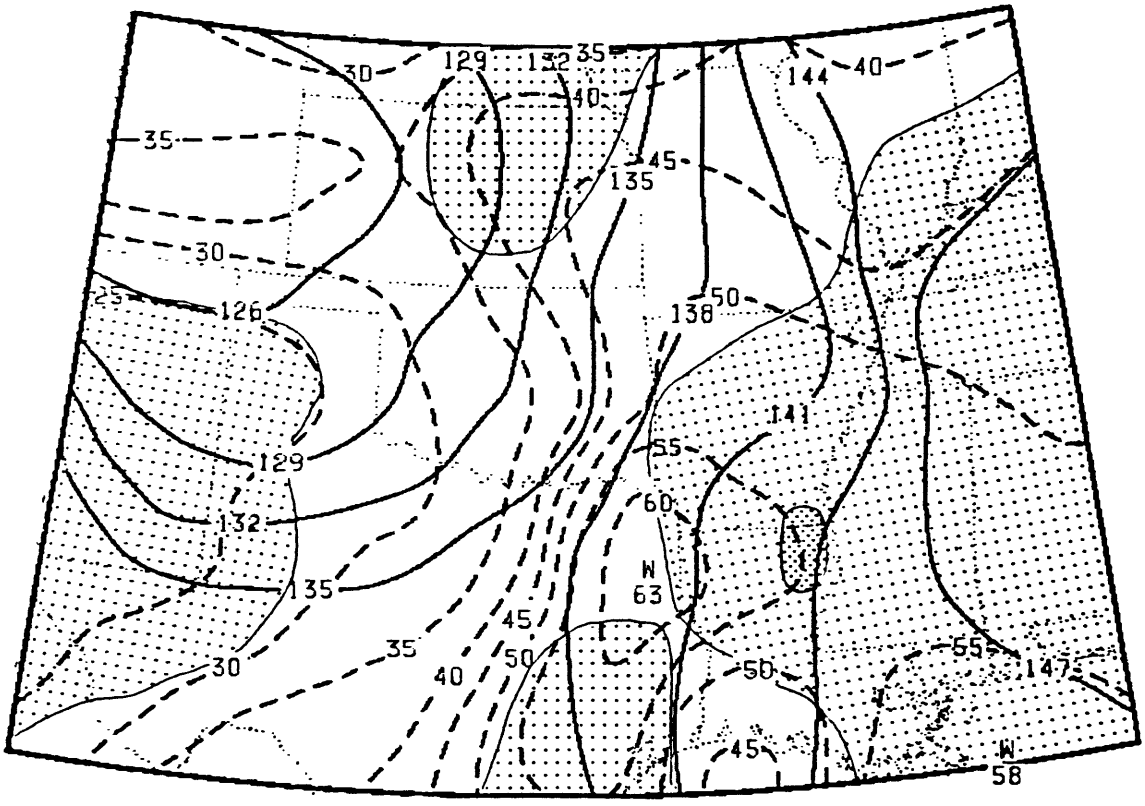
0600 GMT 11 April 1979





0900 GMT 11 April 1979





1200 GMT 11 April 1979

ACKNOWLEDGEMENTS

While conducting this research I was supported by National Science Foundation grant ATM-8019301.

I would like to express my appreciation to Dr. Thomas Carney at Purdue University who was very helpful in making their AVE-SESAME I grid-point data set available and answering my many questions.

I would like to thank the staff of our Center, with special thanks to Jane McNabb, Virginia Mills, Eddie Nelson and Diana Spiegel for their support and friendship. During my stay at MIT Isabelle Kole was very generous with her typing and drafting skills.

I owe a great deal to my thesis supervisor, Professor Fred Sanders, for his instruction and guidance. Of the many thing I've learned from Professor Sanders I think the one thing I will remember the longest is that a truly lucky person is one that is still enthusiastic about their work when they retire.

I want to express my appreciation to my fellow students for all the support that I received from them over the last six years. I would like to mention all those that have already graduated - Frank Colby, John DiStefano, John Gyakum, Jane Hsiung, George Huffman and many others. A special mention of my comrades on the 16^{th} floor that I regrettably leave behind - Tom Nehrkorn, Mike Rocha, Dawn Wolfsberg and Josh Wurman, I hope they all get the support they gave me to succeed in whatever they decide to do. It would be hard to express my appreciation to Mike Rocha for his help in completing this

document. Another person that helped bail me out at the end was Peter Shaffer. His love and encouragement has made it all possible.

An acknowledgement would not be complete without mentioning my family. First of all, my Uncle Wayne will probably be the most relieved of all to know that I'm through. I am grateful to my gradparents who have always given me their selfless and limitless love. My parents have always given me the freedom to make my own decisions and the trust to accept them. They have alway shown an interest in my work and provided that often needed encouragement. Most importantly, I am thankful for their love.

BIOGRAPHICAL NOTE

I was born in Renton, Washington in 1955 and with the exception of single years spent in Wisconsin and New Jersey stayed in the Seattle area through high school. My early interests included the outdoors, sports, and weather, particularly snow. I loved snow. Sometime early in high school I made the choice between becoming a wildlife manager and a meteorologist.

I graduated from Tyee Senior High School in June of 1973 and after spending the summer as a field assistant for the Foundation for Glacier and Environmental Research on the Juneau Icefield in Alaska attended Montana State University in Bozeman where I studied earth sciences and mathematics. In June of 1975 I was hired by the National Weather Service as a Student Trainee and spent the summer in Portland, Oregon at the River Forecast Center. The following summer I worked at the Scientific Services Division of the National Weather Service in Salt Lake City, Utah under Len Snellman.

I graduated from Montana State University in June of 1977 and returned to the Juneau Icefield where I conducted my own project on katabatic winds off an alpine glacier. That fall I enrolled at the Massachusetts Institute of Technology. During my stay at MIT I spent three summers away. The first, 1978, was spent at the National Center for Atmospheric Research in Boulder, Colorado in a computing fellowship program. The next summer, 1979, I returned to Salt Lake City and the Scientific Services Division. Finally, for three weeks during the summer of 1982 I attended the Advanced Studies Institute on Mesoscale Meteorology in Bonas, France.